

**MINERALOGICAL, MORPHOLOGICAL AND GEOCHEMICAL STUDIES
ON KUNDARA AND MADAYI KAOLINS, KERALA**

**Thesis submitted to the
UNIVERSITY OF KERALA
In partial fulfillment of the requirements
For the Degree of
DOCTOR OF PHILOSOPHY
In Geology
Under the Faculty of Science**

by
Manju C. S.

**Clays and Clay Minerals Unit
Regional Research Laboratory (CSIR)
Thiruvananthapuram- 695 019, Kerala, India**

February, 2002

.....dedicated to my beloved father

Declaration

I hereby declare that the matter embodied in this thesis is the result of investigations carried out by me at the Clays and Clay Minerals Unit of the Regional Research Laboratory, Thiruvananthapuram, under the joint supervision of Dr. M. Lalithambika, Deputy Director & Head, Clays and Clay Minerals Unit, Regional Research Laboratory, Thiruvananthapuram and Dr. V. Narayanan Nair, Professor, Department of Geology, University of Kerala, Kariavattom, Thiruvananthapuram and the same has not been submitted elsewhere for a degree.

In keeping with the general practice of reporting scientific observations, due reference has been made wherever the work described is based on the findings of other investigators.

Manju. C.S

Certificate

Certified that the work embodied in this thesis titled “Mineralogical, morphological and geochemical studies on Kundara and Madayi kaolins, Kerala” has been carried out by Ms. Manju C.S under our joint supervision and the same has not been submitted elsewhere for a degree.

*Dr. V. Narayanan Nair
Professor, Department of Geology
University of Kerala, Kariavattom
Thiruvananthapuram- 695 581*

*Dr. (Ms.) M. Lalithambika
Deputy Director & Head
Regional Research Laboratory, C.S.I.R
Thiruvananthapuram- 695 019*

Preface

The geochemical importance of clay minerals stems from their ubiquity in soils and sediments and their manifold industrial applications. Clay minerals, which are grouped as phyllosilicates, share a basic set of structural and chemical characteristics. Kaolin groups of minerals are the most widespread in this phyllosilicate family. Among these, kaolinite is an important weathering product at low latitudes. Geologically, the process of kaolinization occurs under different environmental conditions such as surface weathering and hydrothermal alteration. The product of kaolinization is highly influenced by the geology and geochemistry of the parent rock, the climatic conditions and the topography of the area. Kerala kaolins are mostly the products of surface weathering in tropical climatic conditions. Under this climatic regime primary aluminosilicate minerals are usually weathered to kaolin group minerals either directly or indirectly. The major clay deposits of this region are associated with the Cenozoic sedimentary basins, where kaolinites of both sedimentary and residual origin are well preserved.

The thesis comprises of five chapters. It is an exhaustive study on the geochemical, mineralogical, morphological, and the utilitarian aspects of clays from two major kaolin deposits; Madayi (Kannur) and Kundara (Kollam) in the northern and southern districts of Kerala. The clay deposits are characterised by kaolinites of residual nature, which are the weathered products of Precambrian crystalline rocks overlain by the sedimentary kaolins of Tertiary age.

Chapter one deals with the general introduction on the mineralogical, geological and structural aspects of kaolinite and its industrial versatility. The geological significance of this particular mineral along with an overview on the process of kaolinization is presented in this chapter. Brief descriptions on the topography, climate and geology of Kerala have also been presented.

The second chapter explains the methodology adopted for the geochemical, mineralogical and morphological characterization. The techniques involved X- ray diffraction analysis, Differential Thermal/ Thermogravimetric Analysis, Fourier Transform Infrared Spectroscopy, Diffuse Reflectance FT-IR Spectroscopy, Scanning Electron/Optical microscopy and Chemical analysis. Physical characterization for

industrial evaluation of the clay involved determination of particle size distribution, brightness/yellowness, viscosity, contact angle, linear shrinkage, volume shrinkage, water absorption, bulk density, apparent porosity, green and fired strength measurements.

Detailed characterization of kaolinite from Madayi deposit has been presented in chapter three. The present investigations give evidences on the influence of the environmental conditions on kaolinite formation. Kaolinite formed under different genetic conditions, throw light on the fact that the clay suite can be utilized as a tool to reflect the climate during the time of its formation or deposition. The studies show that the sedimentary clay seams, which overlie the industrially viable residual seam, influence the geochemistry and industrial utility of the latter.

Chapter four is presented in two parts: Part I is a brief description of the mineralogical and morphological features of Kundara kaolinite. The geochemical aspects of quick yellow pigmentation of the residual clay have been studied in detail. The iron impurity, which is mostly in ferrous state at the time of exposure, gets transformed to ferric form due to oxidation. The black patched FeS_2 and its oxidation products in the residual white clay, have a major role in degrading the quality of the white kaolin. The influence of the climatic conditions on the deposits has been explained. Part II deals with the quality improvement studies. The process involved beneficiation by the removal of iron using an efficient chemical leaching technique. The treated clay was tested in bone china formulations.

Chapter five is on the surface modification of kaolinite using organosilane and its application as filler in natural rubber. Silylated clays form 'molecular bridges' to create strong stable bonds between two otherwise weak bonding surfaces. The composite obtained by the incorporation of modified filler clays into natural rubber generate bulk properties of two different phases *i.e.* an inorganic substrate and an organic polymer. This uniform composite structure, exhibits improved thermal and mechanical properties.

The thesis concludes with a note on the future perspectives of this gift of nature, the kaolin.

Acknowledgments

It is with great respect that I place on record of my deep sense of gratitude to my research supervisor, Dr. M. Lalithambika, Head, Clays and Clay Minerals Units, R.R.L., Thiruvananthapuram, for introducing me to the fascinating field of clay science and also for the excellent guidance. I am also thankful to her for giving me profound freedom and support during this work.

I am grateful to my co-supervisor, Dr. V. Narayanan Nair, Professor, Department of Geology, University of Kerala, for constant encouragement and able guidance.

I wish to express my sincere gratitude to the Council of Scientific and Industrial Research (CSIR), Government of India, for providing the research fellowship.

I am thankful to the Director, R.R.L. Prof. (Dr.) Javed Iqbal and the former Director Dr. Vijay Nair for proving all the facilities to work in this laboratory.

I am deeply indebted to Prof. K.P. Thrivikramaji, Head, Department of Geology and Prof. P.K. Rajendran Nair, former Head, Department of Geology, University of Kerala, Kariavattom for the support and facilities made available to me during the course of this research program.

I am thankful to all my teachers and staff members of the Department of Geology in rendering me the necessary help through out the tenure of this work.

With a deep sense of gratitude, I remember DR. C. K. S. Pillai, Dr. A.R.R. Menon, Dr.V.S. Prasad, Dr. Peter Koshi, Mr. Prabhakar Rao, Dr. Sathy Chandrashekar, Shri. P. Raghavan, Dr. Shyama Prasad, Mr. P. Guruswamy, Dr. C. Pavithran, Mr. P. Mukundan, Mr.P. Vijayakumar, Mr. P. Sisupalan and Mr N. Narayanan of this laboratory for the whole-hearted help at various stages of this program.

I specially thank Dr. K. P. Thrivikaramaji, Dr. Sabu Joseph and Mr. V. Velappan Nair of the Department of Geology, University of Kerala, for the help given to me in optical microscopic analysis; Dr. C.P. Sharma and Dr. K. Sreenivasan of Sree Chithirathirunal Institute of Medical Science and Technology for helping in contact angle and mechanical strength measurements; Ms. Mangala Agashe of N.C.L., Pune, for DRIFT spectra and Dr. I. Balakrishnan and Dr. T.J. Nelson of EICL, Thiruvananthapuram, for the help rendered during the course of this research period .

Thanks are due to Dr. D. Bahulayan, Ms Rugmini Sukumar, Mr.V. Sreekantan, Mr.K.M. Prakash, Ms. L. Latha, Ms. Gracy Thomas and all other members of the Clays and Clay Minerals Unit for their sincere and timely help.

It is my pleasure to acknowledge my friends Miss. Yamuna. A, Mr. U. Santhosh, Dr. Raji Mathew, Ms. P. Pushpaleta, Mr. R.P. Aloysius, Mr. G. Narayan, Ms. P. N. Pramada and Mr. S. Ramaswamy for the encouragement given to me.

Above all I am deeply indebted to my parents and sisters for the encouragement given to me in all phases of my life and particularly my husband Mr. K. Sajeev for his kind understanding and moral support which resulted in the successful completion of this work.

Manju. C.S

Content

	Page No.
Preface	(i)
Chapter- 1: Kaolin- an overview on the genesis and applications	
1. Introduction	1
1.1 Phyllosilicates	1
1.2 Kaolin minerals	2
1.3 Genesis of kaolin	4
1.3.1 Kaolinization of feldspar	6
1.3.2 Kaolinization of mica	10
1.3.2.1 Formation of kaolinite from muscovite	11
1.3.2.2 Formation of kaolinite from biotite	12
1.3.3 Formation of kaolinite from halloysite	14
1.3.4 Conversion of gibbsite to kaolinite	15
1.3.5 Formation of kaolinite from smectite	15
1.3.6 Laboratory synthesis of kaolinite	16
1.4 Geology and geomorphology of Kerala	18
1.4.1 Geology	18
1.4.1.1 Precambrian rock	18
1.4.1.1.1 Precambrian rock of North Kerala	19
1.4.1.1.2 Precambrian rock of South Kerala	19
1.4.1.2 Tertiary Formation	20
1.4.1.2.1 Vaikom Formation	21
1.4.1.2.2 Quilon Formation	22
1.4.1.2.3 Warkallai Formation	22
1.4.1.2.4 Quaternary Formation	22
1.4.2 Structural trends	22
1.4.3 Geomorphology	23
1.4.3.1 Topography	23
1.4.3.2 Drainage	23
1.4.3.3 Climate	24
1.4.4 Clay formation in relation with geology and geomorphology	24
1.5 Kaolin resources	26
1.5.1 World resource	26
1.5.2 Indian resource	26
1.6 Application and specifications of kaolin	28
1.6.1 As a paper coating and filler material	28
1.6.2 Ceramics and refractories	29
1.6.3 Plastics, adhesive and fibreglasses	30
1.6.4 Rubber	30
1.6.5 Paints	30
1.6.6 Other uses	31
1.6.7 Special applications through chemical modifications	32
1.7 A brief description of the present work	32

Chapter 2: Methods and techniques of mineralogical, morphological and physico- chemical characterisation.

2.1 Separation of fines from kaolinite	34
2.2 Heavy mineral separation	35
2.3 Mineralogical analysis by X- ray diffraction technique	36
2.3.1 Randomly oriented mounts	37
2.3.2 Oriented mounts	37
2.4 Crystallinity index measurements	38
2.4.1 Pretreatment of samples	39
2.4.1.1 Removal of carbonate	39
2.4.1.2 Removal of organic matter	39
2.4.1.3 Removal of iron oxide	40
2.5 Infrared spectral method	40
2.6 Thermal analysis	41
2.6.1 Differential thermal analysis	42
2.6.2 Thermogravimetry	43
2.7 Optical microscopic analysis	43
2.8 Scanning electron microscopic analysis	44
2.9 Methods for chemical characterisation: major and minor elements	44
2.9.1 Loss on ignition	45
2.9.2 Determination of silica (Gravimetric technique)	45
2.9.3 Preparation of solution for Al ₂ O ₃ , TiO ₂ and Fe ₂ O ₃ determination	46
2.9.4 Determination of Al ₂ O ₃ (Volumetric method)	46
2.9.5 Determination of TiO ₂ (Colourimetric method)	47
2.9.6 Determination of Fe ₂ O ₃ (Colourimetric method)	47
2.9.7 Determination of Na ₂ O, K ₂ O and CaO	48
2.9.8 Determination of ferrous oxide	48
2.10 Determination of pyrite in clays by selective extraction with acid solution	49
2.11 Determination of water soluble sulphate	50
2.12 Organic carbon	51
2.13 Trace element analysis by atomic adsorption spectroscopy	51
2.14 Physical properties of clay	54
2.14.1 Particle size analysis	54
2.14.2 Viscosity	55
2.14.3 pH	56
2.14.4 Brightness measurements	56
2.14.5 Contact angle measurements	56
2.14.6 Determination of water of plasticity	57
2.15 Drying properties	58
2.15.1 Determination of dry linear shrinkage	58
2.15.2 Green strength	59
2.16 Fired properties	60
2.16.1 Determination of fired linear shrinkage	61
2.16.2 Determination of fired volume shrinkage	61
2.16.3 Determination of water absorption	61
2.16.4 Determination apparent porosity	62
2.16.5 Determination of bulk density	62
2.16.6 Determination of fired strength	63
2.17 Physical properties of polymer- kaolinite composite	63
2.17.1 Density measurements	63
2.17.2 Degree of equilibrium swelling and percentage of weight loss measurements	64
2.17.3 Mechanical strength measurements	65

Chapter 3: Mineralogy, geochemistry and utilization study of Madayi kaolin deposit, North Kerala

3.1 Introduction	66
3.2 Geologic setting	67
3.3 Materials and Methods	74
3.4 Results and discussions	75
3.4.1 XRD studies	75
3.4.1.1 Residual white clay (L1a, L1b and L1c)	76
3.4.1.3 Hematitic clay (L16, L17 and L18)	81
3.4.2 Crystallinity index measurements	82
3.4.3 Chemical assay of clays from different layers	83
3.4.3.1 Residual white clay : L1a, L1b and L1c	83
3.4.3.2 Gray carbonaceous clay: L3, L5, L7, L9, L11, L13 and L15	83
3.4.3.3 Hematitic clay: L16, L17 and L18	83
3.4.4 Variation of pH of the clay profile	85
3.4.5 Trace element analysis	85
3.4.6 Thermal studies	86
3.4.6.1 DTA studies	86
3.4.6.2 TG studies	88
3.4.7 FTIR studies	89
3.4.8 Morphological studies	91
3.4.8.1 Residual white clay	92
3.4.8.2 Gray carbonaceous clay	100
3.4.8.3 Hematitic clay	106
3.4.9 Industrial applications of white clay from seam L	110
3.5 Conclusion	112

Chapter 4 I: Geochemical, mineralogical and morphological investigation on Kundara kaolin deposit, South Kerala

4.I.1 Introduction	114
4.I.2 Geologic setting	115
4.I.3 Materials and methods	122
4.I.4 Results and discussions	123
4.I.4.1 XRD studies	123
4.I.4.1.1 Residual white clay (K1a, K1b and K1c)	127
4.I.4.1.2 Black patched residual clay (K1b*)	129
4.I.4.1.3 Gray carbonaceous clay	130
4.I.4.1.4 Hematitic clay	131
4.I.4.2 Crystallinity index measurments	132
4.I.4.3 Chemical analysis	133
4.I.4.3.1 Residual clay (K1a, K1b, K1b* and K1c)	133
4.I.4.3.2 Gray cabonaceous clay (K2, K4, K6 and K7)	134
4.I.4.3.3 Hematitic clay (K8, K9 and K10)	136
4.I.4.4 Trace element analysis	137
4.I.4.5 Thermal studies	138
4.I.4.5.1 DTA analysis	139
4.I.4.5.2 TG analysis	140
4.I.4.6 FTIR studies	141

4.I.4.7 Morphological analysis	143
4.I.4.7.1 Residual white clay	143
4.I.4.7.2 Gray carbonaceous clay	158
4.I.4.7.3 Hematitic clay	159
4.I.4.8 Yellow pigmentation on residual kaolinite	165
4.I.5 Conclusion	166

Chapter 4 II: Deferration and property evaluation of Kundara kaolinite

4.II.1 Introduction	168
4.II.2 Materials and methods	170
4.II.3 Results and discussions	171
4.II.3.1 Mineralogical and chemical characterisation	171
4.II.3.2 Leaching studies	173
4.II.3.3 Mechanism of iron leaching	179
4.II.3.4 Industrial utility	180
4.II.4 Conclusion	182

Chapter 5: Surface modified kaolinite as filler in natural rubber

5.1 Introduction	184
5.2 Materials and methods	189
5.2.1 Sample preparation	189
5.2.2 Surface modification of kaolinites	190
5.2.3 Characterisation of raw and modified kaolinites	190
5.2.4 Mixing of the filler with polymer	191
5.2.5 Composite characterisation	192
5.3 Results and discussion	193
5.3.1 Characterisation of the filler	193
5.3.1.1 XRD studies	193
5.3.1.2 Chemical characterisation	193
5.3.1.3 Particle size distribution analysis	194
5.3.1.4 FTIR studies	195
5.3.1.5 Diffuse reflectance spectral studies	198
5.3.1.6 Morphological analysis by SEM	199
5.3.1.7 Contact angle measurements	201
5.3.1.8 Viscosity studies	201
5.3.1.9 Thermal analysis	203
5.3.2 Properties of kaolinite-natural rubber composite	204
5.3.2.1 Curing characteristics	204
5.3.2.2 Physical property evaluation	204
5.3.2.2.1 Weight loss and equilibrium swelling measurements	204
5.3.2.2.2 Bulk density	205
5.3.2.3 Thermal stability measurements	206
5.3.2.4 Mechanical property evaluation	207
5.3.3 Mechanism involved in coupling	209
5.4 Conclusion	210

Summary and Conclusion	212
-------------------------------	-----

References	220
-------------------	-----

List of Publications	235
-----------------------------	-----

Chapter 1

Kaolin- An Overview on the Genesis and Applications

1. Introduction

Clay had been and continues to be one of the important industrial minerals and are widely utilized in many facets of our day to day life. Clay science during the last three decades, has been characterized by extensive research work in crystallography, mineralogy, geology, pedology and in applied sciences such as agriculture and ceramics. Clays are also the most versatile of all the minerals occurring in the earth's crust. It is a natural earthy material with plastic properties when moist, of very fine grain size ($< 2 \mu\text{m}$) and composed mainly of hydrous aluminium and magnesium silicates.

1.1 Phyllosilicates

The clay minerals have layered structure and are classified as phyllosilicates. They have in common the same type of structural unit (Berry *et al.*, 1985). The basic structural feature of all minerals in this subclass is the combination of layers of pseudohexagonal network of SiO_4 tetrahedra (silica tetrahedral layer) and layers of cations in octahedral coordination (octahedral layer). Two kinds of octahedral layers are known: gibbsite and brucite layers. The gibbsite layer has a dioctahedral arrangement; *i.e.* there are two cations of Al for each six OH ions, whereas a brucite layer is trioctahedral there being three cations (Mg, Fe) for each layer. Composite arrangement of each of the octahedral and tetrahedral layers result in a 1:1 structure as in kaolinite (a two-layer structure); or an octahedral layer sandwiched by two tetrahedral layers resulting in a 2:1 structure (a three-layer structure), as in montmorillonite and illite.

The phyllosilicate types are divided into groups on the basis of charge on the layers and on the nature of octahedral-tetrahedral layers (Bailey, 1980). The schematic representation of the common clay minerals is shown in Fig. 1.1

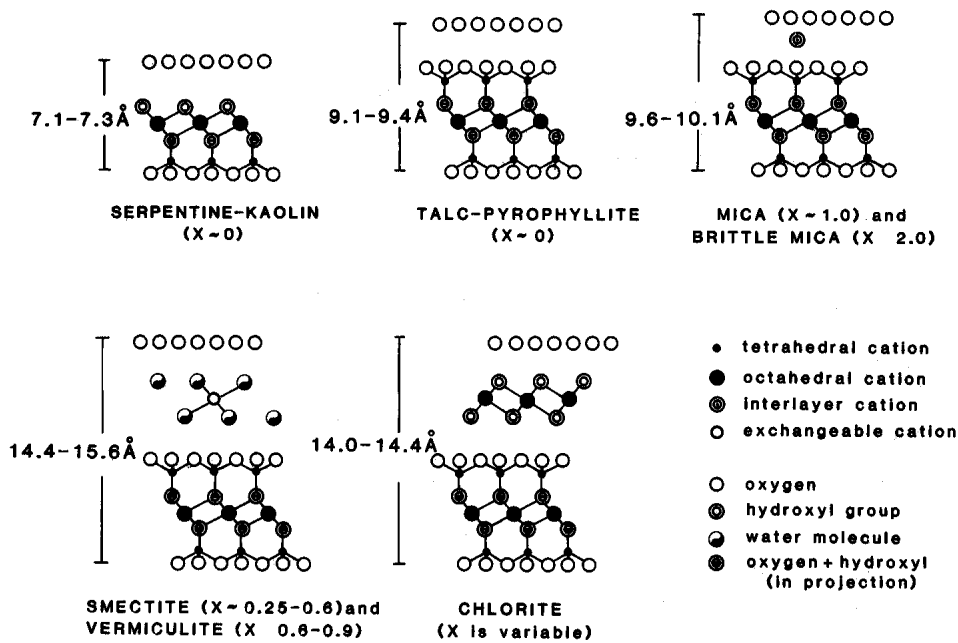


Fig.1.1. Structure of major clay mineral groups (010) view (after Bailey, 1980); X = layer charge per formula unit

The mineral kaolin is geochemically and industrially the most ubiquitous and abundant species of the phyllosilicate family.

1.2 Kaolin Minerals

Kaolin minerals are included under the 1:1 dioctahedral phyllosilicates of kaolin-serpentine family. The name kaolin is derived from the Chinese term “Kauling” meaning high ridge, the name of the hill near Jauchau Fu, China, from where this material was mined (Grim, 1968). The most widespread variety of mineral in kaolin group is kaolinite. Kaolinite is chemically $(\text{Si}_2\text{Al}_2\text{O}_5(\text{OH})_4)$, having an ideal composition of SiO_2 - 46.54%, Al_2O_3 - 39.5% and H_2O - 13.96%, and occurs mostly as flakes or plates ranging in shape from near hexagonal to ragged-edged anhedral. The unit cell dimensions are $a = 5.139$, $b = 8.932$, $c = 7.371$ Å, $\alpha = 91.6^\circ$, $\beta = 104.8^\circ$, $\gamma = 89.9^\circ$

In addition to kaolinite, the polytypes of kaolin mineral include halloysite, nacrite and dickite (Ross and Kerr, 1931; Ross and Kerr, 1934; Bailey, 1963). Halloysites are hydrous forms of kaolinite and are of two principal types: a less hydrous form with a

composition near to that of kaolinite, $\text{Al}_2\text{Si}_2\text{O}_5(\text{OH})_4$ (metahalloysite) and a more hydrous form with a composition, $\text{Al}_2\text{Si}_2\text{O}_5(\text{OH})_4 \cdot 2\text{H}_2\text{O}$ (halloysite). They usually occur as rolled cylindrical or quasi-spherical particles. Dickite (monoclinic, unit cell dimensions $a = 5.15$, $b = 8.94$, $c = 14.736 \text{ \AA}$, $\beta = 103.58^\circ$) and nacrite (monoclinic, unit cell dimensions: $a = 8.909$, $b = 5.146$, $c = 15.697 \text{ \AA}$, $\beta = 113.7^\circ$) have structure similar to that of kaolinite, but are of rare occurrence. These polymorphs of kaolinite result from the variability in the positioning of adjacent layers and in the occupancy of the octahedral sites within each layer (equivalent to layer rotation), which lead to different permissible stacking sequence of layers. Bailey (1969) has shown that there are 12 different trioctahedral 1:1 polytypes, and four enantiomorphs, with periodicities between one and six layers. This variation in the character of the polytypes results from the varying geochemical environment of formation or deposition.

The hydrous form of kaolinite *i.e.* halloysite is a metastable phase and are formed in a low-temperature geological environments (Giese, 1988). Nacrite (with layered stacking sequence shifted by $-1/3a$) is the rarest polymorph and is reported only from high temperature environments (Ross and Kerr, 1931; Firman, 1953 and Hanson *et al.*, 1981). The formation of kaolinite and dickite is not temperature-dependent, as both the polymorphs have been reported from high and low temperature environments (Grim, 1968).

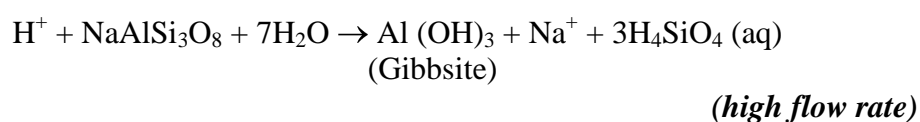
In addition to the above polytypes, kaolinite crystal itself shows structural disorder due to the isomorphous substitution resulting in the incorporation of Fe, Ti and Cr (Meads and Malden 1975; Rengaswamy, 1976; Mestdagh, 1980 and Maksimovic *et al.*, 1981) and also from the structural defects (Plancon and Tchoubar, 1977a,b). Extensive study on the structural order of kaolinite undertaken by Brindley *et al.* (1986), showed that the kaolinite from each locality has a characteristic kind of internal structural disorder which is fairly constant within the suite of the samples from a given locality. The incorporation of foreign ions into the structure of kaolinite results from the variability of chemical environment during its formation. The presence of different types of polymorphs and their structural variation in kaolin group of minerals are of high geological and industrial significance.

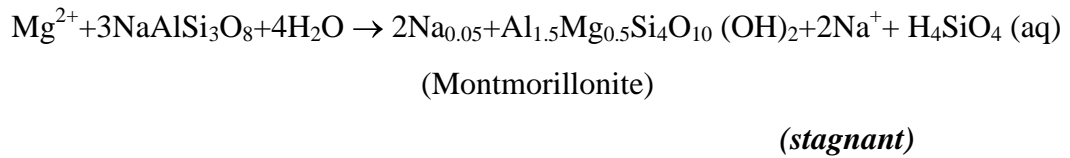
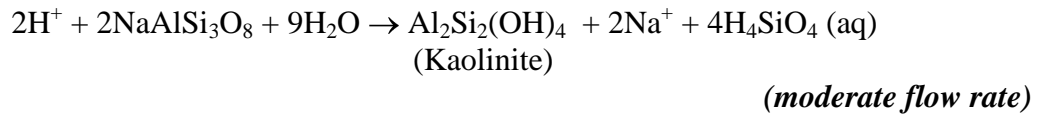
1.3 Genesis of kaolin

The mineral kaolin originates in a variety of diverse environments including: 1) crystallization in cavities within the rock, 2) replacement of other minerals 3) alteration of water-laid clastic silicate parent material, 4) *in situ* alteration of ‘primary’ silicate crystalline rock, 5) kaolinization at an unconformity 6) hydrothermal argillisation, 7) *in situ* alteration of clay parent rock, 8) sedimentary deposition of kaolin mineral, 9) diagenesis and 10) formation under complex geological conditions (Keller, 1977; 1978; 1985). The two natural processes capable of kaolinization of aluminosilicate rocks are weathering and hydrothermal alteration.

The formation of kaolinite and its stability depend upon the changes within its environment. Kaolin minerals tend to develop preferentially in the humid tropics. Under these climatic conditions, the fresh rocks and minerals in the presence of ample amount of water and favourable temperature, chemically modifies them to more stable phyllosilicate phases (Weaver, 1985). Processes leading to the modification/transformation or formation of clay during chemical weathering include hydrolysis, dissolution, hydration, oxidation, chelation and the activities of plants such as fungi, lichen and moss. An increase in rainfall, temperature and moisture enhances the amount of clay formed.

The influx of groundwater has a great influence on the type of clay mineral formed from a particular primary silicate. When a primary silicate hydrolyses in an environment of high activity of H^+ , alkali and alkaline earth metals are removed by replacement. Then the resultant product will be a 1:1 layered phyllosilicate. In contrast, if the activities of the metal ions remain relatively high, 2:1 layer clay minerals tend to form. Such an environment typically represents low intensity leaching, as in either semi-arid weathering or alternatively, in water logged environment, where the metal ions remain at high activity in solution but are not removed. For example, the reaction involved during the hydrolysis and subsequent leaching of feldspar (albite) under three different rates of groundwater flow is as below (Weaver, 1985):





In addition to the above explained factors, the topography of the region also plays a major role during clay formation. For the formation of thick kaolinite deposits, a large influx of water over long period of time is necessary. For that, the terrain should be smooth with quiet tectonic conditions, so that the chemical weathering can be more effective than erosion. Both high relief and high elevation tend to cause a decrease in clay formation.

During the earlier stages of weathering the composition of the parent material can determine the type of clay formation. In addition to the mineralogy of the parent rock, their texture, porosity, density, structure, fabric and the degree of consolidation also influence the clay formation. Kaolinite was reported to be formed from various precursor minerals. A brief description of the methods and pathways of kaolinization as reported by many workers are given below.

“Kaolinization” is the formation of kaolin by the weathering of alumino-silicate minerals or clay minerals (resilication of gibbsite to kaolinite, recrystallisation of halloysite/metahalloysite) (Hurst *et al.*, 1997). Aluminosilicates are common constituents of bedrock and overlying soil. With progressive weathering, primary silicates alter into secondary clay minerals displaying a sequential change of texture, chemistry and mineralogy. Diverse alteration sequences have been reported, depending on the local weathering environment. The most abundant aluminosilicates resulting in kaolinization are feldspars and mica group minerals.

1.3.1 Kaolinization of feldspar

Feldspars are the most abundant constituents of igneous and metamorphic rocks, the product of their weathering is the major source of kaolinite in the earth's surface.

The structure of this group of tectosilicate consists of a continuous three -dimensional network of SiO_4 and AlO_4 tetrahedra, with the positively charged sodium, potassium, calcium and barium situated in the interstices of the negatively charged network (Deer

et al., 1976). The members of this group of minerals include a three component system, the components being KAlSi_3O_8 , $\text{NaAlSi}_3\text{O}_8$ and $\text{CaAl}_2\text{Si}_2\text{O}_8$ and the individual members are:

Sanidine	KAlSi_3O_8	Monoclinic ($2V = 0$ to 12°)
Orthoclase	KAlSi_3O_8	Monoclinic ($2V = 69$ to 72°)
Microcline	KAlSi_3O_8	Triclinic
Plagioclase Series	$(\text{Na,Ca})\text{Al}(\text{Al,Si})\text{Si}_2\text{O}_8$	Triclinic
End members		

Albite	$\text{NaAlSi}_3\text{O}_8$	Triclinic
Anorthite	$\text{CaAl}_2\text{Si}_2\text{O}_8$	Triclinic

The alteration sequences of these minerals show various characters and structural morphologies. The work on feldspar alteration by several authors showed that the major clay mineral resulting from the above process is kaolinite.

In a study of residual kaolin derived from feldspathic rocks in Southern Appalachians, Sand (1956) noted that kaolinite was dominant in Georgia and Virginia samples, with halloysite (10 \AA) increasing in abundance towards the middle of the region (North Carolina). Here mica is found to be the intermediate phase during this transformation.

Studies of surface textures of weathered feldspar minerals by Parham (1969), Lundstrom (1970), Berner and Holdren (1977) indicated that the mode of attack during chemical weathering results in the formation of solution pits

The pathway for feldspar weathering was suggested by various workers. Feth *et al.* (1964) and Helgeson (1971) predicted a sequence of minerals from smectite to kaolinite and gibbsite as the alteration products of feldspar on thermodynamic ground by examination of phase diagram. Feth *et al.* (1964); Loughnan (1969) and Keller (1970) explained that the plagioclase could be replaced sequentially by smectite and kaolinite on the basis of phase diagrams. A similar view was also expressed by Helgeson (1971) for higher temperature alteration (200°C). Similarly, Garrels (1984) traced the pathway for the replacement of muscovite by illite, smectite and kaolinite on a $\log(a\text{K}^+/a\text{H}^+) \text{ Vs } \log(a\text{SiO}_2)$ diagram. Most stability diagrams constructed in the study of the alteration of K-feldspars predict the development of K-mica or illite as the intermediate phase between feldspar and kaolinite (Keller, 1970)

Tardy *et al.* (1973), in their studies on granite, found that plagioclase alters to montmorillonite and vermiculite in narrow fissures, whereas kaolinite forms in well-drained pores.

Clark (1973) in his studies on weathering of granite gneiss from eastern Alabama, Ashland and Opelika Plateaus, found that gibbsite is the major component (upto 30%) of upland, well drained soils. Here plagioclase altered directly to gibbsite and orthoclase to kaolinite. In the poorly drained regions where there is high silica water, both feldspars alter to kaolinite.

Meunier and Velde (1979) found that the secondary clay minerals were related to the precursor mineral composition rather than depth in the profile. Illite is formed at the boundaries between muscovite and orthoclase. Micas and orthoclase altered to vermiculite and beidellite. The fracture where water movement was more rapid contains kaolinite and Fe-oxide.

Suttner *et al.* (1976) concluded that the kaolinite was formed from feldspar under humid conditions, whereas smectite forms in semi-arid climates, the difference resulting from more complete flushing of K^+ under humid weathering.

Keller (1976) stated that the micropitting of feldspar, resulting presumably by incongruent dissolution, is a common process in pre- or early- stage of kaolinization of feldspar.

Berner and Holdren (1977) and Nixon (1979) during their studies on feldspar weathering showed that the access of a solution to the feldspar surface is probably controlled by defects, cleavages, twin planes and cracks. Dissolution appeared to proceed by preferential attack at these energetically favored sites.

Berner and Holdren (1977) and Banfield and Eggleton (1990) in their electron microscopic studies on weathered plagioclase and K-feldspar indicated that the dissolution was initially strongly controlled by the crystallography of the parent feldspar, resulting in the formation of sculpted surfaces, honeycombed by prismatic pits and cracks.

Eswaran and Bin (1978a,b) found that, in a soil developed on Malaysia granite, feldspars altered to kaolinite or gibbsite directly without any intermediate phase of amorphous gel. They also observed that in the same horizon one feldspar crystal may alter to kaolinite while another may alter to gibbsite, depending on the absence or presence of a void adjacent to the feldspar. According to them feldspar alters via

solution to kaolinite and gibbsite. But halloysite is formed through a noncrystalline stage.

Keller (1978a) on his study in weathering of Sparta granite in Central Georgia showed the alteration of feldspar to kaolin. During the early stages of weathering tufts of halloysite (elongate form) grow from silica and alumina released from dissolved feldspar. Eventually grass like mats of halloysite was found to develop on the parent substrate.

Nagasawa (1978) showed that halloysite occurred as a weathering product from feldspar in granite saprolite of Japan, whereas the topsoil on granite consists of kaolinite and 2:1 clay minerals.

Eggleton and Buseck (1980) had revealed a mechanism for the weathering of microcline in a humid, temperate climate. Dissolution of feldspars was found to begin at the boundary of twinned and untwinned domains and produces circular holes, which enlarge to form negative crystals. Amorphous, ring shaped structures develop, about 25 Å in diameter, within the larger holes. These rings, in turn, crystallize to an arcuate phase having a 10 Å basal spacing and then to crinkled sheets of illite or dehydrated montmorillonite.

Aagaard and Helgeson (1982) in their weathering studies of feldspar showed that the rate of hydrolysis of this silicate was controlled by the kinetics of reactions at activated sites at which Al-O and Si-O bonds were disrupted. Many authors (Frederickson, 1951; Garrels and Howard, 1959; Marshall, 1962; Wollast, 1967; Wollast and Chou, 1985) during their studies on the structure of the alteration products have confirmed that hydrogen was involved in the disruption of these bonds, replacing K, Na, or Ca in the feldspar.

Tsuzuki and Kawabe (1983) suggested that dissolution – reprecipitation mechanism might be responsible for the entire sequence of alteration of feldspar to kaolinite.

Anand *et al.* (1985) in the study of weathered feldspars from a saprolite zone (bauxite – laterite profile) developed from a granite (45 km southeast of Perth, Western Australia) showed that the feldspar altered to halloysite, kaolinite and gibbsite with no evidence of a noncrystalline precursor.

In a study of weathered feldspar from a humid, tropical environment from Southern Brazil (Tazaki and Fyfe, 1987), highly weathered K-feldspar has been found to be altered to halloysite (7 Å) and gibbsite. Here they found that the slightly

weathered feldspar has primitive clay, which showed structures like fibers, circle and cylinder with ill-defined structural order.

Banfield and Eggleton (1990) in their studies on weathering of Granodiorite (New South Wales, Australia) suggested that three separate mechanisms are responsible for the development of spherical halloysite, tubular halloysite and kaolinite. Spherical halloysite probably crystallized from a protocrystalline precursor. Tubular halloysite developed as a space filling material growing outward probably *via* solution from corroded feldspar surfaces and kaolinite formed in the early stages of weathering appeared to have crystallized epitactically onto existing phyllosilicates.

Kawano and Tomita (1996) in their study on weathering of K-feldspar from Yakushima island, Kagoshima Prefecture, Japan, showed the formation of amorphous Al(OH)₃ exhibiting two distinct habits: 1) spherical habit less than 1.0 μm in diameter and 2) curled fibrous or circular forms less than 0.02 μm in diameter. These amorphous Al(OH)₃ were found to be formed at the earliest weathering stages of K-feldspar as a metastable phase and transformed into a stable phase of gibbsite as reaction proceeds.

1.3.2 Kaolinization of Mica

The mica group constitutes an isomorphous group within the phyllosilicates. This group of minerals includes the following polytypes (Deer *et al.*, 1976).

Muscovite	$\text{KAl}_2(\text{AlSi}_3\text{O}_{10})(\text{OH})_2$ - (2M ₁)
Phlogopite	$\text{KMg}_3(\text{AlSi}_3\text{O}_{10})(\text{F},\text{OH})_2$ - (1M)
Biotite	$\text{K}(\text{Mg},\text{Fe})_3(\text{Al},\text{Fe})\text{Si}_3\text{O}_{10}(\text{OH},\text{F})_2$ - (1M)
Lepidolite	$\text{K}(\text{Li},\text{Al})_3(\text{Si},\text{Al})_4\text{O}_{10}(\text{OH},\text{F})_2$ - (1M and 2M ₁ and 3T)
Glauconite	$(\text{K},\text{Na})(\text{Fe},\text{Mg},\text{Al})_2(\text{Si},\text{Al})_4(\text{OH})_2$ - (1M, 2M and 3T)

Minerals of this group consist of two sheets of linked SiO₄ tetrahedral structure juxtaposed with the vertices of the tetrahedra pointing inwards. These vertices are cross-linked either with Al, as in muscovite, or with Mg as in phlogopite. Hydroxyl groups, which are present, complete the six coordination of Al or Mg. A firmly bound layer is thus produced with the bases of the silica tetrahedra on both of its outer sides. This layer has a negative charge because of the substitution of Al for Si in some of the tetrahedra. The negative charge is compensated by potassium, or less commonly by

sodium or calcium ions that are located between the layers and serve to link the layers together.

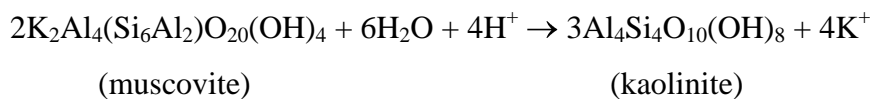
Among this group the most commonly reported phyllosilicates resulting in kaolinite formation during weathering are muscovite and biotite.

1.3.2.1 Formation of kaolinite from muscovite

Muscovite occurs in a wide range of regionally metamorphosed sediments and is found in rocks belonging to each of the zones of progressive regional metamorphism (Deer *et al.*, 1976). This 2:1 mineral is relatively resistant to weathering, and it is found that a relatively intense weathering is required before it is appreciably altered.

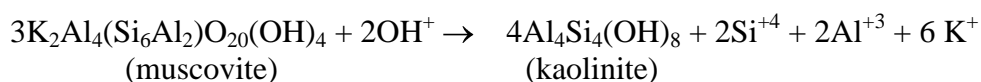
The experimental work by Rausell–Colom *et al.* (1965) indicated that the removal of K from muscovite during weathering is extremely difficult and strongly dependent on the K content of the solution.

Stoch and Sikora (1976) in their study on the Tertiary kaolinite weathering crusts formed on granites and gneisses of Lower Silesia, Poland showed the formation of kaolinite by mica weathering. In this area where K^+/H^+ ratio is low, biotite and muscovite and presumably secondary illite were found to pass directly to kaolinite. They suggested a transition of two muscovite layers to three kaolinite layers, involving the formation of interlayer gibbsite-like sheets and inversion of tetrahedral sheets. The reaction involved during the above mechanism is:



Craw *et al.* (1982) studied the alteration of micas to kaolinite in weathering and hydrothermal environments, using X-ray powder diffraction (XRD), electron microprobe analysis and optical microscopy. They showed that the alteration occurred through fine- scale intergrowths of micaceous phases and kaolinite.

Sharp *et al.* (1990) proposed a mechanism involving the transition of three 2:1 layer to four 1:1 layer for the phlogopite-to-serpentine transition. Similar method of transformation was applied to explain kaolinite formation from muscovite. The reaction involved is:



Banfield and Eggleton (1990) described epitaxial replacement of pre-existing illite and smectite to kaolinite that formed by weathering of muscovite.

Singh and Gilkes (1991) indicated that the kaolinite crystals developed from muscovite faithfully preserved the crystallographic orientation of the parent mica. This alteration involved either epitaxial growth of kaolinite on the surface of the residual layer of muscovite or by a topotactic transformation of muscovite to kaolinite involving the preservation of some components of the octahedral sheet of muscovite.

Robertson and Eggleton (1991) explained that the transition of muscovite to kaolinite minimally involves the removal of interlayer alkali ions and octahedral Mg and Fe, replacement of tetrahedral Si by Al, reorientation of the Si tetrahedra in one of two sheets, formation of one new dioctahedral sheet, and gain of water and / or protons (H^+) to form OH groups coordinating Al. According to them a topotactic conversion of a 10 Å muscovite layer to a 7 Å kaolinite layer occurs by replacement of K by H followed by stripping of Si tetrahedral sheet from one side of a 10 Å layer.

Pevear and Nagy (1993) observed that kaolinite nucleates on the basal surface of muscovite and biotite in a diagenetic environment and also simulated kaolinite overgrowth on muscovite in the laboratory. They concluded that the muscovite and illite act as nucleation sites for kaolinite precipitation.

Jeong (1998b), during a study of the kaolin formation by deep residual weathering of anorthosite in the Sancheong kaolin deposits, Korea reported that biotite, sericite, clinochlore and muscovite were altered into vermicular kaolinite, typically displaying fanning-out textures involving an enormous increase in volume.

1.3.2.2 Formation of kaolinite from biotite

The weathering of biotite differ from that of muscovite due to the variation in the chemical composition of the octahedral and tetrahedral sheets. Kaolinization of biotite is accompanied by a change of chemical composition by exchange of some of its components such as H_2O , K^+ , Mg^+ , Si^{4+} , Al^{3+} , Fe^{2+} , Fe^{3+} with their surroundings.

Wilson (1966) observed that a variety of minerals were found to form as end products of biotite under different weathering conditions. He noted the development of oriented alteration products *i.e.* epitaxial crystallization of gibbsite and kaolinite onto biotite. He also reported that the crystallization of goethite crystals with Z parallel to biotite Y, presumably by nucleation of the iron-oxygen octahedral chains

of goethite parallel to octahedral strips in biotite during the alteration of this phyllosilicates.

Analysis of heavily altered biotite from natural weathering environments (Gilkes and Suddhiprakarn, 1979) exhibited nearly complete oxidation of Fe in the mineral structure during the process of kaolinization.

Muller and Bocquier (1987) found that the kaolinite replacing micas in the tropics are Fe- kaolinite and with increasing weathering (upward) it become more Fe- rich and less well crystallized.

Ahn and Peacor (1987) studied hydrothermal kaolinization of biotite in mica schist and proposed that the alteration mechanism involved dissolution of biotite and crystallization of kaolinite along linear boundaries in biotite layers. They also emphasised the two modes of occurrences of kaolinite from biotite: 1) as packet of layers interstratified within biotite, having thickness of 50 to 300 Å and 2) two layer units irregularly interlayered within biotite. Termination of two- layer tetrahedral-octahedral (T-O) units of kaolinite by single tetrahedral-octahedral-tetrahedral (T- O-T) unit of biotite layers was observed, implying a reaction of one biotite to two kaolinite layers.

Banfield and Eggleton (1988) showed the evidence of a two – stage processes during biotite alteration. An initial stage, dominated by biotite vermiculite reaction and a later stage dominated by the production of kaolinite and goethite. The formation of kaolinite is confined to the surfaces of biotite, resulting from the epitactic crystallisation onto existing tetrahedral sheet. Here, the growth of kaolinite and goethite crystal is controlled by the orientation of biotite. Goethite generally develops with its Y axis parallel to enclosing sheets, whereas kaolinite forms layer which parallel biotite layers

Acker and Bricker (1992) showed that at pH 4 and above the dissolution mechanism of biotite involved the loss of octahedral cations, leading to the formation of a vermiculite type product. At pH 3, biotite dissolves resulting in the destruction of the tetrahedral and octahedral layers.

Samatoin and Checkin (1993) have interestingly observed the spiral growth of kaolinite on mica and chlorite substrate in weathered granite.

1.3.3 Formation of kaolinite from halloysite

Thermodynamic studies by Parham (1969) and Huang (1974) predicted that the halloysites which are polytypes of kaolinite would convert into kaolinite with ageing. This sequence of transformation is also accepted by most investigators (Keller, 1977; Nagasawa, 1978; Tsuzuki and Kawabe, 1983; Churchman and Gilkes, 1989; Steefel and Van Cappellen, 1990).

Robie and Waldbaum (1968); Robie *et al.* (1978) and Anovitz *et al.* (1991) showed that the conversion of halloysite to kaolinite is consistent with thermodynamic considerations. The Gibbs free energy of formation of halloysite is about 4 k cal/mol higher than that of kaolinite.

Banfield (1985), from SEM observations suggested that the platy kaolinite could be formed by the coalescence of halloysite tubes, by a mechanism of simultaneous solution and precipitation.

Thomas *et al.* (1987) in their studies on the weathered crust of Precambrian rock from South Kerala, Kundara showed that halloysite undergoes transformation into well crystalline kaolinites.

Churchman and Gilkes (1989) suggested that halloysite tubes could be altered to kaolinite *via* dehydrated halloysite in a solid state by prolonged dehydration.

Hurst and Pickering (1997) showed that the formation of kaolinite from halloysite involves two steps. During the first stage, irreversible dehydration changes the halloysite habit by shifting the components of the structure, thereby producing metahalloysite. During the second stage, recrystallization of metahalloysite destroys its habit while kaolinite crystallites nucleate and grow. The end product is striking “saw toothed” elongated platelets of kaolinite.

Jeong (1998) suggested the mechanism of kaolinization from halloysites on the basis of the observed micro textures. He proposed a solid – state transformation of the interconnected halloysite grains into large kaolinite plates by coalescence.

1.3.4 Conversion of gibbsite to kaolinite

This aluminum oxide ($\text{Al}(\text{OH})_3$) mineral is more frequent in the intense chemical weathering environment and is mostly associated with kaolinites. However reports on kaolinization of gibbsite are limited.

The karst and lateritic type bauxites were reported to be altered to kaolinite (Goldman and Tracey, 1964; Keller, 1962; Keller and Clarke, 1984; Valenton, 1972; Dangic', 1988) by a relatively simple process of metasomatic resilicification (Keller, 1962; Keller and Clarke, 1984; Valenton, 1972).

Garrels and Christ (1965) considered that both kaolinite and gibbsite form in bauxitic soils where the equilibrium concentration of Si in soil water is between 1.5 and 3 ppm which is near the value of ~ 0.5 ppm predicted for equilibrium between gibbsite and kaolinite.

Dangic' (1985) showed that in the Vlasenica region of Yugoslavia, kaolinization of bauxite had taken place in a complex manner, involving both Si- metasomatism and Al-remobilization. He found that the original bauxite altered progressively to various assemblages of syngenetic or epigenetic boehmite, diaspore and kaolinite, thereby illustrating the complexity of the process.

1.3.5 Formation of kaolinite from smectite

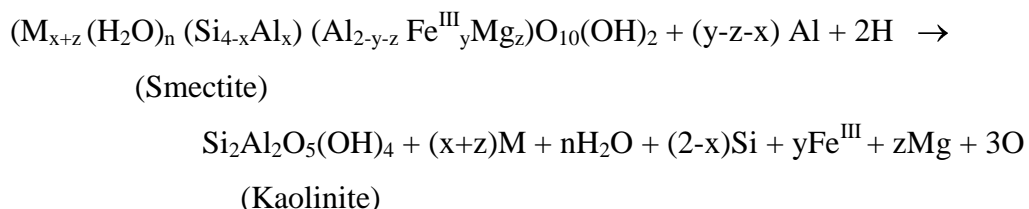
Smectites are 2:1 phyllosilicates with structure similar to muscovite. This clay mineral is reported to be interstratified with kaolinite in a diagenetic environment.

Over large area of Central Florida (Altschuler *et al.*, 1963), Southern Florida, Coastal Alabama and Mississippi (Weaver, 1985), montmorillonite parent material has been altered to kaolinite, often *via* a mixed layer Kaolinite/Smectite (K-S) stage.

Srodon (1980) suggested that kaolinite-smectite (K-S) mixed layers form from smectite by the dissolution of some layers and subsequent crystallization of kaolinite in the interlayer of remaining smectite.

Hughes *et al.* (1993) discussed the mechanism of formation of kaolinite-smectite (K-S) mixed layers by solid-state transformation of pre-existing smectite layers by "stripping" away the tetrahedral sheet.

Amouric and Olives (1998) showed that two types of mechanisms are responsible for the formation of kaolinite from smectite: 1) The transformation of 1 smectite layer into 1 kaolinite layer denoted S → K by stripping of a tetrahedral sheet and the adjacent interlayer region as per the equation:



$M = \text{Na, K, Mg}_{0.5}, \text{Ca}_{0.05}, y+z-x$ may be positive or negative

and 2) The intercalation of kaolinite layer into smectite layer. In this mechanism, all the atoms necessary to create the new kaolinite layer must be provided, from the dissolution of the surrounding smectite.

1.3.6 Laboratory synthesis of kaolinite

Lot of studies have been undertaken on the synthesis of kaolinite, because of its abundance in geological environments and also because of its use in many industrial fields.

Hemley (1959) studied phase equilibrium in the system of $\text{K}_2\text{O}-\text{Al}_2\text{O}_3-\text{SiO}_2-\text{H}_2\text{O}$ and showed alteration of K- feldspar to mica or kaolinite in aqueous solution of various K^+/H^+ activity at 200 to 500°C.

DeKimpe *et al.* (1961; 1964) examined the synthesis of aluminosilicates at low temperatures and under normal pressure with the gels and crystalline phases of various Si/Al ratios. Moreover, they found that the condition of temperature, pH and cationic and anionic impurities are critical for the formation of kaolin mineral.

Helgeson (1971) plotted experimental data activity diagram from the system of $\text{K}_2\text{O}-\text{Al}_2\text{O}_3-\text{SiO}_2-\text{HCl}-\text{H}_2\text{O}-\text{CO}_2$ and suggested that boehmite, kaolinite and illite precipitated as reaction products under equilibrium conditions at 100°, 150° and 200°C.

Eberl and Hower (1975) synthesised kaolinite hydrothermally using amorphous gels with various Si/Al ratios.

DeVijnck (1976) reported the hydrothermal formation of kaolinite from aluminosilicate sols containing alkaline ions such as Li^+ or K^+ . He determined the concentration ranges of Li/K: Al and Si for kaolinite formation.

Tomura *et al.* (1983) synthesized spherical kaolinite for the first time from noncrystalline aluminosilicate material in hydrothermal experiments conducted between 150 and 250°C under autogeneous vapour pressure. Osaka and Kato (1984) also crystallized kaolinite from a mixture of silica and alumina in a strongly acidic medium.

Regarding the mechanism of growth of the kaolinite minerals, Tomura *et al.* (1985) suggested that the spherical particles precipitate from solution with a high

degree of supersaturation at the beginning of the synthesis process, whereas platy kaolinite grows at relatively low degree of supersaturation.

Miyawaki *et al.* (1991) hydrothermally synthesised kaolinite in the $\text{Al}_2\text{O}_3\text{-SiO}_2\text{-H}_2\text{O}$ system to study inhibitory effects of additional ions on the formation of kaolinite. Here the syntheses were carried out with amorphous starting materials and salt solutions of various concentrations in teflon pressure vessels at 220 °C for 5 days. The studies showed that divalent cations Mg^{2+} and Ca^{2+} interfere with the crystallization of kaolinite more than do univalent Li^+ , Na^+ or K^+ cations. Addition of Fe^{3+} or excess Al^{3+} ions interfered mostly with the ions of the same valence, the larger the cation, the greater the inhibition in the formation of kaolinite.

Huertas *et al.* (1993) suggested that the formation of kaolinite from aluminosilicate gels as a two stage process. The first stage corresponds to the formation of spherical domains whereas the second to crystals having platy or lath morphology.

Satokawa *et al.* (1994) showed that the process of kaolinization and properties of synthetic kaolinite were influenced by factors such as structure and composition of starting materials, pH as well as the hydrothermal conditions.

Satakawa *et al.* (1996) in their study on the hydrothermal synthesis of kaolinite discussed the relationship of the rate of kaolinization with the pH condition of the reaction system. It was found that the use of appropriate acidic conditions promoted the dissolution of the starting materials and the crystal growth of kaolinite.

The study on the artificial preparation of clays can to some extent simulate the formation of clays in nature.

As stated earlier the kaolinization in a particular region is found to be dependent upon its climate, geomorphology, and geological factors in the area and their mutual relationships. In this context a brief description of the geological settings of the clay bearing area is of extreme significance.

1.4 Geology and Geomorphology of Kerala

1.4.1 Geology

Kerala state lies between north latitude $8^\circ 17' 30''$ and $12^\circ 27' 40''$ and east longitudes $74^\circ 51' 57''$ and $77^\circ 24' 47''$, covers an area of 38,863 km^2 . Geologically

the major part of Kerala is occupied by Pre-Cambrian crystalline rocks. These crystalline rocks are fringed on the west by sedimentary formations, belonging to Tertiary and Quaternary period. The associations of various rock types, their stratigraphy along with their mineralogy are briefly discussed.

1.4.1.1 Precambrian rock

Geologically, Kerala forms part of the Precambrian shield. The major rock types include granulites and associated gneisses belonging to Precambrian age. Late Precambrian – early Palaeozoic granites and associated pegmatites and Mesozoic-Cenozoic dykes intrude these rocks. The Precambrian rocks of North Kerala varies in composition when compared to those of South Kerala.

1.4.1.1.1 Precambrian rocks of North Kerala

The most widespread rocks in northern and central Kerala are charnockite (pyroxene bearing granulites) and associated gneisses.

Charnockite has been defined as hypersthene granite, which is composed of hypersthene, microcline, quartz and associated iron minerals. They are characterised by the granulitic texture and the invariable presence of rhombic pyroxenes. Holland (1900) defined charnockite as an orthopyroxene – quartzo-feldspathic rock with or without garnet, characterised by a greenish blue feldspar and greyish blue quartz. The mineralogical assemblages in these group of rocks in Kerala consist of 1) quartz-plagioclase-orthopyroxene, 2) quartz- plagioclase-clinopyroxene, 3) quartz–plagioclase-orthopyroxene– clinopyroxene-hornblende 4) quartz-plagioclase-orthopyroxene- clinopyroxene- biotite 5) quartz-plagioclase- clinopyroxene-hornblende 6) quartz-plagioclase-clinopyroxene-biotite. Magnetite, ilmenite, apatite and zircon are the accessory minerals.

Hornblende–biotite gneiss forms a major rock type in segments north of Achankoil shear zone, and covers some region in northern and central Kerala.

Wayanad and Vengad Groups are the greenstone sequence in Kerala, which occurs as a southward extension of Sargur Group in Karnataka. The oldest rock associated with Wayanad Group is represented by bands of quartz- mica schists with kyanite, quartz-sericite schists, quartz magnetites, quartzites, meta-ultramafite and metapyroxenites.

The Vengad Formation consists of schists and quartz with conglomerates. This apparently overlies charnockites, gneisses and Wayanad schist.

1.4.1.1.2 Precambrian rocks of South Kerala

South Kerala (south of Achankovil shear zone) comprises an assemblage of migmatized metasedimentary and metaigneous rocks *i.e.* khondalite–charnockite assemblages. Khondalite Group has been ascribed to the rock assemblage containing garnet-sillimanite-graphite gneiss, garnet- biotite gneiss and garnetiferous –quartzo feldspathic gneiss.

Patches of charnockites are associated with this khondalite group of rocks. Massive charnockites with granoblastic texture are also noticed outcropping in some regions. Their mineralogical association includes hypersthene, garnet, plagioclase, microcline, microperthite and quartz. Ilmenite, rutile, apatite and zircon occur in minor quantities. A few patches of calc –granulites also occur.

Garnet- sillimanite gneiss chiefly consists of plagioclase, K-feldspar, quartz, garnet and sillimanite. Garnet biotite gneiss occurs almost throughout the khondalite terrain of south Kerala as concordant bands within the khondalite. Major minerals of this unit are plagioclase, quartz, biotite, K-feldspar and garnet. Sphene, ilmenite, rutile, zircon and monazite are the accessory minerals.

Cordierite Gneiss: These rock types occur along Achankovil – Konni area (Sinha-Roy *et al.*, 1984). They occur as discontinuous bands. The cordierite bearing gneiss has the following mineral assemblages: quartz- perthite- oligoclase, cordierite, biotite, garnet, sillimanite and ilmenite. Calc granulites also occur as patches and are composed of quartz, clinopyroxene, sphene, plagioclase, calcite, scapolite, grossular-andradite garnet and wollastonite.

1.4.1.2 Tertiary Formation

Most of the major residual and sedimentary deposits including kaolinite deposits are associated with the Tertiary sedimentary formations. This great sedimentary deposit is spread over a major part of the western margin of Kerala. The sequence consists of both marine and non- marine rocks in the on-land part (King, 1882; Foote, 1883), and are distributed in two major basins of deposition 1) between Trivandrum and Ponnani in the south and central Kerala with a maximum width of 16 km between Quilon and

Kundara and 2) between Cannanore and Kasargode in north Kerala with a maximum width of 10 km at Cheruvattur (Paulose and Narayanaswami, 1968).

Paulose and Narayanaswami (1968) have suggested the following general stratigraphic succession of the sedimentary rocks as given in table 1.1

Table 1.1 Stratigraphic succession of sequences of rocks in Kerala

	Soils and alluvium
	Beach sand deposit
	Lime shell deposits of backwaters
Recent to sub-recent	Old and red teri sands of subrecent-marine and lacustrine formations
	Peat beds with semi-carbonised woods
	Calcareous clays with shell etc
	Laterite
	-----Unconformity-----
	Current-bedded friable variegated sandstone interbedded with plastic clay and variegated clays
Warkallai Formation	Carbonaceous and alum clays with (Mio-Pliocene) lignite seams.
	Gravel and pebble beds. Base marked by gibbsitic sedimentary clay.
Quilon Formation (Middle Miocene)	Fossiliferous shell limestone alternating with thick beds of sandy clays, calcareous clays and sandstones
	Base unknown
	-----Unconformity-----
Archean	Crystalline rocks

In addition to the above sequences, Raghava Rao (1976) indicated that the “Vaikom beds” underlie the above thick sedimentary layers.

1.4.1.2.1 Vaikom Formation: This lowest sedimentary sequence consists of gravel, coarse to very coarse sand with greyish and carbonaceous clay with thin seams of lignite. This formation is exposed in the laterite quarries of Vaikom and has a thickness of 100 m and overlies the crystalline rock.

1.4.1.2.2 Quilon Formation: The sequence of deposition of this formation in the type area, Padappakara includes sandy clay II, carbonaceous shale, carbonaceous clay, sandy clay I, limestone, laterite and detrital laterite. Rasheed and Ramachandran (1978) suggested Miocene age for these beds, based on the study by foraminiferal biostratigraphy of this sequence. The overall faunal assemblages also indicated that these formations were deposited during the Miocene age.

1.4.1.2.3 Warkallai Formation: Warkallai Formation unconformably overlies the Quilon bed. King (1882) gave a succession of lignite bed, alum clay, sand, sandy clay and laterites with an overall thickness of 60 m for the type section at Warkallai. This formation has been traced along the entire coast stretching from near Cape Comorin in the south to Ernakulam in the north bordering the coastal tract (Prabhakara Rao, 1968), covering an area of 2000 km². Exposure of these sediments occurs in Kundara, Thamarakulam and Puliur in the south, Cheruvatur, Pazhayangadi, Ramapuram, Nileswaram and Kalnad in the north. Krishnan (1982) gave an age of Late Miocene for these sediments. The carbonaceous and peat beds have well preserved palynoflora, with characteristic features of mangrove swamp and coastal vegetation, indicative of warm, humid climate with heavy rainfall.

1.4.1.3 Quaternary Formation

Quaternary Formation unconformably overlies the Cenozoic sediments and are found in the entire stretch of sedimentary basin. This formation consists of sediments both of fluvial and marine origin.

1.4.2 Structural trends

The Kerala region can be divided into two major tectonic provinces, namely Precambrian tectonic province and the Tertiary tectonic province.

The Precambrian tectonic province constitutes, the high ranges of the Western Ghats, the foothills and parts of midlands. This area forms the western limb of a

NNW plunging synclinorium, the axis of which is traceable from Tuticorin in the south to Dharwar and Belgaum in the north (Rao, 1974). The regional strike of foliation of Precambrian rocks is NW- SE to WNW-ESE with a steep dip towards SW.

The Tertiary tectonic province includes a narrow belt between coastal and midland region extending from Thiruvananthapuram in the south to Kasargode in the north. The Tertiary rocks are almost horizontal to subhorizontal.

A number of lineaments have been identified within Kerala region (Varadharajan and Balakrishnan, 1980; Nair, 1990) and they can be broadly grouped into 1) NW- SE to WNW- ESE 2) NNW- SSE to N-S and 3) ENE- WNW trending lineaments.

1.4.3 Geomorphology

1.4.3.1 Topography: The area is divisible into five physiographic zones (resource atlas of Kerala, 1984). They are – the mountain peaks above 1800 m, the highland at altitudes of 600–1800 m (covering 20.35% of Kerala), the midlands at altitudes of 300- 600 m (8.44%), the low land at 10- 300 m (54.17%) and coastal plains and lagoons below 10 m (16.40%).

1.4.3.2 Drainage: The state Kerala is drained by 44 rivers of which 3 (Kabani, Bhavani and Pambar) are east flowing. The general drainage pattern of these rivers is dendritic although in places trellis, sub-parallel and radial patterns are also noticeable. Most of the river courses are straight indicating structural control and their course coincides with the prominent lineament directions (NW-SE & NE-SW).

Another typical physiographic feature of Kerala coast is the chain of water bodies-backwater - estuaries and lagoons - locally known as kayals. The Kerala Public Works Department (Water Resources of Kerala, 1974) has identified 27 estuaries and 7 lagoons in Kerala.

1.4.3.3 Climate: The territory of Kerala falls within the realm of tropical climate. The variations in the relief feature and proximity to the sea influence the climatic parameters, resulting in sub-tropical climate in certain areas of the eastern parts of the state. Kerala experiences two monsoons, namely the southwest (June to September) and the northeast (October to December), known locally as “Edavapathi” and “Thulavarsham” respectively. The lowland and midland regions experience mean

annual temperature in the range of 25.5 to 27.5°C. Higher temperatures (> 27.5°C) are experienced in a belt in midland parts of central Kerala. Annual mean humidity varies from 79 to 84% in the morning to 73 to 77% in the evening along the coastal areas. During the period from January to March, afternoon humidity reduces to 60 to 63% with variation from 35% in the interior to 71% in the coastal area (Kerala State Gazetteers, Vol 1, 1986). This extensive development of humid tropical climate results in the intense chemical weathering of the country rock leading to lateritization. Laterites are weathered material rich in secondary oxides of iron, aluminium or both and are nearly devoid of bases and primary silicates. Two lateritisation cycles: pre - Tertiary and post -Tertiary are reported from various parts of Kerala (Menon, 1966; Gopalakrishnan and Nair, 1976; Soman and Slukin (1987); Rajendran and Narayanaswamy, 1987).

1.4.4 Clay formation in relation with geology and geomorphology

Thick deposits of kaolin occur in different parts of the state. The clay deposits of Kerala are either primary (*in situ*) or secondary (sedimentary). Primary clays are formed as a result of chemical weathering associated with lateritisation or kaolinization of the basement Precambrian crystalline rock and the secondary clays are formed as a result of transportation and simultaneous deposition of the sediments in a basin during the Tertiary period.

In Kerala, kaolinite deposits are found to spread over major parts of the coastal region (Fig. 1.2). Major clay occurrences are mainly confined to areas around Thonnakkal in Thiruvananthapuram district, Kundara in Kollam district, Payangadi in Kannur district and Nileswaram in Kasargode district. Minor occurrences are also reported from other parts of the state (Fig.1.2).

Since the major portion of Kerala region consists of Precambrian rocks enriched in feldspar and micaceous minerals, kaolinization of the country rock is noticed in almost all parts of the state. These clays were subjected to intense lateritization *i.e.* advanced stage of kaolinization and hence the kaolin suffers quality degradation due to the enrichment of iron oxide and oxyhydroxides.

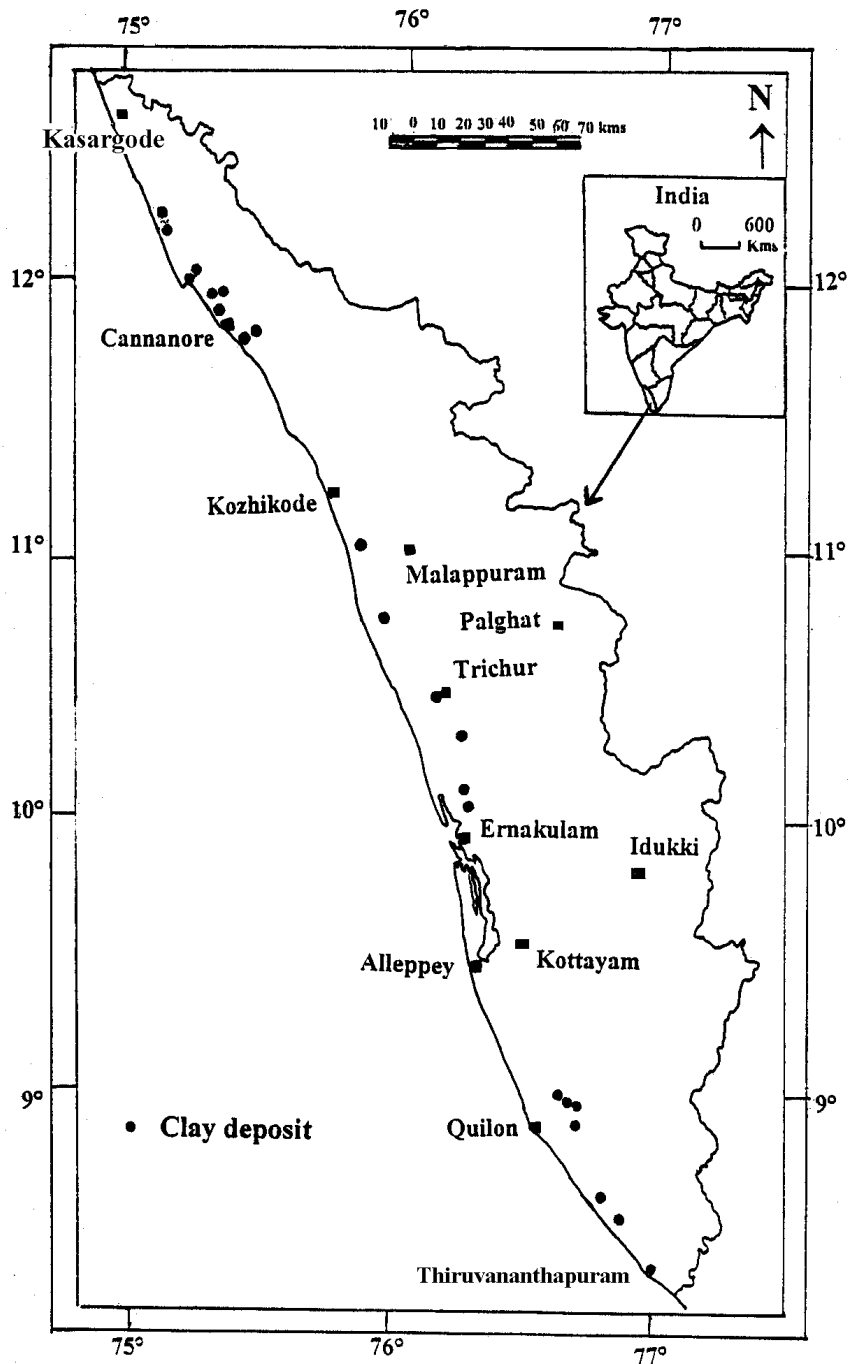


Fig.1.2. Location map of clay mineral deposits of Kerala (synthesized from Geological Survey of India –Resource Map)

The geological and geomorphological factors thus help to explain the mineralogical, morphological and geochemical evidences obtained during the present investigation.

1.5 Kaolin resources

1.5.1 World resource

The world kaolin production as reported by the USGS for the year 1999 is approximately 40 million tons (Dickson, 2000). The major producers and exporters of kaolin are the USA, UK, Brazil, Germany, South Korea and Czechoslovakian Republic. China, India, Uzbekistan and Colombia are also important producers, but mainly serve for internal market. The world kaolin production estimated (in lakh tons) in 1999 is as follows: United States – 97.1; North America – 100.5; Brazil (beneficiated) – 13; Colombia – 80; South & Central America – 95; Germany – 18, United Kingdom – 23; European Union – 52.8; Czech. Republic – 29; Turkey – 5; Ukraine – 8.5; India – 5.6, Uzbekistan – 5.5; Australia – 2.2; Iran – 5; Mexico – 3.4 and Spain – 3.

1.5.2 Indian Resource

India possesses extensive deposits of china clay distributed throughout the country. The total recoverable reserves of kaolin in India are placed at 1042 million tons, which is about 56% of the total reserves. Among these 695 million tons (67%) of the total reserve falls under possible category, 301 million tons (29%) under probable category and 46 million tons (4%) under proven category. The major recoverable reserves of china clay in different parts of the country in percentage are West Bengal-24.08%, Rajasthan-19.67 %, Orissa-15.61%, Kerala-12.18%, Andhra Pradesh -5.09 %, Meghalaya-4.99%, Bihar-4.41 %, Tamil Nadu-4.32%, Gujarat -2.97% and others - 7.13%.

Clay deposits of Kerala are possibly the best in the country. It has remained the largest producer of processed china clay. Of the total reserves of 127 million tons in Kerala, about 5% fall under proven category, 2% in probable category and 93% under possible category. The production of china clay in Kerala comes from four districts namely Cannanore (Kannur), Kasargode, Quilon (Kollam) and Thiruvananthapuram. Thiruvananthapuram remained the leading producer in the state and produced about 74% at 69,304 tons of total state's production in 1996-97 (Indian Bureau of Mines, 2000). Other districts in the decreasing order of productions are Quilon 11%,

Cannanore 8% and Kasargode 7%. In addition to this about 8% of reserve, has been established in Alleppey district.

The estimated consumption of crude and processed kaolin in 1996- 97 all over India and the present demand of the same are shown in table 1.2.

Table 1.2. Internal demand of crude and processed china clay

Industry	Estimated consumption (1996-97) (in tons)	Present demand (2001- '02) (in tons)
I. Crude: (total)	199, 700	236, 600
Cement	150, 400	187, 300
Insecticide	26, 100	26, 100
Refractory	23, 200	23, 200
II. Processed:	219, 850	352, 600
(total)	149, 100	235, 400
Ceramics	15, 500	20, 000
Paper	27, 600	58, 000
Plastics	9, 000	12, 300
Paint	2, 100	2, 900
Rubber	5, 250	9, 500
Fiber glass	11, 300	15, 500
*Others		

* include chemicals, abrasives, textiles, cosmetics, pharmaceuticals etc

1.6 Applications and specifications of kaolin

Kaolin is one of the most important of our industrial minerals. Millions of tons are utilized annually in a large variety of applications (Murray and Keller, 1993). The varied and diverse use of kaolin results from its properties of white colour, softness, small particle size and chemical inertness. The desired properties of kaolin vary greatly depending on the applications.

1.6.1 As a paper coating and filler material

Kaolin when used as a coating pigment an application which requires some of the highest demand in terms of quality, endows the paper with a topographically smooth, bright surface possessing good ink receptive properties and also good opacity. In addition, kaolin possesses rheological properties suitable for modern high-speed paper coating.

Kaolin's principal function as filler is to act as a substitute for the expensive pulpweb, thereby reducing costs. Kaolin also enjoys a principal advantage over its rival calcium carbonate by way of its chemical inertness to other paper making materials, enhances opacity, brightness and printability

Typical specifications of coating and filler grades are shown in table 1.3. Low abrasiveness is important for a filler grade product and the favourable rheological properties along with low particle size and high brightness being the requirements for good coating grade material.

Table 1.3: Typical properties of filling and coating kaolin

Property	Coating clay	Filler clay
% Brightness (ISO)*	81.5 – 90.5	76 – 82
% Yellowness	4 – 6.5	5.7 – 8
Particle size %		
< 2 µm	75 – 95	25 – 60
> 10 µm	0 – 6	6 – 25
> 53 µm	0.02 max	0.05 max
Viscosity concentration (% solids at 5 poise at 22 °C)	64.2 – 74.5	61.2 – 71.5

*International Standards Organization (ISO)

1.6.2 Ceramics and Refractories

The important non-paper end-uses of kaolin are in the ceramics and refractory industries. Clay is the essential raw material in ceramic products, comprising 25-100% of the ceramic body. Kaolin makes up an average of 25% of the earthenware,

60% of porcelain, 20-30% of vitreous china sanitary ware, and 20% of electrical porcelain and wall tiles. Refractory uses include linings of open hearth and blast furnaces in steel industry and other types of high temperature furnaces.

Important properties essential for kaolin in the ceramics and refractories are green strength, dry strength, drying and firing shrinkage and fired color. Shrinkage is also very important to the ceramics manufacturers. The general composition and properties of kaolin used in ceramics are shown in table 1.4.

Table 1.4 Composition and properties of ceramic grade kaolins

Specifications	a*	b*	c*
SiO ₂ (%)	47	48	48
Al ₂ O ₃ (%)	38	37	37
Fe ₂ O ₃ (%)	0.39	0.70	1.00
TiO ₂ (%)	0.03	0.02	0.05
CaO (%)	0.10	0.06	0.07
MgO (%)	0.22	0.30	0.30
Na ₂ O (%)	0.15	0.10	0.10
K ₂ O (%)	0.80	1.85	2.00
LOI (%)	13.0	12.2	12.1
% Kaolinite	93	81	83
% Mica	4	15	13
% Feldspar	1	1	2
% Other minerals	2	3	2
% of particle:			
< 2 μm	85	57	40
> 10 μm	1	10	20
Modulus of rupture (kgf/cm ²) ¹	55.0	25.7	11.0
Casting conc.(weight % solids)	58.0	62.5	64.7
Deflocculent (5 poise) ²	1.5	0.65	0.55
Casting rate (mm ² /min)	0.35	0.80	1.5

% Brightness (1180 °C) ³	95	86	82
% Shrinkage (1180 °C)	10	9	7.5

* a) ECC Super standard porcelain; high quality tableware, porcelain and bone china *b) ECC Grolleg; Earthenware, tablewares,* c) ECC Reinblend; Sanitaryware

1) Dried at 110°C, 2) Amount of sodium silicate required for 5 poise slips 3) At 457 nm wavelength (Source M/S “English china clays” technical literature)

1.6.3 Plastics, Adhesives and Fibreglasses

The use of kaolin in plastics, adhesives and fiberglass industries is as filler to substitute a portion of the resins, which is one of the most expensive materials in the manufacture of these products. The use of kaolin in these products can be separated into uses in which kaolin is important only in lowering raw material costs, and those in which the use of kaolin gives secondary benefits based on the physical properties. The perfect filler for these industries should have a number of characteristics including low cost, good availability, low oil absorption, small and uniform particle size, good dispersion, low density, good chemical resistance, light color and low free-moisture levels. The use of kaolin in fiberglass is facilitated by the unusual characteristic due to its chemically stable nature even at higher temperatures.

1.6.4 Rubber

The use of kaolin in rubber industry is very similar to the use in the fiberglass, plastics and adhesives. The primary beneficial quality of kaolin for rubber is its low cost, since it is much cheaper than either the natural rubber or man made elastomer. Kaolin stiffens the compound and reinforces it when cured. Kaolin is normally used in non-black rubber goods. Kaolin used in the rubber industry must have low amounts of coarse materials, very fine grain size, low amount of impurities, a pH value of 4.4-5.5 and a constant specific gravity so that it can be formulated with other ingredients of the rubber compounds.

1.6.5 Paints

Kaolin is used in interior-exterior water-based and oil-based paints. It increases the whiteness of paint. When used with other pigments, kaolin will increase their

covering power because of its flat shape in which particles arrange themselves in an overlapping pattern. Kaolin is also valued for its hydrophilic characteristics, which make it a premier extender in paint. Because of its high oil absorption characteristic, however, kaolin reduces the gloss in gloss paints and thus its use is limited to ~ 10% weight in this application. Specifications of kaolin for paints are as below.

Table 1.5: Typical property of kaolin used for paints

Property	Grade		
	a	b	c
Seive residue % > 45 μm	0.05	-	0.5
Particle size %			
< 20 μm	99.5	95	90
< 10 μm	99.0	80	70
< 2 μm	70	35	15
Volatile matter at 105 °C	-----2%-----		
Loss on ignition	-----10 – 14%-----		
Matter soluble in water	-----0.5%-----		
pH aqueous suspension	-----4.5 – 9.5 -----		

Source: BS 1795: 1976 Extenders for paints

1.6.6 Other uses

The chemical industry consumes significant quantities of kaolin. Production of aluminum compounds such as aluminum sulphate, phosphate and trichloride account for major applications of kaolin. Another rather significant volume and high value end-use of kaolin is in making synthetic zeolite, or “sieve materials”. Zeolites are mainly used in the petroleum industry as cracking catalysts. They have very high surface area, and thereby can increase the effectiveness of reactions.

A relatively small end-use of kaolin is in the agricultural sector. Kaolins are used by the agricultural industry in the manufacture of fertilizers, pesticides and animal feeds. Kaolin is used in feed and fertilizer mainly as filler to bring the product to the correct consistency, in pesticides as dilutents to dilute the toxic portion of the

pesticide, and as dispersant to make the pesticide easy to apply. Kaolin is used for the above purposes because of its flat particle shape, which improves adhesion of the pesticides to the sprayed plants.

Pharmaceutical industry also uses minor quantities of kaolin. High purity kaolin is used here mainly as inert filler. It can also be effectively used as cosmetic muds.

1.6.7 Special application through chemical modifications

Kaolin is hydrophilic and can be dispersed in water. Because of the nature of the chemistry of its surface, kaolin can be chemically modified so that it will become hydrophobic or organophilic. Generally, an ionic or a polar non-ionic surfactant is used as the surface treating agent. Improvement in functionality of kaolin filler after surface modifications has been noticed in the ink, paint, and plastic industries.

1.7 A brief description of the present work

The present work deals with the study on the geochemical, mineralogical, morphological and the utilitarian aspects of kaolin from the two major deposits of Kerala- Madayi (Kannur, North Kerala) and Kundara (Quilon, South Kerala). The investigation brings out the variation in the environmental conditions, which led to the various mineral assemblages in the above deposits. The laboratory and field data provide an insight into the genetic factors, which contribute to the origin of clay and associated minerals in these deposits. In addition, the study on the surface modification of kaolin using organosilane (triethoxy vinyl silane) has been undertaken. The utilization of this surface modified clay as polymer reinforcement material has also been presented in detail.

Chapter 2

Methods and Techniques of Mineralogical, Morphological and Physico- Chemical Characterisation

As explained in the previous chapter, clays are very diverse in composition and some contain many mineral types. Many of the properties of clays are dependent on the nature and amounts of major and accessory minerals and also the impurities in them, and hence their identification and estimation are of very great significance. The geochemical, mineralogical, morphological and physico- chemical studies of clays involve a variety of techniques. The various methods adopted in the present study are briefly discussed below.

- **Mineralogical, Morphological and Geochemical Characterisation**

- Bulk mineralogy XRD (unoriented mounts of raw and heavy fraction)
- Clay mineralogy XRD (oriented mounts of $< 2 \mu\text{m}$ fraction)
- Structural studies Crystallinity Index Measurements- Hinckley Index and Amigo Index- from XRD ($< 2 \mu\text{m}$)
Fourier Transform Infrared analysis ($< 2 \mu\text{m}$ fraction) and Diffuse Reflectance FTIR analysis of modified clays ($< 45 \mu\text{m}$)
- Thermal studies Differential Thermal and Thermogravimetric analysis($< 2 \mu\text{m}$ fraction)
- Morphological and Textural studies Scanning Electron Microscopic and Optical Microscopic analysis
- Geochemistry Major and minor elements- Classical methods of chemical analysis (raw and $< 2 \mu\text{m}$ fraction)
Trace elements– Atomic absorption spectroscopy (raw and $< 2 \mu\text{m}$ fraction)

- **Physical Property Evaluation**

- Particle size distribution
- Viscosity
- pH
- Brightness/ Yellowness
- Contact angle
- Linear shrinkage (dry and fired)
- Volume shrinkage (fired)
- Water absorption
- Apparent porosity
- Bulk density
- Green strength and fired strength
- Density of polymer- kaolinite composite
- Swelling of polymer- kaolinite composite
- Mechanical strength of polymer- kaolinite composite

2.1 Separation of fines from kaolinite

The principle involved in the separation of fine fraction from the raw clay is based on Stokes law.

$$V = \frac{2}{9} \frac{g \cdot r^2}{\eta} (G_s - \gamma_w)$$

where V = velocity of the falling particle, G_s = Specific gravity of the particle,
γ_w = specific gravity of the liquid medium (water), g = force of gravity ,
η = viscosity and r = radius of the particles

Procedure: The method of separation involves a relative motion between the clay particle and the fluid (water). In order to carry out a particle size analysis based up on the motion between the particles and the fluid, the clay has to be dispersed by a suitable deflocculent. Among the dispersing agents generally used, sodium hexametaphosphate has been found to be the most effective and the widely used one. Here the phosphate ions promote dispersion by the adsorption on the clay edges where they reverse the normally positive edge charge and thus prevent flocculation caused by the formation of the edge to surface bonds among the crystallites. Adequate time was given for settling based on the above principle and the slurry containing < 2 μm clay fraction, which remains in

suspended form was siphoned off and concentrated by evaporation. The concentrated suspension was centrifuged and washed free of the ions of the deflocculating agent.

2.2 Heavy Mineral Separation

Heavy mineral separation is based on mass separation in a liquid with specific gravity between the specific gravities of the minerals to be separated. The separation was accomplished by gravity settling in bromoform (specific gravity 2.89).

Procedure: The heavy mineral separation was carried out in batches in small glass funnel fitted with a pinch clip (Fig. 2.1).

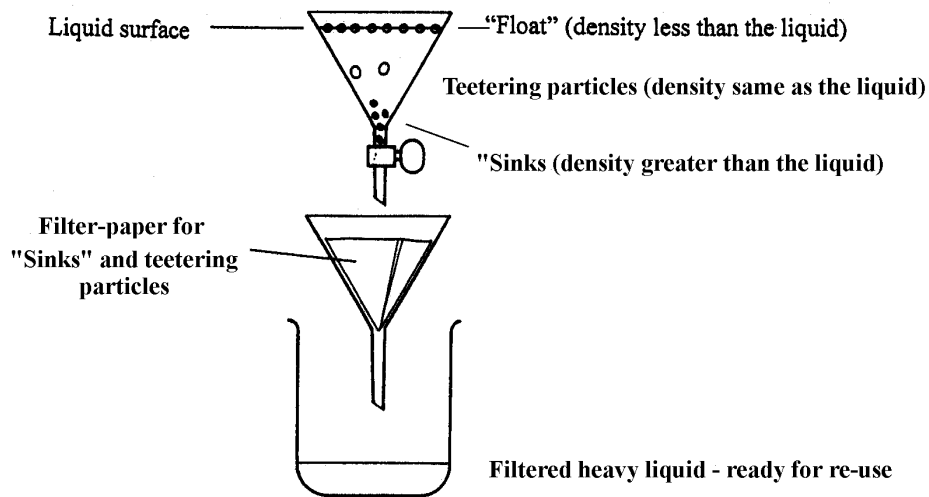


Fig. 2.1. Separation of mineral particles in heavy liquid

The dried raw clay sample was mixed with the heavy liquid taken in a separatory funnel. The sample was stirred well in order to get the mineral grain properly wetted by the liquid and sufficient time was allowed for separation to take place, *i.e.* time must be given for the dense particles to reach the bottom of the funnel. As shown in fig. 2.1, there are three types of particles depending on their movement in the heavy liquid 1) floats – having density less than the liquid, 2) teetering particles- having density same as the liquid and 3) sinks – having density greater than the liquid. After the separation, the heavier “sink” fraction was run out into a filter paper held in a lower funnel. The heavy

liquid was allowed to drain through the filter and collected; it is then ready for immediate re-use. The collected heavy minerals were washed several times with alcohol to make them free from bromoform and are dried in air prior to analysis.

2.3 Mineralogical Analysis by X-ray Diffraction Technique

X- ray diffraction is the most widely used technique for the identification and characterization of clay minerals (Brindley and Brown, 1980; Wilson, 1987).

Clay minerals consist of tiny crystals which are themselves made up of ordered array of atoms arranged in a periodic or repetitive way. X- ray diffraction can be conveniently visualized as a reflection of the incident beam by parallel, closely spaced planes of atom within a crystal. W.L. Bragg in 1912 gave a very simple geometrical interpretation of diffraction by a crystal grating. According to him the condition for diffraction is given by the relation:

$$n\lambda = 2d \sin \theta$$

where n is an integer (order of the reflection), λ is the wavelength of the X- rays, θ is the glancing angle of incidence and d is the interplanar spacing of the crystal. This equation is Bragg's law or the Bragg equation. The X- ray diffraction effects can be used to determine the inter-planar distances in crystals and from this information it is possible to determine the structure of a crystalline substance.

Procedure: Samples were analysed by Philips PW 1710 X-ray diffractometer with Ni-filtered $\text{CuK}\alpha$ radiation (40 kV, 20 mA) at a scan speed of $1^\circ 2\theta/\text{min}$. Two types of sample packing are often used for XRD. These include the preparation of randomly oriented mounts and oriented mounts.

2.3.1 Randomly oriented mounts

The hkl reflection of the mineral is essential to estimate the clay and the non clay mineral abundance in the sample. Such analysis is possible only when there is a perfect random orientation of all the particles in the sample, which is very difficult to achieve. Most crystals break or cleave more readily along some planes than others. When packed as a powder, orientation of the individual grain tends to be governed by the juxtaposition of the faces formed by these preferential breakages, and this process works against the

preparation of randomly oriented aggregates. Various methods for the random orientation have been suggested by Brindley and Brown (1980) and Moore and Reynolds (1989).

In the present work random orientation of the clay sample was achieved by allowing the free fall of the powdered samples into the glass slide pasted with vacuum grease. This method avoids the orientation of clay particles.

2.3.2 Oriented mounts

Preferential orientation of the clay involves either sedimenting a suspension onto a flat surface, usually glass, suction of the suspended material onto a flat unglazed ceramic tile, membrane filters or porous metal surface, smearing a clay paste onto a glass slide; or application of pressure and/or shear to a dry powder (Brindley and Brown, 1980) (Moore and Reynolds, 1989). For oriented mounts any one of the above methods should provide a specimen having maximum amount of preferred orientation of basal planes parallel to the substrate and which is sufficiently thick and homogeneous.

In the present work oriented mounts were prepared by sedimenting the clay slurry on a glass slide after the dispersion of clay sample in distilled water. The sample was dried at room temperature prior to the analysis.

2.4 Crystallinity Index Measurements

Kaolinites from different sources and different locations have different degrees of structural order or “crystallinity”. Mechanical treatments like grinding can also change the order/disorder characteristics. Various methods of crystallinity index measurements were adopted by different authors. Among these, the widely used method is the Hinckley index measurements (HI). In addition, Amigo crystallinity index is also measured in order to avoid the error due to presence of gibbsite, which will interfere with the kaolinite peak during Hinckley crystallinity index measurements.

Hinckley crystallinity index (HI) (Hinckley, 1963) as illustrated in the figure 2.2A, is the ratio of the height above the background of the 110 and 111 peaks occurring between $20-23^\circ 2\theta$ compared to the total height of the 110 above background. Normal values range from < 0.5 (disordered) to > 1.5 (ordered)

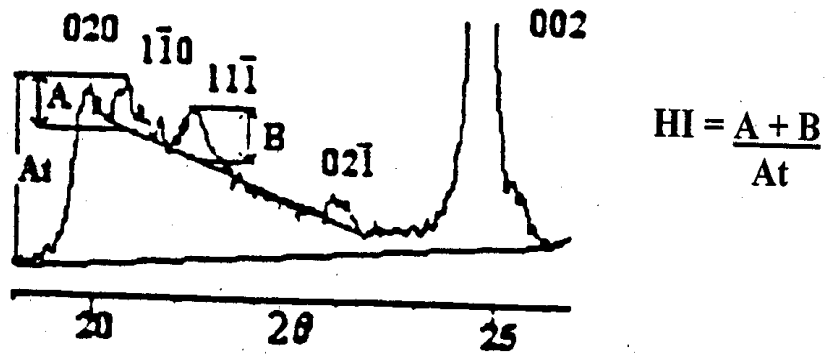


Fig.2.2A.Hinckley Crystallinity Index Measurements

The crystallinity index measurements by Amigo *et al.* (1987) is based on the indices FWHM (001) and FWHM (002). They are determined as the width at half height of the 001 and 002 reflections in degrees (Fig. 2.2B) Normal values range from > 0.4 (disordered) to < 0.3 (ordered).

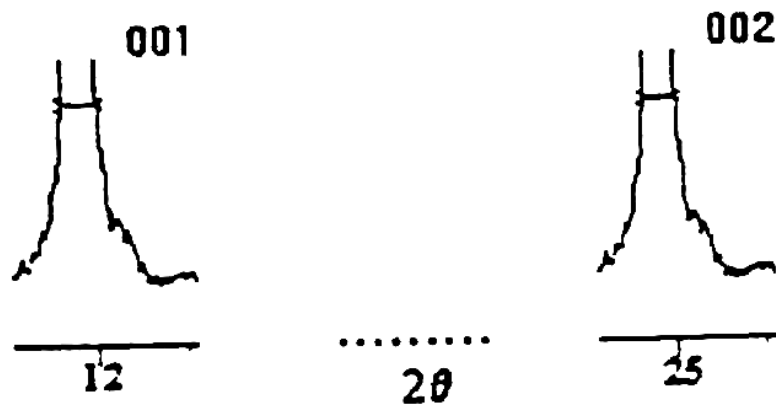


Fig.2.2B. Amigo Crystallinity Index Measurements (FWHM 001 and FWHM 002)

2.4.1 Pretreatment of samples

For crystallinity measurements the size separated < 2 μm samples were chemically treated to remove carbonates, organic matter and oxides of iron as per the methods described below (Al-Khalissi and Worrall, 1982; Moore and Reynolds, 1989).

2.4.1.1 Removal of carbonate

For the removal of carbonates the samples were digested in acetic acid (buffered to pH 5) for 30 minutes with intermittent stirring. The suspension is centrifuged until the supernatant liquid was clear. The experiment is repeated for confirming the complete removal of calcareous impurities.

2.4.1.2 Removal of organic matter

Organic matter can produce broad diffraction peaks, increase the background and inhibit dispersion of other minerals if present in significant amounts. For the removal of organic matter, the samples which were treated for carbonates by the above procedure were treated with H_2O_2 . Each 1-gram sample of the clay was treated with 10 ml of 30% H_2O_2 and the mixture was heated on a boiling water bath. The treatment should be repeated once or twice to remove all the organic matter.

2.4.1.3 Removal of iron oxides

Since iron oxide cement particles together, it will inhibit the dispersion of the clay mineral. In addition, when Cu radiations are used for X- ray analysis of the samples with high amount of iron, it may pose problems since they produce high background that can mask peaks. So the Fe- oxides should be removed chemically. The removal of iron oxides assists the dispersion and separation of fine fraction and facilitates X-ray diffraction analysis. The most commonly used treatment is the citrate – bicarbonate – dithionite (CBD) method (Jackson, 1969). The buffered neutral citrate bicarbonate dithionite was used. Sodium dithionite ($Na_2S_2O_4$) acts as a reducing agent, sodium bicarbonate (pH 7.3) as a buffer, and sodium citrate as a chelating or complexing agent for ferrous and ferric iron.

Oriented mounts were prepared from the above treated clays for crystallinity index measurements.

2.5 Infrared spectral methods

Infrared absorption spectroscopy is a rapid and non-destructive physical method universally applicable to structural analysis. Fourier transform infrared (FTIR) and Diffuse reflectance FTIR methods (DRIFT) were used in the present study.

The absorption of infrared radiation by clay minerals depends critically on atomic mass and the lengths, strengths and force constants of the interatomic bonds in the structure of these minerals (Russell, 1987). The absorption of infrared method is strongly influenced by the degree of crystalline order (Lazarev, 1974; Brindley *et al.*, 1986) and the size and shape of the mineral particles (Farmer and Russel, 1966; Rendon and Serna, 1981; Serna *et al.*; 1982). The infrared spectrum of a clay mineral is therefore sensitive to chemical composition, isomorphous substitution and crystallinity and provides fundamental information not only on the mineral identification, but also on the surface properties and reactions of the minerals with the chemicals in their environment.

Procedure

Sample Preparation: The size separated $< 2 \mu\text{m}$ samples were dispersed in KBr in the ratio (1:200) and are pressed into discs. The sample is scanned and the spectrum is recorded over the range 4000 to 400 cm^{-1} using a Perkin – Elmer spectrometer. The Transmittance (T%) Vs Wavenumber (cm^{-1}) plots are presented.

Similar method of sample preparation was adopted for DRIFT analysis of the modified hydrophobised clay samples. Here the spectra are scanned with an additional DRIFT accessory. In order to study the extent of silylation, the reference spectrum of the unmodified clay was subtracted from the spectra of treated clays. The changes in the band intensities reflect the extent of modification.

2.6 Thermal Analysis

The thermoanalytical methods complement the X- ray diffraction analysis (XRD). In thermal analysis, the physical property of a substance or its reaction products is measured as a function of temperature, while the substance is subjected to a controlled temperature programme (Paterson and Swaffiels, 1987). The primary use of the thermo analytical methods lies in the qualitative and quantitative analysis of the mineral mixture. The

crystal structure, crystallinity and the order/disorder of the mineral species are important factors affecting thermogravimetric analysis of minerals, the composition of a mineral can exert considerable control on thermal reactions, including decarbonation and dehydration reactions (Grimshaw and Searle, 1958). Thermal analysis were carried out using a Seiko 320 TG/DTA analyzer at a heating rate of 10°C/min in the range ambient-1100°C with alumina as standard. A schematic representation of the thermal analyser having the multichannel system analysis is given in fig. 2.3.

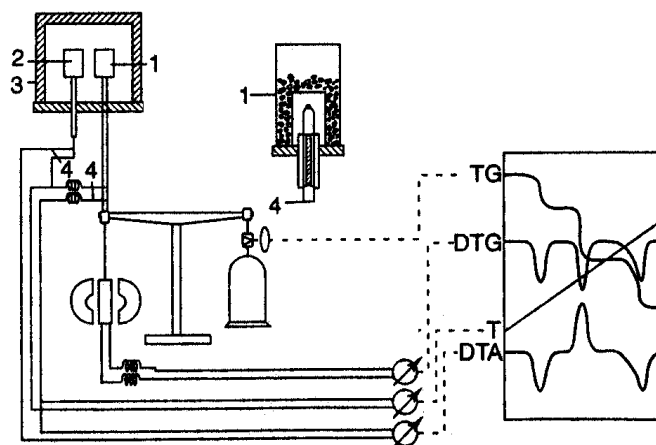


Fig. 2.3. Schematic representation of TG/DTA analyser 1) sample, 2) reference, 3) furnace and 4) thermocouple

2.6.1 Differential Thermal Analysis: Differential thermal analysis is a technique for studying the thermal behavior of material as they undergo physical and chemical changes during heating and cooling. The name is derived from the differential thermocouple arrangement, consisting of two thermocouple wires. The first thermocouple is placed in a sample of material to be analysed and the second one in an inert reference material (Fig. 2.3), which has been selected so that it will undergo no thermal transformations over the temperature range being studied. When the temperature of the sample equals the temperature of the reference material, the two thermocouples produce identical voltages and the net output is zero. When sample and reference temperatures differ, the resultant net voltage difference reflects the difference in temperature between sample and

reference at any point of time. The μV output from the differential thermocouple pair is then amplified, and are recorded.

Differential thermal results are recorded as the DTA curves, in which, by convention, $\Delta\mu\text{V}$ is plotted on the ordinate with endothermic peaks pointing downward, and exothermic reactions as upward deflections from the horizontal base line, while on the abscissa, temperature of the sample, is recorded increasing from left to right. The amount of divergence of the curve from the baseline reflects the difference in the temperature between the sample and the furnace at any given temperature and is therefore, a measure of the intensity of thermal reactions.

2.6.2 Thermogravimetry (TG): The phenomena initiated by heating at a controlled rate or at a fixed temperature above ambient involve a change (usually as loss) in weight (*i.e.* dehydration, desorption, decomposition, oxidation). TG analysis is essentially a means of observing the weight of the sample as a function of temperature (dynamic heating) or time (isothermal heating).

The measured parameter in TG involves the measurement of the mass of a substance as a function of the temperature while the substance is subjected to a controlled temperature program. In reporting the curves, the mass of the sample should be recorded on the ordinate decreasing downwards, while in the abscissa, the temperature or time-should increase from left to right.

Size separated $< 2 \mu\text{m}$ samples were used for thermal analysis.

2.7 Optical Microscopic Analysis

Optical microscope is probably one of the most potent tools in the examination of the mineral grains. Optical analysis of the minerals gives information about the different mineral phases together with their size, shape and distribution pattern. In addition to the morphological features such as twin and cleavage planes, the measurements of the optical properties of the crystals- their refractive indices, birefringence and extinction angles give additional evidences for the mineral identification.

Procedure

Preparation of grain mount: Grain mounts were prepared by impregnation with Canada balsam. Canada balsam (one part Canada balsam in 3 parts of xylene) is poured into a

glass slide. The mineral grains are sprinkled into this, which is then heated to evaporate the solvent and harden the balsam. The grain mount is then polished to smoothen the plane surface. A cover glass is cemented over the thin section prior to the microscopic study using Olympus Polarizing Microscope.

2.8 Scanning Electron Microscopic Analysis

A Scanning electron microscope is a versatile and efficient instrument for obtaining magnified images of small objects with a resolution better than a light microscope. SEM reveals the fine structure of even the smallest clay mineral particle and is an excellent tool for the identification of the principal types.

Scanning electron microscope has an electron source, which creates a beam of electron, an optical system, which focuses the electrons, a scanning system, which directs the beams over the sample, one or more detector systems, which create signals dependent on interactions of the beam electrons with the sample, and display systems which allow the microscope operator to interpret visually the information produced by the microscope. The scanning electron microscope uses a finely focused electron beam incident on the specimen surface. In SEM, the secondary electrons which are generated in the specimen surface are collected and are used to produce an image on a cathode ray tube.

Procedure

Sample preparation: Freshly broken natural surfaces of the clay samples were pasted on the surface of the brass stud using adhesive paste for the morphological analysis of the major and the associated minerals. In addition, in order to analyse the surface features, powder samples were sprinkled on the double-sided adhesive tape. The samples were then sputter coated with gold prior to the examination using JEOL JSM 5600 LV microscope.

2.9 Methods for chemical characterisation: Major and Minor elements

Chemical analysis is an essential step in establishing the nature of minerals, next to the X- ray diffraction analysis. A relatively small difference in the chemical composition of clays can greatly influence the chemical and physical properties and thereby its industrial utility. Classical methods of chemical analysis are widely used for the aluminosilicates

(Bennett and Reed, 1971). The results of chemical analysis are expressed in terms of various oxides present such as SiO₂, Al₂O₃, TiO₂, Fe₂O₃, FeO, CaO, Na₂O, K₂O, MgO and LOI. Of the various constituents SiO₂ is determined by gravimetric, Al₂O₃ by volumetric, TiO₂ and Fe₂O₃ by colourimetric and Na₂O, K₂O and CaO by flame photometric techniques.

2.9.1 Loss on Ignition

1 gram of the finely ground, dried sample (110°C, 1 hour) was weighed in to a platinum crucible and heated in a muffle furnace at a temperature of 1025 ± 25°C for 60 minutes. Then the loss in weight was determined as:

$$\% \text{ LOI} = \frac{A-B}{A} \times 100$$

where A = initial weight, B = weight obtained after ignition.

Loss on ignition reflects the loss of weight due to the oxidation of organic coatings (humic acid), carbonaceous and graphitic impurities and the water loss due to dehydroxylation.

2.9.2 Determination of Silica (Gravimetry technique)

Procedure: 0.5 g of the finely powdered dried sample (105° – 110°C, 1 h) was weighed in a platinum crucible. 3 g 1:1 mixture of Na₂CO₃ and K₂CO₃ was added and the mixture fused in a high temperature furnace. The melt after cooling was disintegrated with 30 ml 1:1 HCl and 1 ml of 1:1 H₂SO₄. The resultant solution was evaporated and baked in an oven at 110 °C for 5-6 h. The residue was cooled and digested with 10 ml of conc. HCl and 40 ml of hot water. The resultant mass was filtered through a whatman No. 40 filter paper and washed free of chloride with hot water. The filtered residue along with the filter paper was ignited at 1000°C for 30 minutes and weighed after cooling in a desiccator. The precipitate was treated with 10 ml of HF (40%) and a few drops of 1:1 H₂SO₄ and evaporated to dryness. The crucible was ignited cooled and weighed. During the HF treatment silica completely volatilises as hydrofluosilicic acid. Any impurity other than silica only is left in the crucible.

$$\% \text{ of SiO}_2 = \frac{A- B}{W} \times 100$$

where A = weight of the sample and the crucible after ignition of the residue, B = weight of the sample and crucible after HF treatment, W = initial weight of the clay sample

2.9.3 Preparation of solution for Al₂O₃, TiO₂ and Fe₂O₃ determination

0.5 g of well agated dried sample (110°C) was weighed in a platinum basin and moistened with water. 10 ml of H₂SO₄ (1:1) and 10 ml HF (40%) was added and evaporated on a sand bath to fume off sulphuric acid. The basin was cooled and 10 ml HF was again added, evaporated to copious fumes and ultimately to near dryness. The residue was fused with 5- 6 fold quantity of Na₂CO₃ and about 4 fold quantity of potassium bisulphate. Cooled the basin and dissolved the melt with 3% H₂SO₄ in a steam bath to a clear solution and made it up to 250 ml.

2.9.4 Determination of Al₂O₃ (Volumetric method)

The principle involved in this method is to complex aluminium with EDTA and estimate the excess complexing agent by titrating with zinc acetate solution.

Procedure: 20 ml of the sample solution (2.9.3) was pipetted into a conical flask. 25 ml of EDTA (0.02 N) and a drop of methyl orange indicator was added. Dropwise addition of NH₄OH changes the colour of the solution from red to yellow. 10 ml of buffer (pH 5.3) was added and titrated with zinc acetate using xylenol orange as indicator, till the solution gets an orange colour. 1 g of NaF was added and boiled for five minutes. The solution was cooled and buffered to pH 5.3 followed by titration with zinc acetate. Then the concentration of Al₂O₃ was calculated as.

$$\text{Percent alumina (Al}_2\text{O}_3) = \frac{A \times x \times 100}{W} - 0.6378T$$

where A = the titre value in ml of zinc acetate solution, x = equivalent Al₂O₃ in g per ml of zinc acetate, W = weight in gram of the sample present in 25 ml of the stock solution and T = percent titania in the sample.

2.9.5 Determination of TiO₂ (Colourimetric method)

Procedure: 20 ml of the aliquots of the solution (2.9.3) was transferred to 100 ml standard flasks A and B. 10 ml of hydrogen peroxide was added to A and both were

diluted with water to the mark. Optical density at 410 nm was measured for A against that in B without peroxide. The unknown titania concentration was calculated from the calibration curve.

When the Fe_2O_3 content in the sample was above 1%, 5 ml of the acid mix (20 ml- H_2SO_4 , 50 ml- H_3PO_4 , 30 ml- H_2O) was added to each flask and the absorbance were measured at 398 nm after the addition of H_2O_2 as in the previous case.

2.9.6 Determination of Fe_2O_3 (Colourimetric method)

Procedure: 5 ml of the prepared solution (2.9.3) was transferred to a 100 ml standard flask and 1 or 2 drops of paranitrophenol indicator and 10 ml of tartaric acid were added. The solution was neutralized with conc. ammonia to the yellow colour of the indicator and acidified with a few drops of 1:1 HCl. 2 ml hydroxylammonium chloride and 10 ml 1:10 phenanthroline were added and diluted to the mark. The optical density was measured at 510 nm in a cell against reference test blank prepared in the same way without the sample. Calibration graph was drawn with 0, 1, 2, 3, 4 and 5 ml of standard Fe_2O_3 solution and the iron content in the unknown sample was determined from this graph.

2.9.7 Determination of Na_2O , K_2O and CaO

The concentration of sodium, potassium and calcium in clay samples were determined by flame photometric technique. The essential features of the instrument are a suitable flame and a means of ejecting a solution of the sample into it at a predetermined rate. A filter designed to transmit only the characteristic emission of a particular element is placed between the source and a photocell, so that the intensity of radiation can be measured and compared with standard samples tested under the same conditions.

Procedure: 0.1 g of well agated dried (110°C , 1 h) sample was weighed in a platinum basin and moistened with water. 1 ml perchloric acid and 5 ml of HF were added and evaporated in a sand bath to fume of perchloric acid. The basin was cooled, a few drops of water was added and evaporated to dryness. To the dry mass in the basin, 5 drops of 1:1 HCl and water were added and dissolved by keeping it over a steam bath for 5 minute. The content was transferred to 100 ml flask and diluted to the mark. The concentrations

of K_2O , Na_2O and CaO in the unknown clay samples were determined using a flame photometer with their corresponding filter. Calibration graphs are drawn with the varying standard concentrations.

2.9.8 Determination of Ferrous oxide

Hey (1941) and Schafer (1966) have reviewed various methods available for determining Fe^{2+} in silicates.

Procedure: 1 g of the oven-dried sample ($110^\circ C$, 1 hr) was weighed into a platinum crucible of about 30 ml capacity. 10 ml of 1:1 sulphuric acid was added and stirred with a glass rod, 10 ml hydrofluoric acid (40% w/w) was also added and digested in a sand bath. Boiled sample was plunged into a 600-ml beaker containing 300 ml of cold, freshly boiled distilled water in which 15 g of boric acid has been dissolved. Swirl the beaker to remove the lid from the crucible and the solution was mixed gently. 15 ml of sulphuric acid-phosphoric acid mixture and 10 drops of barium diphenylamine sulphonate indicator were added and titrated to a purple color with 0.1N potassium dichromate solution.



2.10 Determination of Pyrite in Clays by Selective Extraction with Acid solution

The pyrite in the sample was quantitatively analysed as per the analytical procedure adopted by Schneider and Schneider (1990).

The method involved two selective extractions: A) overnight dissolution of nonpyritic iron, including hematite (Fe_2O_3) in concentrated hydrochloric acid and then diluting the sample with distilled water to 2.5 N and boiling it for 1 h under atmospheric pressure; and B) dissolution of total pyritic and non-pyritic iron, including hematite, from a separate sample in a two-step extraction. This two step extraction involves a) initial dissolution in concentrated HCl followed by dilution to 2.5 N and boiling for 30 minutes, followed by b) the addition of 3 N nitric acid (to dissolve pyrite) and boiling for the next 30 minutes. The filtrates (or aliquots) from extractions A and B were then used for the determination of iron. The pyritic iron was determined as a difference in iron content of the two extractions (B-A).

Selective extraction of nonpyritic and total (pyritic and nonpyritic) iron:

1 g dried pulverised sample was weighed into a 250 ml conical flask. 11 ml of concentrated HCl was added, mixed thoroughly, closed and kept overnight. The content was diluted to 50 ml and an additional 50 ml of 2.5 N HCl was added. The flask was covered and boiled for 60 minutes. Sample was cooled, rinsed with 20 ml HCl (1:10) and filtered through a double slow filter paper (whatman no.5) with a small amount of paper pulp in it and washing it 5 or 6 times with 2 ml of HCl solution (1:10). Transparent and colourless or yellow-green filtrate was obtained depending on the content of acid soluble compounds. The acid-insoluble part, which remained in the filter paper, was discarded and the filtrate was treated with 5 ml con H_2SO_4 and a few ml of HNO_3 and was evaporated to dense sulfur trioxide fumes. After cooling, the residue was diluted with distilled water to 250 or 500 ml (depending on the content of Fe) in the measuring flask. An aliquot of the solution was taken for the determination of Fe.

In the case of extraction of total pyritic and nonpyritic iron, the pulverised 1 g sample was transferred to 250-ml conical flask. Overnight treatment of the sample with 11ml of concentrated HCl was done as given above. Diluted it to 50 ml with distilled water (acidity of 2.5 N) and is boiled for 30 minutes. Then, 50 ml of 3 N HNO_3 was added, and boiling was continued for the next 30 minutes. The sample was cooled and filtered through whatman no.5 filter paper after rinsing the flask with 20 ml of 2 N HNO_3 . Subsequently, flasks and the filters were washed 5 to 6 times with 2 N HNO_3 . The filtrate is treated with 5 ml of concentrated H_2SO_4 and evaporated until the dense SO_3 fumes appeared. After cooling, the residue was diluted with distilled water and boiled for a few minutes. If silica precipitates, it has to be removed by filtering. The filtered solution was diluted to 250 or 500 ml in a standard flask and an aliquot of the solution is taken for the determination of Fe.

Percentage of pyritic Fe = Percentage of Fe from extraction B – Percentage of Fe from extraction A

From pyritic iron the percentage concentration of pyrite in the samples were calculated.

Spectrophotometric method was used for the determination of iron in the extract.

2.11 Determination of water soluble sulphate

Water soluble sulphate in the samples were determined as BaSO_4 by precipitation using BaCl_2 (Jeffery *et al.*, 1989).

Procedure: 5 g of the dried clay (110°C) was weighed into a 400-ml beaker containing 100 ml distilled water for SO_4^{2-} dissolution. The solution was filtered, 0.3 – 0.6 ml of concentrated HCl was added and diluted to 200 – 250 ml. Filtrate was boiled and barium chloride solution was added drop wise from a burette by constant stirring. The precipitate was allowed to settle and the supernatant liquid was tested for complete precipitation of SO_4^{2-} by the addition of a few drops of barium chloride solution. Then the solution was covered and kept hot without boiling for an hour for complete precipitation. The precipitate was transferred through an ashless filter paper (whatman No. 40) using a rubber tipped rod and washed free from chloride. The residue along with the filter paper was transferred to a silica crucible and ignited in a muffle furnace to a clear white precipitate. Then the percentage of SO_4 in the sample calculated.

2.12 Organic Carbon

Procedure: Organic carbon content in the clay samples were determined by wet combustion method (Gross, 1971)

Principle: 0.5 g of ground and dried sample was transferred into a 500 ml flask and 10 ml $\text{K}_2\text{Cr}_2\text{O}_7$, followed by 20 ml of $\text{H}_2\text{SO}_4 - \text{Ag}_2\text{SO}_4$ solutions were added. The flask was gently heated to 150°C for 1 minute and allowed to cool. Excess $\text{K}_2\text{Cr}_2\text{O}_7$ was estimated by back- titration with FeSO_4 solution after dilution to 200 ml and addition of 10 ml 85% H_3PO_4 , 0.2 g NaF and 30 drops of diphenylamine indicator. The endpoint is a change of colour from blue to bright green. A blank analysis was conducted for each series of samples. The percent organic carbon in the sample was calculated as follows.

$$\text{Percent of organic carbon} = \frac{(\text{ml FeSO}_4) \text{ blank} - (\text{ml FeSO}_4) \text{ sample} \times 0.3}{\text{Weight of the sample}}$$

2.13 Trace Element Analysis by Atomic Adsorption Spectroscopy

Atomic adsorption spectroscopy is one of the oldest and most well established of the analytical methods particularly for trace element analysis. The principle involved here is atomic adsorption and atomic emission. Every element has a specific number of electrons associated with its nucleus. The normal and most stable orbital configuration of atom is known as the ground state. If energy is applied to an atom, the energy will be absorbed and an outer electron will be promoted to a less stable configuration known as the excited state. As the number of atom in the light path increases, the amount of light absorbed also increases. By measuring the amount light absorbed, a quantitative determination of the amount of analyte can be made. The process involved in atomic absorption is illustrated in fig.2.4A



Fig. 2.4A Atomic Absorption Process

Since this excited atom state is unstable, the atom will immediately return to the ground state, releasing light energy. Atomic emission involved the processes of excitation and decay as shown in fig. 2.4B.

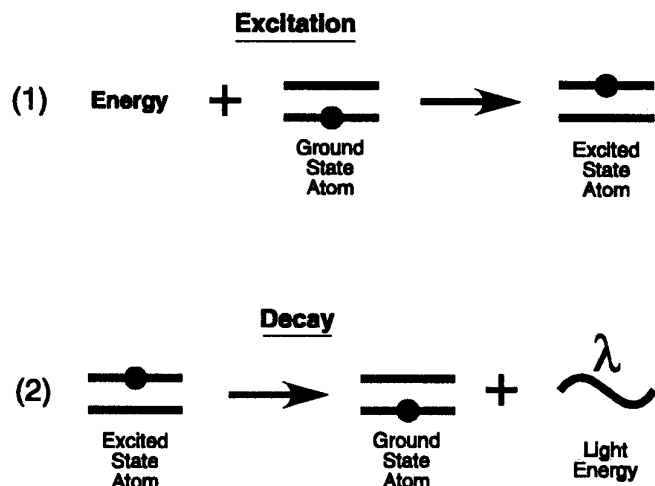


Fig. 2.4B Atomic emission processes

Basically in atomic emission, the flame serves a dual purpose: it converts the sample aerosol into an atomic vapour and then thermally elevates the atoms to an excited state. When these atoms return to the ground state, they emit light, which is detected by the instrument. In atomic absorption, the only function of the flame is to convert the sample aerosol into atomic vapour, which can then absorb light from the primary light source (hollow cathode lamp or electrodeless discharge lamp). The intensity of light emitted is related to the concentration of element of interest in solution. The use of specific light source and careful selection of wavelengths allow the specific determination of individual elements. The trace elements analysed in the present study include Cu, Co, Cr, Ni, Pb, Zn, Mn and Mg.

Procedure: The underlying requirement for all atomic methods of analysis is that a sample be decomposed to the greatest extent possible into its constituent atoms. For the analysis a known weight of the dried sample (110°C, 1 hour) was decomposed using HF followed by dissolution in 1:1 HCl. The prepared solution was atomised through a nebulizer. The nebulisation serves to increase the surface area of the sample solution, so that solvent evaporation can proceed more rapidly and the resulting dried solute particles can be volatilized better. Once formed, droplets in the nebulized spray are sent into a high – temperature flame. The solute-particle vaporization takes place, and the resulting vapor is

converted more or less efficiently into free atoms. Once formed, the concentration of the atoms can be measured by atomic adsorption spectroscopy. Varian Spectra AA- 10 Model atomic adsorption spectroscopy has been used for the trace element analysis.

The essential components of an atomic absorption spectrometer (Fig. 2.4C) involve:

- ◆ a light source, usually a hollow cathode lamp, which provides a sharp line emission at the resonance wavelength for the element to be measured (analyte).
- ◆ an atomiser which produces free atoms of the analyte
- ◆ a wavelength selection device (usually a monochromator) which allows the isolation of this resonance line from other lines produced in the spectrum of the lamp.
- ◆ a detector (usually a photomultiplier tube) which measures the intensity of the signal which is passed by the wavelength selection device.
- ◆ an amplifier –read-out device which processes the signal from the photomultiplier and converts into a suitable form from which the result is obtained.

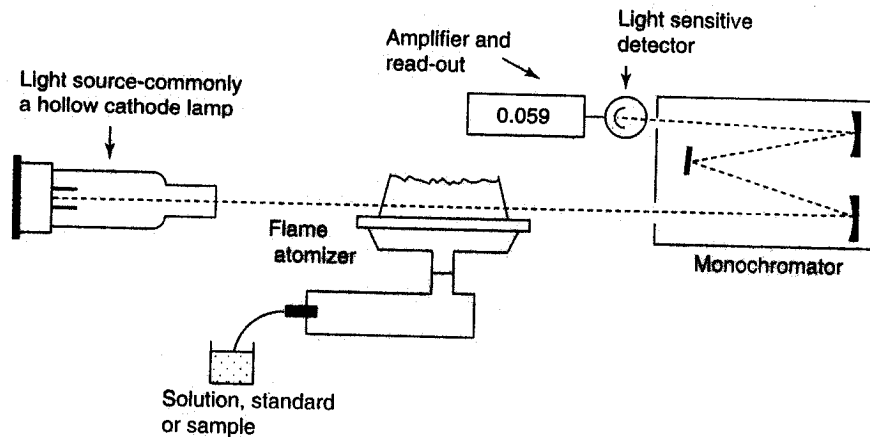


Fig. 2.4C Schematic representation of atomic absorption spectrometer

2.14 Physical properties of clay

2.14.1 Particle Size Analysis

Particle size measurements of the clay samples were carried out by Sedigraph 5100 based on Stokes law as explained earlier. Schematic representation of the particle size analyser (Sedigraph 5100) is given in fig. 2.5.

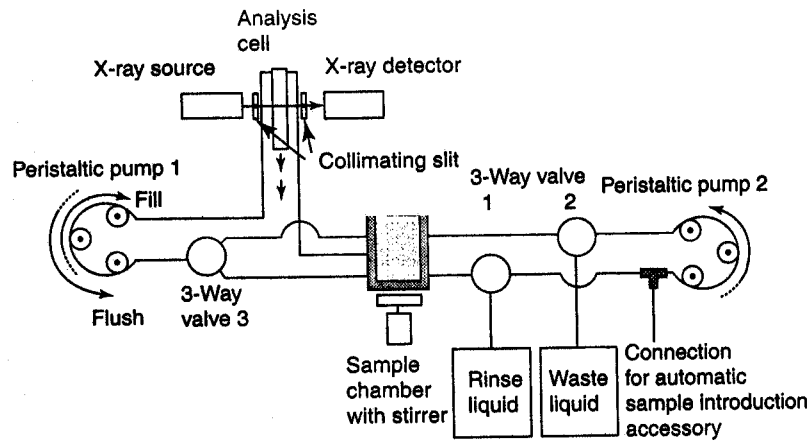


Fig. 2.5 Schematic diagram of particle size analyser (Sedigraph 5100)

Procedure: Approximately 5 g of the sample was taken in a container and dispersed with water using sodium hexametaphosphate as the deflocculating agent. The dispersed slurry was transferred into a sample chamber. A magnetic stirrer located under the mixing chamber keeps the particle suspended. A well-dispersed suspension in the sample chamber is transferred to the analysis cell by means of a peristaltic pump. At the start point of the analysis the pump stops and the particles are allowed to settle inside the analysis cell under the influence of gravity. The Sedigraph 5100 then determines the particle size distribution by means of X- ray beam. The percentages of total particle mass at different point in the cell were analysed by X- ray absorption. After the analysis the suspension is pumped to a waste reservoir and using a second peristaltic pump, fresh rinse liquid flows through the system.

The results are plotted as graphs with the diameter of the particles on the abscissa and cumulative weight percentage on the ordinate.

2.14.2 Viscosity

The viscosity of a liquid is the internal friction opposing its flow. The unit of viscosity is poise. The equation for viscosity determination as expressed by Frenchman Poiseuille is

$$V = \frac{\pi Pr^4}{8l\eta}$$

where V = volume of the liquid flowing per sec

P = pressure of the liquid (g/cm^2)

r = radius of the tube (cm)

l = length of the tube (cm)

η = viscosity of liquid

Procedure

Viscosity measurement of 63% w/w slurry was undertaken with a Brookfield Viscometer using minimum concentration of sodium polysalt as dispersing agent.

2.14.3 pH

The hydrogen ion concentration or pH is expressed as the logarithm to the base 10 of the reciprocal of the hydrogen ion concentration.

Procedure: 20 g of the raw sample was mixed in 80 ml distilled water (in the ratio 1:4) and stirred for 5 minutes. The slurry was filtered through whatman 40 filter paper. Discarded the first 20 ml. The remaining filtrate was collected and pH measured using a Systronic μ pH system 361.

2.14.4 Brightness measurements

The optical properties of kaolin are of much importance in most commercial applications. The brightness/yellowness of the clay samples are usually interpreted in terms of absorption coefficient (K) and scattering coefficient (S) by using K- M theory (Starr and Young, 1978). The absorption of kaolin can be modified by chemical treatment or by beneficiation to remove coloured impurities.

Procedure: Minus 350 mesh oven dried samples (110°C , 1 h) were powdered for 10 seconds in a high-speed mixer. The powdered samples were pelletized at a pressure of 55 kg/cm^2 for 30 seconds and the discs were subjected to brightness/yellowness measurement using Colour Touch Model ISO Brightness Meter. AR BaSO_4 was used as standard. Brightness was measured at 457 nm and yellowness as the difference in brightness between 570 and 457 nm.

2.14.5 Contact Angle Measurements

The contact angle measures the wetting tendency of a liquid on a solid and is thus of particular importance in the fields where wetting is important (Hunter, 2001). The measurement of contact angles is dependent on the nature of the substrate under consideration.

The commonly used method for contact angle measurement is by Sessile drop method (Neumann and Good, 1979). Here the wetting and non-wetting behaviour is obvious when a drop of liquid (water) is placed on the solid surface. The possible shape that can be attained for a liquid is shown as in fig. 2.6. The shapes of the liquid reflect the value of the contact angle and in turn the behaviour of the solid surfaces.

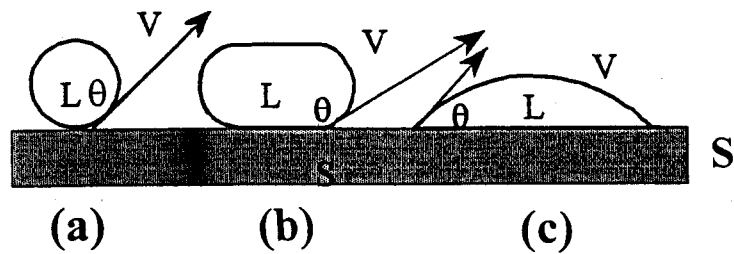


Fig. 2.6. Possible shapes of sessile drop a) small drop of completely non-wetting liquid with very high surface energy, so that gravitational forces have little effect b) large drop of liquid showing partial non-wetting character ($\pi/2 < \theta < \pi$) and sagging under gravity c) partially wetting drop ($0 < \theta < \pi/2$); V- vapour, L- liquid, S- solid substrate, θ - contact angle.

Procedure: Kaolinite samples were pressed into disc at a pressure of 100-250 kg/cm² by the method described by Janczuk and Bialopiotrowicz (1988). The discs were placed in the measuring chamber filled with saturated vapour for 20 minutes. Using a microsyringe, a drop of (2 μ l) water was settled onto the disc surface, and the contact angle was read immediately on the left and right sides of the drop, using a Reflective – Microscope-goniometer, Kernco Model II at 25 times magnification. At least 5 discs of a particular sample were used for contact angle determinations. Six or more drops were settled on the surface of each pellet and the average value taken. If the contact angle measured on both sides of the drop differed by more than 2°, they were not included.

2.14.6 Determination of Water of Plasticity

Plasticity is the ability of a clay- water mass at its maximum consistency to be shaped and to hold its shape after the forming forces are removed (Grim, 1962). The water content of the clay at the point of maximum workability, when expressed as a percentage gives the value of water of plasticity.

Procedure: 500 g of clay was dried thoroughly at a temperature of 70°C and crushed to pass through 45 micron IS sieve. Seived clay was mixed with water from the burette, thoroughly wedged and kneaded by hand to a soft plastic mass of appropriate consistency. Allowed it to age for 24 h by keeping it covered by wet cloth during the period. After 24 h this plastic mass was kneaded again and was pugged well by further small additions of water until proper working consistency was attained in order to extrude or mould into bars. Three equal proportions of the clay mass at this consistency from different portions were taken, the edges and corners rounded to avoid any handling loss and weighed immediately to the nearest 0.01 g.

Then the clay masses were dried in an air oven (70°C for 4 h) after room temperature drying for 24 h. The temperature of the air oven was again raised (110 ± 5°C) and the samples were dried further for 12 h. Cool them in a desiccator and weigh to the nearest 0.1 g. The water of plasticity was calculated as

$$\text{Water of Plasticity, percent} = [(A-B)/ B] \times 100$$

where A= weight in grams of the plastic clay mass and B= weight in grams of the dried clay mass.

2.15 Drying Properties

2.15.1 Determination of Dry linear shrinkage

When a clay sample is mixed with water and made into a plastic mass, it can be shaped in any form required. However on drying, the clay shrinks and the extent of shrinkage is dependent on the nature of clay as well as the grit content in the mass.

Procedure: A portion of the 24 h aged and kneaded clay as prepared in the plasticity determination was taken (2.14.6). The inner sides of the brass mould was coated with a

thin layer of petroleum jelly or kerosene oil and a lump of the plastic mass was pressed into the mould without any entrapment of air. The excess clay was stripped off with a straight edge spatula from the top of the mould and finally wiped of any adhering clay. Two reference points approximately of 10 cm apart were made on the surface of the smooth clay. The distance between the two points was accurately measured using the micrometer. Prepare five such specimens. The test specimens were released carefully from the mould and allowed to dry slowly under a wet cloth for 48 h. Air dry the specimen for another 48 h at room temperature, occasionally turning sides of the specimen to expose new surface for evaporation. The test specimens were placed in an air oven, with automatic temperature control and was dried at $110 \pm 5^{\circ}\text{C}$ for 24 h. Specimens were then cooled in a desiccator and the distance between the points were again measured.

Dry linear shrinkage was calculated as follows

$$\text{Dry linear shrinkage, percent} = [(L_p - L_d)/L_d] \times 100$$

where L_p = length of the plastic clay mass in cm, and L_d = length of dry clay mass in cm.

2.15.2 Green Strength

The property of the dried clay to hold together, known as the ‘green strength’, is essential for preparing ceramic materials (Singer and Singer, 1978). It depends on the electrostatic attractions between clay colloid particles which increase as the separating water film is removed. The green strength of the clay body increases as the water content decreases. The strength of the dry clay is an important property with direct practical bearing on the problems of moulding, handling and drying of wares, since a high strength enables the clay to withstand the shocks and strain of handling. The green strength of the clay is generally determined by finding its transverse strength and expressed as the modulus of rupture.

Determination of Modulus of Rupture

Preparation of samples: < 45 µm fraction, of the clay was mixed with sufficient quantity of water, kneaded into a soft, plastic and homogeneous mass and aged for 48 h. After ageing, the plastic mass was vacuum extruded (50 cm of mercury). Extruded bars of 25 mm diameter from the air dried plastic mass was cut into bars of 180 mm length. These bars were placed on the glass plates very lightly oiled and marks at 100 mm apart were put on each test bar. Test bars were covered with a piece of wet cloth and was allowed to dry in air at room temperature. After five days of room temperature drying, samples were oven dried at $110 \pm 2^\circ\text{C}$. Cooled the test bars in a desiccator. The test bar should be straight free from warpage. Ten such test bars were prepared to find out the average value of MOR.

Place a test bar on two of the bearing edges, in such a way that the bearing edges coincide with the mark made on the test bar. Apply the load uniformly at the centre point at a rate of 5 kg/s approximately. Note the load, which just breaks the test bars. The average load was calculated.

Then the dry modulus of rupture was calculated as follows

$$\text{Modulus of rupture, } S, \text{ kg/cm}^2 = \frac{8PL}{\pi d^3}$$

where P = total load in kg, L = span of the bar in cm and d = diameter of the test bar in mm.

2.16 Fired Properties

The irreversible hardening reaction that occurs when clay is strongly heated is another feature that has been of fundamental interest to the ceramic industry. Briefly, on further heating of dried clay more, water is given off and in due course a hard but porous piece forms. Thereafter vitrification occurs leading to a strong dense piece but is eventually followed by softening and fusion. Release of gases may also give rise to a swollen appearance known as 'bloating'. During these reactions some expansion may occur, but there is always an overall shrinkage. The whole series of reactions is governed by the mineralogical, chemical and grain size distribution of the clay and is therefore different for each clay sample.

The fired properties of the clay include fired linear shrinkage, fired volume shrinkage, fired strength, water adsorption, bulk density and apparent porosity.

2.16.1 Determination of Fired linear shrinkage

Rectangular bars were prepared from the plastic clay mass as in the case of dry linear shrinkage (2.15.1). These bars were fired at varying temperatures with a soaking period of 3 h. Then the fired shrinkage was measured as

$$\text{Fired linear shrinkage, percent} = [(L_p - L_f) / L_f] \times 100$$

where L_f = length of the fired mass, L_p = length of the dry clay mass (dried at 110°C).

2.16.2 Determination of Fired volume shrinkage

Procedure: Sufficient quantity of clay was mixed with water to form a soft mass and allowed to stand covered with a wet cloth for 24 h. About 10 mm thick discs having a diameter of 25 mm were prepared by hand pressing the soft clay mass in the steel moulds. The discs were covered with wet cloth and were dried slowly at room temperature to avoid warpage and cracking. These discs were again oven dried by gradually raising the temperature and drying it at 105 to 110°C for 6 h. Fired the disc in a furnace at the required temperatures (soaking period 3 hour). Measure the volume of the disc. The fired volume shrinkage was measured as:

$$\text{Fired volume shrinkage, percent} = [(V_p - V_f) / V_f] \times 100$$

where V_f = volume of the fired mass, V_p = volume of the dry clay mass (dried at 110°C)

2.16.3 Determination of water absorption

Pellets prepared from the plastic mass (2.16.2) were fired at various temperatures and the water absorption was determined by soaking the fired buttons in water and measuring the amount of water absorbed.

Procedure: Clay pellets were prepared and fired as described above. These fired samples were immersed in a beaker containing distilled water and boiled for 5 h, taking care that the specimens were covered with water at all times. After 5 h, allowed the pieces to soak in water for 24 h. Wipe each piece lightly with tissue paper to remove water from the

surface. Avoid excessive blotting so that it will remove water from the pores. Then the water absorption was calculated as follows.

$$\text{Water absorption, percent, } A = [(W-D)/D] \times 100$$

where W = weight of saturated test piece and D = weight of the fired test piece.

2.16.4 Determination of Apparent Porosity

The apparent porosity is defined as the ratio between the volume of water or liquid capable of being absorbed into it and the total volume of the article.

Samples were prepared as in the case of volume shrinkage (2.16.2). Then the apparent porosity in percentage is given as:

$$P_a = [(W_c - W_a) / (W_c - W_b)] \times 100$$

where W_a = weight of the dry test piece, W_b = weight of the dry piece soaked with and suspended in the immersion liquid (water), W_c = weight of the test piece soaked with the immersion liquid and suspended in air.

2.16.5 Determination of Bulk Density

It is defined as the ratio of the mass of the sample to its bulk volume *i.e.* the volume of the material plus all its pores. It was determined by the boiling water method. Samples for the analysis were prepared by the procedure adopted for volume shrinkage determination (2.16.2). Then the bulk density was calculated as

$$\text{Bulk Density, } D_b = [W_a / (W_c - W_b)] \times D$$

where W_a = weight of the dry test piece, W_b = weight of the dry piece soaked with and suspended in the immersion liquid (water), D = density of the immersion liquid at the temperature that prevailed during the test (for water $D = 1$), W_c = weight of the test piece soaked with the immersion liquid and suspended in air.

2.16.6 Determination of Fired Strength

Fired strength of the clay samples was measured as in the procedure for green strength measurement (2.15.2). MOR of the samples fired at 1250°C has been calculated.

2.17 Physical Properties of Polymer- Kaolinite composite

The scope of the application of the polymeric materials has been widened by the incorporation of kaolinite into the polymer. This additive, when incorporated into a polymer, modifies the properties of the composites. The measured properties of the polymer-kaolinite composite include density, degree of equilibrium swelling and percentage of weight loss in toluene and mechanical strength properties.

2.17.1 Density Measurements

Cured natural rubber-kaolinite composites were analysed for the variation in density in order to evaluate the effects of surface modification. Samples of dimensions 10 × 10 × 1 mm were used for the measurements. Density was measured at room temperature after calculating the specific gravity of the samples by the ASTM D 792 test method as follows.

$$\text{Sp. Gravity, } S = a/(a + w - b)$$

Where a is the apparent weight of the specimen, without wire or sinker in air, b is the apparent weight of the specimen and of the sinker completely immersed and of the wire partially immersed in pure water and w is the apparent weight of the totally immersed sinker and the partially immersed wire. Thus the density of the composite was calculated as follows

$$D \text{ (g/cc)} = \text{Sp. Gravity, } S \times 0.9975$$

2.17.2 Degree of Equilibrium Swelling and Percentage of Weight Loss Measurements

The natural rubber can absorb liquids to a greater or lesser degree. The absorption of the liquid causes the rubber to increase in volume, and this is the phenomenon of swelling- a consequence of which is the deterioration in physical properties. Raw rubber is

completely soluble in certain liquids, but vulcanized rubbers are virtually insoluble. Strong bonds, such as chemical crosslinks between the rubber chains, prevent rubber molecules becoming completely surrounded by the liquid and restrict the deformation of the rubber. The swelling of the rubber by a liquid is a diffusion process. At the start of the process, the surface of a composite has a high liquid concentration while the liquid concentration in the bulk of the component is zero. Subsequently, the liquid molecules diffuse into the rubber just below the surface and eventually into the bulk of the rubber. As the diffusion process proceeds the dimensions of the rubber component increases until the concentration of the liquid is uniform throughout the component and equilibrium swelling is achieved. The amount of a given solvent that will diffuse into the rubber until it reaches equilibrium depends upon the number of crosslinks per unit volume of the rubber. The degree of swelling (V_r) is expressed as the volume fraction of the rubber in the swollen gel. The high swollen ratio, *i.e.* low V_r would indicate a very low crosslinking density of the bound rubber and vice versa.

Procedure: Cured test pieces of dimensions $10 \times 10 \times 1$ mm were allowed to swell in toluene until equilibrium swelling occurred (for a period of 120 h). After reaching the equilibrium, the swollen test pieces were weighed, then dried under vacuum, and again weighed. The swollen and deswollen weights were used to calculate the volume fraction of the rubber in the network swollen to equilibrium V_r , according to the following equation

$$V_r = \frac{D \times \rho_r^{-1}}{D \times \rho_r^{-1} + (S-D) \times \rho_s^{-1}}$$

where D = deswollen weight, S = swollen weight, ρ_s = density of the solvent and ρ_r = density of the rubber blend.

The cured test piece of above dimensions is used for weight loss measurements in toluene after ageing for 5 days. The percentage weight loss of the rubber composite is measured by the following equation

$$\text{Weight loss \%} = \frac{W_0 - W_1}{W_0} \times 100$$

where W_0 = original weight of the cured test piece, W_1 = weight of the vacuum dried test piece after ageing in toluene for 120 h.

2.17.3 Mechanical Strength Measurements

Mechanical strength measurements include the evaluation of the tensile properties such as break stress, break strain, modulus at 100% and modulus at 300%.

The tensile properties were measured by ASTM D412 test method with a Universal Testing Machine, Instron Model 1193, Instron Corporation UK with a crosshead speed of 500 mm/min. The dumb-bell shaped specimen of width 3.2 mm, gauge length – 15 mm and grip distance 32 mm was used for the analysis. Six samples were analysed consecutively from the same formulation. The tests were undertaken at $22.0 \pm 2^\circ\text{C}$ with an environmental humidity of $50 \pm 5\%$.

The tensile modulus, the break strain and modulus at 100% and 300% was calculated by applying varying loads.

Chapter 3

Mineralogy, Geochemistry and Utilization Study of Madayi Kaolin Deposit, North Kerala

3. 1. Introduction

Kaolin is an important industrial mineral and a potent geological indicator. The study of kaolinite is of great importance at basic and applied levels because of its ability to modify the structure in accordance with the surrounding environment and also its industrial versatility. The mineralogy, structure and morphology of kaolinite depend on different environmental factors (Keller, 1985). The clay mineral in a deposit represents the response of its constituent elements to the environmental energies impressed upon it. In other words a change in energy correspondingly reflects the properties of the clay minerals.

In the present work, a systematic study was carried out to show the variations in chemistry, structure and morphology of kaolinite collected from the deposit at Madayi village, ($75^{\circ} 15' 00'' - 75^{\circ} 16' 00''$ E; $12^{\circ} 01' 45'' - 12^{\circ} 02' 30''$ N) (Fig.3.1A), Kannur district, Northern Kerala. The availability of the different types of clays in this location was identified by the Department of Mining and Geology, Kerala (internal report, 1995) (Fig.3.1B). The characterization of clays collected from different layers gives a detailed picture of the mineralogical assemblages and the nature of the mineral species, which has been formed under the varying environmental conditions within the deposits. An attempt has been made to define the processes that lead to the formation of genetically different varieties of kaolinite within the same deposit by characterising different clay layers (Fig.3.1C). Laboratory tests were also conducted to identify the uses of china clay seam L (Fig.3.1C). It is a reserve of ~ 17 million tons within an area of 1.2 sq. kms, with proven industrial viability.

3.2. Geologic Setting

Geologically the area consists of Precambrian crystalline rocks overlain unconformably by thick sequence of Warkallai Formation of Miocene age. Thick deposits of residual and sedimentary clay sequences, having an overall thickness of

~45 meters are found associated with these. This clay deposit is confined within the Tertiary sedimentary basin, of North Kerala. Since it was found to be a potential and viable deposit, detailed investigation of the same was undertaken.

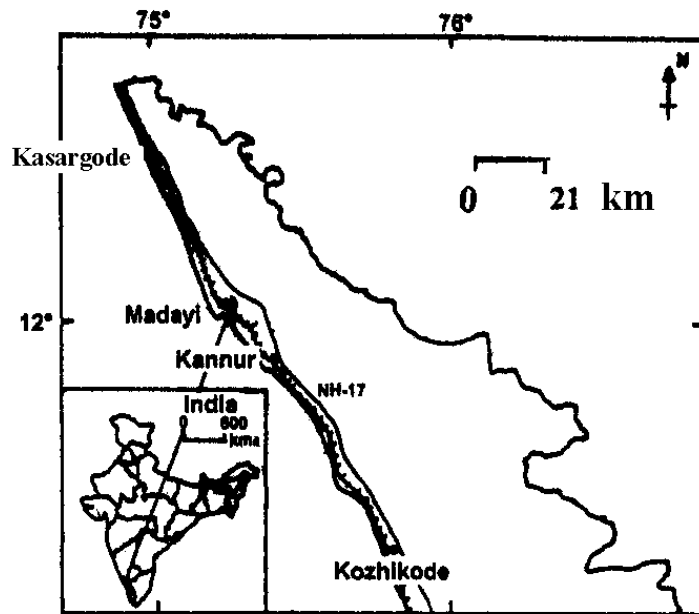


Fig.3.1A Schematic representation of the area under study.

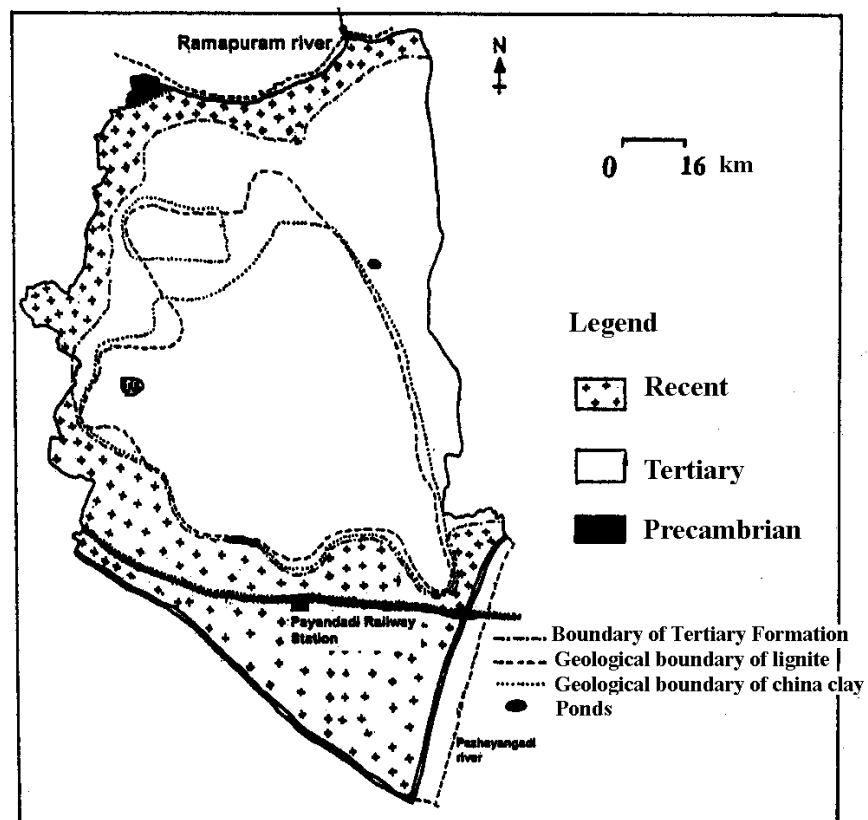


Fig. 3.1B. Geological map of Madayi.

The sedimentary deposit of this region belonging to Warkallai Formation of Miocene age is characterised by thin layer of sand, alternate layers of carbonaceous clays and lignite seams followed by iron rich variegated clay, laterite and bauxite with ferricretes at the top (Fig.3.1C).

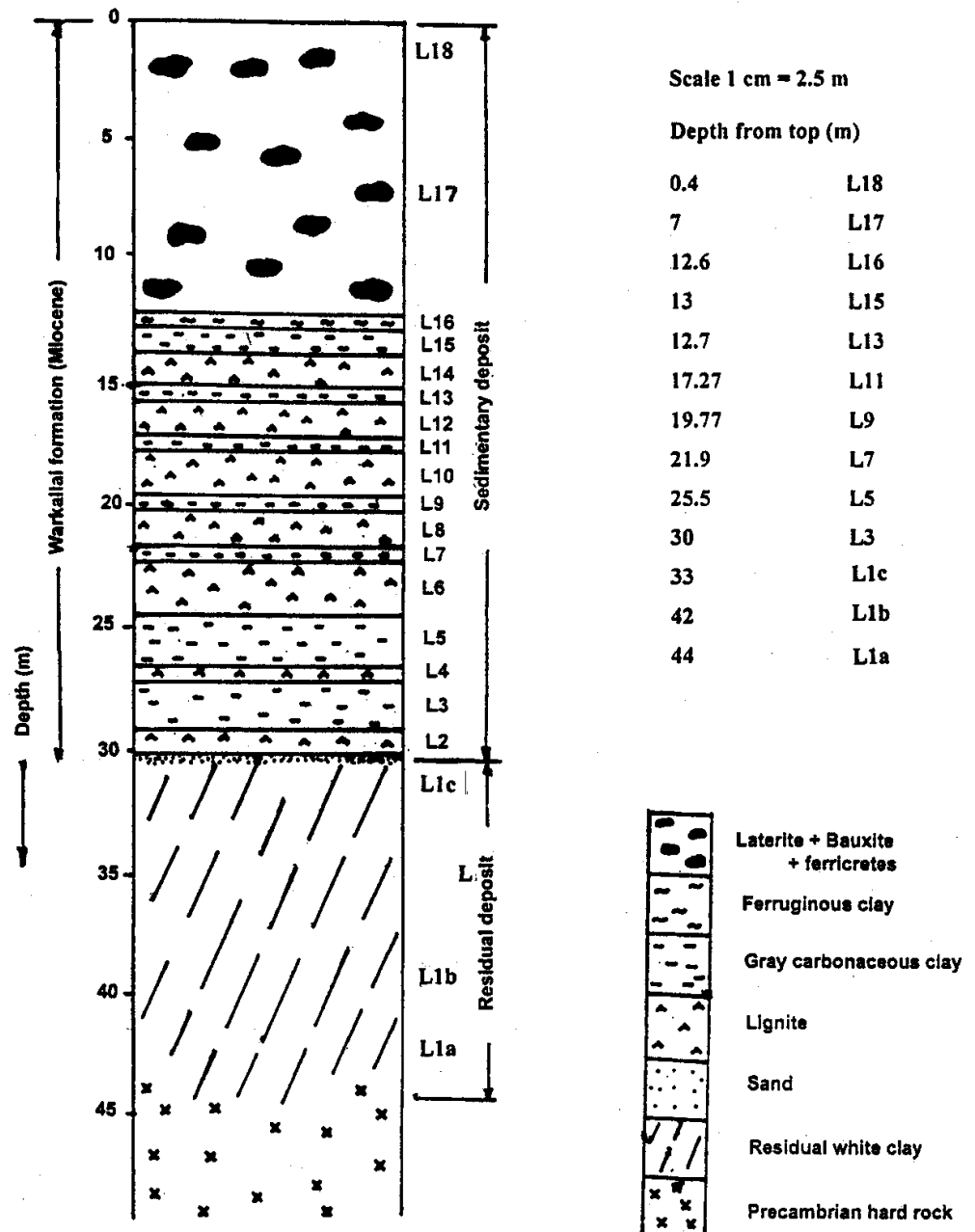


Fig.3.1C. Schematic cross section of Madayi deposit

Detailed field studies were undertaken and the field photographs of the three different types clays: white residual, gray carbonaceous and hematitic clays are shown in Fig 3.2 (A-F).

The bauxitic crust (L18), laterite (L17) and clay from L16 layer are grouped under the “hematitic clays”. The topmost bauxitic layer L18, which is found as a capping on the deposit, is too hard with numerous vesicles. The segregation of iron during bauxitization is evident from the banding of iron with different hue in these bauxitic samples (Fig.3.2A). The surface of bauxite shows encrustation of iron forming ferricretes. Some of them are of needle shape (Fig.3.2B). The lateritic bed having a thickness of around 11 meters underlie the bauxitic layer. Below these layers, the clay layer L16 occurs which is highly reddish in colour and has a thickness of around 0.6 meters. Figure 3.2C shows the association of lateritic clay layer (L17) and the ferruginous layer, L16.

The gray carbonaceous clay layers, L15, L13, L11, L9, L7, L5 and L3 alternate with lignite seams L14, L12, L10, L8, L6, L4 and L2 forming an overall thickness of about 17.5 meters. The upper two carbonaceous clay seams L15 and L13 show mottled reddish yellow patches. Black coloured patches of FeS_2 can be seen within the lower L9, L7 and L3 clay seams (Fig.3.2D). Fossilized plant remains such as roots and stems are found both in the carbonaceous clay and lignite seams. The entire sedimentary deposit is approximately 30 meters in thickness and is underlain by residual white clay. A thin veneer of sand separates the overlying sedimentary and the underlying residual clay.

The residual white clay L has a thickness of around 15 meters. Sampling from this thick seam of clay was done at 5 meters interval (L1a, L1b and L1c), in order to analyse the variation in the geochemical factors with depth (Fig. 3.1C). These clays show relict structures like foliation and quartz vein (Fig.3.2E) that is inherent from the parent rock, quartzo-feldspathic mica gneiss, which is of Precambrian age. Numerous fossilized plant roots confining approximately to 0.1-0.35 meters of the topmost portion of residual clay L, were identified during field studies (Fig.3.2F). This shows evidence of plant growth and subsequent weathering prior to Tertiary sedimentation. Field evidences and geological studies of the regions around North Kerala by Rajendran *et al.* (1987) indicate the influence of two spells of lateritisation of pre-Warkallai and post-Warkallai-pre-Quaternary age on the country rock. The pre-Warkallai lateritisation resulted in the formation of the thick white residual clay. In addition, weathering after the deposition of Warkallai Formation resulted in thick deposits of laterites and bauxite which overlie the gray carbonaceous clay seams.

Fig.3.2A. Bauxitic clay sample chipped out from the L18: Layering of iron. Cavities are seen indicating recrystallization/remobilization of the parent material.

Fig.3.2B. Hematite needles from the bauxitic crust resulting from the remobilization and leaching of Al_2O_3 and SiO_2 .

Fig.3.2C. Field photo of L16/L17 ferruginous layer lateritised clay layers (arrow).

Fig.3.2D. Pyrite patch within the gray carbonaceous clay L9.

Fig.3.2E. Residual white clay showing quartz vein.

Fig.3.2F. Fossilized plant remains from the topmost portion of residual white clay.

3.3. Materials and Methods

Representative clay samples were collected from each of the recognisable layers (Fig. 3.1C). Sampled materials were crushed in an agate mortar and a fraction of the raw clay was used for mineralogical and chemical analysis. Heavy mineral fractions in raw clay were separated by bromoform for mineralogical analysis. The < 2 µm clay fraction separated by sedimentation and centrifugation was analyzed for clay minerals and associated impurities by XRD and DTA. Structural characterization of the < 2 µm fraction of kaolinite was carried out by FTIR spectroscopy and Crystallinity Index measurements. Hinckley Index (Hinckley, 1963) and Amigo Index (Amigo et al., 1987), were calculated for crystallinity index measurements.

XRD analysis was performed using Ni-filtered Cu-K α radiation (40 kV, 20 mA) at a scan speed of 1° 2 θ /min. DTA was carried out using a Seiko 320 TG/DTA analyser at a heating rate of 10°C/min in the range ambient-1100°C with alumina as standard. The FTIR spectra of 1 mg pretreated fraction, mixed and pelletised with 200 mg of KBr, were recorded after overnight drying at 60°C. The samples were scanned over the range of 4000 – 400 cm⁻¹ using a Perkin Elmer Spectrometer.

The pH of the raw clay samples was measured using 1:4 clay water ratios. Organic carbon in these samples was determined by oxidative decomposition using K₂Cr₂O₇ as the oxidizing agent (Gross, 1971). The concentration of pyritic and non-pyritic iron was determined by acid dissolution technique (Schneider and Schneider, 1990). The raw clay and < 2 µm fraction were analyzed for SiO₂, Al₂O₃, Fe₂O₃, TiO₂, K₂O, CaO, Na₂O, MgO, and LOI (Bennett and Reed, 1971). The trace element analysis of selected raw samples (L1a, L7, L16, L17 and L18) was carried out by AAS.

Scanning electron microscopic analysis of raw clay and hand picked plant remains was performed using a JEOL JSM 5600 LV Microscope as explained in chapter 2.

Petrographic studies were undertaken using polarizing microscope for mineral characterisation.

From the technological point of view extensive laboratory investigations were conducted on the < 45 µm fraction of residual china clay L, as it is an economically viable seam within the Madayi deposit. The physical properties and firing behaviour

were tested for evaluating their utilization in the ceramic industry. Grain size analysis was carried out by Micromeritics Sedigraph 5100 using calgon as the dispersant. Viscosity measurement of 63% w/w slurry was undertaken with a Brookfield viscometer using minimum concentration of sodium polysalt as dispersing agent. Brightness improvement studies of crude and calcined samples (350°C, 1 h) (Kogel *et al.*, 1999) were undertaken by chemical leaching using sodium hydrosulphite and oxalic acid as leaching agents. In the case of leaching with sodium hydrosulphite, the clay slurry was treated for 30 minutes with stirring. For oxalic acid treatment, samples were kept undisturbed for a reaction time of 12 h after thorough mixing. All the experiments were conducted at room temperature in 1:2 clay: water ratio with various concentrations of the leaching agents. The efficiency of the two reagents on the brightness improvement for the clays were measured using Color Touch Model ISO brightness meter. Brightness was measured on dried samples (110°C, 1h) at 457 nm and the yellowness as a difference in brightness between 570 and 457 nm. The water of plasticity, green MOR, fired MOR (1250°C) and linear shrinkage (dry and fired, 1250°C), were measured as specified in ASTM standards. Volume shrinkage, bulk density, water absorption and apparent porosity (ASTM) of the samples were analysed by firing the samples at temperatures 600, 800, 1000 and 1250°C (one hour soaking). The fired color of the sintered samples was also noted.

Detailed procedure of all the experimental methods adopted are presented in Chapter 2.

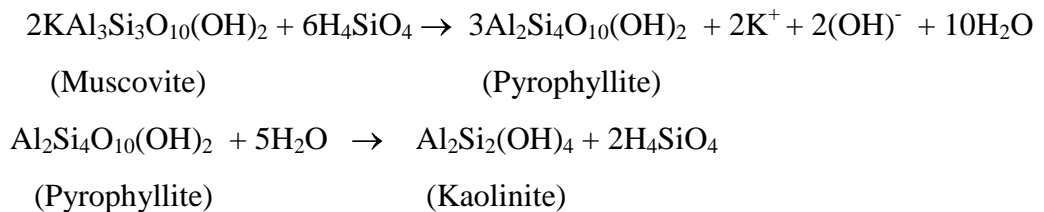
3.4. Results and Discussions

3.4.1 XRD studies

The mineralogical analysis of raw clay and the < 2 µm fraction are summarized in Table 3.1. The constituent minerals are expressed as major, minor and trace depending upon their concentration. In addition, heavy mineral fraction of the samples from the selected clay layers was also analysed for mineral characterisation. The mineralogical evaluation of the three different clays: residual white, gray carbonaceous and hematitic clays are discussed below.

3.4.1.1 Residual white clay (L1a, L1b and L1c)

The residual clays L1a, L1b and L1c consist chiefly of kaolinite and quartz with appreciable amount of muscovite (Fig.3.3A). Muscovite, which is present in the parent rock, is relatively more in L1a. Considerable amount of gibbsite and pyrophyllite are also present in L1b and L1c, along with muscovite. Their absence in L1a is attributed to lower degree of alteration for these clays. The fine fractions (< 2 µm) (Fig.3.3B), of L1b and L1c are devoid of pyrophyllite, showing its complete conversion to kaolinite. The same conclusion was reported by Heckroodt *et al.* (1987) suggesting the formation of pyrophyllite from muscovite during early stages of weathering and its alteration to kaolinite at a later stage. The reaction involving the formation of pyrophyllite and its subsequent alteration to kaolinite is as follows:



The presence of this 2M1 mica, pyrophyllite in the raw clay samples in uppermost portions of the weathered profile (L1b and L1c) and their absence with depth (L1a), where there is higher amount of muscovite supports the above view of alteration. Microcrystalline quartz and fine-grained mica *i.e.* illite constitute minor ingredients. The entire sequence of these residual clays L1a, L1b and L1c shows a similar value for the mica (illite) crystallinity index (half – height peak breadth of the white mica 10 Å peak); Kubler Index (0.3 Δ2θ), (Kubler, 1968). This is indicative of the absence of any diagenetic transformation. The occurrence of illite in these clays solely results from the disintegration of muscovite.

The concentration of heavy mineral fraction is very little in L1b and L1c. Muscovite is the major mineral found in this fraction of L1a clay (Fig. 3.3C).

Table 3.1. Semiquantitative mineralogical analysis by XRD (raw clay and <2 μm fraction)

Sample	K	Sm	M	Py	I	Gi	Q	P	Ma	He	A
Raw clay:											
L1a	***		***				***				
L1b	***		**	**	*	*	***				
L1c	***		**	**	*	*	***				
L3	***					**	***	**	**		*
L5	***					**					
L7	***					**	***	**	**		*
L9	***					**	***	**	**		
L11	***					**	***	**	**		
L13	***						***	*	*		
L15	***							**	**		
L16	***						*			***	
L17	***						***			***	
L18	*					***	*			***	
< 2 μm											
L1a	***		**								
L1b	***				**	*	*				
L1c	***				**	*	*				
L3	***					**	**	**	**		
L5	***	*				**					
L7	***					**	***	**	**		
L9	***						***	**	**		
L11	***					**					
L13	***							*	*		
L15	***						**	*	*		
L16	***									**	
L17	***									**	

K-kaolinite, Sm- smectite, M- muscovite, Py- pyrophyllite, I- illite, Gi- gibbsite, Q- quartz, P- pyrite, Ma- marcasite, He- hematite, A- anatase.
 major ***, minor **, trace* minerals

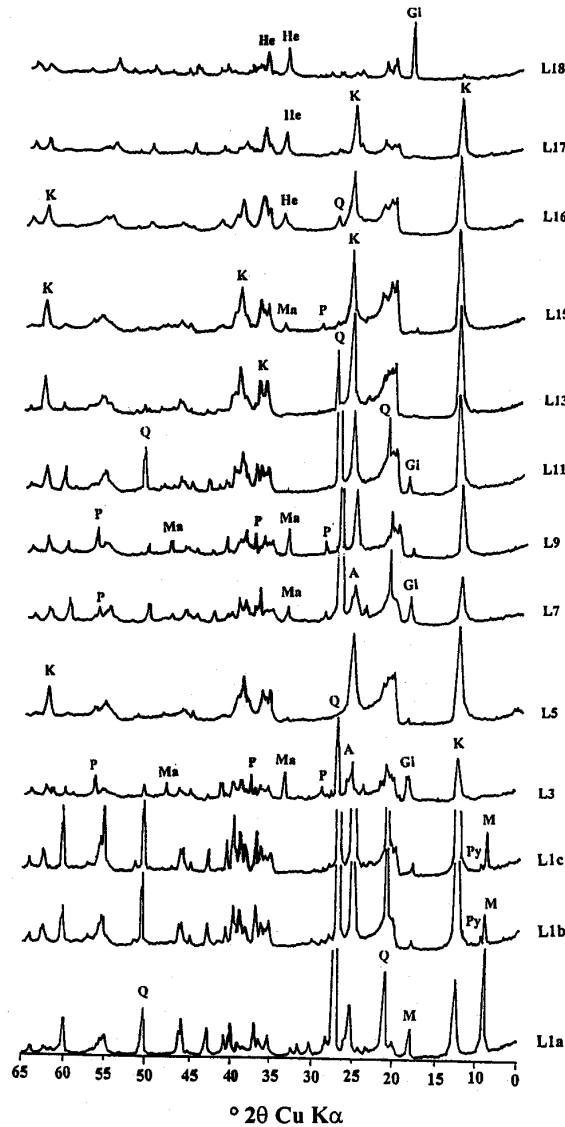


Fig.3.3A. X-ray diffractograms of raw clay samples: L1a, L1b and L1c- the lowermost residual clay layer, L3, L5, L7, L9, L11, L13, L15- the carbonaceous gray clay with decreasing order of depth from the top, L16- ferruginous clay, L17-lateritised clay and L18- bauxite. K- Kaolinite, Py- Pyrophyllite, Gi- Gibbsite, Q- Quartz, P- Pyrite, Ma- Marcasite, M- Muscovite, He- Hematite, A- Anatase.

3.4.1.2 Gray carbonaceous clay (L3, L5, L7, L9, L11, L13 and L15)

Most of the gray carbonaceous clays, except L5, exhibit an association of pyrite and marcasite along with kaolinite, quartz and gibbsite. Sedimentary pyrite formation occurs during the reaction of detrital iron mineral with H_2S , which was formed by the reduction of sulphate by bacteria in the presence of organic matter (Berner, 1984). The XRD analysis of the sample from the black patched portion indicates the presence of FeS_2 (Fig.3.3D - a). The small shoulder at 3.52 \AA in the XRD patterns (Fig.3.3A) of L3 and L7 indicates anatase. Trace amounts of smectite (14 \AA) was identified in

L5 (Fig.3.3B). The formation of smectite is favoured by a microenvironment with poor drainage and hence, minimum leaching condition with relatively high metal ion concentrations (Keller, 1985).

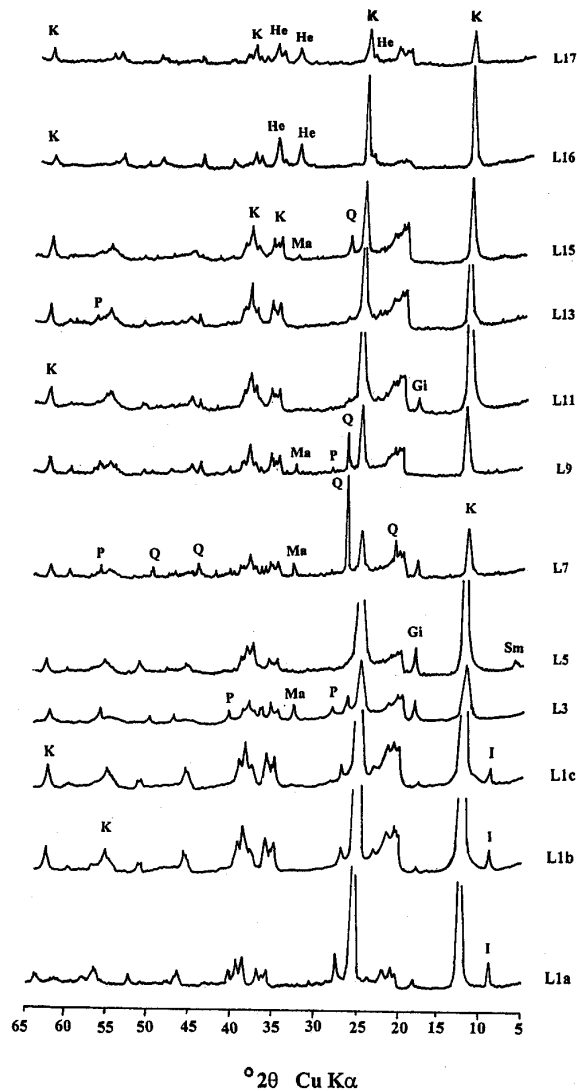


Fig.3.3B. XRD patterns of oriented $< 2 \mu\text{m}$ clay fraction: L1a, L1b, L1c- the lowermost residual clay layer; L3, L5, L7, L9, L11, L13, L15- the carbonaceous gray clay with decreasing order of depth from the top; L16- ferruginous clay and L17- lateritised clay. K- Kaolinite, Gi- Gibbsite, Sm- Smectite Q- Quartz, P- Pyrite, Ma- Marcasite, I- illite, He- Hematite, A- Anatase.

Gibbsite identified by the 4.84 \AA peak in L3, L5, L7, L9 and L11 give evidences of intense leaching in strongly deionized environment under tropical climate (Vazquez, 1981) during desilication *i.e.* dissolution of Si from its aluminosilicate parent material. From the available information it is not clear whether the gibbsite found in these carbonaceous clay is the product of post or pre-depositional alteration. The

association of the above minerals, gibbsite and smectite in the same clay resulted from the changes in the microenvironment during the clay deposition or formation. Fine quartz grains ($< 2 \mu\text{m}$) were noted in the carbonaceous clays having high amounts of marcasite/pyrite (evident from peak intensity, Fig.3.3B). Chen *et al.* (1997) suggests formation of microcrystalline quartz as a result of rearrangement of feldspar and muscovite structure during kaolinization or kaolinite recrystallisation. Heavy mineral fraction of the selected samples L3 and L11 are shown in Fig. 3.3C. For L3, the mineralogical association includes pyrite, marcasite, anatase and rutile. Sillimanite is the sole mineral identified in this fraction of L11 clay.

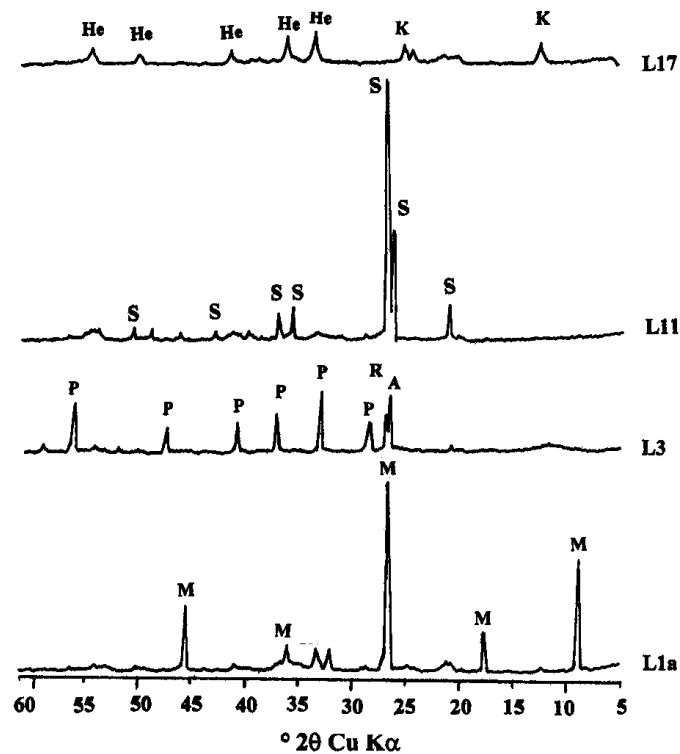


Fig.3.3C. XRD patterns of heavy mineral fraction of the selected samples L1a, L3, L11 and L17: M- Muscovite, S- Sillimanite, P- Pyrite, A- Anatase, R- Rutile, K- Kaolinite and He- Hematite.

3.4.1.3 Hematitic clay (L16, L17 and L18)

The ferruginous clays L16 and L17 show an assemblage of kaolinite, quartz and hematite. Hematite is concentrated in the fine clay fraction. The uppermost hard bauxitic crust consists entirely of gibbsite and hematite. Here kaolinite is found only in traces. The intensity of leaching of silica and alumina from this rock, which is present in the topmost portion of the profile, is evident from the presence of small iron nail like material strewn through out the uppermost portion of the bauxitic crust

(Fig.3.2B). The XRD analysis shows that this material is entirely of hematite (Fig.3.3D-b), which has a higher crystallinity than that of the hematite in laterite and bauxite as evident from the sharp peaks (Fig.3.3A). The concentration of hematite in the uppermost portion of this clay profile shows a congruent dissolution of kaolinite by removal of SiO_2 and Al_2O_3 and simultaneous enrichment of Fe_2O_3 , which occurs at the final stage of intense tropical weathering. The XRD analysis indicates that, as the intensity of weathering progresses, the crystallinity of the above iron mineral also increases. The above mineralogical evidences confirm that the hematite needles are the products of leached out remains of the bauxitic crust. Such hard iron oxide crusts are extremely wide spread in tropical countries due to lateritic weathering (Bruckner, 1952). Low intensity peak of kaolinite in heavy fractions in these clays shows the presence of this aluminosilicate as occlusion within hematite (Fig 3.3C).

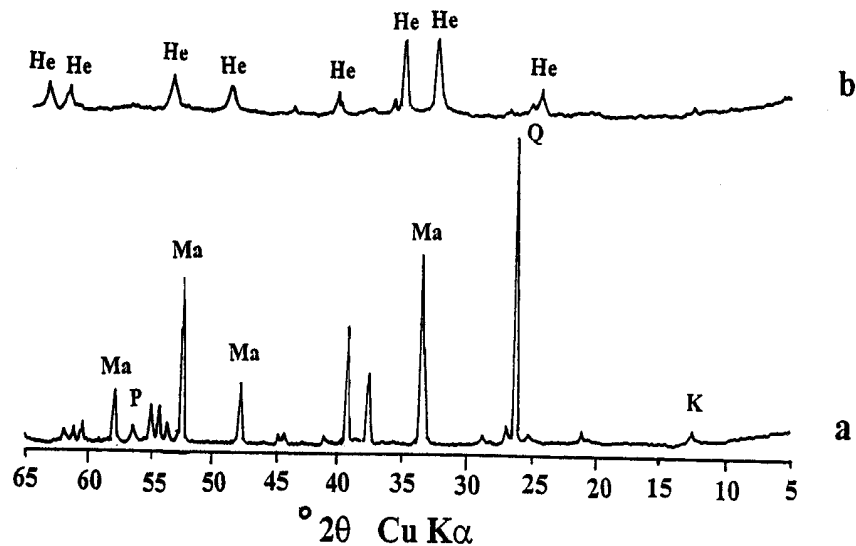


Fig.3.3D. XRD patterns of a) Pyrite patch from gray carbonaceous clay L9 and b) Iron needles from the topmost bauxitic clay L18. K- Kaolinite, Q- Quartz, Ma- Marcasite, P- Pyrite, He- Hematite.

The presence of hematite indicates an oxidizing environment and the presence of Fe-sulphide a reducing environmental condition during the formation or deposition of gray carbonaceous and ferruginous clay layers.

3.4.2 Crystallinity Index Measurements

Kaolinite crystallinity index measurements: HI- Hinckley Index (Hinckley, 1963), FWHM 001 and FWHM 002- index of Amigo et al. (1987) are given in table 3.2. The crystallinity indices of the kaolinite from different layers show variation.

The Hinckley crystallinity index of kaolinite varies from one clay layer to the other (Table 3.2). This variability may be attributed to the differences in the geological environment *viz.* the intensity of weathering and the extent of transportation suffered by the clay during their formation/deposition (Brindley *et al*, 1986). Hinckley crystallinity index varies between 0.44(L5) to 1.10(L1a). The Amigo index also shows a similar trend in order- disorder for clays from different layers.

3.4.3 Chemical assay of clays from different layers

The chemical analysis data and pH values of the samples from residual white, gray carbonaceous and hematitic clay layers are briefly discussed below (Table 3.2).

3.4.3.1 Residual white clays: L1a, L1b and L1c

The SiO₂ and Al₂O₃ contents of L1a, L1b and L1c were consistent with the mineralogical observations. Percentage of K₂O was found to be in the order L1a>L1b>L1c. The relatively lower K₂O concentration in L1b and L1c compared to L1a from the same seam at 5-10 meters of depth difference indicates its preferential leaching from muscovite. Higher Fe₂O₃ (2.17%), Na₂O (0.26%), CaO (0.22%) and MgO (0.23%) for this clay (L1a) reflects a lower intensity of leaching of the parent material with depth.

3.4.3.2 Gray carbonaceous clays: L3, L5, L7, L9, L11, L13 and L15

The major oxide, SiO₂ in gray carbonaceous clay is relatively lower than that in the residual clays described above. This might possibly be due the winnowing action during transportation and sedimentation. Lack of a particular trend in the TiO₂ distribution with depth, indicates its immobile nature, during weathering. MgO concentrated in fines is attributed to smectite. High Fe₂O₃ accounts for the presence of FeS₂ minerals, marcasite and pyrite (Table 3. 2).

Table 3.2. Chemical analysis of clay samples from different layers (wt%)

	L1a	L1b	L1c	L3	L5	L7	L9	L11	L13	L15	L16	L17	L18
SiO ₂	67.44	65.03	63.9	34.92	51.07	46.49	35.02	52.60	43.24	37.67	43.47	28.54	9.86
	46.86	45.26	46.02	36.82	38.98	38.06	37.59	40.31	41.38	39.76	28.21	34.42	
Al ₂ O ₃	18.77	21.61	23.91	26.23	26.92	25.45	28.72	27.08	33.69	37.30	29.77	31.72	41.57
	35.42	38.02	37.17	29.20	36.85	34.06	37.01	36.89	37.02	38.06	35.22	35.52	
Fe ₂ O ₃	2.17	1.43	1.27	10.76	1.97	6.64	9.81	1.35	2.36	2.89	11.90	22.66	27.57
	1.59	0.38	0.75	6.82	1.26	5.34	2.87	1.42	1.34	2.68	22.20	13.47	
TiO ₂	0.57	0.02	1.30	1.00	0.98	1.44	1.59	1.35	1.84	3.35	1.85	4.40	1.13
	0.89	0.06	0.32	0.10	0.81	2.27	2.86	3.62	2.54	1.05	0.16	2.15	
Na ₂ O	0.26	0.16	0.12	0.26	0.18	0.29	0.22	0.21	0.17	0.18	0.37	0.41	0.34
	0.19	0.45	0.33	0.45	2.04	0.67	0.53	0.67	0.58	0.98	0.36	0.24	
K ₂ O	2.51	1.90	1.08	1.05	0.60	2.24	2.24	3.73	1.50	1.20	0.09	0.04	0.05
	1.89	0.65	0.39	0.37	1.83	0.55	0.51	0.49	0.58	0.54	0.58	0.05	
MgO	0.33	0.23	0.01	0.04	0.07	0.01	0.03	0.01	0.05	0.27	0.21	0.19	0.39
	0.16	0.06	0.11	0.13	0.52	0.02	0.15	0.06	0.33	0.40	0.49	0.21	
CaO	0.22	0.10	0.13	0.13	0.28	0.39	0.41	0.18	0.13	0.14	0.38	1.10	1.38
	0.33	0.11	0.13	0.41	0.55	0.42	0.28	0.28	0.13	0.28	0.70	0.82	
LOI	9.10	9.59	9.38	24.49	18.20	17.33	21.62	13.04	17.13	17.13	12.81	11.64	18.20
	13.34	14.41	14.69	25.56	17.04	18.36	17.93	16.02	15.43	16.75	12.08	13.00	
C [#]	bdl	0.21	0.45	7.23	1.08	3.31	5.84	0.99	0.64	0.73	0.42	0.09	0.16
FeS ₂ [#]	bdl	0.18	0.31	9.96	1.15	8.47	15.37	1.34	0.95	1.36	bdl	bdl	bdl
pH [#]	5.01	3.99	3.49	2.64	3.14	2.75	2.67	3.29	2.77	2.77	5.48	5.66	5.88
HI [*]	1.10	0.86	0.69	0.72	0.44	0.70	0.70	0.51	0.64	0.50	0.67	0.57	0.53
^δ AI													
	(001)	0.45	0.50	0.45	0.45	0.50	0.50	0.40	0.55	0.45	0.35	0.40	0.45
(002)	0.45	0.45	0.40	0.40	0.50	0.40	0.38	0.50	0.40	0.40	0.30	0.40	0.35

Upper readings relate to raw clay, Lower readings relate to < 2 μm fraction

[#] raw clay, ^{*} < 2 μm fraction, HI- Hinckley Index, ^δ - Amigo Index,

bdl - Less than detection limit

3.4.3.3 Hematitic clays: L16, L17 and L18

Hematite contributes to the major source of iron in ferruginous clay (L16), laterite (L17) and bauxites (L18) and the maximum iron content of this deposit is found in

raw fraction of bauxite (27.57%)(Table 3.2). An upward increase of this transition element concentration in these layers might have resulted from the leaching out of silica and alumina from the structure of kaolinite and quartz and simultaneous enrichment of Fe₂O₃ mostly in the form of hematite. This is also reflected in the depletion of concentration of the major element, SiO₂ (9.86%).

3.4.4 Variation of pH of the clay profile

The pH of the clays ranges from 2.64 to 5.88. The high acidity implies the effect of ongoing weathering. The acidity correlates with FeS₂ and organic carbon content. The pH is the lowest in L3 (2.64) where organic carbon (7.23%) and FeS₂ (9.96%) are relatively high. FeS₂ is highly concentrated in L9 (15.37%), L7 (8.47%) and L3 (9.96%) where the carbon content and Fe₂O₃ are also high.

3.4.5 Trace Element Analysis

The behaviour of trace element during rock weathering has been discussed by several investigators (Goldschmidts, 1958; Rankama and Sahama, 1952). The distribution of trace elements: Cr, Cu, Ni, Pb, Zn, Co and Mn from clay layers: L1b, L7, L16, L17 and L18 show a definite pattern (Fig.3.4).

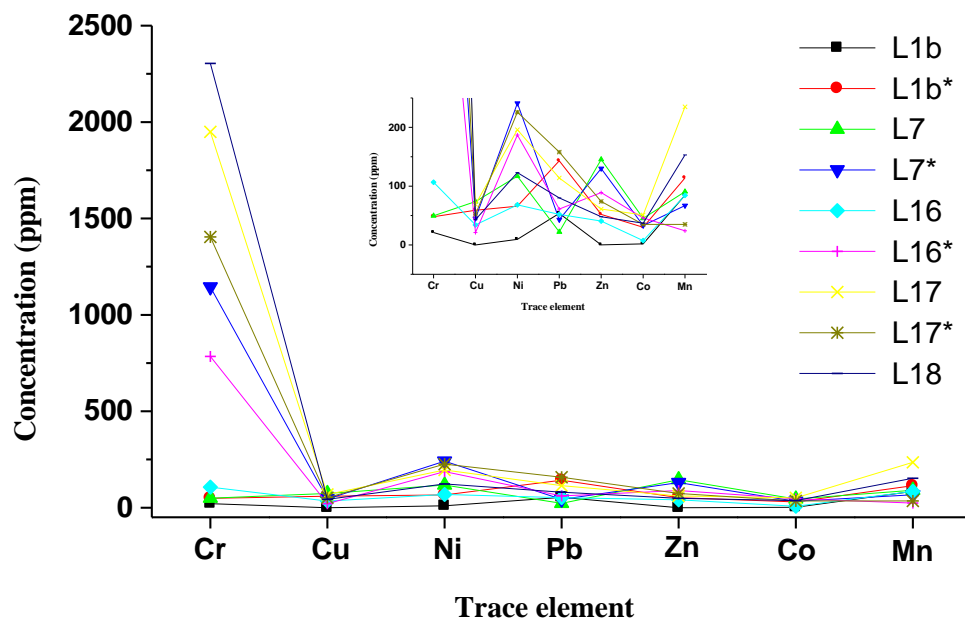


Fig.3.4. Trace element patterns of selected clay samples L1b, L7, L16, L17 and L18 (Sample code with * represents the corresponding < 2 μm fraction)

The concentration of Cr^{3+} is maximum relative to other ions. Cr^{3+} (0.64 Å) has a radius very similar to those of aluminum Al^{3+} (0.57 Å) and ferric iron (Fe^{3+} 0.67). Higher Cr content in bauxite could be explained because of the isomorphous substitution of these ions in aluminous and ferric oxyhydroxy minerals. Elemental analysis of major constituents also confirms this view, since maximum concentrations of the above oxides are present in the bauxitic clays.

Cu content falls in the same range in all the clay samples. This element exhibits a correlation with that of Zn *i.e.* for an increase in the concentration of Cu, the Zn content also increases indicating the same trend. Co also shows a comparable relationship with Zn. For a sample with very high concentration of Co, Zn shows a high value. The Ni content is maximum for the sedimentary clays and is concentrated more in the fine fractions, suggesting their concentration during the course of weathering, transportation and deposition. Mn shows a relatively higher concentration for the raw fraction of laterites. The concentration of trace elements has a strong relation with the concentration of total iron. Total trace element concentration is maximum in bauxite (2788 ppm), where there is a higher amount of iron. This phenomenon is evident from the chemical analysis data as well. The above evidences of variation in the trace constituents resulted from the varying petrogenetic conditions that the rock was subjected to.

3.4.6 Thermal studies

The thermal studies of kaolinite are undertaken using differential thermal and thermogravimetric analysis. The characteristic patterns of the fine fractions (< 2 µm) have been presented in Fig. 3.5A & B.

3.4.6.1 DTA studies

DTA patterns (Fig. 3.5A) show features related to the mineralogical assemblage and the kaolinite structure. The endotherm due to dehydroxylation and exotherm resulting in a new phase formation (mullite) are seen in the range 487 to 542°C and 955 to 1003°C respectively. Higher exothermic temperatures for kaolinite were noted in L1b (1000.9°C) and L1c (1003.5°C) and lower peak temperatures were noted in the uppermost bauxite, where the concentration of kaolinite is the least (954.8°C). Compared to the residual clays L1b and L1c, the sample L1a has relatively lower

endothermic and exothermic peak temperatures. This results from the presence of illite, *i.e.* finely divided mica which remains in the system as an impurity.

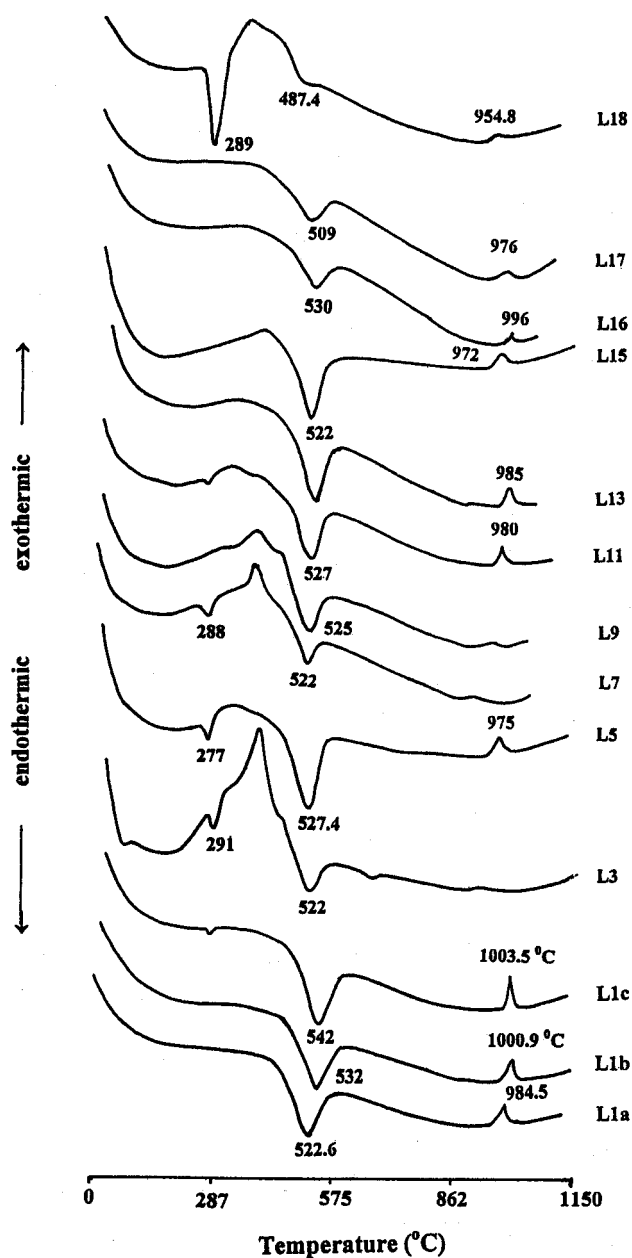


Fig. 3.5A. Differential thermal analysis curves of < 2 μm fraction showing varying endothermic-exothermic temperature

The exothermic peak typical of kaolinite is not prominent in L3, L7 and L9 where there is higher concentration of pyrite, which can give a mild fluxing action affecting the thermal property. An additional peak at 450°C was also noticed in the above clays, which is characteristic of pyrite (Grimshaw and Searle, 1958). X- ray analysis and chemical assay also support this evidence. The dehydroxylation temperature at 277 to

291°C is of gibbsite. The above mineral is concentrated more in the uppermost bauxite, as evident from the intensity of the endothermic peak at 289°C.

3.4.6.2 TG studies

The thermogravimetric patterns (Fig.3.5B) of the fine fraction is consistent with mineralogical and chemical analysis.

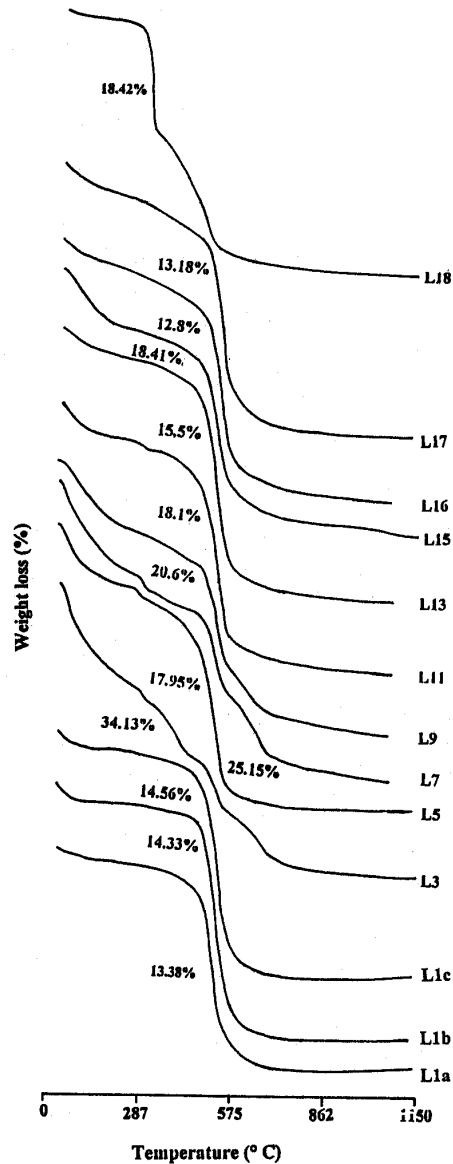


Fig. 3.5B. Thermogravimetric curves of < 2 μm fraction indicating varying percentage weight loss depending on mineral assemblages.

The weight loss during thermal treatment is maximum for the carbonaceous clays. The maximum value of weight loss is for L3 (34.13%) where there is higher FeS_2 and organic matter and a lower value is noticed for the L16 (12.8%), the ferruginous clay

layer. In bauxite the abrupt weight loss at around 289°C results from the dehydroxylation of gibbsite. Very low weight losses around this temperature were also noticed for the samples L11, L7, L5 and L3 due to the presence of the above mineral in traces. This is also confirmed from the mineralogical analysis.

3.4.7 FTIR studies

The structural analysis of kaolinite by XRD and DTA was further complemented by its detailed FTIR studies as well. Fine < 2 µm fractions of clay samples after the removal of iron, organic carbon and carbonates (Al-Khalissi and Worrall, 1982) were subjected to IR spectral studies. The spectra (Fig.3.6) gave valuable information about the degree of crystallinity and regularity of the structure of the clay minerals (Russell, 1987). IR spectra show the prominent peak of kaolinite: 3620- 3700 cm⁻¹ (-OH stretching), 1000-1120 cm⁻¹ (-Si-O stretching), 910-940 cm⁻¹ (-OH bending) and 400-550 cm⁻¹ (-Si-O bending) vibrations (Farmer, 1979). The difference in band intensities as evident from the peak height differences, suggest the variation of defects in kaolinite structure. The doublet between 3694 and 3619 cm⁻¹ for L1b, L3, L7, L11, L13 and L15 is indicative of well ordered kaolinite structure (Farmer, 1979; Russell, 1987). Degree of order for the above clays is also clear from the band intensities at 791 and 751 cm⁻¹. The relative intensity of these bands is the same for ordered kaolinite and the band at 791 cm⁻¹ becomes weak with increasing disorder. The presence of the doublet in the above gray carbonaceous clays, which has lower Hinckley index (Table 3.2), might be due to the mixture of ordered and disordered kaolinite. The above features could be explained based on the order/disorder index proposed by Placon *et al.* (1989), which measures the relative proportion of high-defect components. The ordered kaolinites as evident from FTIR spectra are found to be formed as a result of the recrystallization of low order detrital ones. The above evidence of recrystallization is further clear from SEM studies. But in the case of bauxite, L18 the IR peak shows a different pattern. The OH bands around 3653 cm⁻¹, shows a slight shift towards the lower value of wavenumber *i.e.* around 3647 cm⁻¹. In addition, the intensity of the 3694 cm⁻¹ peak is much less compared to the 3619 cm⁻¹ peak, indicating a lower order of crystallinity. In all other clay samples, 3694 cm⁻¹ peak is more intense compared to the other. In addition prominent peaks characteristic

of gibbsite occurs at 3529, 3449, 3392 and 3377 cm^{-1} in the OH stretching region. The -Si-O stretching, -OH bending and -Si-O bands show slight shift in the peak values.

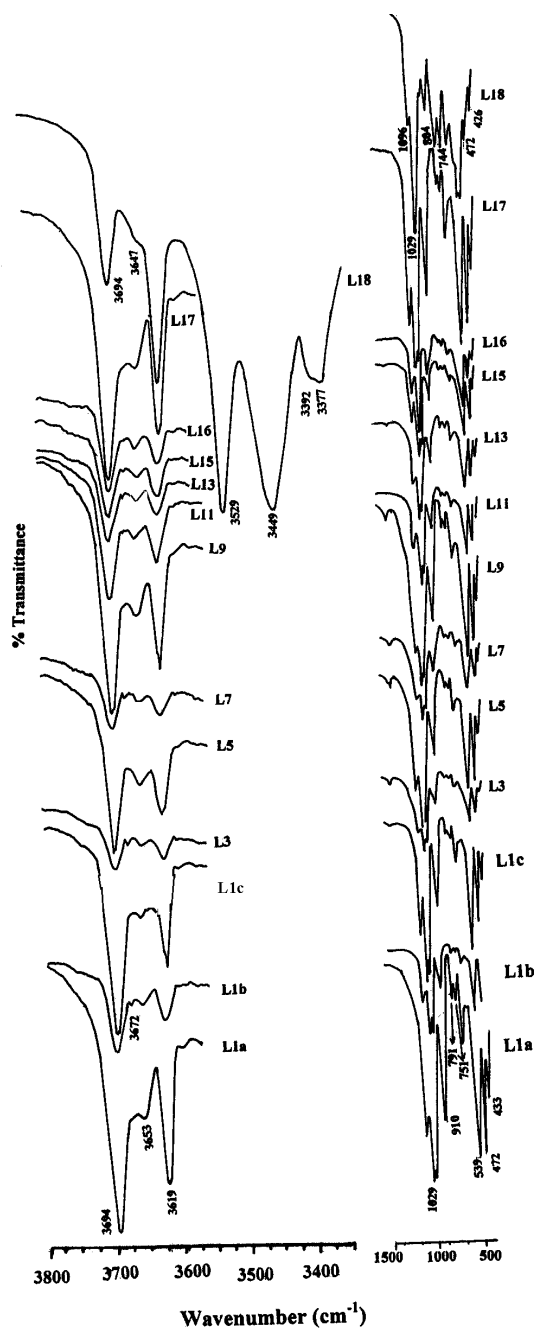


Fig. 3.6. FTIR spectra of $< 2 \mu\text{m}$ clay sample ($3800 - 3350\text{cm}^{-1}$) ($1500-400\text{cm}^{-1}$) with weak doublet between 3694 and 3619cm^{-1} and relative intensities of 791cm^{-1} and 751cm^{-1} reflecting the crystalline order of kaolinite; note the variation in the peak value of L18 reflecting high gibbsite concentration.

3.4.8 Morphological Studies

Scanning electron micrographs and Optical micrographs of clay from L1b, L3, L5, L15, L16, L17, L18 and the fossilized plant remains clearly indicate the geochemical

processes and the environment in the genesis of the three distinct clays, residual white clay, sedimentary gray carbonaceous and the hematite rich clays in this particular deposit.

3.4.8.1 Residual white clay

Optical microscopic studies of mineral grain collected from the residual clay layer, shows the variation in the intensity of alteration which reflects the leaching conditions. This variation is very prominent from the textural features of muscovite (Fig.3.7). The residual clay L1a, which is at greater depth compared to L1b and L1c of the same seam shows ample well developed platy muscovite grains with a little alteration (Fig.3.7a- d). The grains a, b and d show sharp grain outline. Some of the grains show coating of iron oxide on their surfaces (Fig.3.7c). The extent of alteration of muscovite increases upward in the clay profile. For L1b most of the muscovite grains are corroded with numerous etch pits on their surfaces and edges (Fig.3.7 e-h). The muscovite grain from the uppermost residual clay layer L1c is found to be altered with features such as etched surfaces and embayed edges (Fig.3.7i). The crystal edges are found to be rounded in contrast with the one from the lower most L1a sample depicting the intensity of weathering under acid rich environment.

Quartz grains show rainbow like features on their surfaces due to difference in the order of interference colours (Fig.3.8a- c), reflecting the non-uniformity in the thickness of the grains. Some of these grains show inclusions of anatase/rutile and zircon (Fig.3.8b and c).

The heavy minerals from L1a show some opaque grains, with alteration features (Fig.3.8 d & e). These opaque grains are absent in the uppermost layers showing their complete leaching or transformation during weathering. In addition to this, the mineral anatase (TiO_2) in traces is also present in all the layers, L1a-c (Fig.3.8.f&g). Considerable amount of zircon grains of varying size and shapes are also noticed (Fig.3.8 h – l).

Fig.3.7. Optical micrographs of muscovite from the residual clay profile showing features indicative of varying intensity of leaching:

[a - d] : Muscovite from L1a: relatively less altered with sharp edges;

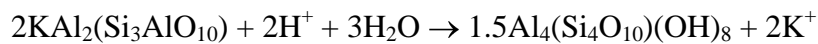
[e - h] : Muscovite from L1b: corroded with etch pits;

[i] : Muscovite from L1c: highly altered with embayed edges.

(X denotes magnification; o- under open nicols, c- under crossed nicols)

Fig.3.8. Optical micrographs of heavy and light fractions from the residual clay layer:
[a – c] : Quartz grains with rainbow features resulting from varying thickness of the grain surface, inclusions of anatase/ zircon are numerous within these grains;
[d & e] : Opaque iron mineral from L1a with features of alteration;
[f & g] : Anatase;
[h – l] : Zircon of different color and crystal features
(X denotes magnification; o- under open nicols, c- under crossed nicols)

SEM pictures show vermicular and book like morphology for the residual L1b clay (Fig.3.9A). Almost all kaolinite grains exhibit a face-to-face pattern of arrangement of platy crystals (Fig.3.9A). The residual kaolinite shows crystals with angular edges (Fig.3.9A&B), suggesting their lack of wearing of edges due to *in situ* formation. The irregular angular kaolinite edge is characteristic of actively growing crystals (Keller, 1985). Kaolinite grains were found at the edge of micaceous stacks or books suggesting the alteration of muscovite to kaolinite (Fig.3.9B). This particular morphology implies the initiation of kaolinization from the edge and weak cleavage planes of the muscovite stacks. For the formation of kaolinite from muscovite, it is necessary to remove potassium from the muscovite structure and to bring protons from the surrounding water that gets transformed to OH group, which finally coordinates with the aluminum according to the equation:



Rebuilding of a 2:1 mica layer into a 1:1 kaolinite layer requires displacement of part of Si^{4+} and Al^{3+} ions. The muscovite stacks show a typical fanning out texture, formed by the release of K during hydration or hydrolysis (Stoch and Sikora *et al.*, 1976; Chen *et al.*, 1997) forming numerous lenticular voids along the cleavage planes. The formation of these lenticular voids during weathering is attributed to the volume decrease during the collapse of the muscovite structure (Robertson and Eggleton, 1991). These lenticular voids indicate an incomplete stage for kaolinization, since they disappear during the completion of weathering of the primary phyllosilicates (Chen *et al.*, 1997; Robertson and Eggleton, 1991). Compact tabular muscovite grains (Fig.3.9C) without any indication of alteration could also be identified. The K deficient muscovite crystals characteristically had a more irregular shape than the typical prismatic laths of fresh muscovite.

Fig.3.9. Scanning electron micrographs illustrating residual clay A) Kaolinite books (arrow), with irregular edges showing *in situ* crystallization and friated appearance, indicative of mica alteration. B) Fanning out of muscovite (m), along with kaolinite (k) at the edges, with numerous lenticular voids (v) between the flakes due to K leaching C) Muscovite grain (m) without alteration, embedded within the kaolinite platelets.

Fig.3.9A

Fig.3.9B

Fig.3.9C

Fossilized plant roots from the uppermost residual clay shows mineralization. Figures 3.10 (A-D) show the features of mineralisation within handpicked plant remains from uppermost portion L1c of the residual clay. These roots show solution pits formed as a result of the percolation of ion enriched weathering solution (Fig.3.10A). Numerous crystals were found within the plant roots exhibiting *in situ* crystallising morphology. These crystals were found to grow from the side wall towards the centre of the pit suggesting localised area of supersaturation of the precipitating solution (Fig.3.10B). *In situ* pyrite crystals show morphology of octahedron, pyritohedron, dodecahedron and octahedron-cube combination (Fig.3.10C). These particular crystal morphologies are similar to that of pyrite forming from an undersaturated solution (White *et al.*, 1991). The euhedral texture of FeS₂ develops due to the crystallization of iron sulphide by concentration of Fe and S after transportation over a distance of many centimeters in the enclosing sediments (Raiswell, 1982). Numerous etch pits were also found on the surface of the grain (Fig.3.10C), formed as a result of ongoing weathering, during the percolation of ions enriched solutions. Partially developed pyrite crystals with octahedral and dodecahedral crystal morphology were also identified (Fig.3.10D). By applying the general law of crystallization imperfect crystals develop as results of irregular rate of crystallization. These FeS₂ mineralization in the residual white clay might have been resulted from the influence of the leached out acid rich pore water from the overlying organic and FeS₂ enriched gray carbonaceous clay layers during oxidation.

Fig.3.10A. Solution pits within fossilized plants remain.

Fig.3.10B. *In situ* mineralization in the pits of fossilised plant remains indicating local area of supersaturation of crystallizing solution.

Fig.3.10C. *In situ* crystallization of Fe-sulphide crystals with o) octahedral, d) dodecahedral, p) pyritohedral, c) cube-octahedral combination. The grains show etched pits on their surface.

Fig.3.10D. Partially developed pyrite crystal showing octahedral-dodecahedral morphology.

3.4.8.2 Gray carbonaceous clay

SEM analysis of these clays shows two types of kaolinite formation in addition to its detrital character. Clay fraction (L5) shows a swirl texture (Fig.3.11A) with face-to-face arrangement of grains suggesting their detrital origin (Keller., 1978). In the sedimentary clay L15, finer clay grains are agglomerated during their deposition by the cementing effect of organic matter (Fig.3.11B), thereby giving a flower like appearance.

The lowermost gray carbonaceous clay (L3) has two types of grains (Fig.3.11C), suggesting the diversity of the environment for their formation. The smaller kaolinite grains are angular with a typical face-to-face arrangement, surrounding larger hexagonal grains having smooth edges. These bimodal features indicate that the finer grains are a recrystallized product and the coarser grains are of detrital origin. Such a texture in kaolinite occurs due to *in situ* formation of this particular mineral in a waterlaiden condition from silicate parent material (Keller, 1978).

The fossilized plant remains collected from the gray carbonaceous clay L15 show percolation pits (Fig.3.11D). Within these pits a second type of *in situ* kaolinite mineralization are found. Here stacks of kaolinite platelets are found grown into the

cubic etched pits formed by the dissolution of the cubic pyrite (Fig.3.11E), suggesting the kaolinite crystallization, after the removal of FeS₂ during oxidation. Oxidation of organic matter along with FeS₂ leads to the formation of acid rich pore fluid which will disintegrate and dissolve the kaolinite and reprecipitating this Al-Si rich ionic solution within the microenvironment of plant fossils, thereby developing authigenic kaolinite. Simultaneously dissolution of FeS₂ under oxidizing condition allows the percolation of acid rich water through the available pores and cavities within the clay. The iron released during dissolution precipitates as Fe-oxyhydroxides. The overall reaction for complete pyrite oxidation and hydrolysis of iron to Fe³⁺ is:



Microscopic examination of reddish yellow clay encircling the plant fossils in mottled L15 clay shows some minerals, which are amorphous and with corn flake like texture. This may be smectite, probably formed as a result of low leaching environment due to the precipitation of amorphous Fe-oxyhydroxides (Fig.3.12A) during FeS₂ dissolution. The typical morphology of Fe-oxyhydroxide grain indicating *in situ* crystallization is shown in Fig.3.12B.

Fig.3.11A. Swirl texture with face-to-face arrangement of platy grains indicating the detrital origin of gray carbonaceous clay.

Fig.3.11B. Agglomeration of kaolinite by organic matter giving a flower like appearance.

Fig.3.11C. Kaolinite of bimodal origin, face-to-face arrangement of fine platelets of kaolinite (arrow) surrounding larger ones, product of *in situ* crystallization from water laid environment.

Fig.3.11D. Percolation pits within the fossilized plant remains from the gray carbonaceous clay layer L15.

Fig.3.11E. Plant remains from uppermost gray carbonaceous clay L15: kaolinite crystals, product of crystallization from Si & Al rich solution which is found to be intergrown into the etched pits of cubic Fe-sulphide.

A

B

Fig.3.12. Scanning electron micrographs showing smectite and secondary iron oxides A) smectite precipitation (s) with corn flake like texture and amorphous Fe-hydroxides (a); B) Crystal of Fe-oxyhydroxide showing *in situ* crystallization.

Optical microscopic analysis showed that most of the heavy minerals in these layers are opaque. The heavy fraction separated from the L11 clay shows the assemblages of sillimanite of varying crystal features (irregular and long slender prismatic crystals). The presence of this mineral in major amount is confirmed from the XRD analysis of the heavy fraction (Fig.3.3C). In these clays traces of rutile and anatase are also present (Fig.3.13 b & d).

Fig. 3.13. Optical micrographs of heavy minerals from sedimentary clay layers:
[a – d] : Association of sillimanite, anatase & rutile from L11-gray carbonaceous clay;
[e – h] : Non magnetic fraction of heavy minerals L17 (lateritic clay); e- anatase, f- zircon with inclusion, g- iron oxide coated grain, h- hematite with earthy appearance;
[i & j] : Magnetic fractions from L7 & L17 respectively. (X denotes magnification; under open nicols)

3.4.8.3 Hematitic clays

Morphological features of hematitic clays are different from that of the residual and gray carbonaceous clays. Figures 3.14 (A-D) show scanning electron micrographs of clays from hematite rich layers, L16, L17 and L18.

The SEM examination of L16 clay shows the agglomeration of finer particles, by the cementing effect of hematite or amorphous Fe-oxyhydroxides (Fig.3.14A). In this genetic environment the *in situ* kaolinization or the features of kaolinite recrystallization are absent. This is also evident from the FTIR patterns, where kaolinite shows a lower crystallinity.

The hematite rich lateritic clay layers show an entirely different morphological feature (Fig. 3.14B). Here crystal features of the kaolinite grain could not be identified due to the coating of iron. Numerous studies exist on the petrographic and morphological character of laterites (Alexander and Cady 1962; Hamilton, 1964; Kubiena, 1954, 1970; Eswaran *et al.*, 1981). During the intense lateritisation, recrystallization and mobilization of iron occurs at the early stages, which gets accumulated in the kaolinite matrix. Later the intensity of deposition of iron on kaolinite matrix increases due to the leaching of SiO₂ and these Fe- oxyhydroxides form a coalescing mass (Hamilton, 1964). Eswaran, *et al.* (1977; 1978) indicated the crystallization of gibbsite at this stage of transformation. The SEM (Fig.3.14B) shows such an *in situ* formation of fine gibbsite crystals in voids along with the coalescence mass of iron (arrow) indicating the intensity of lateritisation for this layer.

The uppermost iron rich bauxitic layer megascopically shows alternate dark (cherry red) and bright layering (yellowish) in some portions giving a banded appearance (Fig.3.2A) This again emphasises the segregation of iron in this weathering environment. The hard, highly compact bauxite shows vesicles in some portions exhibiting vesicular texture, which occurs due to leaching of SiO₂ and consequent remobilization of the oxides, Fe₂O₃ and Al₂O₃.

Scanning electron micrograph (Fig.3.14C) indicates that the coalescence mass of iron gets aggregated in the form of tubes due to the advanced stage of remobilization. The bauxite surface is found to be more or less massive except these aggregates. This hard, compacted bauxitic crust might have resulted by the cementing action of the cryptocrystalline iron mineral. Figure 3.14D shows the magnified portion of the

cryptocrystalline phase of these iron minerals. This cement gives the material its rigidity and toughness.

The above process of hardening has received considerable attention. According to Alexander and Cady (1962) these hardening effects resulted from an increase in the crystallinity of the iron oxide during the hardening phase of lateritization. Eswaran and Raghumohan (1973) established the interlocking network nature of the goethite in SEM analysis in their studies of lateritic crust. Apart from the crystallinity, a change from one kind of mineral to another is postulated by several workers to explain the hardening. The XRD analysis confirms the presence of higher hematite concentration having good crystallinity in these bauxitic clays (Fig.3.3A).

Fig.3.14A. Agglomerated kaolinite platelets with amorphous iron oxide coating in hematite-rich clay, L16.

Fig.3.14B. Collomorphous precipitation of amorphous Fe-oxides on kaolinite surface with *in situ* cryptocrystalline gibbsite in voids (arrow) indicative of recrystallisation of lateritised clay, L17.

Fig.3.14C. Remobilization of iron into tubes as a result of incongruent dissolution of Al_2O_3 and SiO_2 during bauxitisation

Fig. 3.14D. Magnification of the cryptocrystalline iron mineral from bauxite

The optical microscopic features show ferric coating on the surface of most of the grains. Good amount of anatase and zircon are also present (Fig.3.13 e & f). Zircon shows inclusions along the axis of the grain (Fig.3.13f). Brownish-red grain with earthy appearance is characteristic of hematite (Fig.3.13h). Photomicrograph (Fig.3.13j) shows the opaque magnetic heavy fraction of L17 (laterites).

Above evidences indicate that both oxidizing and reducing conditions have influenced the entire clay deposit. The oxidized weathering condition which led to the formation of hard bauxitic crust, laterite and hematite rich clay enhanced the dissolution of the FeS_2 present in the gray carbonaceous clay layers, creating a high acid environment in which dissolution and reprecipitation of microcrystalline quartz and authigenic kaolinite occurred. In addition, the percolation of these SO_4^{-2} ions rendered the deposit more acidic resulting in the subsequent crystallization of FeS_2 in the microenvironment within the plant fossils in the residual white clay. The presence of overlying sedimentary deposits of Warakallai Formation preserves the underlying residual white clay deposit from intense post-Warkallai–pre-Quaternary lateritisation.

3.4.9 Industrial applications of white clay from seam L.

Chemical characterisation of the < 45 μm samples are given in table 3.3.

Table 3.3 Chemical characterisation of < 45 μm fraction (wt %)

SiO ₂	Al ₂ O ₃	Fe ₂ O ₃	FeO	TiO ₂	CaO	Na ₂ O	K ₂ O	LOI
45.41	38.88	0.72	0.06	0.03	0.14	0.17	0.48	14.19

Commercial evaluation of the representative sample of white clay from L is given in table 3.4. The recovery of < 45 μm fraction was 46% (Table 3.4). In this fraction, the < 2 μm fraction is 48%. Calcination of kaolinite prior to bleaching using sodium hydrosulphite causes an enhancement in brightness of about 7.91 units compared to the crude clay. Correspondingly the yellowness value also decreases by 1.57 units. Such an improvement indicates that the clay contains goethitic iron impurity (Kogel *et al.*, 1999) which converts into hematite during calcining and is leached more efficiently. But bleaching using oxalic acid as sequestering agent could not improve the property as that of sodium hydrosulphite. The pinkish white fired colour of the clay even after bleaching shows the presence of colour imparting impurities. Table 3.4 presents the fired properties of the samples *viz.* fired shrinkage, water absorption, apparent porosity and bulk density at 600, 800, 900 and 1250°C. Samples sintered at 1250°C exhibit increase in fired shrinkage (24.26%) and bulk density (0.82), with a corresponding reduction of apparent porosity (17.3%) and water absorption (33.26%). This also results in a drastic increase in MOR of about 235 kgf/cm².

Table 3.4. Physical properties of china clay (< 45 µm sample)

Clay recovery					46%
Raw colour					Buff
Particle size distribution:					
< 2 µm					48%
< 5 µm					72%
< 10 µm					89%
< 20 µm					99.5%
> 20 µm					0.5%
Brightness/Yellowness of raw clay					58.48/10.9%
Brightness/Yellowness of calcined clay					62.32/11.02%
Brightness/Yellowness after bleaching using 0.4%:					
	Sodium hydrosulphite				58.48/10.5%
	Oxalic acid				58.90/10.5%
Brightness/Yellowness after calcination and bleaching using 0.4%					
	Sodium hydrosulphite				66.26/9.35%
	Oxalic acid				64.56/10.1%
Viscosity					621 cps
Water of plasticity					40.2%
Dry linear shrinkage					3.9%
Green MOR					5.59 kgf/cm ²
Fired properties:					
Fired colour					Pinkish white
Fired linear shrinkage (1250°C)					16.08%
Fired MOR (1250°C)					235 kgf/cm ²
	600°C	800°C	1000°C	1250°C	
Fired volume shrinkage %	1.17	2.30	10.00	24.46	
Water absorption %	44.35	42.69	38.27	33.26	
Apparent porosity %	22.40	21.35	19.13	17.3	
Bulk density g/cm ³	0.66	0.68	0.69	0.819	

3.5 Conclusion

The present investigation indicates that the mineralogy, chemistry and morphology of the associated minerals in this deposit have a close bearing on the formation environment. The nature of the agents, which were active during the formation or deposition of clays are evident from the above evaluations. The variation in kaolinite character in each layer as evident from XRD, DTA, FTIR, chemical analysis and SEM is related to the petrogenetic, stratigraphic and post depositional conditions. It is found that kaolinite within the same deposit itself has been formed under three genetic environmental conditions:

1. Oxidizing conditions for the detrital hematite rich layers L16, L17 and L18.
2. Reducing environment for the deposition of FeS₂ enriched gray carbonaceous kaolinite seams and
3. Intense lateritised weathering conditions for the formation of the economically viable residual white clay L.

The structural and morphological studies indicate that the remobilization of Al₂O₃ and SiO₂ and consequent crystallization of Al(OH)₃ (gibbsite) in this hematite enriched environment results from bauxitization under an intense tropical climate. In addition, the above study shows the recrystallisation of kaolinite in the gray carbonaceous clays, which is enriched in FeS₂. Clay in L3, showed textures characteristic of detrital and also *in situ* crystallization under water laden condition. *In situ* kaolinization into etched FeS₂ pits from Al-Si enriched ionic solution occurs within the plant remains of (L15) carbonaceous clay in an organic enriched environment. Mineralization in plant remains in L1c indicates that this microenvironment does not favour the *in situ* kaolinite crystallization in the absence of ample amount of organic chelators as in gray carbonaceous clay. The mineralogical assemblages such as pyrophyllite and muscovite with its typical morphology of fanning out texture with lenticular voids and leached pits in pyrite crystals found within the plant remains from L1c indicate that the kaolinization of this deposit is not yet complete. This is further proven by the trace element analysis where their concentration is the least for the residual clay L1b, which has undergone relatively less weathering. The sedimentary clay deposits of the Warkallai formation has a major role in preserving the underlying residual white clay form the ongoing lateritisation.

Technological evaluation of this clay, which has a recovery of 46%, points out that this spatially wide deposit could be commercially exploited in ceramic industry. A comparison of the specifications of this clay with ASTM indicates that this clay is suitable for white ware and sanitary ware applications.

Chapter 4

Part – I

Geochemical, Mineralogical and Morphological Investigation on Kundara Kaolin Deposit, South Kerala

4.I.1 Introduction

Kaolinite deposits of Kerala are closely associated with lateritization. Lateritic weathering of Fe bearing rock in tropical areas produces various mineral sequences. Almost all kaolin deposits formed under the above weathering mechanism are invariably associated with both amorphous and discrete forms of Fe and Ti minerals. These include goethite (α -FeOOH), hematite (α -Fe₂O₃), lepidocrocite (γ -FeOOH), ferrioxyhyte (δ -FeOOH), maghemite (γ -Fe₂O₃), ferrihydrite (5Fe₂O₃.9H₂O), ilmenite (FeTiO₃) and rutile/anatase (TiO₂). Each of the above forms of iron minerals is a natural indicator for the evaluation of geochemical environment of kaolinite formation (Schwertmann and Taylor, 1977). These mineral impurities within a deposit impart an undesirable property of impairing whiteness and increasing yellowness thereby degrading the quality of kaolin.

The kaolin deposit of Kundara, Southern Kerala (8° 54' N; 76° 40.5' E) (Fig. 4.I.1A) is associated with a vast reserve of ~ 6 lakh tons of kaolinite. The peculiarity of this deposit is that, the residual white clay on exposure develops yellow pigmentous coating much faster than kaolinite deposits occurring elsewhere in the state, probably resulting from the rapidity in the geochemical phenomenon of Fe²⁺ to Fe³⁺ transformation. The aim of the present study is to understand the geochemistry of this particular deposit, giving emphasis to the distribution of iron, in order to reveal the unique geochemical feature of quick colouration of the white clay.

4.I.2 Geologic Setting

Kundara kaolinite deposit of southern peninsular India is located in the eastern periphery of the Cenozoic sedimentary basin of South Kerala (Fig.4.I.1A).

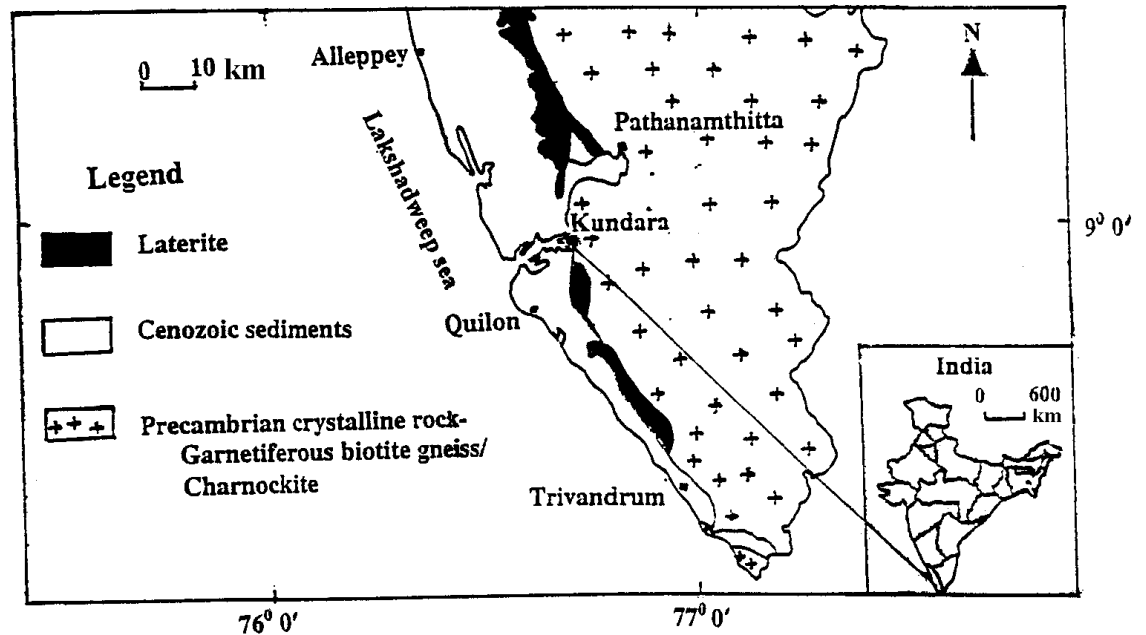


Fig. 4.I.1A. Location map of Kundara clay mine

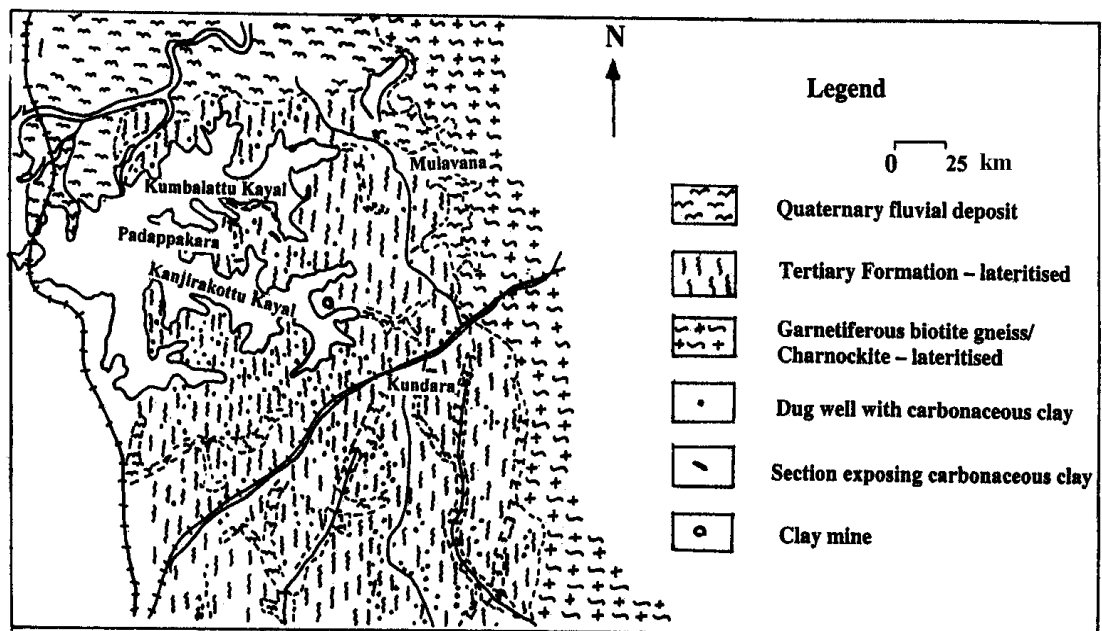


Fig. 4.I.1B. Geological map indicating the association of different types of rock in and around Kundara (after Nair and Chandran, 1989).

The Geological Survey of India has demarcated an area around 250 Sq km in Kundara region of Quilon district as a potential reserve of kaolinite deposit (Fig.4.I.1B).

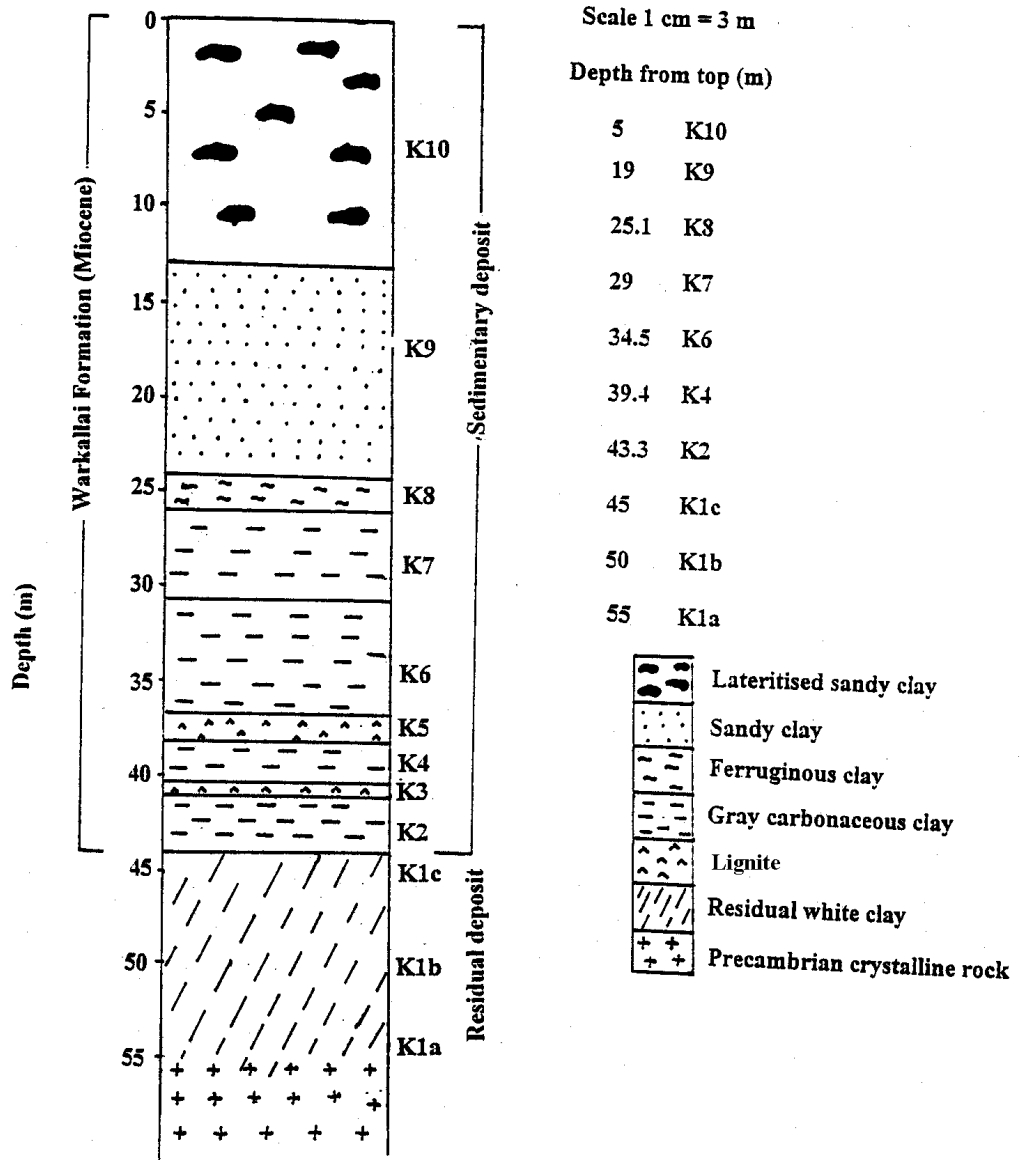


Fig. 4.I.1C. Schematic cross-section of Kundara clay deposit.

Geologically the area is dominated by a thick sequence of white residual clay, formed from Precambrian crystalline rock. The sedimentary Warkallai bed of Upper Tertiary age is found above this primary deposit (Fig.4.I.1C, 4.I.2A). These Tertiary sedimentary sequences are extensively lateritised in the uppermost portions and are found to overlie

the entire region. The entire sequences of the clay in this deposit have an overall thickness of 55 meters. The clay sequences in the mine profile are divided into three groups: white residual clay, gray carbonaceous clay and hematitic clay for convenience. The field photographs of the same are given in Fig.4.I.2 and 4.I.3.

The residual white clay is approximately 15 meters thick and sampling from this seam is done at 5 m interval (K1a, K1b and K1c). These clays show the presence of garnet patches (Fig.4.I.2B), relict foliation and quartz vein of parent rock, the garnetiferous biotite gneiss. In addition, prominent black patches (coded as K1b* in the text of the chapter) of FeS₂ almost circular in shape of ~ 5-10 cm in diameters are seen in certain portions of the residual clays, K1b (Fig.4.I.2C). These patches are frequent up to a depth of 2-8 meters from the top of the residual clay layer and the frequency of the same decreases with depth. In addition, size of the patches also reduces with depth. Yellow coloured precipitation is found to encrust these occluded patches at some portions as a result of oxidation in areas of intense surface weathering. Numerous fossilised plant roots are preserved at the top 0 - 0.5 meters of the residual clay, indicating an intense growth of vegetation and consequent weathering of the Precambrian rock prior to Tertiary sedimentation (Fig.4.I.2D).

The Warkallai beds, which overlie the residual clay are horizontally bedded and consist of layers of gray carbonaceous clay (K2, K4, K6, K7) and lignite seams (K3, K5) together making an approximate thickness of 20 meters followed by layers of ferruginous and variegated clay- K8, sandy clay-K9 and lateritised sandy clay- K10 having maximum thickness of 1.8, 10.8 and 12.3 meters respectively (Fig.4.I.1C and 4.I.3A-C). The entire Tertiary deposit has a maximum thickness of around 44 meters and the individual bed has varying thickness. The intensity of ongoing weathering under tropical climate of this area is evident from the extent of lateritisation of uppermost Tertiary sandy clay bed.

The entire region is fringed by younger fluvial sediments of Quaternary age towards the northwestern side and the lateritised Precambrian hard rock borders the east (Fig.4.I.1B). Tertiary sedimentary sequences of Lower Miocene age with hard fossiliferous limestone and marl of Quilon Formation are exposed in the cliff section of Padappakara (towards north west of Kundara mine).

Fig. 4.I.2A. Association of thick sequences of Warkallai sediments and residual white clay.

Fig.4.I.2B. Garnet patches within the residual white clay.

Fig. 4.I.2C. Black FeS₂ patches within the residual clay (K1b*).

Fig. 4.I.2D. Fossilised roots at the topmost portion of residual clay, indicative of intense plant growth prior to Tertiary sedimentation.

Fig. 4.I.3A. Hematite rich ferruginous clay layer overlain by the sandy lateritised clay layer - note the sharp boundary (arrow) which demarcates the two layers.

Fig. 4.I.3B. A thick sequence of sandy lateritised clay layer showing prominent laminations.

Fig. 4.I.3C. Vermicular lateritised clay overlying the sandy clay layer showing the intensity of lateritisation.

4.I.3 Materials and Methods

Systematic geological observation, documentation and sampling were carried out during the field visit. Samples were collected from each horizon of the vertical mine profile and from portions which show the concentration of a particular mineral. Schematic cross section of Kundara clay deposit (Fig.4.I.1C) shows the sequence and the code of the samples collected.

Samples were crushed and fine ($< 2 \mu\text{m}$) clay fractions were separated by sedimentation technique. The $< 2 \mu\text{m}$ fraction separated from all the seams are designated as 'fines' in the text of the paper. Heavy mineral content was determined by separation using bromoform (2.2).

Mineral identification was undertaken using powder diffraction analysis using Philips PW 1710 X-ray diffractometer with Ni- filtered $\text{CuK}\alpha$ radiation (40 kV, 20 mA) at a scan speed of $1^\circ 2\theta/\text{min}$. Hinckley Index (Hinckley, 1963) and Amigo Index (Amigo et al., 1987), were calculated for crystallinity index measurements.

Chemical analysis was carried out by classical analytical techniques (Bennett and Reed, 1971). Concentration of ferrous iron in selected samples was determined by titration against $\text{K}_2\text{Cr}_2\text{O}_7$ after digestion in $\text{HF} + \text{H}_2\text{SO}_4$. Water soluble SO_4^{2-} and Fe in the raw clay of residual layer were also analysed by precipitation using BaCl_2 and colourimetric techniques respectively (Jeffery *et al.*, 1989). Organic carbon content in the raw fractions was determined by oxidative decomposition using $\text{K}_2\text{Cr}_2\text{O}_7$ (Gross, 1971). The pH of the bulk fractions was determined using 1:4 clay: water ratio. Trace element analysis of the selected samples, K1b, K6, K7 and K10 was done by AAS (Varian Spectra AA- 10 Model).

DTA/TGA of the fines was carried out using a Seiko 320 TG/DTA analyser at a heating rate of $10^\circ\text{C}/\text{min}$ in the range ambient- 1100°C with alumina as standard.

FTIR absorption spectra of the pretreated fines (Al-Khalissi and Worrall, 1982), were recorded using Perkin-Elmer spectrophotometer by scanning at a wavelength of $4000 - 400 \text{ cm}^{-1}$ using KBr pellets

SEM analysis of fractured clay surfaces and mineral grains was carried out using JEOL JSM 5600 LV Microscope. Petrographic studies were undertaken using polarizing microscope for mineral characterization.

Detailed experimental procedures are given in Chapter 2.

4.I.4 Results and Discussions

4.I.4.1 XRD studies

X-ray diffractograms indicate that the clays in different layers show variation in mineral concentration (Fig.4.I.(4-7)). The mineralogical analysis of raw clay, fines and heavy fractions of residual white clay, gray carbonaceous clay and hematitic clays are summarised in Table 4.I.1. The constituent minerals are expressed as major, minor and trace based on their concentration.

Table 4.I.1. Semiquantitative mineralogical analysis by XRD (raw clay, fines and heavy fraction)

Sample	Raw	Fines	Heavy
K1a	K [#] , Q [#] , B [#] , I ^δ	K [#] , Q ^β	B [#] , I [#] , A ^β , Pr ^β
K1b	K [#] , Q [#]	K [#] , Q ^β	A [#] , R ^δ , Pr ^β , S ^β , Go ^β
K1b*	Me [#] , Q [#] , K [#] , P [#] , J ^β , A ^β	-	-
K1c	K [#] , Q [#] , A ^β	K [#] , Q ^β	R [#] , A [#] , Pr ^β
K2	Gi [#] , Q [#] , K [#] , A ^β	Gi [#] , K [#] , Q ^β , A ^β , R ^β	Ma [#] , R [#] , A [#] , J ^β , S ^β
K4	Q [#] , K ^δ , Gi ^β , A ^β	Gi [#] , K [#] , R ^β , Q ^β , A ^β	A [#] , R [#] , J ^β , Go ^β , S ^β
K6	Gi [#] , K [#] , R ^β , Q ^β	Gi [#] , K [#] , Q ^β , R ^β	A [#] , R [#] , S ^δ
K7	Q [#] , Gi [#] , R ^δ , K ^δ , A ^β	K [#] , Gi [#] , Q ^β , R ^β	Ma [#] , A [#] , R [#] , S ^δ
K8	K [#] , Q [#] , He ^β	K [#] , Q ^β	A [#] , R [#] , He ^δ , S ^β , Go ^β , K ^β
K9	Q [#] , K ^δ	K [#] , Q ^β	S [#] , R [#] , A ^β
K10	Q [#] , K ^δ , He ^β	K [#] , Q ^β , R ^β	R [#] , S ^δ , He ^δ , K ^β

K1b* represents black patched portion from K1b

K- kaolinite, Q- quartz, B- biotite, Gi- gibbsite, I- ilmenite, Pr- pseudorutile, A- anatase, R- rutile, S- sillimanite, Me- melanterite, P- pyrite, Ma- marcasite, J- jarosite, He- hematite, Go- goethite

-major, ^δ - minor and ^β trace

The sequence of minerals from left to right is in the decreasing order of concentration

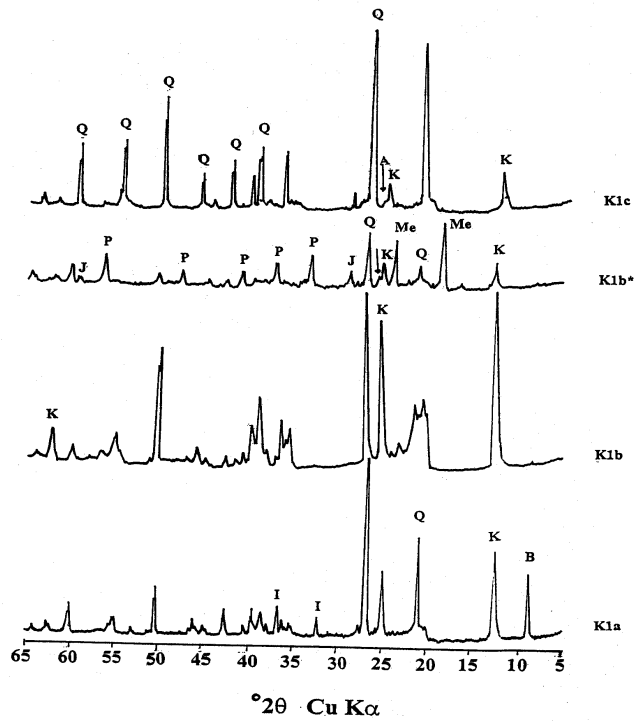


Fig. 4.I.4A: X-ray powder diffraction patterns of raw clays from K1a, K1b, K1b* and K1c of the residual clay at varying depths (K1b* represents black patched portion from K1b layer): K-Kaolinite, Gi- Gibbsite, Q- Quartz, A- Anatase, R-Rutile, I- Ilmenite, B- Biotite, Me- Melanterite, P- Pyrite and J- Jarosite.

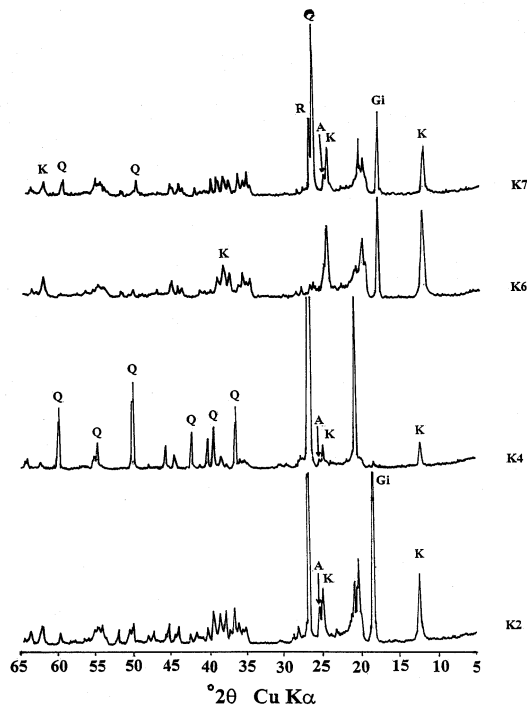


Fig. 4.I.4B: X-ray powder diffraction patterns of raw clay from carbonaceous clays K2, K4, K6 and K7: K-Kaolinite, Gi- Gibbsite, Q- Quartz, A- Anatase, R-Rutile.

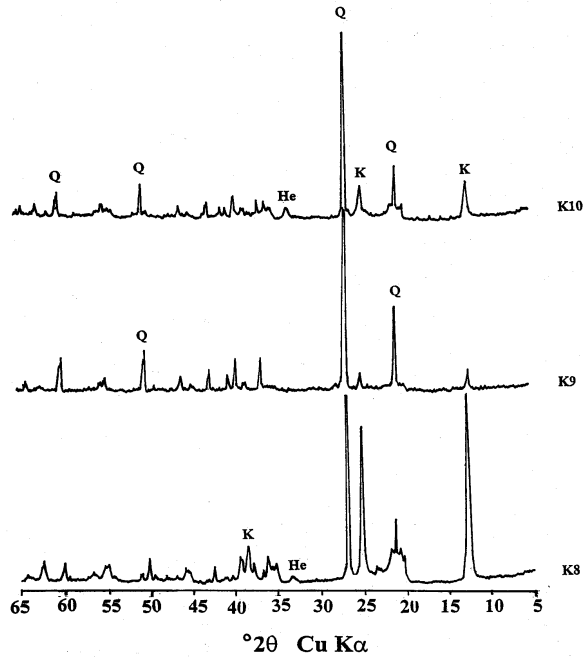


Fig. 4.I.4C: X-ray powder diffraction patterns of raw clays from ferruginous clays- K8, K9 and K10: K- Kaolinite, Gi- Gibbsite, Q- Quartz, A- Anatase, R- Rutile and He- Hematite.

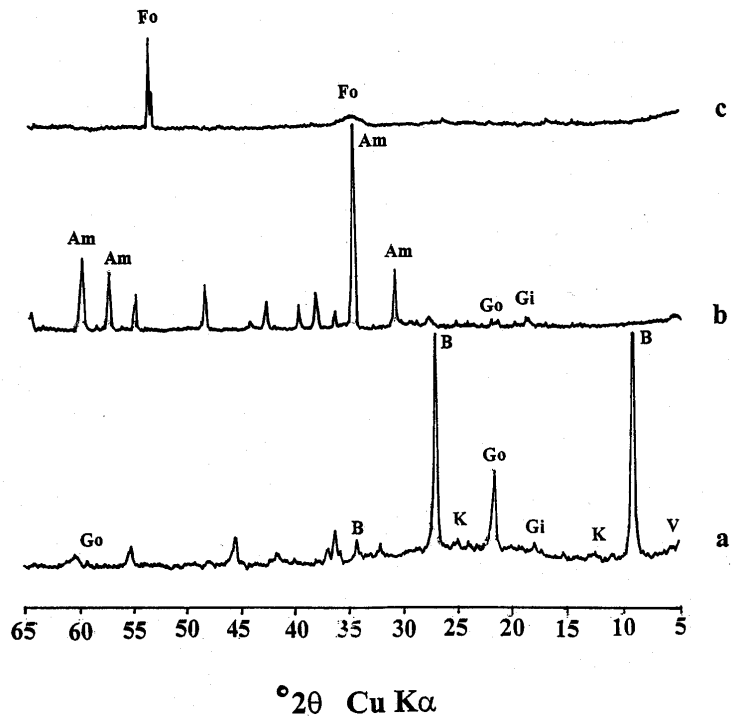


Fig. 4.I.5. X- ray powder diffraction patterns of a) hand picked biotite grains from the residual clay- K1a; b) hand picked garnet grains from the residual clay -K1b; c) yellow precipitation from the seeped out water of the residual clay: B- Biotite, Go- Goethite, Am- Almandine, K- Kaolinite, Gi- Gibbsite, V- Vermiculite, Fo- Ferroxyhyte.

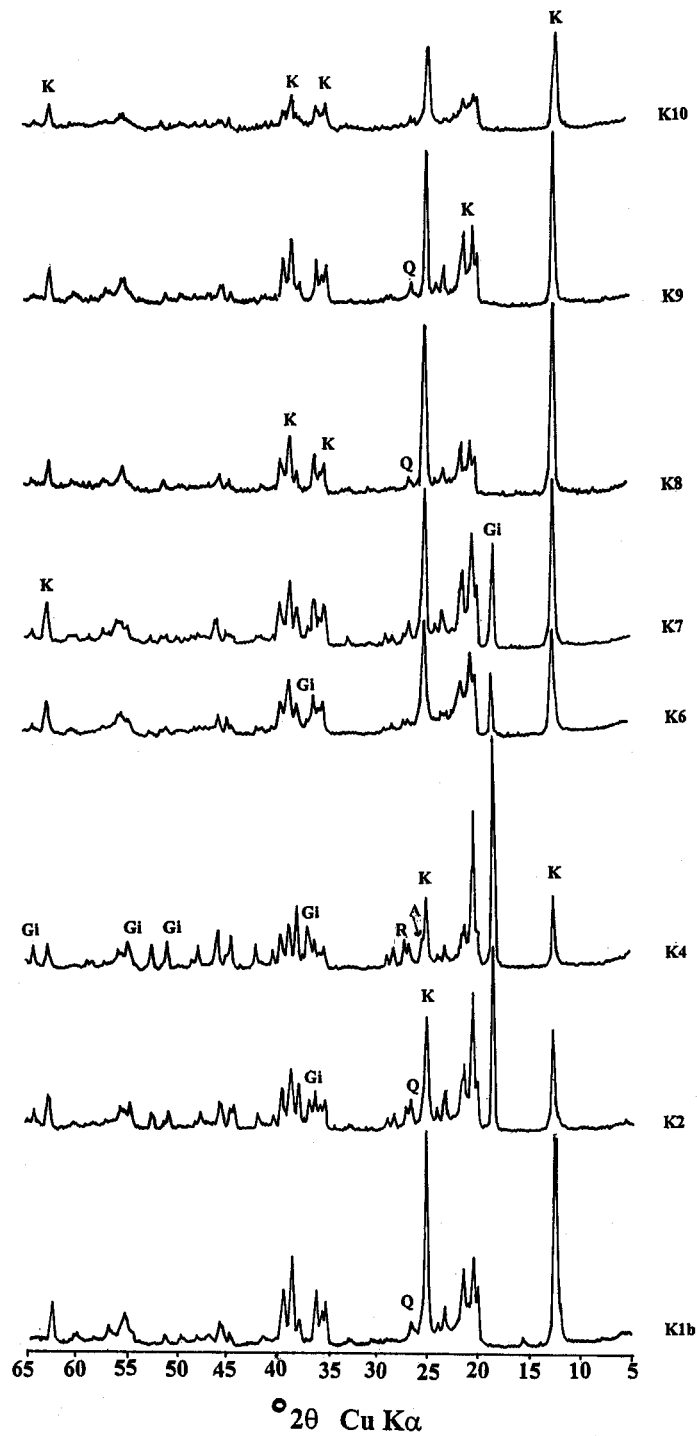


Fig. 4.I.6. X-ray powder diffraction patterns of $< 2 \mu\text{m}$ fraction from different clay layers: residual clay – K1b; carbonaceous clays- K2, K4 and K6; and ferruginous clays - K7, K8 and K9: K- Kaolinite, Gi- Gibbsite, Q- Quartz, A- Anatase and R- Rutile.

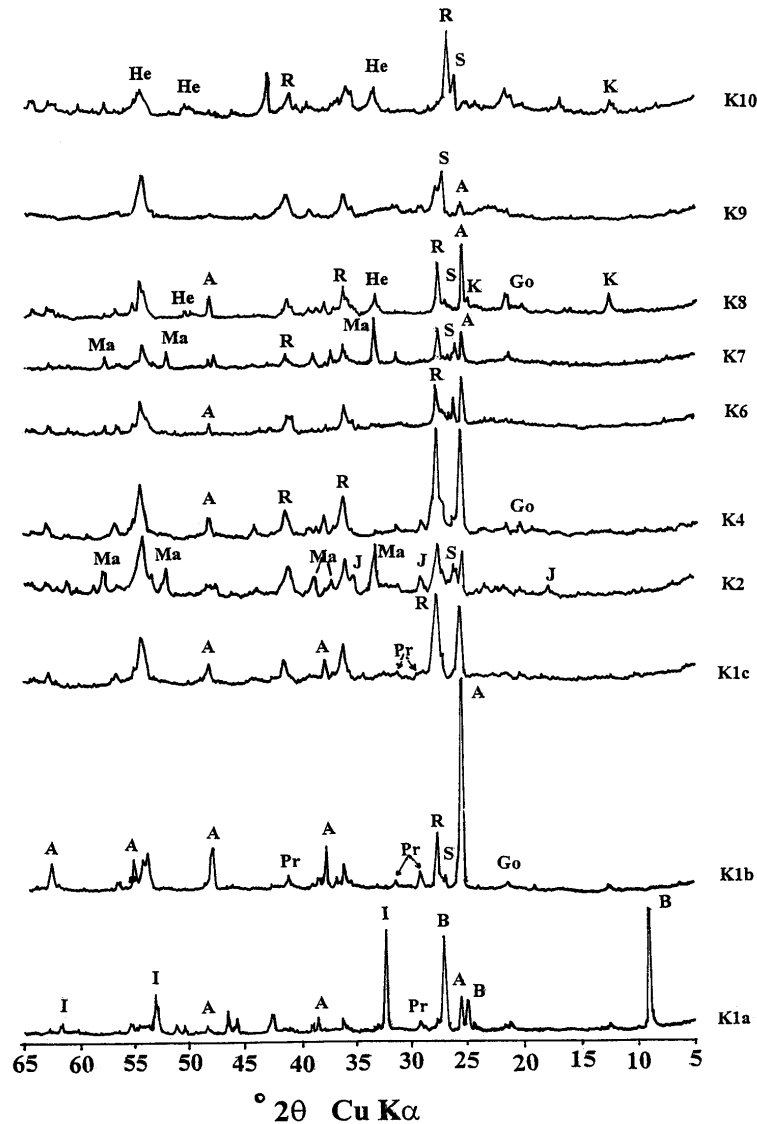


Fig. 4.I.7. X-ray powder diffraction patterns of the heavy fraction of Kundara kaolinite from different layers residual clay - K1a, K1b and K1c; carbonaceous clays - K2, K4, K6 and K7; ferruginous clay - K8, K9 and K10: I- Ilmenite, Pr- Pseudorutile, A- Anatase, R- Rutile, S- Sillimanite, J- Jarosite, Ma- Marcasite, Go- Goethite, He- Hematite and K- Kaolinite.

4.I.4.1.1 Residual white clay- (K1a, K1b and K1c)

The bulk mineralogy of the residual clay K1a, K1b, and K1c (Fig.4.I.4A) includes kaolinite along with ample amount of quartz. Sample K1a, which is in the lowermost portion of the residual clay layer, has good amount of biotite and ilmenite. The biotite peak is absent in K1b and K1c indicating their alteration during the course of weathering.

Biotite which is common in granitic and high grade metamorphic rocks, is reported to be altered to hydrobiotite, a regularly interstratified biotite-vermiculite phase, vermiculite and kaolinite (Sawhney, 1977; Brindley *et al.*, 1983). The sample K1a does not show any evidence of the presence of the interstratified mineral indicating a direct conversion of biotite to kaolinite as described by Harris *et al.* (1985). For further confirmation, concentrated handpicked biotite flakes were examined for its alteration products (Figure 4.I.5 a). The X-ray diffractogram shows only a small hump at lower angle region (around 14 Å) indicating a very low amount of vermiculite in this clay. This might be due to the influence of intense acidic weathering environment, where enhanced destruction and loss of Fe from mineral surface would occur rapidly. In such geochemical environment structural transformation to vermiculite is relatively low (Acker and Bricker, 1992). In addition, prominent 4.13 Å peak shows the precipitation of goethite, as evident from the XRD pattern (Figure 4.I.5 a).

The presence of major concentration of ilmenite in raw fraction of K1a was evident from the peaks at 2.75, 1.86 and 1.72 Å. Heavy fractions of the residual clay show major concentrations of ilmenite- pseudorutile- anatase/rutile (Fig.4.I.7). Temple (1966) indicated that ilmenite will be converted to TiO₂ on oxidation and leaching of the structural iron. The peaks at 3.04, 2.47 and 2.30 Å for K1a indicate the presence of pseudorutile, the intermediate product of ilmenite weathering. The above mineral is concentrated more in K1b and found only in traces in K1c. But in these clays, ample amount of anatase and rutile are present. Anatase concentration was maximum in K1b. The formation of more amount of anatase than its polymorph rutile in this environment might be due to the presence of various ions in solution in the weathering environment (Anand and Gilke, 1984). Rutile is the predominant form of TiO₂ mineral in K1c. The presence of the entire paragenesis of the mineral, ilmenite- pseudorutile-anatase/rutile in the weathering profile confirms the above sequence of formation. The XRD results indicate that most of the ilmenite was converted to pseudorutile and then to anatase/rutile. The presence of more amount of pseudorutile in K1b indicates that weathering of this profile reached a stage in which most of the Fe⁺² and Fe⁺³ from ilmenite structure are removed by solid state oxidation and diffusion (Teufer and Temple, 1966). Later these altered ilmenite is congruently dissolved under acidic reducing condition producing Fe²⁺

and authigenic TiO₂ (Temple, 1966; Grey and Reid, 1975). The intensity of the peak also indicates the extent of alteration.

Fines of residual clays (Table 4.I.1)(Fig.4.I.6) are devoid of titaniferous mineral. Along with kaolinite, quartz was also present in traces in this fraction.

The black patched portions of the clay from K1b were also analysed for the mineralogical assemblages.

4.I.4.1.2 Black patched residual clay (K1b*)

Mineralogical assemblages in the raw clay from black pockets in the K1b layer (K1b*) include kaolinite, quartz, pyrite, melanterite and jarosite (Table 4.I.1)(Fig.4.I.4A). Pyrite is the widespread sedimentary authigenic mineral, which forms under reducing environmental condition in the presence of adequate organic carbon, reactive iron mineral and dissolved sulphate (Berner,1984). Melanterite and jarosite are the secondary iron minerals formed as a result of FeS₂ oxidation. Jarosite (KFe₃(SO₄)₂(OH)₆) is the most commonly identified basic iron sulphate formed as a result of FeS₂ leaching (Bigham,1994). The reaction for the formation of jarosite, as given by Baron and Palmer (1996), is



Potassium ions needed for the precipitation of the above mineral might have been taken from the leached out K of feldspars or biotite. The environmental condition prevailed during the deposition of gray carbonaceous clay influenced the *in situ* FeS₂ formation in the residual clay as a result of elution of the sulphate enriched organic solution into the residual clay. This probably has resulted in the *in situ* FeS₂ mineralisation in regions of enriched iron, which results from the parent rock alteration.

Later on exposure of the clays during weathering under oxidising environment, results in the leaching of FeS₂, forming jarosite and melanterite. The oxidation of FeS₂ on exposure is also clear from the field evidences where the seepage near pyrite patches in the mine shows reddish-yellow colour, indicating the formation of Fe – aquo complex. The water from the seepage was collected and the clay is filtered off using whatman No. 42 filter paper. The resultant solution is kept at room temperature and the precipitate

formed as result of ageing has a reddish colour. XRD analysis of the reddish iron formed from the above leached out water shows prominent diffractions at 1.72, 1.69 and a hump at 2.54 Å, indicative of mineral feroxyhyte and also iron- oxyhydroxides of poor crystallinity (Fig.4.I.5c). Feroxyhyte is reported to be present in the natural environment where oxidation of Fe^{2+} is rapid. Chukrov *et al.* (1977) postulated the formation of feroxyhyte in nature as a result of rapid abiotic oxidation of Fe at neutral to slightly acid pH.

4.I.4.1.3 Gray carbonaceous clay- (K2, K4, K6 and K7)

Carbonaceous clays contain gibbsite, kaolinite and quartz as the major components and anatase and rutile as minor constituents (Table 4.I.1)(Fig 4.I.4B). The fine fraction contains more gibbsite, which is indicative of a strongly deionised environment with intense and rapid water circulation. The coarser fabric of this clay layers dominated by sand- sized quartz allowed water to drain more freely, making the silica level in the soil solution sufficiently low for the formation of gibbsite. This is confirmed from the presence of maximum concentration of gibbsite in fines of K4, where the coarser raw fraction contains gibbsite in traces and with abundant quartz. Gibbsite, the widespread aluminum hydroxide mineral has a tendency to form in acidic solutions (Hsu, 1977). Schoen and Roberson (1970) stated that, in addition to warm conditions and high rainfall, good drainage was also required for gibbsite formation. In these conditions equilibrium between the liquid and solid phases is not reached, which helped to eliminate the mobile components of the weathering system (bases and silica) allowing alumina to concentrate in the residual phase.

Titanium mineral anatase/rutile is present in the fines of K2, K4 and K6, indicating their wearing down or precipitation during the course of transportation or deposition (Fig. 4.I.6). In all these carbonaceous clays the iron bearing titanium mineral ilmenite/pseudorutile is absent which is attributed to the conversion of these minerals to more stable rutile or anatase.

The above TiO_2 polymorphs are almost in equal concentrations in the carbonaceous clays as evident from the intensity of their peaks (3.2 and 3.4 Å) in heavy fraction (Fig. 4.I.7). The FeS_2 mineral, marcasite was present in K2 and K7, the uppermost and

lowermost carbonaceous layers. Traces of jarosite were also noticed in K2, K4 and K7 indicating the oxidation of the above authigenic mineral. Traces of goethite were identified from the hump at 4.18 Å showing the effect of oxidation. Goethite is the stable Fe³⁺ oxide formed at low temperature in saturated sediment (Trady and Nahon, 1985). The peaks at 3.36 and 3.41 Å indicate the presence of sillimanite (Al₂O₃.SiO₂). The presence of the above mineralogical assemblages of iron makes clear the influence of dual environment, reducing and oxidizing on the carbonaceous layers.

4.I.4.1.4 Hematitic clay (K8, K9 and K10)

The reddish hue in clay beds K8, K9 and K10 indicates the presence of hematite. This is confirmed by its characteristic broad peak at 2.68 Å (Fig. 4.I.4C). The formation or precipitation of hematite is considered to be an indicator of arid and tropical environment (Walker, 1974) with long dry season. Quartz and kaolinite are the major phases in ferruginous, sandy and lateritised sandy clays. But kaolinite is relatively less in the sandy laterite and lateritised clay region, indicating higher permeability for these layers. Even though the presence of iron and the typical lateritic texture is indicative of intense weathering, gibbsite is almost absent in these layers.

‘Fines’ of this clay contains only traces of hematite (Fig. 4.I.6). The concentration of the above mineral is more in the uppermost layer K10. The < 2 µm fraction of K9 (sandy clay layer) is devoid of hematite indicating an initial stage in lateritisation.

The presence of kaolinite with broad diffraction peaks of the heavy fraction (Fig. 4.I.7) shows the formation of this primary clay mineral as an occluded phase within hematite. This indicates the precipitation of the above iron mineral after kaolinite deposition or crystallization. The TiO₂ mineral, rutile, is concentrated more in the uppermost layers, K9 and K10 than its polymorph anatase. Sillimanite is a prominent phase in these lateritised layers.

The presence of sillimanite, anatase and rutile in the residual, carbonaceous and ferruginous clays indicate same suite of precursor parent material- khondalite for all the layers. Variations in the assemblages result due to varying intensity of weathering and environmental conditions of deposition.

4.I.4.2 Crystallinity Index Measurements

Kaolinite crystallinity index measurements by Hinckley, (1963) and Amigo *et al.* (1987) methods showed that almost all clays have a lower index. Among these, hematitic clays K8 and K9 have relatively higher order (Table 4.I.2). The HI ranges from 0.67 (K10) to 1.24 (K9). Amigo index, which measures the width of the 001 and 002 peaks of kaolinite at half height also, shows similar inference as HI. The variation in the crystallinity index for different layers reflects the diversity of geochemical environment of kaolinite formation / deposition.

4.I.4.3 Chemical Analysis

The chemical assays of fine and raw samples from the residual white clay, gray carbonaceous clays and hematitic clays are shown in Table 4.I.2.

4.I.4.3.1 Residual Clay (K1a, K1b, K1b* and K1c)

Among the residual clays, SiO₂ is maximum for the uppermost K1c layer (75.67%). The Fe₂O₃ content of K1b and K1c are comparable to TiO₂ concentration indicating their presence in titaniferrous minerals pseudorutile and rutile/anatase. An interesting feature noticed in this study was the sharp increase in the concentration of ferrous ion with depth (except for the pyrite concentrated fraction). Ferrous iron was concentrated more in the lowest region of the residual clay, K1a (2.29%) rationalising the presence of biotite and ilmenite. The black occluded patches (K1b*), shows higher iron content (19.05%), which further substantiates the presence of Fe-sulphide minerals and their oxidation products as evident from XRD. Here the water-soluble iron and sulphate are 1.98 and 8.22% respectively. For K1c water soluble iron (0.95%), and SO₄²⁻ (2.18%) were more when compared to K1a and K1b, showing higher ferrous sulphate concentration. K₂O increases with depth and was maximum in K1a (1.14%) showing their presence in unaltered biotite. The easy leachable MgO (1.04%), CaO (0.71%) and Na₂O (0.25%) are also concentrated more in the lowermost clay and their leachability is evident from the lower concentrations of the above oxides in K1b and K1c respectively.

Higher weight loss, 20.38 % for K1b* in the absence organic carbon is attributed to the decomposition of FeS_2 . The 0.08% of organic carbon of K1a shows the evidence of downward percolation of organic enriched solution. The upper most portion of the residual clay (K1c) has an organic carbon concentration of 0.72%. This higher concentration is attributed to the presence of plant remains as evident from field observations. For K1b the pH is 7.5, but on exposure due to oxidation in the mine environment the pH of the same clay reduces to 3.2 indicating a rapid acid leaching condition. The black patched clay has a pH of 2.58 showing the oxidation of FeS_2 mineral as identified in the XRD by the presence of melanterite and jarosite. For fines, the oxides have similar range of distribution.

4.I.4.3.2 Gray Carbonaceous clay (K2, K4, K6 and K7)

The raw clay has appreciable amount of SiO_2 . But their fine fractions have lower SiO_2 content, almost half the amount that of residual clays ($< 2 \mu\text{m}$), due to higher gibbsite. Enriched gibbsite concentration in sedimentary carbonaceous clay layers indicates that the above layers might have formed either by the transportation and consequent deposition of gibbsite enriched parent lateritised clay or by an intense *in situ* leaching of the deposited parent materials. On the contrary, the typical feature of laterite, *i.e.* the Fe encrustation is less, as evident from the chemical assay, which shows the remobilization of this particular oxide in the highly reducing environment. TiO_2 and Fe_2O_3 are concentrated more in the coarser fractions. Maximum concentration of iron was for K7 (2.74%) where the iron sulphide mineral, marcasite is present. The concentration of ferrous iron could not be estimated in these clays due to the masking of the colour by organic carbon during titration.

Table 4.I.2. Chemical characterisation of clay samples (wt%)

	K1a	K1b	K1b*	K1c	K2	K4	K6	K7	K8	K9	K10
SiO ₂	63.02 45.72	65.55 46.36	46.63	75.67 47.42	31.14 23.87	71.3 22.03	29.88 33.99	39.73 34.45	51.73 45.04	81.03 45.92	57.02 44.16
Al ₂ O ₃	19.73 37.46	22.82 36.97	11.95	13.24 36.49	35.92 43.75	12.12 44.62	37.37 42.94	26.96 42.67	34.33 38.02	10.57 37.29	21.12 37.71
^δ Fe ₂ O ₃	2.53 0.90	1.27 0.88	19.05	1.29 0.87	0.96 0.57	1.87 0.07	0.59 0.72	2.74 0.69	1.58 0.93	1.60 0.43	7.88 2.81
FeO	2.29	1.02	3.18	0.91	-	-	-	-	Bdl	bdl	bdl
[#] FeO	0.05	0.75	1.98	0.95	bdl						
SO ₄ ²⁻	0.02	1.38	8.22	2.18	bdl						
TiO ₂	3.97 0.01	1.35 0.03	2.01 -	3.03 0.11	4.41 0.11	3.31 0.12	2.83 0.06	4.09 0.02	0.28 0.47	1.42 0.10	3.57 0.37
CaO	0.71 0.78	0.16 0.09	0.33 -	0.12 0.14	0.11 0.14	0.14 0.14	0.15 0.14	0.28 0.14	0.27 0.33	0.50 0.28	0.59 0.72
K ₂ O	1.14 0.18	0.17 0.14	0.35 -	0.06 0.05	0.04 0.62	0.19 0.26	0.07 0.05	0.12 0.05	0.06 0.29	0.06 0.02	0.14 0.32
Na ₂ O	0.25 0.48	0.15 0.14	0.16	0.11 0.04	0.04 0.12	0.20 0.11	0.03 0.18	0.13 0.22	0.10 0.23	0.17 0.17	0.20 0.40
MgO	1.04 0.26	0.11 0.06	0.09 -	0.02 0.01	0.03 0.15	bdl bdl	0.02 0.03	0.02 0.02	Bdl Bdl	bdl bdl	bdl bdl
LOI	7.98 14.46	8.59 14.63	20.38	5.53 14.59	27.01 30.42	10.85 32.11	29.08 21.79	26.49 21.33	11.64 14.57	5.27 15.08	9.30 13.51
[*] OC	0.08	0.03	-	0.72	8.20	5.56	8.67	9.09	0.12	2.89	0.02
[*] pH	5.59	7.5 (3.2)	2.58	2.80	3.32	3.37	3.00	3.05	4.62	4.43	4.81
^{\$} HI	1	1.1	-	1.07	1.01	0.97	0.71	0.91	1.23	1.24	0.67
^β A (001) (002)	0.35 0.35	0.35 0.3	- -	0.35 0.35	0.4 0.3	0.35 0.35	0.45 0.4	0.35 0.3	0.4 0.35	0.3 0.3	0.5 0.45

Upper reading corresponds to the raw fraction, Lower reading corresponds to < 2 μm fraction (fines),
 bdl – below detectable limit, OC- organic carbon, LOI- Loss on ignition , [#] Fe- Water soluble iron.,
^{*} raw fraction.

^{\$} Hinckley crystallinity index of < 2 μm fraction, ^β Amigo crystallinity index of < 2 μm fraction (width at half height of 001 and 002 kaolinite peaks).

Water-soluble SO_4^{2-} and iron were below detection limits. FeS_2 in these layers is much lower even though these layers are formed in the presence of highly organic rich environment. This might be due to its removal of either the SO_4^{2-} or Fe^{2+} or both by leaching under the tropical climatic condition through the highly permeable sandy clay layers. Studies on the similar sedimentary sequence, *i.e.* the Warkallai Formation of Northern Kerala showed the crystallization of ample FeS_2 minerals in the carbonaceous clay seams (Manju *et al.*, 2001). Here in this deposit geochemical evidences indicate that the lower concentration of FeS_2 could be attributed to the lack of reactive iron needed for crystallization of FeS_2 . The XRD results also confirm the above evidences, where the marcasite is found only in minor amounts even in the heavy fractions. Presence of FeS_2 and ample amount of water leachable SO_4^{2-} in the residual white clay, is a clear indication of the elution of these from the carbonaceous seams. The loss on ignition of the samples are in accordance with the concentration of organic carbon and the associated minerals-gibbsite and kaolinite. The organic carbon content is maximum for K7 (9.09%) and minimum for K4 (5.56%). pH values of the raw clays vary somewhat randomly between 3 to 3.37.

4.I.4.3.3 Hematitic clay (K8, K9 and K10)

The uppermost hematite rich layers are enriched in quartz as evident from high SiO_2 content. Fe_2O_3 (7.88%) and TiO_2 (3.57%) are maximum for the uppermost lateritised clay, K10. Water-soluble iron and SO_4^{2-} are absent in these highly oxidized clays. K_2O content is more in the fine fractions showing the presence of disintegrated fine feldspar. The clays are slightly acidic with pH around 4.5. In these layers, organic carbon is maximum (2.89%) for the coarser and friable sandy clay layer.

The changes in chemical composition are fully consistent with the mineralogical data as described above.

4.I.4.4 Trace Element Analysis

The type and amount of trace elements in the clay profile reflect the environmental condition encountered by the rock during the course of geological time. Trace element

analysis of the raw and fine clay fractions of selected clay samples from three types of clay layers (residual, carbonaceous and ferruginous) show wide variations in concentration (Fig. 4.I.8).

Lead having an ionic radius (Pb^{2+} 1.32 Å) replaces potassium (1.33 Å) (Goldschmidt, 1958), which is a major constituent of most common rock forming mineral. Appreciable concentration of Pb is noticed in almost all the samples and it is maximum in clay fraction of K8 (409ppm), indicating lesser leaching compared to other samples and least was noticed for the fine fraction of the residual clay (29.80 ppm).

Chromium Cr^{3+} (0.64 Å) having ionic radius similar to that of ferric iron (0.67 Å) is found to show isomorphous substitution. The above element was found to be highly concentrated in bulk fraction of K10 (469 ppm), where Fe_2O_3 is maximum. Conversely the least concentration is noticed for the residual K1b clay (5.40 ppm). These wide differences reflect the variation in the character of the parent rock material.

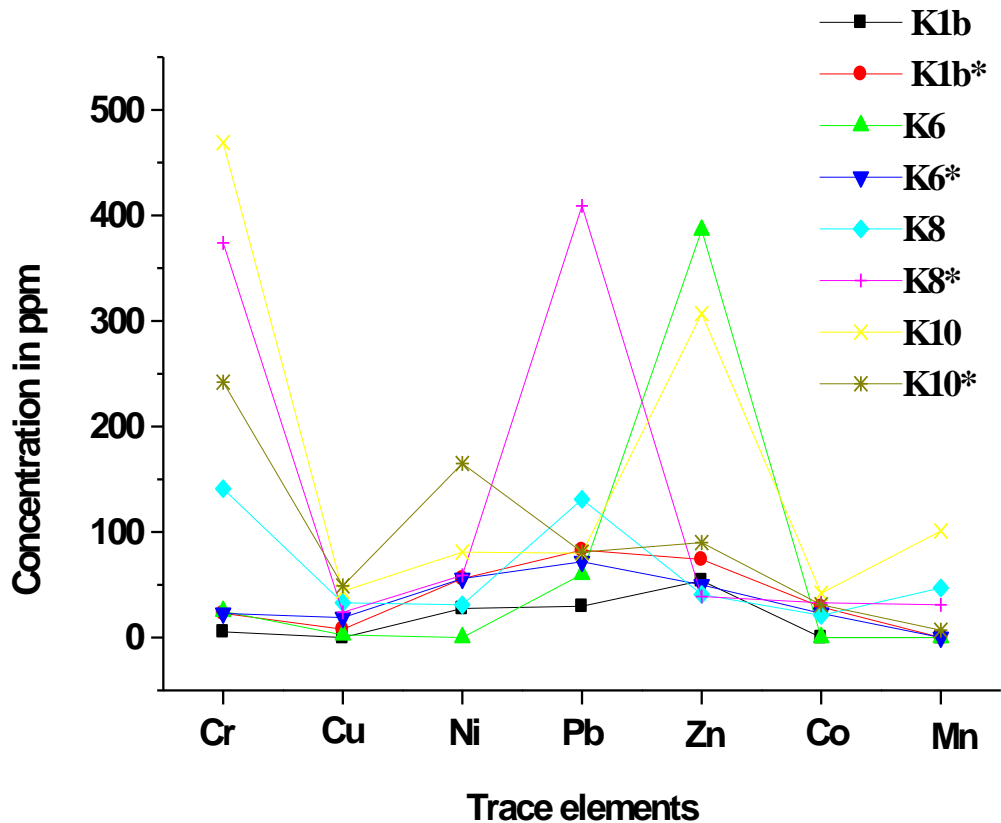


Fig. 4.I.8. Trace element analysis of raw and fines of selected clay samples: K1b, K6, K8, and K10 (sample code with * represents the corresponding $< 2 \mu m$ fraction).

Cobalt and nickel probably expected to be incorporated in the parent ferromagnesian minerals (Rankama and Sahama, 1952; Goldschmidt, 1958) might get concentrated in ferric oxide/ferric hydroxide, the alteration products of the above parent minerals. The above geochemical behavior is clear from the higher concentrations of Co and Ni in the uppermost laterite layer (K10), which has a higher concentration of Fe.

Copper expected to be soluble due to its lower ionic potential, is found in lower concentrations in all the samples. Comparatively higher value of this element in fines could be explained based on its surface adsorption property.

The divalent Mn^{2+} ion, which occurs as a substitute for Fe^{2+} in the ferromagnesian mineral of the parent rock gets depleted since it is more liable to leaching than any other elements. The above element is absent in both the fractions of the residual clay K1b, owing to the basic nature of the element which gets leached away even in slightly acidic condition in an anaerobic environment. On the other hand their concentration in the oxidized hematite rich environment K8 and K10 is due to its precipitation under aerobic conditions.

Trace element distribution patterns also shows the influence of reducing and oxidizing climatic conditions. The total trace elemental concentration is maximum in the raw fractions of uppermost lateritised clay (1124 ppm), which substantiates its high residual nature.

4.I.4.5. Thermal Studies

Thermal studies on fine fraction of the clays: residual white clay, gray carbonaceous clay and hematitic clay were undertaken by DTA/TG analysis. The DTA/TG analysis (Fig. 4.I.9A&B) complements the evidences obtained from XRD analysis. The intensity of leaching as evident from relative concentration of the mineralogical assemblages, kaolinite and gibbsite could be confirmed from DTA/TG curves.

4.I.4.5.1. DTA analysis

The DTA patterns (Fig. 4.I.9A) show endothermic peaks of gibbsite, ranging from 288.2 to 298.5°C for the gray carbonaceous clay and it is maximum for K4. The range of the

endotherm reflects the variation in crystallinity of the mineral. The endothermic peaks for the above minerals were absent in the residual and hematite rich clay layers.

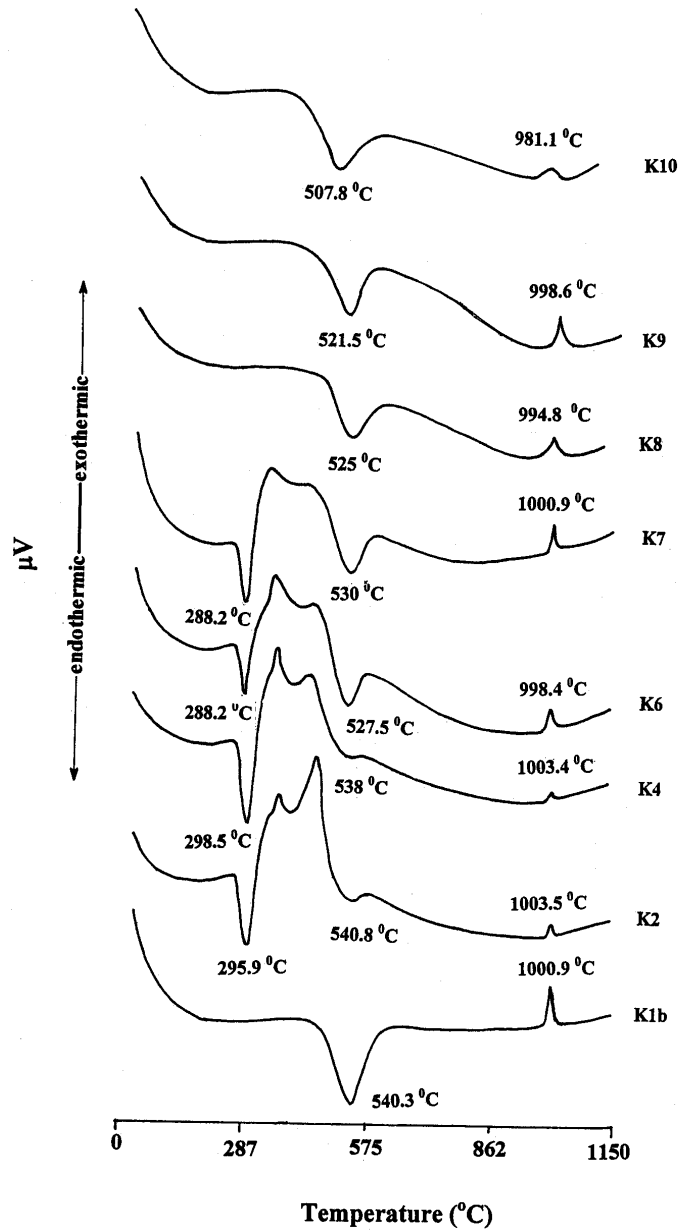


Fig. 4.I.9A. DTA curves for < 2 μm fraction, indicative of variation in the environmental condition of deposition / formation for the different types of clays as evident from the peaks of gibbsite.

The endothermic peak characteristic of kaolinite also ranges between 507.8 and 540.8°C. The intensity of this peak is not sharp for the samples with relatively high gibbsite content. Corresponding changes were noticed in the exothermic peak also, where formation of the new phase mullite occurs. The exotherm of kaolinite falls between

981.1 to 1003.5°C. The lowest temperature of exotherm was for K10, the topmost lateritised clay where the Fe₂O₃ concentration is high. The kaolinite, which has the higher endothermic peak, has a relatively higher range for the exotherm also.

4.I.4.5.2. TG analysis

The thermogravimetric curves (Fig. 4.I.9B) show weight losses corresponding to the type of minerals present.

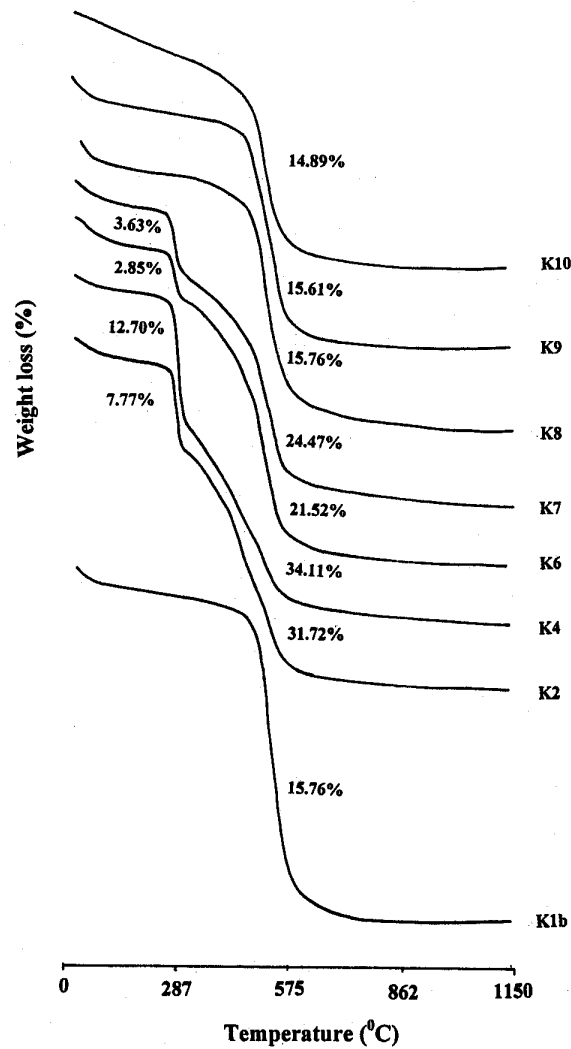


Fig. 4.I.9B TG curves for < 2 μm fraction, indicative of variation in the environmental condition of deposition / formation for the different types of clays as evident from the weight loss characteristic of gibbsite; weight loss due to gibbsite (left) and cumulative weight loss (right).

Higher cumulative weight loss is noticed for samples K4 (34.1%), K2 (31.72%), K7 (24.47%) and K6 (21.52%), where there is appreciable amount of gibbsite and organic carbon. Weight loss corresponding to gibbsite around 288°C is maximum for K4 (12.70%) where maximum concentration of above mineral occurs, as evident from the XRD peak intensity. For the hematite rich clay layers- K8 and K9, TG weight loss is 15.76 and 15.61% respectively. But for the lateritised clay it is much less *i.e.* about 14.89%. For the residual clay (K1b) weight loss is around 15.76%. The range of the percentage weight loss is similar to the weight loss noticed during chemical characterisation.

4.I.4.6 FTIR studies

The infrared spectra of pretreated clay (< 2 µm) fraction (complement the above analytical evidences (Fig. 4.I.10). Well-developed band characterising gibbsite at 3522, 3456 and 3390 cm⁻¹ are found in all the carbonaceous clays. The clay, which has higher gibbsite as evident from the XRD, has higher intensity for the corresponding IR peaks. The effect of the intense leaching environment for gray carbonaceous clay is evident from the gibbsite peaks. Kaolinite is the sole clay mineral, which could be detected in the residual clays- K1a, K1b, K1c and sedimentary ferruginous clays- K8, K9 and K10. The bands of kaolinite are around 3622 - 3695(-OH stretching), 1000-1096 cm⁻¹ (-Si-O stretching), 910-940 cm⁻¹ (-OH bending), and 400-550.cm⁻¹ (-Si-O bending) vibrations (Farmer, 1979). Here the peaks indicating the presence of gibbsite is absent in the residual clay- K1a, K1b and K1c and sedimentary ferruginous clays- K8, K9 and K10. The doublet between 3695 and 3622 cm⁻¹, which reflect the crystalline perfection is, absent in all the clays. This lower degree of crystallinity is confirmed from the Hinckley and Amigo index where the crystallinity index values are below 1.5 and ≥ 0.3 respectively.

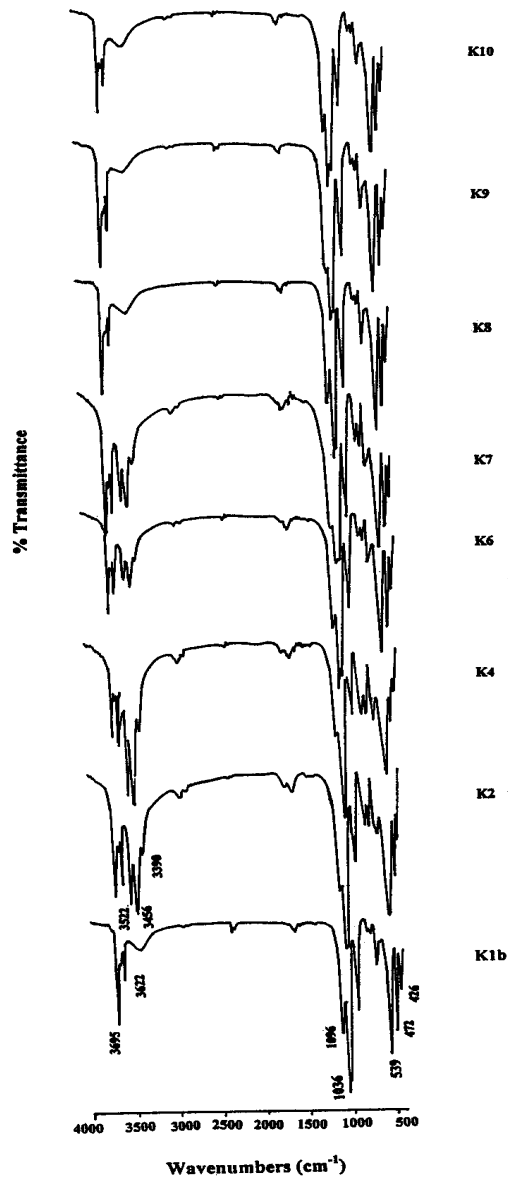


Fig. 4.I.10. Fourier-transform infrared absorption spectra of $< 2 \mu\text{m}$ clay indicating the association of gibbsite along with kaolinite for the carbonaceous clays (K1a and K1c not shown since their IR patterns are similar to that of K1b)

4.I.4.7 Morphological Analysis.

Petrographic data obtained by scanning electron microscopic and optical microscopic examination of the raw clay and handpicked minerals from the residual white, gray carbonaceous and hematitic clays give some interesting geochemical features characteristic of this particular deposit.

4.I.4.7.1 Residual white clay

The mineralogical association in residual white clay as revealed from XRD and field studies include kaolinite, almandine, ilmenite, pseudorutile, rutile, anatase, pyrite,

melanterite and jarosite along with quartz, which is the common impurity in the clay deposit. The scanning and optical micrographs of minerals from the residual clay layer K1a, K1b, K1b* and K1c are shown in Fig.4.I.(11-17).

Kaolinite from this clay layer occurs as microporous tightly arranged booklets characteristic of *in situ* crystallisation. These grains (Fig. 4.I.11) occur as closely spaced stacks having a size of 3 to 6 μm with the individual plates showing face-to-face arrangement. Here kaolinite replaces the feldspar grains through layer-by-layer growth along parallel planes, which are believed to be the cleavage planes. This particular morphology implies kaolinite to be pseudomorphs after feldspar. Loughnan (1969) indicates that the clay minerals will retain their parent mineral structure during weathering. The presence of this typical morphology of kaolinite implies that the major silicate responsible for the clay formation is feldspar.

Fig. 4.I.11 Scanning electron micrograph illustrating stacks of microaggregates of kaolinite, resembling feldspar morphology.

Scanning electron microscopic analysis of biotite indicated that it is in the process of alteration (Fig.4.I.12). The dissolution /alteration of biotite is found to be favoured at edges. Micron sized crystals of kaolinite are found to grow from the edge of biotite grain. The remaining part of this particular grain is partially altered with irregular, curved edges. Step like or terrace like retrograding layers are found for this grain (arrow). This typical alteration feature for kaolinite was also reported by Tarzi and Protzi, (1978). The

dissolution of these primary silicates resulted in the release of ferrous iron and the remaining iron in the lattice is oxidised (White and Yee, 1985; Gilkes and Suddhiprakarn, 1979; Cleaves *et al.*, 1970; Velbel, 1985a, b).

Fig. 4.I.12. Scanning electron micrograph of biotite from the lowermost residual clay K1a, with kaolinite formation at the edges of the grain, the terrace like retrograding layers (arrow) are typical for biotite alteration.

The optical microscopic examination of biotite shows features indicative of alteration. Gradation in the alteration features was noticed for the grain (Fig.4.I.13 a-d). Megascopically most of the grains show a rusty brown colour indicating the removal of some amount of iron from their structure. Exfoliation features were noticed on most of the grain surfaces. The biotite grains show jagged edges exhibiting its residual character. Here, most of the grains have relatively lower interference colour and its typical pleochroic feature is absent indicating advanced stage of alteration. Several irregular, curved lines were found on the surface of the entire grain. Similar manifestation of weathered biotite was noticed by Acker and Bricker (1992). Some black materials were found to fill these curved features. In addition the grain shows pitted appearance indicative of alteration. Inclusions of some minerals similar to that of zircon were also found in some grains (Fig. 4.I.13d) A few grains shows the typical platy habit with a greenish tinge under open nicols, indicative of the presence of more amount of ferrous iron (Fig.4.I.13 e).

Fig. 4.I.13. Optical micrographs of hand picked minerals from residual white clay layer.
**[a - e] : Biotite grains from K1a: showing alteration features such as irregular cracks – (b),
pitting on the surface & filling of the cracks with alteration products – (c)
inclusion of zircon – (d), biotite grain with coating of ferrous iron – (e).**
[f] : Quartz grain from K1a with coating of ferrous iron.
[g] : Quartz from K1c with ferric coating.
**[h] : Garnet grains from K1b with concoidal fracture surfaces and pitted appearance.
(under open nicols ; X denotes magnification) .**

Field observations revealed the presence of Fe rich garnet, almandine $\text{FeAl}_2(\text{Si}_3\text{O}_{12})$ patches strewn throughout the residual white clay.

Optical analysis of garnet grains reveals their isotropic nature with typical concoidal fracture (Fig. 4.I.13 h). Some of the grains show a pitted appearance.

SEM studies reveal the irregular massive nature of this particular mineral (Fig. 4.I.14A). A few grains exhibit partially developed isometric crystal faces with typical rhobododecahedral (r) and trapezohedral (t) crystal face combinations (Fig. 4.I.14B). Further magnification of the same grain shows some interesting morphological and textural features on the grain surface (Fig. 4.I.14C). Numerous etch pits are found on the grain surface indicating the selectivity of surface leaching. Two types of etch pits (o) and (i) show two different genetic microenvironments indicating differential rates of leaching of the almandine grain. Fine etch pits (i) were found to be oriented in particular direction parallel to the crystal face. These etch surfaces are found to be coated with some amorphous substance. Large etch pit (o), show *in situ* crystallisation and these minerals are formed by the alteration of the above parent mineral. This secondary product occurs as vermiform pseudo-hexagonal stacks where the grains are arranged in a face- to -face manner (Fig. 4.I.14D). The morphology exhibited by this particular grain indicates *in situ* crystallisation. In these etch pits, amorphous coating is absent. Velbel (1984) explains the formation of gibbsite and goethite as the by-products of weathering during his study of alteration of almandine. The XRD analysis of the garnet grains (Fig. 4.I.5 b) shows the presence of gibbsite. Most probably the above *in situ* crystallising mineral would be a vermiform gibbsite. The characteristic feature of the two types of etch pits indicates two sets of weathering conditions, inorganic and biochemical (involving organic chelating agent). Weathering of almandine under inorganic conditions results in the formation of amorphous coated material in this weathered product (Velbel, 1984). In addition the effect of organic chelators, resulting from the leached out material from the above organic/sandy clay layers also contribute to the weathering of almandine with *in situ* gibbsite mineralization there by, leaching out the Fe from the proximity of the mineral. The almandine grains were found affected by both organic and inorganic weathering processes.

Fig. 4.I.14A. Almandine grains in low magnification.

Fig.4.I.14B. Partially developed isometric garnet grain with its rhombododecahedral (r) and trapezohedral (t) faces.

Fig 4.I.14C. On magnification of the above almandine grain, two sets (arrow) of etched pits were found on the surface of the above grain, indicating two types of environmental conditions inorganic (i) and biochemical (o) suffered by this mineral during the course of weathering.

Fig. 4.I.14D Almandine grain showing *in situ* mineralization within the etch pits (arrow).

An interesting geochemical feature noticed in the residual clay is the presence of FeS₂ and Fe-oxyhydroxide minerals as pockets strewn throughout the white clay. FeS₂ crystals (Fig. 4.I.15A) occur in various morphologies, cube-octahedral combination (c), and pyritoheron (p). Numerous etch pits on their surfaces (arrow) indicate the influence of ongoing weathering. The crystal morphology of FeS₂ alteration product, melanterite and jarosite is also evident from scanning electron microscopic analysis. Melanterite show a bushy tubular appearance (Fig. 4.I.15B). On magnification these microtubules show the typical monoclinic habit (Fig 4.I.15C). The arrow points to the 001 face of the melanterite crystals. Figure 4.I.15D shows the association of fine kaolinite grains at the edges of tubular melantarite grains. The reddish yellow precipitation identified as feroxyhyte, from the leached out water from the clay shows rounded aggregates of 1-2 micron sized particle with grassy surfaces (Fig. 4.I.15E). This typical poorly crystalline iron oxide is reported to be formed in an environment enriched in SO₄²⁻ (Brady *et al.*, 1986). These particles have similar feature to the natural stream precipitate as described by Chukhrov, *et al.*(1970).

Fig. 4.I.15A. FeS₂ crystals showing the typical crystals of cube-octahedral combination (c) and pyritoheron (p) with numerous leach pits (arrow).

Fig 4.I.15B. Melanterite with its bushy appearance

Fig 4.I.15C. Magnification of the above bushy feature showing well developed monoclinic crystals of melanterite (arrow points to 001 face).

Fig.4.I.15D. Melanterite in association with fine kaolinite grains at its edges.

Fig 4.I.15E. Feroxyhyte, the poorly crystalline iron- oxide aggregations with grass like projections on their surface, precipitated from leached out solution in Fe and SO_4^{2-} enriched environment.

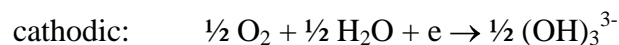
Alterites. Another typical characteristic feature of this residual clay layer (K1a) is the presence of ample amount of altered minerals commonly named as alterites. Here the features of the parent mineral could not be identified due to the obliterated nature (Fig. 4.I.16 a-d). Ferrous iron with characteristic greenish tinge is found to coat the grains. Some of them show a pitted appearance. The bleaching effect, *i.e.* the removal of Fe from the proximity of the grain is noticed for some of the grains (Fig. 4.I.16 b, c, d). For grain d, most of the ferrous iron coating was removed under the influence of a reduced leaching condition. Later the remaining ferrous iron is found to be transformed to ferric form as evident from the change of the colour of the pigment from green to reddish brown. Some of the grains show *in situ* crystallisation of some minerals at edges (Fig. 4.I.16 e and f). The newly formed crystals with pyramidal terminations and yellowish appearance at the edges of the grain indicates that the mineral is zircon, which results from the alteration of the ferromagnesian minerals.

Ilmenite, pseudorutile, anatase and rutile are the Fe-titanium minerals present in the residual clay as identified by optical microscopic and XRD analysis. Petrologic analysis of heavy fractions (Fig. 4.I.16 g), show ilmenite grain with corroded appearance. Different stages of ilmenite alteration are revealed by optical microscopy. The grains show gray patches of unaltered ilmenite (Fig. 4.I.16 h, i, j). At the periphery the colour of the grain becomes more reddish brown accompanied by an increase in reflectivity. The term leucoxene is used for this type of alteration product. Fig. 4.I.16k, shows a grain which is completely altered to leucoxene. Some of the ilmenite grains show another type of alteration feature. These partially altered ilmenite grains consisting of a core of dark gray phase, rimmed by a light gray alteration product which might probably be pseudorutile with granular appearance (Fig.4.I.17 a). Anand and Gilkes (1984) explain the association of this particular mineral in lateritic pallid zone as a result of Fe leaching from the ilmenite grain. This mineral is found as the intermediate phase in the alteration of ilmenite to rutile or anatase (Teufer and Temple,1966; Anand and Gilkes, 1984). Lynd (1960) and Temple (1966) explain such a granular character for the ilmenite alteration product due to decrease in the Fe and subsequent increase in porosity.

Photomicrographs also show the typical stage of alteration of ilmenite to anatase (Fig. 4.I.17 b & c). These grains show features of partial conversion of ilmenite to rutile. Here the portion having higher reflectivity is that of anatase and the darker portion is unaltered ilmenite. Temple (1966) explains such an optical stage for the ilmenite-anatase during its course of alteration. Even though the XRD analysis of the heavy mineral fractions do not show any evidence of the precipitation of ferric oxides on the grain surface, the features on the photomicrographs indicate their formation on anatase surfaces, pointing towards the influence of oxidising environment (Fig. 4.I.17 d-h). Few grains show the precipitation of the exsolved iron as yellowish brown coloured ferruginous granules at the boundary of the crystal (Fig. 4.I.17 i). The anatase grains are found in different forms. Well-developed crystals are rare. Even though the XRD analysis indicates good amount of rutile from K1c, the features of this mineral could not be discriminated from that of anatase by optical analysis.

The mechanism of transformation of ilmenite \rightarrow pseudorutile \rightarrow rutile is evident from the above analysis. Grey and Reid (1975) explained a feasible mechanism for the alteration of ilmenite on the basis of an electrochemical corrosion model. Here the oxidation and leaching proceeds *via* electrochemical corrosion process in zone of saturation. The material leached *via* a dissolution and reprecipitation process in zone of oxidation.

The ilmenite containing some ferric iron (e.g. as Fe_2O_3 - FeTiO_3 solid solutions) are quite good conductors, and in suitable groundwater situations this might also be expected to oxidise by the following processes. Possible half- cell reactions may be written

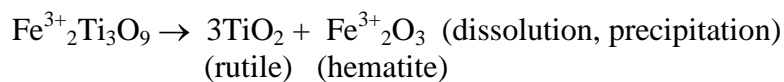
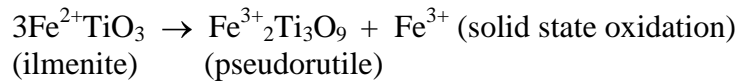


In situ anodic oxidation of ferrous ions produces electrons, which can move through the conducting surface to the surface (or to a crack in the grains) and take part in the cathodic reduction of oxygen in the pore water. The above half- cell reaction show that the complete oxidation of ferrous iron in ilmenite to ferric iron releases one electron; this will produce just enough hydroxyl ion (or some anion) at the cathode to remove one –

third of the ferric ions produced. The product of electrochemical alteration of ilmenite is $\text{Fe}^{3+} \frac{2}{3}\text{TiO}_3 = \text{Fe}_3\text{Ti}_3\text{O}_9$, the pseudorutile. The changes of the ilmenite to pseudorutile results in a volume reduction of about 6 percent which would produce considerable elastic stress in the oxygen lattice at the coherent interface between segments of ilmenite and its alteration product, pseudorutile. This would result in the development of considerable microcracking and poring. Consistent with this the microscopic study of the surface of pseudorutile shows evidences of its very fine granularity.

On the contrary, the mineralogical and microscopic analysis revealed the formation of the TiO_2 with a coarser microstructure from ilmenite. This suggests that alteration beyond the pseudorutile composition occur *via* a leaching and reprecipitation process whereby both iron oxide and titanium reprecipitates on the seed materials. Such a mechanism could change the microscopic features such as granularity or crystallite size, while maintaining the overall macroscopic morphology. Epitactic reprecipitation of titanium oxide on the original material occurs in this case. This type of alteration occurs in a reducing condition at the top few feet of the deposit where there is ample amount of organic matter.

In short the reactions involved in the alteration of ilmenite to rutile/anatase can be written as:



The iron thus formed may either be precipitated on the surface of the grain or can be removed under reducing conditions. The above sequence of formation of the TiO_2 mineral anatase/ rutile from pseudorutile emphasises the influence of reducing environment in residual clays.

Fig. 4.I.16. Optical micrographs of heavy minerals from the residual clay layers K1a, K1b, K1c.
[a - d] : Stages of leaching of ferrous iron from alterites in K1a; d) conversion of Fe^{2+} to Fe^{3+} and consequent precipitation of Fe^{3+} on the grain surface;
[e & f] : *In situ* crystallization of zircon during alteration of ferruginous minerals;
[g - k] : Stages of ilmenite weathering; (g) corroded ilmenite grain; (h-j) remnants of ilmenite (black) in reddish brown altered leucoxene ; (k) completely altered ilmenite. (X- denotes magnification, under open nicols).

Fig. 4.I.17. Photomicrographs of ilmenite- anatase showing different morphological features.
[a] : Ilmenite from residual clay K1b rimmed with granular pseudorutile;
[b & c] : Ilmenite to rutile transformation, portion with high reflectivity indicates rutile;
[d - h] : Ferric iron coated anatase;
[i] : Association of granular amorphous iron with anatase;
(X denotes magnification, under open nicols).

4.I.4.7.2 Gray carbonaceous clay

The mineralogical analysis indicates the presence of major amount of gibbsite, kaolinite, anatase and rutile along with the ubiquitous quartz.

The clays of K7 layer is found as vermicular stacks with face to face packets in loosely expanded books of 10 μm , in thickness (Fig. 4.I.18A). The above texture indicates an open crystallising environment depicting the unconsolidated nature of the parent material. The typical morphological feature indicates the parent rock to be enriched in feldspar. Most probably this type of kaolinite might have resulted from the alteration of arkosic sand. Kaolinite rich carbonaceous layer (K6) shows agglomeration of the fine grain (Fig. 4.I.18B) suggestive of its sedimentary nature. The morphological feature of the gibbsite in these clays was indistinguishable from that of kaolinite due to their pseudohexagonal habit and ability to form *in situ* vermicular grains.

Optical microscopic analysis of the heavy fractions from these layers shows the presence of anatase, zircon, and sillimanite along with some opaques (Fig. 4.I.19 a- h). Sillimanite shows high refractive index. The grains have the typical irregular termination of its edges (step like appearance) (Fig. 4.I.19 f & g). Some of the grains show vertical striations and exhibit a greenish tinge on the surface. Opaque grains show a varying size range ($\sim 4 - 40 \mu\text{m}$) (Fig. 4.I.19 h).

Fig. 4.I.18A. Kaolinite in K7, gray carbonaceous clay with vermicular appearance indicating an open crystallizing environments with ample space, most of the grains are coated with amorphous carbonaceous matter.

Fig.4.I.18B. Feature indicative of sedimentation: K6 clay showing agglomerated kaolinite/gibbsite.

4.I.4.7.3 Hematitic clay

The mineralogical analysis indicates the presence of appreciable hematite with major quartz and kaolinite.

Kaolinite occurs as vermiform stacks (Fig. 4.I.20A). Here the individual grains are much larger and have a vermicular morphology typical of *in situ* kaolinization. Some portion of the layer K8 shows morphology indicative of sedimentation (Fig. 4.I.20B). Here the particles are much finer and the grains are arranged in an edge to face manner.

Feldspar grains from the lower ferruginous clay layer shows prismatic etch pits (arrow) (Fig. 4.I.20C). They are characteristically developed on the principal (001) cleavage surface with their long axis approximately parallel to the c- axis. Their elongated prismatic shape is prominent from SEM.

Iron minerals are found as coating on the kaolinite surfaces giving the aluminosilicates an amorphous appearance. In addition some of the grain shows a mushroom shaped feature indicative of *in situ* crystallisation (Fig. 4.I.20D). The lower most portions of these grains entirely cover clay surfaces like a coating.

Fig. 4.I.19. Optical micrographs of heavy minerals from the carbonaceous and ferruginous clay layers.

[a] : Anatase;

[b - e] : Zircon;

[f & g] : Sillimanite with irregular edges (saw tooth) and parallel striations;

[h] : Magnetic heavy mineral fraction from K7 layers - note the variation in the grain size;

[i - k] : Ferric iron coated rutile;

[l & m] : Zircon with inclusions;

[n & o] : Tabular and rounded monazite grain with its typical straw yellow color and smooth concoidal surface;

[p] : Magnetic fraction of K8; (X denotes magnification; under open nicols).

Fig. 4.I.20A. Ferruginous clay (K8) showing features of *in situ* kaolinization.

Fig 4.I.20B. The ferruginous clay layer (K8) showing character typical of sedimentary nature.

Fig. 4.I.20C. Etched feldspar grain of the ferruginous clay K8 indicating the intensity of chemical leaching under a tropical climatic condition, most of the pits exhibit prismatic habit (arrow).

Fig. 4.I.20D. Hematite showing mushroom shaped feature, coating the entire clay surface camouflaging its morphological features.

Optical microscopic analysis also revealed the presence of feldspar in this clay enriched environment (Fig.4.I.21a). These grains are enclosed with ferric iron, most probably the hematites, as identified from their cherry red colour. The presence of these unaltered

detrital primary minerals might be due to the iron coating, which perhaps prevented the diffusion of water and consequent alteration of the above primary aluminosilicates. Highly altered hypersthene without any cleavage traces and pleochroic habits were noticed in this clay (Fig. 4.I.21 b, c). The grain shows irregular outline due to corrosion. Some of the grains show pitted appearance. Sillimanite grains with ferric iron patches are also found (Fig. 4.I.21 d - f). Fig. 4.I.21 (g & h) are hematite grains with brownish red earthy appearance. Rutile in these layers is identified by their reddish brown color and its typical slender prismatic/acicular nature (Fig. 4.I.19 i - k). Zircons of different habits are abundant in these layers (Fig. 4.I.19 l & m). Most of them show inclusions. Another typical mineral noticed in the heavy fraction is monazite, $(\text{Ce,La,Di})_2\text{O}_3\text{P}_2\text{O}_5$ with some $\text{ThO}_2.\text{SiO}_2$. They show a typical straw yellow colour with smooth edges. The surface of the grains shows small conchoidal habit. Both rounded and tabular grains are present (Fig. 4.I.19 n & o). The magnetic fractions of the heavies of lateritic clays are shown in Fig. 4.I.19p.

The above mineralogical, geochemical and morphological evidences make clear the influence of the dual environmental conditions on the entire clay deposit.

The typical feature of quick yellow pigmentation of the kaolinite deposit by Fe precipitation could be explained from all the above geochemical and mineralogical evidences. Both oxidation and reducing condition were found to influence the yellow pigmentation character of kaolin.

Fig. 4.I.21. Optical micrographs of heavy- light minerals separated from the hematite-rich layers K8, K9 and K10:

[a] : Feldspar grain from K8 with coating of ferric iron on the surface;

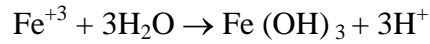
[b & c] : Hypersthene from K8 layer;

[d - f] : Sillimanite grain coated with ferric iron under intense lateritisation.

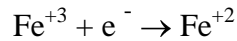
**[g & h] : Hematite from K8 & K9 layers respectively with earthy appearance
(X- denotes magnification, under open nicols)**

4.I.4.8 Yellow Pigmentation on residual kaolinite.

The iron mineral in any of the transition states *i.e.* Fe⁺³ or Fe⁺² can precipitate Fe-hydroxides as shown below. The sudden change in the colour of the white kaolinite emphasises the dominance of the following geochemical processes.



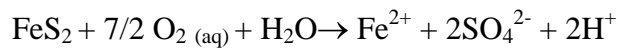
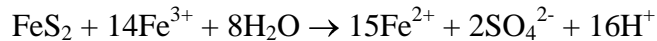
Higher Fe⁺² concentration in this particular deposit which is under relatively neutral pH, prior to oxidation indicates the existence of a coupled half-cell reaction. Here in this type of reaction the iron bearing silicates on weathering releases Fe⁺³. These ions get reduced to Fe⁺² by surface oxidation –reduction reaction which happens for the Fe-bearing silicate minerals as given below (White and Yee., 1985).



(where M represents the cation of charge +z)

These Fe⁺² which were released from the primary iron bearing mineral will be mobilised by thin film of water surrounding each grain and subsequently get deposited on the mineral surface as amorphous ferrous iron layer which on exposure rapidly get oxidised to ferric iron.

In addition, oxidation of Fe- sulphide either in the presence of oxygen or Fe⁺³ ions also provides good amount of Fe⁺² to the surrounding environment.



The Fe⁺² source for the Fe-hydroxide precipitation in presence of high concentration of SO₄²⁻ is again evident from the formation of feroxyhyte. The release of SO₄²⁻ and consequent precipitation of ferrous iron produces high level of acidity in mine. This is also evident from the acidic nature attained by the clay after its exposure.

In addition to the iron hydroxides formed at the clay surface during oxidation, optical microscopic analysis indicates a reddish iron coating for most of the altered mineral, which shows the precipitation of Fe⁺³ ions on the mineral surface during the

course of transformation. The presence of Fe^{3+} on silicate surface was previously documented by Berner and Schott (1982) and Schott and Berner (1983).

The oxidation of FeS_2 and Fe^{2+} and the simultaneous leaching of their oxidation products, Fe^{2+} , Fe^{3+} and SO_4^{2-} along with the percolating water resulted in the precipitation of this iron on the surface of the clays.

The study clearly indicates that the oxidative and reductive processes play a major role in controlling the quality of kaolinite.

4.I.5 Conclusion

The geochemical studies on the kaolinite deposit of Kundara provided valuable information about the influence of the dual environmental conditions on the clay deposit. The mineralogical assemblages and the features of almost all minerals within the residual clay give fingerprints on the influence of oxidising/reducing environment on the deposit.

Pre-Tertiary lateritization of Precambrian crystalline rock – garnetiferous biotite gneiss resulted in the formation of *in situ* residual white clay. This clay has been affected by leaching and weathering processes. The acid reducing condition that developed during the deposition of carbonaceous clay results in the leaching of SO_4^{2-} forming *in situ* FeS_2 in the white residual clay. The decrease in concentration of biotite, ilmenite and pseudorutile in the upper portions of the residual clay profile and consequent increase in anatase and rutile and etch pits of almandine indicate the influence of organic chelating agents on mineral alteration. Later oxidation of FeS_2 during the exposure of the white residual clay resulted in the formation of melanterite, jarosite and ferrosiderite.

The influence of dual environment in carbonaceous clay layers (K2, K4, K6 and K7) is evident from the mineralogical assemblages – gibbsite, marcasite, jarosite and goethite. Intense post-Tertiary lateritisation and oxidising environment at the time of formation/deposition of clay layers K8, K9 and K10 resulted in the hematite enrichment in these clays. In addition to the sedimentary nature, *in situ* kaolinizations of these sedimentary clays are evident from its vermicular morphology.

The entire cycle of reduction and oxidation of iron have an influence on the quality of the industrially viable residual white clay. The rapid yellow pigmentation of this clay resulted from the oxidation of ferrous iron, which is formed by the leaching of Fe-

bearing silicates and non-silicates. The presence of more amounts of iron in ferrous form emphasises the existence of coupled half-cell reaction. In addition accelerated FeS_2 oxidation by Fe^{3+} is evident from the formation of the iron mineral ferrosulphate.

Mineralogical, thermal, spectroscopic and morphological analysis give evidences to substantiate the climatic and environmental conditions during the formation/deposition of kaolinite. Thus, the sequence and pattern of lithologies, mineral content and chemical composition clearly bring out the complete record on geochemistry of the deposit. The texture and morphology of the minerals help to substantiate the conditions of microenvironments under which the formation of this valuable deposit has taken place.

Chapter 4

Part – II

Deferration and Property Evaluation of Kundara Kaolinite

4.II.1. Introduction

Iron staining has been widely researched in kaolin industry because of the yellow shade imparted by it to the commercial products like bone china, tableware, sanitary wares etc. Kaolin containing substantial quantities of free Fe- oxides and oxyhydroxides cannot be used commercially. These clays have red or yellow tint and would therefore be unwanted in paper applications. If used in ceramic bodies they would give poor fired colour possibly accompanied by ‘specking’.

The untoward feature of Kundara deposit is the degradation of the kaolinite quality due to yellow pigmentous coating on short periods of exposure. This occurs due to the ubiquitous phenomenon of $\text{Fe}^{2+} \rightarrow \text{Fe}^{3+}$ transformation, as explained in Part I of this chapter. It is noticed that the kinetics of the above transformation is so fast in this case that the brightness reduces by 7 - 8 units and yellowness increases by 3 – 4 units within a fortnight of atmospheric exposure. Because of the above ionic transformation, the beneficiation of kaolinite becomes more energy intensive as Fe^{3+} leaching is a difficult process.

Iron in any kaolin deposit can be present in different forms: a) as coating on the clay surfaces b) as discrete mineral species like hematite, goethite, ilmenite, iron stained rutile and anatase and c) in isomorphic substitution *i.e.* replacing Al and Si by Fe in the crystal lattice (Jepson, 1988).

The physical separation techniques adopted for the removal of discrete impurities include magnetic separation, flotation and selective flocculation (Fuerstenau, 1976; Shoumkov *et al.*, 1987). But when the impurity is in pigmentous form chemical leaching techniques could only be successfully employed. Various mineral acids viz. HCl, HClO_4 and H_2SO_4 as well as organic acids such as citric, formic, acetic, tartaric, ascorbic and

oxalic acids were found to be effective in deferration by leaching (Cornell *et al.*, 1987; Waite and Morel, 1984; Stumm *et al.*, 1991; Chiarazia and Horwitz, 1991). Ammonium oxalate- oxalic acid mixtures were extensively tried for extracting amorphous inorganic and organic Fe from soils (Stucki *et al.*, 1988). Later the use of oxalic acid for dissolution of Fe from bauxite, goethite, hematite, kaolinite and silica sands have been elucidated by several authors (Ubal dini *et al.*, 1996; Cornell *et al.*, 1987; Bonney, 1994; Ambikadevi *et al.*, 2000). The above investigations have proved that oxalic acid works as an excellent reagent for deferrating mineral surfaces or dissolving oxides of Fe. The investigation of Ambikadevi *et al.* (2000) has indicated that a brightness improvement of 4-9 units could be achieved for Fe-stained kaolinites, which have a yellow to brown pigmentous coating.

The mechanism of reductive dissolution was suggested by Panias *et al.* (1996) which involved adsorption of the ligand on the mineral surface followed by autocatalytic dissolution. Ferrous ions can accelerate the reaction and increase the kinetics of the dissolution.

Since the clay under investigation has a fairly high brightness value (77% ISO) at the time of mining which decreases on exposure very fast, indicates that it contains significant amount of ferrous ions at its surface at the time of mining. Hence it was felt worthwhile to investigate the brightness improvement studies of this clay using oxalic acid as chelating agents.

The objectives of the present investigation are a) the identification of the type of iron mineral impurities in this deposit 2) to extract Fe before it develops yellow colour, that is arresting the oxidation of ferrous Fe by complexing with oxalic acid 3) to compare the leaching efficiency of oxalic acid with H₂SO₄ and sodium hydrosulphite and finally 4) to carry out the utilization studies by incorporating the processed clay in bone china formulations.

4.II.2 Materials and Methods

Raw clay samples were collected from the white residual clay seam. The coarse fraction was size separated by wet sieving using 350 mesh BS sieve. Less than 350 mesh fraction has been denoted as '*finer*' in the text of this chapter. In order to minimize atmospheric oxidation the size separation was done immediately after the sample collection.

Chemical characterisation of the '*finer*' was carried out by classical chemical analysis (Bennett and Reed, 1971). The major oxides SiO₂ and Al₂O₃ were determined by gravimetric and titrimetric techniques respectively. The total iron content was determined as Fe₂O₃ by spectrophotometry. The percentage of ferrous iron, as FeO was analyzed by volumetric techniques by the wet combustion method. SO₄²⁻ in the '*finer*' was estimated after extraction with 1% hot HCl followed by precipitation as BaSO₄ (Jeffery *et al.*, 1989).

Mineral assemblages in *finer* were analyzed by X-ray diffraction. The samples were scanned from 5 to 65° 2θ at 40 kV and 20 mA in Philips PW 1710 X-ray diffractometer.

Deferration studies were undertaken at room temperature in 33% slurry (solid to liquid ratio 1: 2). The required amount of oxalic acid /H₂SO₄/both in combination (E.Merck, AR grade) was added to the clay slurry, stirred for 5 minutes for uniform mixing and kept undisturbed for iron extraction for a fixed period of time where iron is brought into solution by complexation.

For sodium hydrosulphite treatment, a 50 g clay dispersed in 350 ml water at pH-3 (using dil. H₂SO₄) is treated with 0.15 g of the reagent at room temperature by stirring for 30 minutes.

The leached liquor was analyzed for Fe by spectrophotometric technique using 1: 10 phenanthroline as colour developing agent.

The treated clay was filtered, washed free of iron and the brightness/yellowness measured as per the procedure 2.14.4 (chapter 2). The effect of chemical leaching on kaolinite structure was analysed by Hinckley crystallinity index calculation (Hinckley, 1963) and Scanning electron microscopic studies. The dried samples were sprinkled on double sided carbon coated tape pasted on brass stud and sputter coated with gold prior to the analysis.

Particle size distribution of < 45 μm fraction (*finer*) was carried out using Micromeritics Sedigraph 5100 with sodium hexametaphosphate as deflocculent. Viscosity of the sample was measured in 63% slurry.

The physical properties *viz.* water of plasticity, viscosity, green MOR, fired MOR, linear shrinkage, volume shrinkage, bulk density, water absorption and apparent porosity

were measured as per ASTM standards. Detailed experimental procedures adopted are given in Chapter 2.

Deferrated clay was incorporated in bone china body and the results compared with those of the standard formulation. The experiments were carried out at Tata ceramics, Cochin Export Processing Zone, Kakkanad, Cochin, India.

4.II.3 Results and Discussion

4.II.3.1 Mineralogical and Chemical characterisation

X-ray diffraction patterns (Fig.4.II.1) indicate that the major mineral present in the above clay is kaolinite. Quartz was identified as minor constituent.

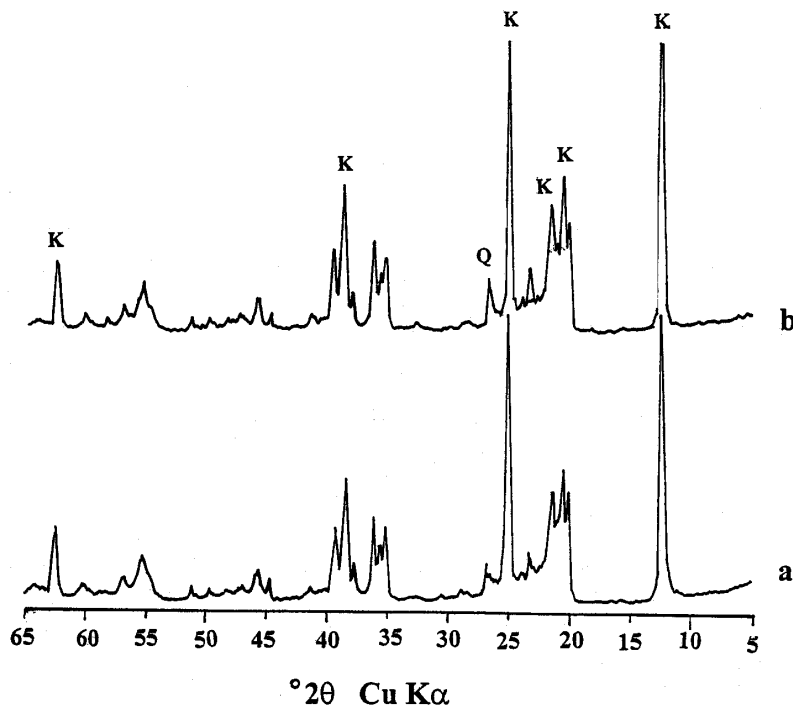


Fig. 4.II.1 X-ray diffractograms of (a) $<45 \mu\text{m}$ fraction of kaolinite (b) $<45 \mu\text{m}$ fraction treated with 0.5 g (for 50 g clay) oxalic acid, K- Kaolinite, Q- Quartz.

The chemical characterisation of the clay presented in Table 4.II.1 indicates that the composition is more or less in the same range as that of standard kaolinite (SiO_2 - 46.33% and Al_2O_3 – 37.84%).

Table 4.II.1. Chemical assay of < 45 μm fraction (wt%)

SiO_2	Al_2O_3	$^{\$}\text{Fe}_2\text{O}_3$	FeO	$^*\text{SO}_4^{2-}$	TiO_2	CaO	Na_2O	K_2O	LOI
46.33	37.84	0.70	0.31	0.10	0.14	0.02	0.07	0.28	14.08

$^{\$}$ - total iron, LOI – Loss on ignition (1025 $^{\circ}\text{C}$), * SO_4^{2-} as BaSO_4

The total iron present is 0.70 % of which 0.31% is in the ferrous form (~ 44.4%). SO_4^{2-} leached out from the clay was around 0.10 %.

The above chemical and mineralogical evidences and geochemical characteristics of the clay as explained in Chapter 4.I showed that the Fe contamination in this kaolinite are of the following types: ferrous/ ferric hydroxides or sulfates and surface coating on ilmenite, anatase, rutile, and pseudorutile.

4.II.3.2 Leaching studies

Table 4.II.2 shows the results of iron removal from the fines (< 45 μm fraction) for three sets of leaching conditions 1) with oxalic acid 2) with oxalic acid in presence of H^+ ions (0.1 N H_2SO_4) and 3) with just mineral acid alone (H_2SO_4). All experiments were conducted at different acid concentrations and reaction periods. All experiments were carried out in 50 g batch of clay with solid to liquid (clay to water) ratio of 1:2 at room temperature.

As evident from table 4.II.2, A 1-5, it was found that the iron leaching increased with increasing acid concentration. Correspondingly, the improvement in brightness and reduction in yellowness also could be observed. 0.1gm oxalic acid in 50-g clay (2 kg/ton) improved the brightness by 7.29 and reduced the yellowness by 4.09 units. The leached out iron was around 37.11% of the total iron present in the clay (0.71%).

Table 4.II.2. Brightness measurement and chemical assay of the treated sample

Experiments	Brightness/ Yellowness%	% Fe ₂ O ₃ removed	% Al ₂ O ₃ removed	% SiO ₂ removed	Hinckley Index
Raw sample (RS)	77.48/8.66	-	-	-	0.85
RS after 2 weeks of exposure	69.99/12.30	-	-	-	-
Deferrating agents:					
#Sodium hydrosuphite (commercial deferrating agent; 0.15g)	84.11/4.9	33.01	0.14	0.27	-
*A.Oxalic acid (g):					
1) 0.10	84.77/4.57	37.11	0.13	0.30	-
2) 0.15	84.84/4.44	44.06	0.26	0.42	-
3) 0.20	84.91/4.27	53.34	0.38	0.57	-
4) 0.25	85.40/4.15	54.45	0.51	0.60	-
5) 0.50	85.65/3.82	67.25	0.55	0.63	0.91
*B. Oxalic acid (g) + 0.1 N H₂SO₄ :					
1) 0.10	84.96/3.68	47.74	0.45	0.91	-
2) 0.15	85.38/3.43	50.56	0.52	0.93	-
3) 0.20	85.51/3.36	58.91	0.56	0.96	-
4) 0.25	85.63/3.26	60.90	0.59	0.96	-
5) 0.5	85.80/3.18	79.27	0.63	0.99	0.59
*C. H₂SO₄ (N) :					
1) 1 × 10 ⁻⁴	77.50/8.66	1.11	0.01	0.05	-
2) 1 × 10 ⁻³	77.69/8.55	1.15	0.04	0.09	-
3) 1 × 10 ⁻²	77.40/6.8	2.32	0.14	0.42	-
4) 1 × 10 ⁻¹	82.86/4.77	20.87	0.42	0.91	0.65
5) 1 × 10 ⁰	83.32/4.44	47.54	0.70	2.32	-

* Reaction time - 15 hours, Temperature of reaction - room temperature, Feed ratio - clay: water 50: 100; # Reaction time- 30 minutes, Temperature of reaction –room temperature, with 30 minutes stirring, Feed ratio –clay: water 50:350 at pH –3 (dil. H₂SO₄).

A further increase in the complexing agent (0.5 g per 50 g of clay *i.e* 10 kg/ton) could extract nearly 67.25% of the total iron. The brightness/ yellowness achieved was 85.65/ 3.82%.

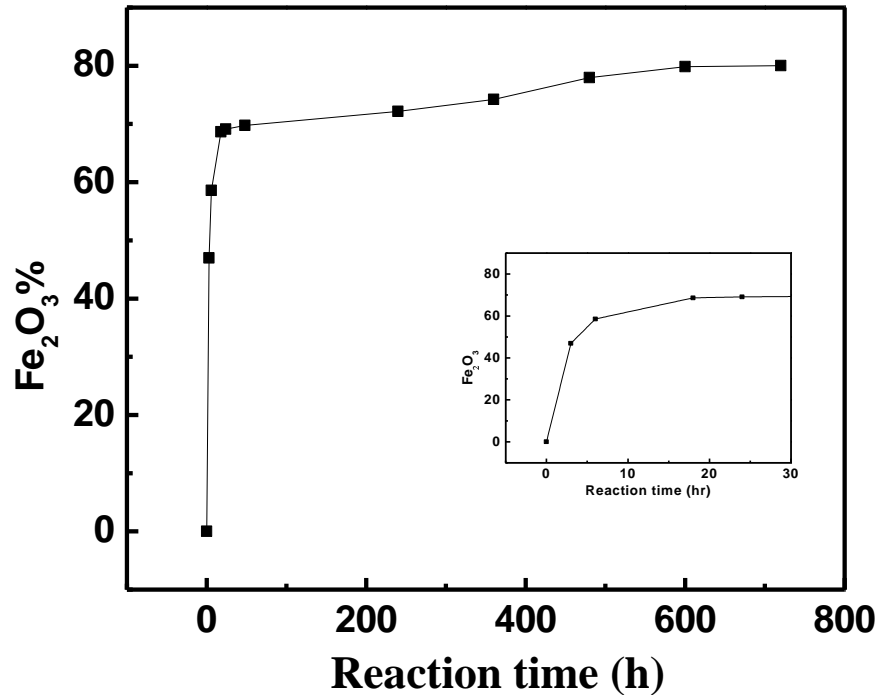


Figure 4.II.2A. Extent of iron removal with reaction time
Oxalic acid concentration 10 kg/ton; solid: liquid ratio (clay: water) 1:2.

Figure 4.II.2.A shows the kinetics of Fe leaching with oxalic acid (10 kg/ton). Even a 3-h reaction could leach out 46.97% of Fe₂O₃ improving the brightness to 84.57%. The results indicated in figure 4.II.2.B imply that increase in reaction period increases the brightness. After a reaction period of 18 h brightness of clay remained almost steady. The kinetics of reaction clearly indicates the leachability of the ferrous and ferric iron in oxalic acid solution. After 720 h (30 days) of treatment brightness/yellowness achieved for the clay was 85.65/4.57%. Almost 80% of iron was found to be leached out.

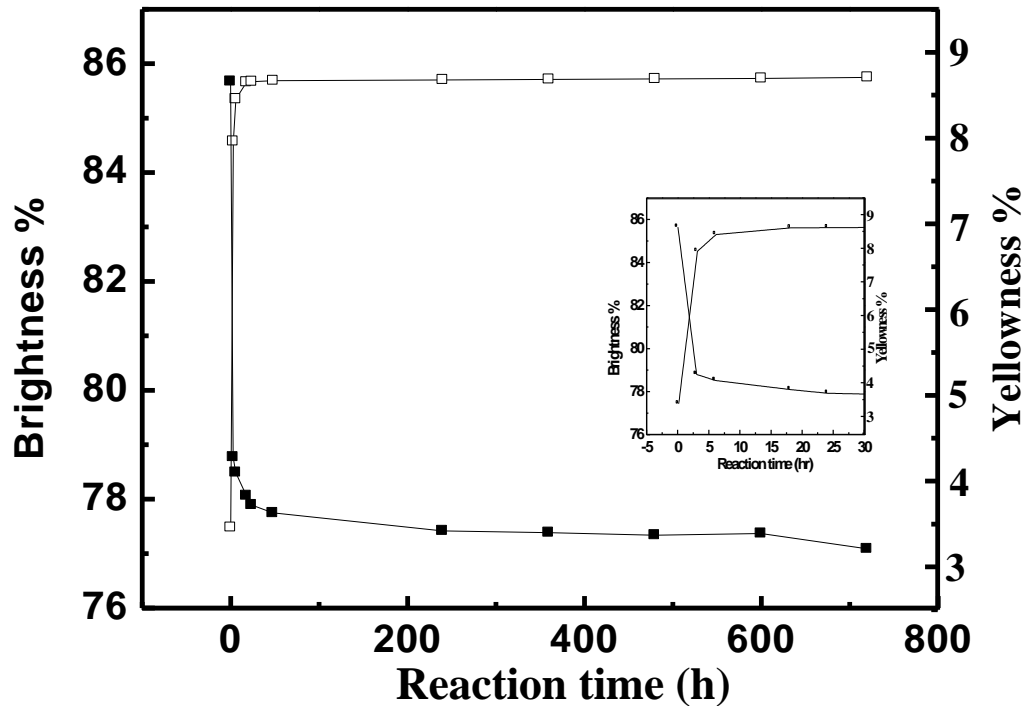


Fig. 4.II.2.B. Variation of Brightness/yellowness with reaction time.
Oxalic acid concentration 10 Kg/ton solid: liquid (clay : water) ratio 1:2.

Chemical assay of the leached clay indicates that increase in acid concentration resulted in increased leaching of SiO_2 and Al_2O_3 . When 2 kg/ton of oxalic acid was used 0.13% of Al_2O_3 and 0.30% SiO_2 were removed. An increase of the sequestering agent to 10 kg/ton dissolved out 0.55% Al_2O_3 and 0.63% SiO_2 .

However the structural analysis of the above clay by X-ray diffraction analysis and Hinckley index studies indicated that the structure remains intact by this treatment. The major basal kaolinite peaks (001) and (002) remained unaffected. But the (110) and (111) peaks of treated clay showed a slight increase in intensity indicating very slight improvement in the crystallinity after treatment. This was also confirmed by the Hinckley crystallinity index measurements.

The promotion of dissolution of cations by H^+ is a widely accepted phenomenon. The tests (A 1-5), carried out with just oxalic acid were conducted in presence of oxalic acid- H_2SO_4 (0.1 N) to understand the Fe dissolution behaviour in organic acid- mineral

acid combination (B 1-5). Although the Fe removal was improved the results indicated that the structure was seriously affected in the latter case evidenced by the increased dissolution of Si and Al and also the lower value of crystallinity index.

Experiments C 1-5 indicate that Fe_2O_3 leaching was fairly low in mineral acid alone. A comparison of C 1-4 to its counter parts B 1-1 and A 1-1 amply illustrates this experimental finding. When 0.1 N H_2SO_4 leaches out 20.87% of the surface iron (as Fe_2O_3) B 1-1 and A 1-1 can leach out 47.74 and 37.11% of Fe_2O_3 respectively. Only a very high dosage of 1 N can leach out Fe_2O_3 equivalent to B 1-1 *i.e.* oxalic acid- mineral acid mixture.

The kaolinite treated by usual method using sodium hydrosulphite as the bleaching agent shows only a lesser improvement in the properties (brightness of 84.11% and yellowness 4.9%), compared to that of oxalic acid treated samples.

Since the crystallinity index was affected in mineral acid and organic-mineral acid combinations, oxalic acid treatment itself was found to be the most suitable for Fe removal from kaolinite of this particular deposit. The oxalic acid treatment does not affect the crystallinity index and morphology (Fig. 4.II.3.A & B). The figures indicated that although the stacks of kaolin aggregates were found delaminated to a certain extent, the individual platelet morphology was preserved during treatment.

A

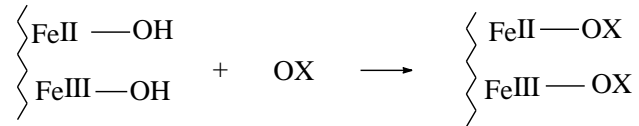
B

Fig. 4.II.3. Morphology and textural feature of kaolinite A) Before treatment B) after treatment with 0.5 g oxalic acid- delamination of kaolinite stacks occurs.

4.II.3.3 Mechanism of iron leaching

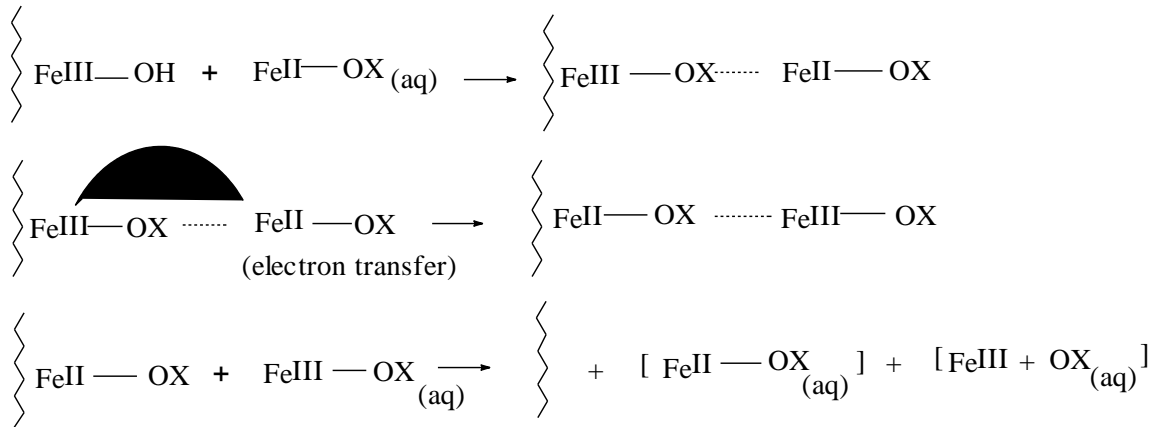
Chemical assay indicated that 44.4% of the total Fe is present in the ferrous form in a freshly mined and size separated sample. Hence an iron dissolution mechanism operative in presence of ferrous iron could be envisaged in this case.

The ferrous and ferric irons on the clay surface form complexes with oxalic acid.



These $\text{Fe}^{\text{II}} - \text{OX}$ and $\text{Fe}^{\text{III}} - \text{OX}$ are water-soluble and are brought into the solution. Meanwhile a simultaneous mechanism of a combined process of complexation by $\text{Fe}^{\text{II}} - \text{OX}$ followed by reduction of the surface Fe^{III} operates, promoting fast dissolution of the Fe^{III} from the clay surface. The reduction mechanism of Fe^{III} by Fe^{II} resulted by the electron transfer, which occurs *via* the bridging ligand, the oxalate. Subsequently both the ferrous and ferric ions get detached from the surface of kaolinite into the solution.

The resultant situation is as follows:



Where $\left\{ \begin{array}{l} \\ \end{array} \right\}$ is the surface of the substrate

OX - oxalic acid

Here the autocatalytic reductive dissolution promoted the accelerated leaching of iron in oxalic acid.

The experiments indicated that 5 kg/tons of oxalic acid could leach out 54.45% Fe₂O₃ and when the amount is raised to 10 kg/tons the leached out Fe₂O₃ increased to 67.25%. Brightness of the deferrated clay was 85.65% (ISO).

Obviously the presence of ferrous ions have played a catalytic role in the reaction mechanism. An increase in the kinetics of iron dissolution by Fe²⁺ addition as ferrous sulphate was found to be effective for iron leaching in goethite (Cornell *et al.*, 1974, 1976) and kaolinite (Ambikadevi *et al.*, 2000) using oxalic acid. Since a good amount of Fe is in the ferrous form during clay mining, the possibility of arresting the oxidation of ferrous ions to ferric by oxalic acid has been advantageously employed in this deferration process.

4.II.3.4 Industrial Utility

Physical and fired behaviour of the clay sample were analyzed and the results presented in table 4.II.3. For industrial evaluation, the treated clay (A1.5) was tested for bone china formulation (Table 4.II.4). Testing of this clay for bone china was carried out to confirm the laboratory results for its utilization. The plastic mass of bone china formulation: 46% bone ash, 23% K-feldspar and 31% china clay (Grimshaw and Searle, 1958) was extruded and moulded into various artifacts and fired properties were measured.

Table 4.II.3: The physical and fired properties of the < 45 μm clay fraction.

Physical properties:				
Particle size distribution analysis:				
< 2 μm	43%			
< 5 μm	68%			
< 10 μm	83.5%			
< 20 μm	92.5%			
> 20 μm	7.5%			
Water of plasticity	40.6%			
Viscosity	639 cps			
Dry linear shrinkage	3.09%			
Green MOR	2.20 kgf/cm ²			
Fired properties:				
Fired colour	white			
Linear shrinkage (1250 °C)	15.97%			
Fired MOR (1250 °C)	234 kgf/cm ²			
	a	b	c	d
Volume shrinkage %	1.76	2.98	12.4	19.34
Apparent porosity %	23.22	23.56	21.49	18.17
Water absorption %	35.16	34.90	32.06	22.08
Bulk density g/cc	0.65	0.66	0.72	0.87

a- 600°C, b- 800°C, c-1000°C and d- 1250°C

Table 4.II.4: Comparison of bone china body (prepared with Kundara clay) with the standard.

Properties	Standard bone china body	Bone china body using Kundara clay
Green shrinkage	2-3.5%	3.10%
Green MOR	> 25 kg/ cm ²	22.94 kgf/ cm ²
Fired shrinkage	7- 8.5 %	9.54%
Fired MOR	> 1100 kg/ cm ²	1007 kgf/ cm ²
Loss on ignition	4.7 – 5.5 %	5.25 %
Water absorption	< 0.2%	< 0.2%
Bulk density	2.5- 2.65 g/cc	2.56 g/cc
Closed pores	7.14%	6.25%

Bone china formulation: bone ash - 46%, K- feldspar - 23% and china clay - 31%

The above results indicate that this clay certainly qualifies for applications in bone china bodies.

4.II.4 Conclusion

The rapid $Fe^{2+} \rightarrow Fe^{3+}$ transformation of the transition metal in the Kundara clay resulted in the degradation of kaolinite quality by reducing brightness and increasing yellowness by 7.49 and 3.68 units respectively, within a fortnight of atmospheric oxidation. Chemical assay indicated that 44.4% of the total iron (0.70%), is in ferrous state. Mineralogical examination showed that the colour imparting iron impurities present in the clay are hydroxides/oxyhydroxides/sulphates of iron, psuedorutile, ilmenite, iron-coated anatase and rutile. Deferration studies indicate fast room temperature dissolution

of Fe with oxalic acid by autocatalytic reductive mechanism. The fast and efficient removal of Fe from clay resulted from the presence of Fe^{II} ion which complexes with oxalate dissolving the Fe^{III} rapidly by electron transfer mechanism. Since the clay surface contains chemically leachable Fe^{2+} ions, low dosage of the sequestering agent is sufficient for quality enhancement of kaolinite if Fe^{2+} to Fe^{3+} conversion is arrested. Presence of the mineral acid affected the composition and structure of kaolinite. The experiments indicate that ~ 4 kg/ ton of oxalic acid can improve the brightness of Kundara clay by 7.43 and reduce the yellowness by 4.39 units. The oxalic acid is found to be an efficient sequestering agent for iron removal from Kundara kaolinite. The clay treated by above method qualifies for bone china formulations.

Chapter 5

Surface Modified Kaolinite as Filler in Natural Rubber

5.1 Introduction

Fillers are important ingredients of rubber and their use in compounding is as old as the industry itself (Barrot, 1968). A filler may be regarded as finely divided solid which, on adding and bonding to the polymer matrix, modify the properties of the system in certain direction. Fillers are incorporated in polymers for a variety of functional reasons including reinforcement, abrasion resistance, dielectric strength, electrical conductivity, fire resistance, UV radiation resistance, colour and other physical properties (Blow and Hepburn, 1982).

Kaolin has been traditionally employed as an inert diluent for compounding of polymers (Nugay and Erman, 2001). The success of mineral platelets reinforcement is due to their desirable combination of cost and properties such as i) price per unit mass, which is typically less than one- fifth of the common rubber composites ii) ability to improve stiffness and strength of polymer and iii) the anisotropic alignment providing reinforcement in all directions. The mineral kaolinite satisfies all the above conditions due to its favourable properties. However, the surface of kaolinite mineral filler is hydrophilic and this impedes their dispersion in and rapid wetting by the organic phase. In order to overcome this problem the surface of the fillers are made hydrophobic for blending or compounding the filler with the polymer. The simplest way to achieve hydrophobicity is to attach a suitable organic compound to the mineral surface (Murray, 1963). Plueddemann (1982) showed that coupling agents could improve the rubber filler interaction in the case of mineral filler. A rank order of most commonly used fillers, according to their effectiveness when combined with silanes for promoting substrate adhesion is summarised in Table 5.1.

Table 5.1 Efficiency of the filler to react with the silane

Silane filler reactivity	Fillers
excellent	Precipitated and fumed silicas, cristobalite, quartz, wollastonite, hydrous and calcined clays, glass, aluminum trihydrate
good	mica, talc, magnesium dihydrate, inorganic oxides (Fe_2O_3 , TiO_2 , Cr_2O_3 etc), other silicate fillers (nepheline syenite, feldspar etc)
slight	Calcium carbonate, barium sulfate, graphite, gypsum
bad	Carbon black

Earlier studies have shown that kaolinite as such or in modified forms are widely used in rubber, paper and in paint industries for the enhancement of the desired properties. Surface modified kaolinite using chemical coupling agents such as organotitanate, organosilanes and other chemical products were reported to enhance several properties of the polymer composites (Theng, 1979; Blow and Hepburn, 1982). Modification of the surface of this inorganic solid is important in controlling the adhesion of the matrix to polymer (Fowkes, 1987). A brief overview of surface modification of kaolinites and their use in various industries are given below.

Rehner *et al.* (1960) and Libby *et al.* (1967) successfully modified clay surfaces to enhance the polymer filler interaction with a variety of organosilanes. Kukharskaya and Skorik (1966) evaluated the effect of kaolinite modification using organo-silicon compounds. They added diethylpolysiloxane to kaolinite and mixed it by ultrasonic vibrators. The product obtained by mixing the grafting polymer, when blended and vulcanised with rubber, showed substantial improvement in tensile strength over the

polymer material filled with unmodified clay. Hawthorne *et al.* (1974) prepared a series of kaolinite filler, by making the clay surface initially acidic so as to initiate the cationic polymerization with various vinyl monomers, and neutralized the remaining acidity with ammonia or an organic base. Polyethylene filled with such surface modified clay showed significant improvement in processability, tensile and impact strengths as compared with unfilled polymer or the material containing untreated filler. Helmer *et al.* (1976) reported the filling of polyamides with organo- titanium kaolinites. These treated fillers were found to be more compatible with the polymer matrix. Using an amino silane, Libby *et al.* (1967) were able to attach the hydrolysed silanol group of the reagent to the kaolinite surface leaving the pendant amino group free to react with the rubber during vulcanization. The work on surface modification of kaolinite using tetramethoxy silane and tetraethoxy silane was patented (Brown *et al.*, 1990). These products were effectively incorporated in paper and were found to enhance the gloss, light scattering, opacifying and printability properties. Bei and Huang (1990) and Dai *et al.* (1995b, 1999) modified kaolinite by surface activation of clays by treating with sulfuric acid. The resultant products were found to show excellent adhesion behaviour with the silane coupling agent and were found to be highly compatible in rubber. Kaolin was found to be an excellent modifier for the improvement of the toughness of diglyceryl ether of bisphenol, an epoxy resin with polyamino-imidazoline as curing agent (Fellahi, *et al.*, 2001). These organo mineral derivatives are of interest because they show combined structural, physical and chemical properties of both the inorganic host material and the organic guest species at a nanometer scale (Rausell- Colom *et al.*, 1987). In the case of polymer composites, strong adhesion of the matrix polymer to the surface of the reinforcing filler is required in order to obtain tough and flexible composites (Fowkes, 1987).

As described earlier, although silane-coupling agents have been widely used for surface modification of minerals and in the composite field and their performance was studied widely, the information on the surface modification of kaolinite and its modified forms is quite inadequate. During surface modification of kaolinite with organosilane the silanol groups react with the hydroxyl group on the mineral surface (Braggs *et al.*, 1994; Johansson *et al.*, 1999). The type and presence of the hydroxyl groups has a major role in controlling the silylation reaction. In kaolinite the exposed Al and Si centers at kaolinite

edges are terminated by hydroxyls. In addition the other hydroxyl groups of kaolinite are those on the octahedral planes, which are coordinated to two underlying aluminium atoms and are thought to be appreciably less reactive than the edge aluminols and silanols (Sposito, 1984). A schematic representation of the structure of kaolinite is given in fig.5.1.

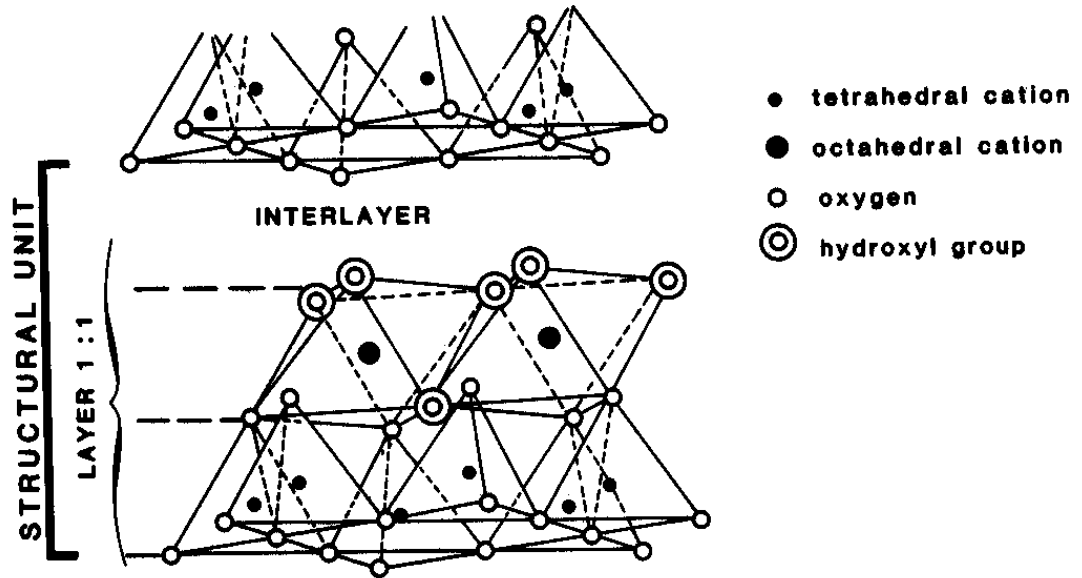


Fig. 5.1 Tri-dimensional sketch of the structure of kaolinite

Arkles (1977) had put forward the reaction mechanism involved during silylation of the mineral surfaces. The properties of organofunctional silanes are due to their special molecular structure and reactions. The chemical structure of organofunctional silanes is:



Y = organofunctional group, H_2N- , $CH_2=CH-$, $CH_2=C-COO-$, HS^- , Cl^-



X = siliconfunctional group, $-OCH_3$, $-OC_2H_5$, $(-OR, -Cl, -O-C-CH_3)$

The silicon, which is the central unit of a silane, is combined with two different functional groups. Organofunctional group Y, is strongly bound to the silicon *via* a stable unreactive carbon chain. The adhesion to the polymer occurs *via* this organofunctional group. The siliconfunctional groups, mostly alkoxy groups, which are directly attached to

the silicon, can react after their hydrolysis with active centers of an inorganic substrate by condensation with other silicon compounds and thus form stable bonds. The mode of action of organofunctional silanes involves the following sequence of reactions (Fig. 5.2).

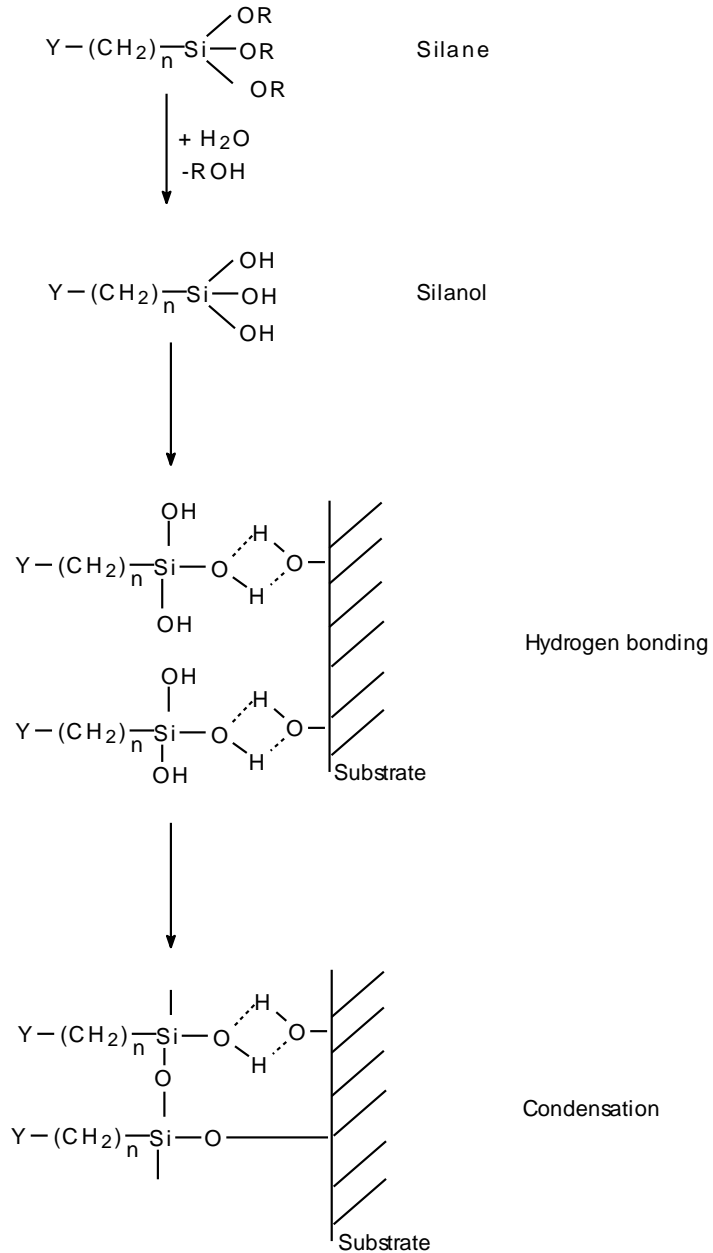


Fig.5.2 Reaction of the siliconfunctional group to the inorganic substrate

The first step comprises of the initial hydrolysis of the three labile X group attached to the silicon. The second step is the formation of hydrogen bond with the OH group of the

substrate and finally during curing, a covalent linkage is formed with the substrate with the elimination of a water molecule. At the interface, usually only one bond is formed with silicon of the organosilane and the substrate molecule. The two remaining silanol groups present are either bonded to the other coupling agent silicon atom by condensation or exist in free form.

The silylation of the interlayer silanol groups of layered silicates may lead to novel functional inorganic-organic supramolecular systems (Ogawa *et al.*, 1998). This technique of surface modification of kaolinite results in surface tailored products, with excellent coupling properties and is found to be able to fulfill predetermined specific applications.

The present work details the efforts to study 1) the effects of silylation on the properties of raw and thermally modified kaolinites and 2) the use of these surface modified organo-inorgano hybrids as filler in rubber composites. The interaction of kaolinite and natural rubber is analyzed by evaluating the mechanical, physical and thermal properties of the natural rubber – filler composites.

5.2 Materials and Methods

5.2.1 Sample Preparation

The < 45 µm fraction collected by wet sieving of the specimen sample of kaolinite deposits of Kundara region (Quilon district, South Kerala), was dried and fractions of the same were calcined in a muffle furnace at 600 and 900°C for a soaking period of 3 h. In order to reduce the size of the clay agglomerates, the thermally treated and untreated clays were subjected to micronization by dry grinding using an oscillatory disc mill (Siebtechnik, Germany). About 50 g of the clay was subjected to milling for a period of 10 minutes and the powdered samples were dried to remove the excess moisture by oven drying at 110°C for 1 h. The uncalcined and the calcined kaolinites (600 and 900°C) are designated as C0, C6 and C9 respectively.

5.2.2 Surface modification of kaolinites

In order to improve the surface property, both calcined and uncalcined samples were treated with organosilanes. Surface modification was effected by mixing and blending the

powdered dry kaolinites with 1.5 and 3% concentration of triethoxyvinyl silane (TEVS) ($\text{H}_2\text{C} = \text{CHSi}(\text{OC}_2\text{H}_5)_3$, b.p 160-161°C, $d = 0.903$ (Aldrich, AR grade, 97%), in a high speed mixer for approximately 30 minutes, by externally heating the sample at a temperature around 80°C during mixing. The treated filler was oven dried at 110°C for 1 h. The modified samples were dried in a desiccator and are stored in airtight plastic bag for further experimental analysis.

5.2.3 Characterisation of raw and modified kaolinites

Studies on variation of properties of the treated and untreated fillers were accomplished by chemical characterisation, X- ray diffraction analysis (XRD), Fourier transform infrared analysis (FTIR), Diffuse reflectance Infrared analysis (DRIFT), Thermogravimetric analysis (TG) and Contact angle and Viscosity measurements.

Chemical characterisations of the thermally treated and untreated samples were carried out by adopting classical methods of silicate analysis (Bennett and Reed, 1971).

Mineralogical and structural variations of calcined kaolinites were evaluated by X- ray diffraction analysis, using a Philips X- ray diffractometer.

Fourier transform analysis of the kaolinite was obtained using Perkin Elmer IR spectrometer. The raw and modified samples were mixed with KBr in the ratio of 1: 200 and pressed into pellets and are scanned over the range of 4000 – 400 cm^{-1} .

Diffuse reflectance spectral analysis was carried out to determine the extent of silylation for the thermally treated and untreated clays, using Shimadzu 8300 IR spectrophotometer, equipped with DRIFT accessory and a reference mirror.

A Dupont Thermal Analyser model was used for thermogravimetric studies. The heating rate was maintained at 20° C/ min.

Contact angle measurements of kaolinite were carried out as per the procedure adopted by Janczuk and Bialopiotrowicz (1988a), using a goniometer – telescope at 25 times magnification.

Viscosity measurements of the clays were carried out using a Brookfield viscometer. Since the modified clays do not disperse in water due to its hydrophobic nature, paraffin oil was used as the liquid medium.

The particle size measurements of the untreated kaolinite are made using Micromeritics Sedigraph 5100. Calgon was used as the dispersant.

5.2.4 Mixing of the filler with polymer

Formulation of the mix is given in Table 5.2. Mixing of natural rubber, filler, curing agents and antioxidants was carried out at 50°C in a Brabender Plasti-Corder Mixer using a rotor speed of 30 rpm. The mix was discharged and sheets were moulded / crosslinked at 150 ± 1°C using an electrically heated press at a pressure of 50 kg/ cm² using a spacer of 1 mm. The time needed for curing of each set of mixing was determined in the same Plasti-Corder Mixer at 150°C. This curing time is used for crosslinking of the rubber – filler composites. In both mixing and the curing studies, the variation of torque with time is plotted and the torque needed for mixing of each formulation is calculated.

Table 5.2 Mix Formulation

	Ingredients	Weight in gram
1	Natural rubber	30
2	ZnO	1.5
3	Stearic acid	0.6
4	Filler	9
5	MBT*	0.6
6	Sulphur	0.6
7	Napthenic oil	3

* 2- Mercaptobenzothiazole

5.2.5 Composite characterisation

The experimental methods adopted for the evaluation of the properties of the composites include the measurements of density, equilibrium swelling, percentage weight loss, thermal and mechanical properties of the cured samples. Density for the cured test specimen was measured at room temperature after calculating the specific gravity of the samples by the ASTM D 792 method. Degree of equilibrium swelling measurements (V_r) were undertaken

using cured test pieces of dimension $10 \times 10 \times 1$ mm in toluene (Oliveira and Soares, 2000). Thermal properties of the cured samples were measured using a DuPont thermal analyser at a heating rate of $20^\circ\text{C}/\text{min}$ to measure temperatures at 5, 10 and 50 % weight loss. In addition the temperature at final weight loss (i.e. while it reaches a steady state) and weight of the residue at 600°C were also calculated. Mechanical properties were analysed by tensile strength measurements by ASTM D412 method. (Detailed experimental procedures in chapter 2).

5.3 Results and Discussions

5.3.1 Characterisation of the filler

5.3.1.1 XRD studies

Figure 5.3 shows the XRD patterns of calcined and uncalcined clays.

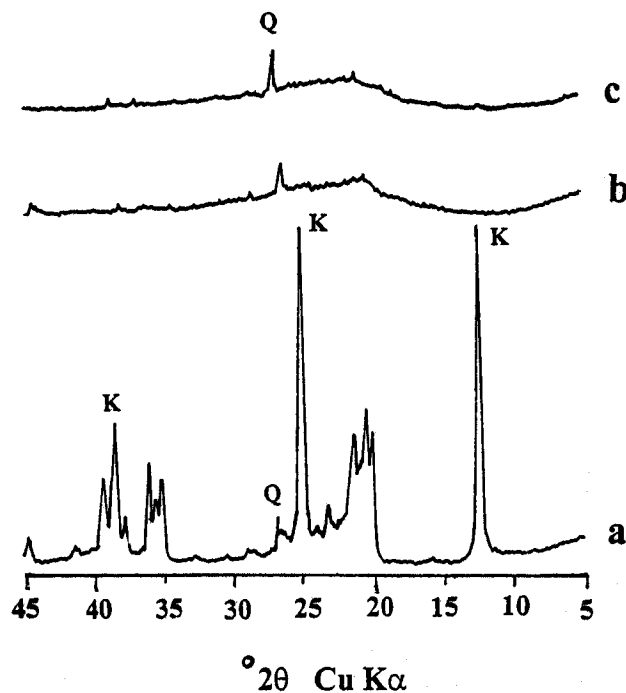


Fig. 5.3. X-ray diffraction patterns of (a) Kaolinite, (b) Kaolinite calcined at 600°C and (c) Kaolinite calcined at 900°C : K- kaolinite, Q- quartz.

Untreated sample shows characteristic peaks of kaolinite at 7.15 and 3.56 \AA and these peaks disappeared in the case of calcined kaolinite, leaving only the peaks of quartz and an amorphous material between 2θ : 15 and 30 degrees.

5.3.1.2 Chemical characterisation

The raw and calcined samples have been subjected to chemical assay and the results are reported as the oxides of the respective elements (Table 5.3). The dehydroxylation during calcination is responsible for the increase in percentages of the constituents. The SiO₂ content reaches around 53.02% for C6 and 53.54% for C9. The Al₂O₃ content was 42.30 and 43.26% for C6 and C9 respectively. The LOI is in accordance with the temperature of dehydroxylation.

Table 5.3. Chemical composition of the kaolinities used as the filler (wt %)

Sample code	SiO ₂	Al ₂ O ₃	Fe ₂ O ₃	TiO ₂	CaO	K ₂ O	Na ₂ O	LOI
C0	47.87	36.05	0.47	0.06	0.21	0.07	0.11	14.98
C6	53.02	42.30	0.54	0.07	0.22	0.08	0.13	3.41
C9	53.54	43.26	0.55	0.07	0.32	0.12	0.20	1.71

5.3.1.3 Particle size distribution analysis

The size of the particles has a great influence on the property enhancement of the polymer. Smaller particle size results in higher tensile strength, higher abrasion resistance, higher electrical conductivity and higher Mooney viscosity, with minor effect on extrusion shrinkage and modulus (Blow and Hepburn, 1982).

Figure 5.4 shows the variation in the range of particle size of the fillers. Particle size distribution analysis indicates that the < 2 µm fractions are more for C9 (52%) and C6 (48%). For C0 less than 2 µm fractions is only 24%, half of that for the calcined one (Fig. 5.4). The results show that the calcined samples are more amenable to size reduction by dry grinding.

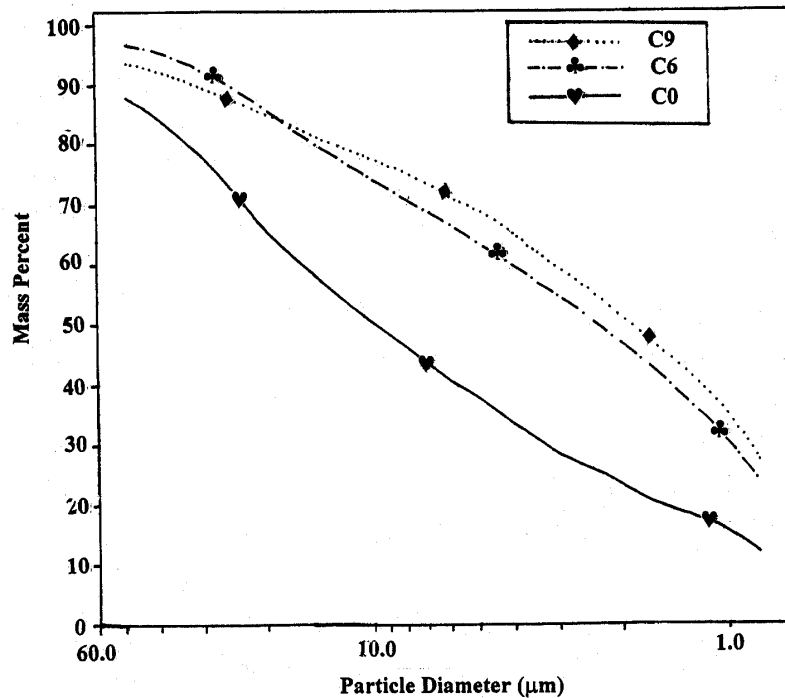


Fig. 5.4 Particle size distribution pattern of kaolinite and metakaolinities: C0- raw kaolinite, C6- kaolinite calcined at 600°C, C9- kaolinite calcined at 900°C.

5.3.1.4 FTIR studies

Figure 5.5 shows the FTIR spectra of raw and calcined kaolinite. The bands at 3695, 3648, 3615, 1102, 1029, 1009, 917, 797, 758, 698, 539, 472 and 426 cm^{-1} are characteristic of kaolinite. The higher frequency bands at 3695 and 3621 cm^{-1} arise from the stretching of the inter and intrasheet hydroxyl groups respectively. The absorption frequency observed around 1100 – 1000 cm^{-1} region corresponds to the Si– O –Si asymmetric stretching vibrations and the bands observed at 917 and 539 cm^{-1} are characteristic of Al- O- H deformation of intrasheet hydroxyls present in kaolinite. The kaolinite–metakaolinite transformation taking place during heat treatment is confirmed by the absence of the major peaks of hydroxyl bands at 3695 and 3621 cm^{-1} and Al-O-H bands at 917 cm^{-1} (Figure 5.5). The disappearance of band at 539 and 917 cm^{-1} and the appearance of a new band at 817 cm^{-1} are connected with the change from the octahedral coordination of Al^{3+} in kaolinite to tetrahedral coordination in metakaolinite. The band at 1102 cm^{-1} is assigned to the Si-O-Si asymmetric vibrations of amorphous SiO_2 . From the FTIR pattern, it is evident that the

sample calcined at 900°C has more intense Al-O-H band compared to the one calcined at 600°C, resulting from the segregation of octahedral ions. On the contrary adsorbed water molecules as evident from the OH peak at 3429 cm^{-1} of C9 (calcined at 900°C, Fig.5.5c) metakaolinite is less intense than that of the C6.

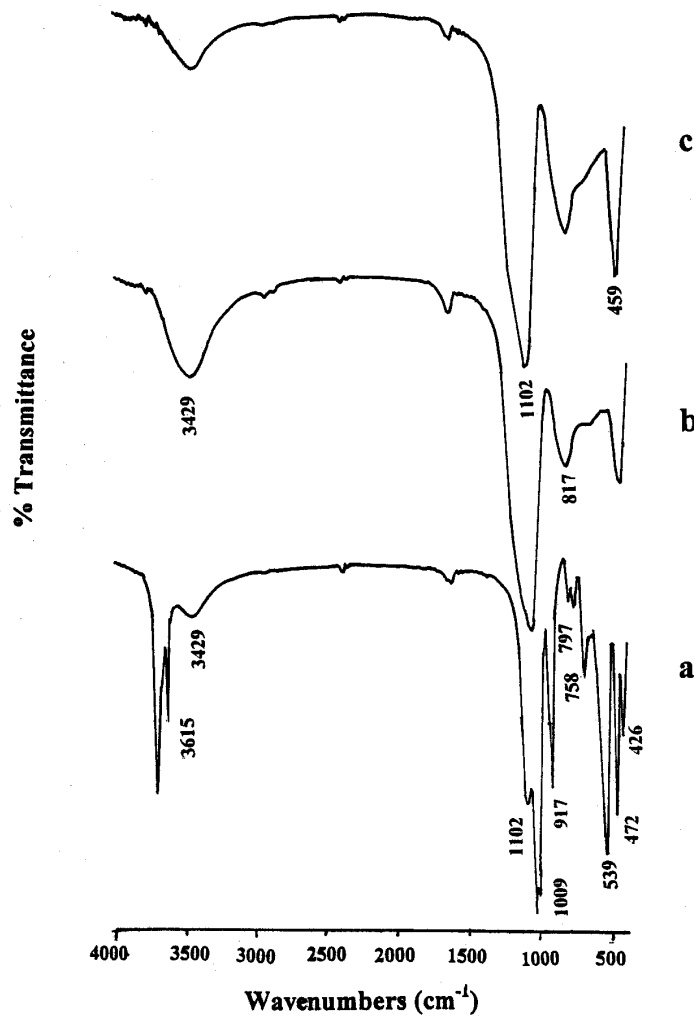


Fig. 5.5. FTIR patterns showing the structural variation during thermal treatment of kaolinite (a) kaolinite (b) kaolinite calcined at 600°C and (c) kaolinite calcined at 900°C.

A schematic representation of the reaction sequence of well- ordered kaolinite to metakaolinite and the collapsed reaction product (bottom) as suggested by Freund (1966) is shown in Fig. 5.6.

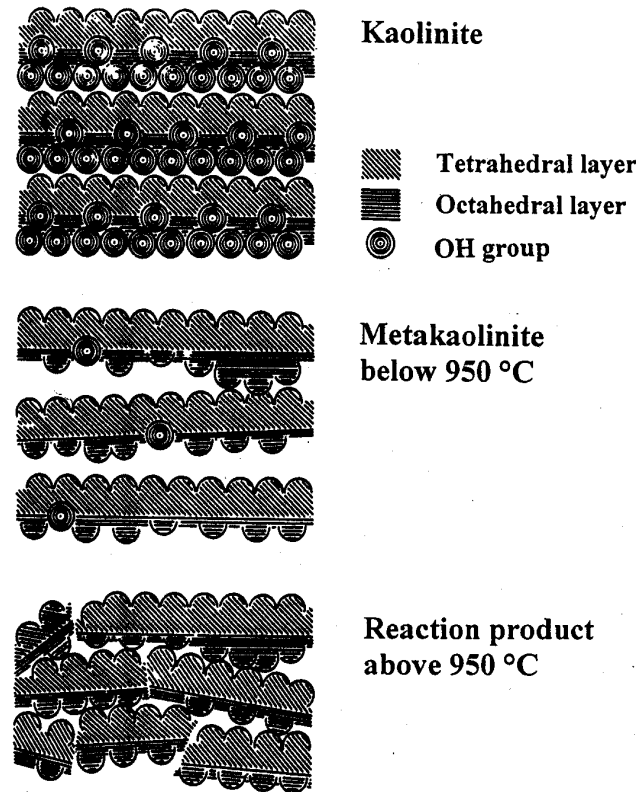


Fig. 5.6. Schematic representation of structural transformation of kaolinite during calcination.

According to Freund's model, the dehydroxylated metakaolinite contains residual hydroxyls even at higher temperatures of calcination. MacKenzie *et al.* (1985) showed metakaolinitisation reaction as:



According to this reaction, at least 10 % of residual hydroxyl groups are present within the metakaolinite structure even at the dehydroxylation temperature of 500-600°C. Further increase of calcination temperature removes the remaining hydroxyl ions but the rate of removal is very low. So the residual OH groups were found within the structure even for the metakaolinite prepared at higher temperatures. At temperature in the range 720 to 850

°C, the collapse of the metakaolinite pseudo- lattice gives way to extensive segregations of amorphous silica. These observations are well in agreement with the FTIR patterns recorded for the metakaolin studied. However the FTIR patterns of the silylated kaolinites and metakaolinites do not show any change in the intensity or any shift of the wave length. Hence Diffuse Reflectant Infrared Spectral studies were undertaken to understand the surface characteristics.

5.3.1.5 Diffuse Reflectance Spectral studies

Diffuse reflectance IR spectral characteristics of silylated kaolinites were extensively studied by Porrio and Pattacini (1990).

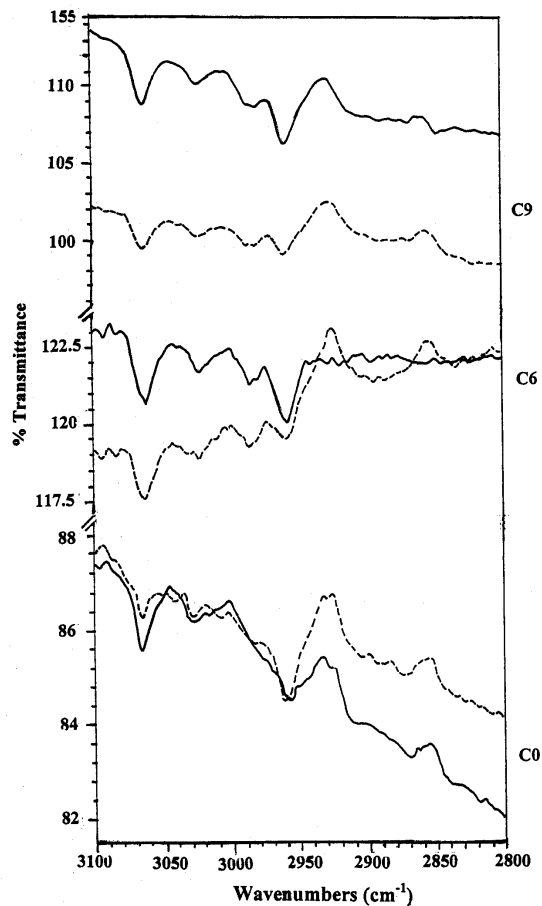


Fig.5.7. DRIFT spectra (3100–2800 cm^{-1}) of surface modified kaolinite using triethoxyvinyl silane (TEVS): the unmodified clay is used as the reference material (dotted line represents 1.5% TEVS treated and bold line represents 3% TEVS treated samples) - note the variation in the band intensities of raw and calcined samples; C0- raw clay, C6- sample calcined at 600°C, C9- sample calcined at 900°C.

The DRIFT spectra (Fig. 5.7) show distinct bands of silanes adsorbed on the kaolinite-metakaolinite surfaces. The variation of the intensity of reflectance patterns of silylated raw and calcined kaolinite C0, C6 and C9 is attributed to the variation of silane consumption of these materials. The characteristic peaks of vinyl silanes like the C-H stretching bands between 2850 and 2925 cm^{-1} and unsaturated C-H stretching bands between 2925 and 3100 cm^{-1} , show a relation with the silane concentration (1.5 and 3%). The maximum intensity of the peaks for the vinyl group is observed for the sample C9 (3%) (calcined at 900° C; 3% silane treated) and the least is for the raw sample. The intensity variation is in consistency with the calcining temperature and the concentration of silane used for silylation.

5.3.1.6 Morphological analysis by SEM

Scanning electron micrographs of kaolinite indicate that the raw kaolinite consists of densely packed pseudo-hexagonal sheets (Fig. 5.8A) and this platy nature is retained even at a temperature of 900°C (Fig. 5.8B). But in this case, most of the platelets were broken and the stacked platelets were found to be much more dispersed (Fig. 5.8B). It is quite probable that the fracturing of the surfaces might have taken place during dry milling of the sample after calcination. Surface modified silylated samples do not show any variation in the morphological or textural features (Fig. 5.8C).

A

B

C

Fig. 5.8. Scanning electron micrographs of < 45 μm fraction of (A) raw kaolinite (B) kaolinite calcined at 900°C (C) 3% triethoxyvinyl silane treated raw kaolinite

5.3.1.7 Contact angle measurements

Values of the contact angle for the kaolinite (calcined and uncalcined) and for the kaolin treated with varying silane concentrations are listed in the table 5.4. The value of the contact angle of water drops increases with increasing silane concentration, on the filler. The contact angle of the untreated raw kaolin is around 26.1 degree, similar in range to the one reported by Janczuk *et al.* (1989), in the study of surface energy of kaolinite. On increasing the silane concentration from 1.5 to 3%, contact angle also increases from 39.7 to 61.4 degrees. For untreated calcined kaolinite C6 and C9 (600 and 900°C) the measurements of contact angle were difficult, because of the spreading of the water droplets due to absorption. On the contrary, their surface modified products showed higher contact angles. The increase in the contact angle is consistent with an increase in calcination temperature and silane concentrations. Highest value in the angle (116.64°) is noticed for 3 % triethoxyvinyl silane treated calcined clay, C9 3%. This is due to the inducing of hydrophobic nature of the clay surface through treatment with organosilanes. The increase in contact angle for calcined clays results from an increase in adhesion/bonding of these silanes on metakaolinite. If the kaolinite surface is progressively coated with triethoxyvinyl silane, the dispersive force increases making the surface more and more hydrophobic or in other words, less wettable by water.

5.3.1.8 Viscosity studies

Since the silylated kaolinites are hydrophobic, viscosity measurements were undertaken in a hydrocarbon medium using liquid paraffin oil. The results show the extent of particle-particle interaction and the degree of dispersion of kaolin (Table 5.4). Silane treated raw clay C0 (1.5%) has a lower viscosity value (760 cps), compared to the untreated one (1180 cps). Calcined kaolinite shows a higher viscosity value and is directly proportional to the temperature. For sample treated at 600°C (C6), the viscosity is around 5900 cps and for C9 (900°C) it is much higher, 6400 cps. This variation resulted mainly from the reduction in particle size during dry milling as evident from the particle size measurements and also from the reconstitution of the crystal structure during calcination. The aggregated structure produced by metakaolinization followed by dry milling imparts major surface irregularities

to the particles with sharp protrusions, as evident from the scanning electron micrographs. These surfaces are more resistant to shear (Bundy and Ishley, 1991) leading to higher viscosities. On the contrary silylated calcined clays, show lower viscosity than the silylated raw clay C0 (1.5 and 3%). The decrease in the viscosity is in accordance with the percentage of silane. It has been reported that the use of the silane coupling agent is an effective means of reducing viscosity of polymer formulations (Nugay and Erman, 2001). The lowering of the viscosity values is attributed to the breakdown of the structure of filler-filler agglomerate and also due to the masking of the electronic edge-face interaction between kaolinite particles. The results obtained during the viscosity studies indicate that the structure and morphology of kaolinite play a major role in the silylation and consequent reduction in viscosity.

Table 5.4. Viscosity and Contact angle measurements of raw and calcined kaolinities.

Sample Code	Contact angle (θ)	Viscosity in cps at 50 rpm
C0	26.10	1800
C0 1.5%	39.71	1180
C0 3%	61.44	760
C6	-	5900
C6 1.5%	97.63	300
C6 3%	113.7	220
C9	-	6400
C9 1.5%	105.5	520
C9 3%	116.64	230

5.3.1.9 Thermal Analysis

Thermogravimetric analysis was used to examine the extent of stability of organic coatings on the clays. The results are given in table 5.5. A regular variation in weight loss is observed for the filler calcined at different temperatures and it was also found to depend on

the nature of the clay samples. At 100°C, raw kaolinite shows a weight loss of 3.34% and the calcined variety exhibits relatively lower percentage of weight loss and the least was for the silylated ones. Lower weight loss observed for calcined and silylated kaolinites compared to raw clay may be due to the low amount of hydroxyls. The trend of decreasing hydroxyl weight loss follows an increased loading of silane, there may be a direct correlation of the extent of grafting of these silanes with the hydroxyl groups of kaolinite. A steady state condition for dehydroxylation is achieved at 600°C, for all the samples. These studies indicate that the silane modification causes the kaolinite surface to become hydrophobic and hence moisture adsorption during the storage of the filler can be significantly reduced. The observations are well in correlation with the results obtained by DRIFT analysis and contact angle measurements.

Table: 5.5 Thermal characterization of the filler (% cumulative wt loss)

Sample code	100°C	200°C	300°C	400°C	500°C	600°C
C0	3.34	5.69	6.64	7.41	13.44	17.63
C0 (1.5%)	2.09	4.93	5.26	5.43	11.11	15.75
C0 (3%)	1.96	3.74	4.25	5.15	10.62	16.10
C6	0.89	1.79	2.23	1.89	2.07	2.55
C6 (1.5%)	0.32	1.06	2.04	0.90	1.60	2.09
C6 (3%)	-	-	0.10	0.57	0.92	1.19
C9	-	-	0.55	1.19	1.32	1.56
C9(1.5%)	-	0.24	0.65	0.88	1.14	1.15
C9 (3%)	-	-	-	0.20	0.26	0.26

5.3.2 Properties of Kaolinite-Natural Rubber Composite

5.3.2.1 Curing characteristics

Curing characteristics are shown in table 5.6. The curing time required for different filler added rubber composites were found to be dependent on the calcination temperature and the concentration of the silane. The minimum curing time was observed for C9 (calcined at 900°C, 3% silane) and the maximum was observed for raw kaolin having no silane coating.

The curing time required for various filler-rubber composite shows a gradation. Higher calcination temperature and silane loading need only lower curing time. The above features of reduction in cure time on addition of thermal and chemically modified kaolinite is indicative of curative adsorption on the filler surface.

The final torque attained by the composite during mixing also varies depending on the surface modification (Table 5.6). Silylated samples, both calcined and uncalcined show reduction in their final torque values during mixing.

5.3.2.2 Physical property evaluation

The physical properties such as the equilibrium swelling, density, loss of weight in toluene etc show variation in the value depending on the filler treatment.

5.3.2.2.1 Weight Loss and Equilibrium Swelling Measurements

The results of the degree of equilibrium swelling measurements and weight loss in toluene for NR-kaolinite composite are given in table 5.6. For raw clay C0, the weight loss is significantly higher than those obtained for C6 and C9. The value of equilibrium swelling in toluene (V_r) is found to be inversely proportional to the percentage weight loss in toluene. For a sample, which has a higher V_r , the percentage of weight loss is lower *i.e.* the percentage of bound rubber is more in this sample. Addition of silylated raw kaolin (C0-1.5 and 3%) and metakaolin (C6-1.5% and 3%) leads to a lower value of weight loss. On the contrary, V_r for C9 (1.5 and 3%) shows much higher value (0.28) and an increase in weight loss (8.61 and 8.91%), compared to C6 (1.5% and 3%). The lower values of V_r and a reduction in the weight loss indicate an improved crosslinking for the corresponding filler- polymer composites. These observations are well in agreement with similar studies reported by Bandyopadhyay et al. (1996), for carboxylated rubber filled with silane treated carbon black. Based on these observations, it can be inferred that the silane promotes the rubber-kaolinite interface reaction. It is further observed that the extent of interfacial reaction is greater in the case of silylated calcined kaolinite as compared to the uncalcined one. The silane coupling agent improves the interfacial bonding and thereby reduces the weight loss in toluene.

5.3.2.2.2 Bulk Density

The variation in bulk density of the composites is given in Table 5.6. Bulk density of the composites increases with the temperature of calcination and also increases with an increase in the concentration of silanes. The composite with filler calcined at 900°C has a relatively higher density than other composites having fillers treated at lower temperatures. The above results indicate that the property of the composite greatly depends on the filler. In addition, the coupling action of silane also influences the density of the composite. The density increases with the amount of treatment of TEVS on the filler. This property results from the good interface adhesion between polymer matrix and filler due to the reduction of voids and vacuoles.

Table 5.6 Physical properties of the cured rubber sample

Sample code	Final torque during mixing (Nm ⁻¹)	Optimum cure time (min)	Bulk density g/cc	Vr* (ratio)	Weight loss after ageing in toluene (%) [#]
C0	10.8	3.8	1.14	0.16	9.72
C0 (1.5%)	10.4	3.6	1.16	0.20	9.24
C0 (3%)	10.2	3.4	1.16	0.22	9.04
C6	10.9	3.0	1.14	0.26	8.61
C6 (1.5%)	10.4	2.9	1.16	0.28	8.37
C6 (3%)	10.2	2.8	1.17	0.27	7.61
C9	10.5	2.0	1.19	0.26	8.32
C9 (1.5%)	9.8	2.0	1.21	0.28	8.61
C9 (3%)	9.7	2.0	1.23	0.28	8.91

* equilibrium swelling in toluene (after 5 days),

percentage weight loss in toluene (after 5 days)

5.3.2.3 Thermal stability measurements

TGA has been effectively used to study the thermal properties of these composites. The temperature required for 5%, 10%, 50%, and final weight loss percentage has been taken as

an index of thermal stability. The decomposition temperatures are given in table 5.7. The temperature for 50% weight loss increases with an increase in the content of coupling agent. Surface modified raw kaolinites (C0 1.5% and 3%) have higher degradation temperature for 50% weight loss compared to the composite having untreated filler. In addition, surface modification of the calcined filler improves the thermal stability of the composites. The temperature at 5% weight loss is the highest for the composites containing kaolinite filler (900°C, 3%). The highest value of temperature at 50 % weight loss is for the composites with 600°C calcined 3% silane treated kaolinite filler. The improvement in the thermal stability is brought about by the enhancement in bonding between matrix and the filler as well as the improvement on the interface bonding by coupling agent treatment. From TGA it is clear that the thermal degradation commences at a temperature around 600°C. Percentage of residual material after degradation is much more for the composites with silane treated calcined fillers. These variations observed in thermal stability are solely attributed to the property changes of the kaolinite filler, which occurred during thermal and chemical modifications. Higher residues in the case of calcined fillers are due to the lower amount of structure hydroxyls in them (Table 5.7).

Table 5.7 Thermal analysis of rubber- modified kaolinite filler composites

Sample code	* T ₅	*T ₁₀	*T ₅₀	*T _F	Residue at 600° C (% wt)
C0	295.7	324.5	337.9	546.6	19.60
C0 1.5%	307.22	334.6	372	532.2	20.29
C0 3%	313	343.3	383.7	535	21.93
C6	314.4	336	389.42	542.3	23.54
C6 1.5%	324.5	344.7	389.42	542.3	23.57
C6 3%	307.9	343.3	393.7	543.7	23.93
C9	302	338	384.6	533.7	24.93
C9 1.5%	311.3	343.3	392.1	551.9	26.45
C9 3%	324.5	349	392.3	572.1	27.1

* T₅ – Temperature at 5% weight loss, * T₁₀ – Temperature at 10% weight loss,

* T₅₀ – Temperature at 50% weight loss, * T_F – Temperature at final weight loss

5.3.2.4 Mechanical property evaluation

It is well known that the filler affects the tensile properties according to the packing characteristics, size and interfacial bonding of the polymer composite (Milewski and Katz, 1978). Table 5.8 shows the variation in the stress, elongation at break and modulus at 100% and 300%. The results show a synergetic effect of the coupling agent and the improvement of the tensile strength of the composites as compared to the composites with unmodified kaolin. A considerable enhancement of the mechanical properties with both thermal and chemical modifications of the kaolinite surfaces was observed in all the cases. Effect of thermal modification is evident from the increase of the breaking stress from 13.4 ± 1.26 for the raw clay to 16.37 ± 2.39 and 17.69 ± 2.82 Mpa for the samples calcined at 600 and 900° C respectively. Elongation at break increases with the addition of thermally treated fillers. The mechanical strength of the composite material is also influenced by the amount and adsorption behaviour of the silane coupling agent. Incorporation of C0 (1.5 and 3%) and C6 (1.5 and 3%) kaolinites results in an increase in the breaking stress, breaking strain and modulus at 100 and 300%. This shows the ductile nature of the composite on treatment. On the other hand the elongation at break decreases for C9 (1.5 and 3%). Stress at break and modulus at 100 and 300% for these samples are relatively higher. Even though the higher modulus and breaking stress indicate higher crosslinking density for the metakolinite C9, C9 1.5% and C9 3%, the lower value of elongation compared to the composites with filler C6 shows the higher stiffness. This variation solely depends on the structural variation taking place in the filler.

The variation in the above mechanical properties of the composites results from the variation in the filler character and the effects of silane bonding on the inorganic surface. The filler encapsulated with silane can bond the matrix to the mineral surface and act as a seal, reducing the formation of deleterious stress concentration at the matrix filler interface. The surface of the kaolinite treated with the silane coupling agent gets more desirable dispersion in the polymer matrix and enhances the wetting-adhesion between the filler and the polymer and thereby improving the interface of both and increasing the mechanical properties. When kaolinite is calcined, the efficiency of bonding of silane on the kaolinite

surface is improved and this enhances the coupling action resulting in the improvement of mechanical properties. Addition of unmodified filler kaolinite itself gives reinforcing property in natural rubber. The silylated counterpart further enhances the extent of reinforcement.

Table 5.8 Mechanical strength of kaolinite- polymer composite

Sample(n= 6)	Break stress (Mpa)	Break Strain (%)	Modulus at 100% (Mpa)	Modulus at 300% (Mpa)
C0	13.40 ± 1.26	1544 ± 73	0.845 ± 0.134	0.551 ± 0.103
C0 (1.5%)	13.84 ± 2.04	1551 ± 145	0.836 ± 0.013	0.576 ± 0.101
C0 (3%)	13.61 ± 1.45	1616 ± 74	0.780 ± 0.121	0.536 ± 0.101
C6	16.37 ± 2.39	1633 ± 146	0.781 ± 0.109	0.528 ± 0.111
C6 (1.5%)	16.55 ± 2.31	1585 ± 182	0.882 ± 0.122	0.615 ± 0.116
C6 (3%)	18.27 ± 2.12	1779 ± 137	0.832 ± 0.119	0.559 ± 0.101
C9	17.67 ± 2.82	1596 ± 147	0.903 ± 0.049	0.618 ± 0.031
C9 (1.5%)	17.01 ± 3.28	1559 ± 179	0.893 ± 0.027	0.624 ± 0.014
C9 (3%)	19.53 ± 3.50	1676 ± 183	0.916 ± 0.04	0.636 ± 0.024

The values indicate the average of six measurements

5.3.3 Mechanism involved in coupling

The mechanism involved in the coupling of the modified filler is schematically represented in Fig. 5.9.

In the initial step, it is believed that the -OH group of kaolinite surface interacts chemically with the -OC₂H₅ groups of TEVS and a hydrogen-bonded complex is formed (Fig.5.2). This then interacts with the natural rubber, forming a kaolinite –natural rubber bond in the presence of TEVS. These rubber filler bonds which are formed during mixing are converted into a crosslinked structure during high temperature moulding. Thus they form a network of molecular bridges to create a strong, stable bond between the two otherwise weak bonding surfaces. The above reaction, which occurs within the polymer, results in the enhanced interfacial bonding of the composite.

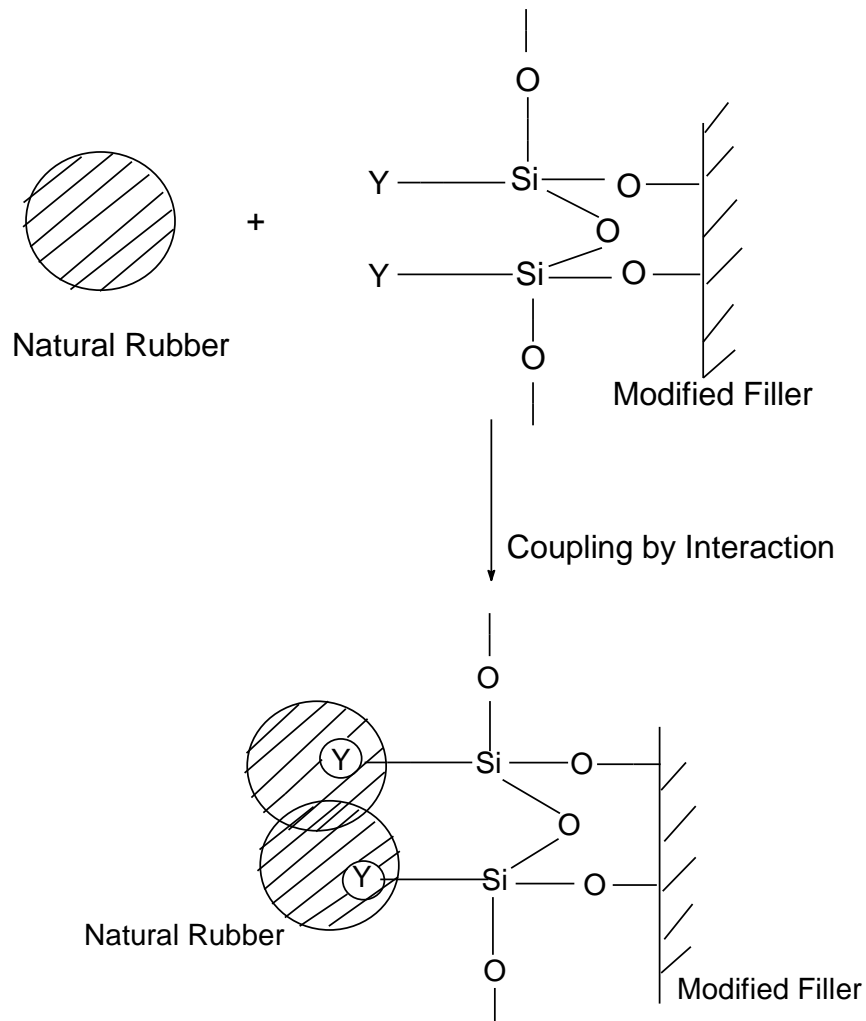


Fig. 5.9 Modified Filler Natural Rubber Composite

5.4 Conclusion

Kaolinite filler improves the mechanical and thermal properties of natural rubber. Raw and calcined fillers have been surface modified by silylation. The viscosity, contact angle, DRIFT and thermal property studies of kaolinite and its surface modified forms reflect the adhesion of organosilane on the inorganic host material. Incorporation of silylated kaolinite in natural rubber enhances the rubber-filler interactions. In addition, the enhanced mechanical, thermal, curing and swelling characteristics of modified kaolin incorporated

natural rubber composites reflect the higher crosslink density. This improvement is also evident in the properties of the composites with fillers which are both thermally and chemically modified. The present study indicates that the silylated clays act as excellent molecular bridges, thereby bonding the otherwise weak-bonded surfaces resulting in a manifold increase in the rubber-filler interactions. The studies showed that the use of surface modified kaolinite, as filler in polymer is a versatile, efficient and cost effective technique for achieving the desired physical and mechanical properties required for specific industrial application.

References

- Aagaard, P. and Helgeson, H. C. (1982) Thermodynamic and kinetics constraints on reaction rates among minerals and aqueous solutions I. Theoretical considerations. *American Journal of Sciences*, **282**, 237-285.
- Acker, J.G. and Bricker, O.P. (1992) The influence of pH on biotite dissolution and alteration kinetics at low temperature. *Geochimica et Cosmochimica Acta*, **56**, 3073- 3092.
- Ahn, J. H. and Peacor, D. R. (1987) Kaolinization of biotite: TEM data and implications for an alteration mechanism. *American Mineralogist*, **72**, 353–356.
- Alexander, L.T. and Cady, J.G. (1962) Genesis and hardening of laterite in soils USDA Tech. Bulletin, 90 pp.
- Al-Khalissi, F.Q. and Worrall, W.E. (1982) The effect of crystallinity on the quantitative determination of kaolinite. *Transaction British Ceramic Society*, **81**, 43-46.
- Altschuler, Z.S., Dwornik, E.J. and Kramer, H. (1963) Transformation of montmorillonite to kaolinite during weathering. *Science*, **141**, 148-152.
- Ambikadevi, V.R. and Lalithambika, M. (2000) Effect of organic acids on ferric iron removal from iron stained kaolinite. *Applied clay science*, **16**, 133-145.
- Amigó, J.M., Bastida, J., Garcia Agramut, M.J., Sanz M. and Galván J. (1987). Crystallinity of Lower Cretaceous kaolinites of Teruel. In *EUROCLAY Conf; Sevilla '87; Sevilla; Spain*, Galan E, Perez- Rodriguez JL, Cornejo J. eds., 74-75.
- Amouric, M. and Olives, J. (1998) Transformation mechanisms and interstratification in conversion of smectite to kaolinite: An HRTEM study. *Clays and Clay Minerals*, **46**, 521-527.
- Anand, R. R. and Gilkes, R. J. (1984) Weathering of ilmenite in a lateritic pallid zone. *Clays and Clay Minerals*, **32**, 363-374.
- Anand, R.R., Gilkes, R.J., Armitage, T.M. and Hillyer, J.W. (1985) Feldspar weathering in lateritic saprolite. *Clays and Clay Minerals*, **33**, 31-43.
- Anovitz, L. M., Perkins, D., Essene, E. J. (1991) Metastability in near-surface rocks of minerals in the system Al_2O_3 - SiO_2 - H_2O . *Clays and Clay Minerals*, **39**, 225- 233.
- Arkles, B. (1977) Tailoring surfaces with silanes. *Chemtech*, **12**, 766-777
- Bailey, S.W. (1963) Polymorphism of kaolin minerals. *American Mineralogist*, **48**, 1196-1206.
- Bailey, S.W. (1969) Polytypism of trioctahedral 1:1 layer silicates. *Clays and Clay Minerals*, **17**, 355-371.
- Bailey, S.W. (1980) Structures of layer silicates. In *Crystal structure of clay minerals and their X-ray identification*, G. W. Brindley and G. Brown, eds., Mineralogical Society London, Monograph, **44**, 78-114.
- Banfield, J.F. (1985) The mineralogy and chemistry of granite weathering. MSc. Thesis, Australian National University, Canberra, Australia, 229pp.
- Banfield, J. R. and Eggleton, R. A. (1988) Transmission electron microscopic study of biotite weathering. *Clays and Clay Minerals*, **36**, 47– 60.
- Banfield, J.F. and Eggleton, R. A. (1990) Analytical transmission electron microscope studies of

- plagioclase, muscovite and K- feldspar weathering. *Clays and Clay Minerals*, **38**, 77- 89.
- Bandyopadhyay, S., De, P.P., Tripaty, D.K. and De, S.K. (1996) 3- Aminopropyltriethoxysilane as a promoter in the crosslinking of carboxylated nitrile rubber by surface-oxidized carbon black. *Journal of Applied Polymer Science*, **61**, 1813-1820.
- Baron, D and Palmer, C.D. (1996) Solubility of jarosite at 4 – 35°C, *Geochemica et Cosmochimica Acta*, **60**, 185- 195.
- Barrot, R.J. (1968) Interest of lamellar minerals in rubber compounding. Rubber Meeting of the Swedish Institution of Rubber Technology, Falsterbo, 14 pp.
- Bei, Y.L. and Huang, J.T. (1990) Study on clay surface modified by coupling agents. *Journal of Huaqiao University*, **11**, 278-283, in Chinese, with English Abstract.
- Bennett, H. and Reed, R.A. (1971) Chemical methods of silicate analysis. A handbook Academic Press Ind., London, 272 pp.
- Berner, R.A and Holdren, G.R. Jr. (1977) Mechanism of feldspar weathering. I. Some observational evidences. *Geology*, **5**, 369-372.
- Berner, R.A. (1984) Sedimentary pyrite formation: An update. *Geochimica et Cosmochimica Acta*, **48**, 605-615.
- Berry, L.G., Mason, B. and Dietrich, R.V. (1985) Mineralogy concepts description and determination. W.H Freeman and Company, U.S.A., 560 pp.
- Bigham, J.M. (1994) Mineralogy of ochre deposits formed by sulfide oxidation. In. *Handbook on environmental geochemistry of sulfide mine waste*, J. Jambor and D. Blowes eds., Mineralogical Association of Canada, **22**, 103-132.
- Blow, C.M. and Hepburn, C. (1982) Rubber technology and manufacture. Published for the plastics and rubber institute, Butterworth Scientific, London, 608 pp.
- Bonney, C.F. (1994) Removal of iron from kaolin and quartz dissolution with organic acids. Proceedings of International Symposium on Hydrometallurgy, London, 313-323.
- Brady, K.S., Bigham, J.M., Jaynes, W.F. and Logan, T.J. (1986). Influence of sulfate on Fe-oxide formation: Comparisons with a stream receiving acid mine drainage. *Clays and Clay Minerals*, **34**, 266-274.
- Braggs, B., Fornasiero, D., Ralston, J. and Smart, R.St. (1994) The effect of surface modification by an organosilane on electrochemical properties of kaolinite. *Clays and Clay Minerals*, **42**, 123-136.
- Brindley, G.W. and Brown, G. (1980) Crystal structure of clay minerals and their X-ray identification, Mineralogical Society, London, 495 pp.
- Brindley, G.W., Zalba E, and Bethke C.M. (1983). Hydrobiotite, a regular 1:1 interstratified cation of biotite and vermicullite layers. *American Mineralogist*, **68**, 420-425.
- Brindley, G.W., Kao, C-C., Harrison, J.L., Lipsicas, M., and Raythatha, R. (1986) Relation between structural disorder and other characteristics of kaolinite dickite. *Clays and Clay Minerals*, **34**, 239 – 249.
- Brown, A.J., Brannen, J.O., Andrews, W., May, J.R. and Raythatha, R.H. (1990) Kaolinite aggregation using organo-silicon compounds. June 19, Patent number.4,935, 062.

- Bruckner, W. (1952) The mantle rock ("laterite") of the Gold coast and its origin. *Geol Rdsch.*, **43**, 307-327.
- Bundy, W.M. and Ishley, J.N (1991) Kaolin in paper filling and coating. *Applied Clay Science*, **5**, 397-420.
- Busenberg, E (1978) The product of the interaction of feldspar with aqueous solution at 25°C. *Geochimica et Cosmochimica Acta*, **42**, 1679-1686.
- Chen, P.-Y. Lin, M.-L and Zheng, Z. (1997) On the origin of the name kaolin and the kaolin deposits of the Kauling and Dazhou areas, Kiangsi, China. *Applied Clay Science*, **12**, 1-25.
- Chiarizia, R., Horwitz, E.P. (1991) New formulation for iron oxides dissolution. *Hydrometallurgy*, **27**, 339-360.
- Churchman G.J. and Gilkes R.J. (1989) Recognition of intermediates in the possible transformation of halloysite to kaolinite in the weathering profiles. *Clay Minerals*, **24**, 549-590.
- Chukrov, F.V., Zvyagin, B.B., Gorshov, A.I., Yermilova, L.P., Korovuskov, V.V., Rudnitskaya Ye. S. and Syakubovskaya. N. Yu (1977) Feroxyhyte a new modification of FeOOH. *Int. Geol. Rev.*, **19**, 873-890.
- Clarke, O. M. Jr. (1973) Gibbsite in weathered granitic rocks of Alabama, Southeast. *Geology*, **14**, 203-212.
- Cleaves E. T., Godfrey, A. E. and Bricker O. P. (1970) Geochemical balance of a small watershed and its geomorphic implications. *Geological Society of America Bulletin*, **81**, 3015 – 3032.
- Cornell, R.M., Posner, A.M. and Quirk, J.P. (1974) Crystal morphology and the dissolution of goethite (α - FeOOH). *Journal of Inorganic Nuclear Chemistry*, **36**, 1937-1946.
- Cornell, R.M., Posner, A.M and Quirk, J.P (1976) Kinetics and mechanisms of the acid dissolution of goethite (α -FeOOH). *Journal of Inorganic Chemistry*, **38**, 563-567
- Cornell, R. M. and Schindler, P.W. (1987) Photochemical dissolution of goethite in acid/oxalate solution. *Clays and Clay Minerals*, **35**, 347-352.
- Craw, D., Coombs, D.S. and Kawachi, Y. (1982) Interlayered biotite kaolin and other altered biotites and their relevance to the biotite isograd in eastern Otago, New Zealand. *Mineralogical Magazine*, **45**, 79-85.
- Dai, J.C., Bei, Y.L., Lin, Q.Y. and Huang, J.T. (1995b) Reinforcement of rubber by silane modified clay. *Journal of Huaqiao University*. **16**, 159-164, in Chinese, with English Abstract.
- Dai, J.C. and Huang, J.T. (1999) Surface modification of clays and clay- rubber composites. *Applied Clay Science*, **15**, 51-65.
- Dangic', A. (1985) Kaolinization of bauxite: A study in the Vlasenica bauxite area, Yugoslavia. I. Alteration of matrix. *Clays and Clay Minerals*, **33**, 517-524.
- Dangic', A. (1988) Kaolinization of bauxite: A study of the Vlasenica bauxite area, Yugoslavia, II. Alteration of oolites. *Clays and Clay Minerals*, **36**, 439-447.
- Danneberg, E.M. (1975) The effects of surface chemical interactions on the properties of the filler-reinforced rubber. *Rubber Chemical Technology*, **48**, 410-444.
- Debnath, S., De, S.K. and Khastagir, D. (1987) Effect of silane coupling agent on vulcanization

- network structure, polymer-filler interaction, physical properties and failure mode of mica filled styrene butadiene rubber. *Journal of Material Science*, **22**, 44-53.
- Deer, W.A., Howie, R.A. and Zussman, J. (1976) *Rock forming minerals*. Volume 3, Longman Group Limited, London, 270 pp.
- DeKimpe, C., Gastuche, M.C. and Brindley, G.W. (1961) Ionic coordination in alumino-silicic gels in relation to clay mineral formation. *American Mineralogist*, **46**, 1370-1381.
- DeKimpe, C., Gastuche, M. W. and Brindley, G. W. (1964) Low temperature synthesis of clay minerals. *American Mineralogist*, **49**, 1-16.
- De Vijnck, Y. (1976) Action des ions alcalins sur la transformation hydrothermales de gels silico-alumineux . II. Influence de 1 ions K⁺. *Silic. Ind.* **41**, 67- 81.
- Dickson, T. (2000) Global kaolin supply and industrial structure. *Industrial Clays*, **3** 39-47.
- Eberl, D. and Hower, J. (1975) Kaolinite synthesis. The role of the Si/Al and (Alkali)(H⁺) ratio in hydrothermal systems. *Clays and Clay Minerals*, **23**, 301-309.
- Eggleton, R.A. and Buseck, P.R. (1980) High resolution electron microscopy of feldspar weathering. *Clays and Clay Minerals*, **28**, 173-178.
- Eswaran, H. and Raghumohan, N.G. (1973) The microfabric of petroplinthite. *Soil Science Society of America Proceedings*, **37**, 79- 81.
- Eswaran, H., Stoops, C and Sys, C. (1977) The micromorphology of gibbsite forms in soils. *Journal of Soil Science Society of America Proceedings*. **37**, 79-81.
- Eswaran, H. and Bin, W.C. (1978 a) A study of a deep weathering profile on granite in Peninsular Malaysia: III. Alteration of feldspar. *Soil Science Society of American Journal*, **42**, 154-158.
- Eswaran, H. and Bin, W.C. (1978b) A study of a deep weathering profile on granite in Peninsular Malaysia: II Mineralogy of the clay, silt and sand fraction. *Soil Science Society of American Journal*, **42**, 149-153.
- Eswaran, H., Comerma, J. and Sooryanarayanan, V. (1981) Scanning Electron Microscopic observations on the nature and distribution of iron mineral in plinthite and petroplinthite. In *Proceedings of the International Seminar on Lateritisation Processes*, Oxford & IBH Publishing Co. New Delhi, 335- 341.
- Farmer, V.C and Russell, J.D. (1966) Effects of particle size and structure on the vibrational sequences of layer silicates. *Spectrochimica Acta*, **22**, 389- 398.
- Farmer, V.C. (1979) Infrared Spectroscopy. In *Data Handbook for Clay Minerals and other Non metallic* M, H. Van Olphen and J.J. Fripiat, eds., Pergamon Press, New York, 285-337.
- Fellahi, S., Chikhi, N. and Bakar, M. (2001) Modification of epoxy resin with kaolin as a toughening agent. *Journal of Applied Polymer Science*, **82**, 861-878.
- Feth, J. H., Roberson, C.E. and Polzer, W.L. (1964) Sources of mineral constituents in water from granitic rocks, Sierra Nevada, California and Nevada, U.S. Geological Survey Water Supply Paper, 170pp.
- Firman, R.J. (1953) On the occurrence of nacrite at Shap, Westmorland. *Mineralogical Magazine*, **30**, 199-200.
- Foot, R. B. (1883) On the geology of south Travancore. *Record of Geological Survey of India*, **16**,

20–35.

- Fowkes, F.M. (1987) Role of acid – base interfacial bonding in adhesion. *Journal of Adhesion Science*, **1**, 7- 27.
- Frederickson, A. F. (1951) Mechanism of weathering. *Geological Society of America Bulletin*, **62**, 221–232.
- Freund, F. (1966) Nature of high temperature reaction products of dehydroxylated clay minerals. In *Silicate Science Volume V, Ceramic and Hydraulic Binders*, Wilhelm Eitel, ed., 133-151.
- Fuerstenau, M.C. (1976) Flotation. American Institute of Mining, Metallurgical and petroleum Engineers, New York, Vol 2, 1341pp
- Garrels, R. M. and Howards, P. (1959) Reactions of feldspar and mica with water at low temperature and pressure. In *Clays and Clay Minerals, 1957, A. 6th Natl. Conf., Berkeley California, 1957, A.* Swineford, ed., Pergamon Press, New York, 66- 88.
- Garrels, R. M. and Christ, C. L. (1965) *Solutions, minerals and equilibria*, New York, 450 pp.
- Garrels, R.M. (1984) Montmorillonite/ illite stability diagram. *Clays and Clay Minerals*, **32**, 161-166.
- Giese, R.F. Jr. (1988) Kaolin minerals: structure and stabilities. In *MSA Rev. Mineral Hydrous phyllosilicates (exclusive of micas)*, Bailey S.W, ed., **19**, 29- 66.
- Gilkes, R.J. (1973) The alteration products of potassium depleted oxybiotite. *Clays and Clay Minerals*, **21**, 303-313.
- Gilkes, K.J and Suddhiprakarn, A. (1979) Biotite in deeply weathered granite. Morphologic, mineralogical and chemical properties. II. The oriented growth of secondary minerals. *Clays and Clay Minerals*, **27**, 349 – 367.
- Goldman, M. I. and Tracey, J. I. Jr. (1964) Relation of bauxite and kaolin in the Arkansas bauxite deposits. *Economic Geology*, **14**, 567-575.
- Goldschmidts, V.M. (1958) *Geochemistry*. Oxford University Press, 491 pp.
- Gopalakrishnan, L.S. and Nair, M.M. (1976) Pre and post – sedimentary laterites-critical appraisal of the Karruchal Cliff section. *Proceedings of. Symposium On Geology and Geomorphology of Kerala (Abstr.) Geological Survey of India*, 58 pp.
- Grey, I.E. and Reid, A.F. (1975) The structure of psuedorutile and its role in the alteration of ilmenite. *American Mineralogist*, **60**, 898-906.
- Grim, R.E. (1962) *Applied clay mineralogy*. Mc Graw-Hill Book Company, Inc. London, 422pp.
- Grim, R.E. (1968) *Clay Mineralogy*. McGraw- Hill Book Co., New York, 596 pp.
- Grimshaw, R.W. and Searle, A. B. (1958) *Physics and Chemistry of Clays*. Western Printing Service Ltd., Bristol, 742 pp.
- Gross, M.G. (1971) Carbon Determination. In *Procedure in Sedimentary Petrology*, Robert. E. Carver ed., Wiley Interscience, 573-596.
- Hamilton, R. (1964). A short note on droplet formation in iron crusts. In *Proc IInd. Ind. Work. Meeting on Soil Micromorphology Arnheim*, A. Jorgesius ed., Nederlands, Elsevier, Amsterdam, 277- 278
- Hanson, R.F., Zamora, R. and Keller, W.D. (1981) Nacrite, dickite and kaolinite in one deposit in Nayarat, Mexico. *Clays and Clay Minerals*, **29**, 451-453.

- Harris, W.G., Zelazny L.W., Baker, J.C. and Martens D.C. (1985) Biotite kaolinization in Virginia Piedmont Soils: 1. Extent, profile trends and grain morphological effects. *Soil Science Society of American Journal*, **49**, 1290-1297.
- Hawthorne, D.G., Hodgkin, J.H., Loft, B.C. and Solomon, D.H. (1974) Polymerisation of vinyl monomers on mineral surfaces a novel method of preparing reinforcing fillers. *Journal of Macromolecular Science, Chemistry, A*, 649-657.
- Heckrodt, R.O. and Buhmann, D. (1987) Genesis of South African residual kaolins from sedimentary rocks. In *Proceedings of the International Clay Conference, Denver, 1985*, L.G.Schultz, H.van Olphen and F.A.Mumpton, eds., The Clay Minerals Society, Bloomington, Indiana, 128-134.
- Helgeson, H.C. (1971) Kinetics of mass transfer among silicates and aqueous solution. *Geochimica et Cosmochimica Acta*, **35**, 421-469.
- Helmer, B.M., Prescott, P.I. and Sennett, P. (1976) Surface –modified kaolin in plastics. In *Proceedings of 31st Annual Technical Conference, Reinforced Plastics/Composite Institute*, The society of the plastic industry, Inc. Section 8-G, 1-4.
- Hemley, J.J. (1959) Some mineralogical equilibria in the system K_2O - Al_2O_3 - SiO_2 - H_2O . *American Journal of Science*, **257**, 241- 270.
- Hey, M.H. (1941) The determination of ferrous iron in resistant silicates, *Mineralogical Magazine*, **26**, 116-118.
- Hillebrand, W.F., Lundell, G.E.F., Bright, H.A. and Hoffmann, J.I. (1953) *Applied Inorganic Analysis*. John Wiley, New York. 296 pp
- Hinckley, D.N. (1963) Variability in crystallinity values among the kaolin deposits of the coastal plain of Georgia and South Carolina. *Clays and Clay Minerals*, **11**,229- 235.
- Hoda, S.N and Hood, W.C. (1972) Laboratory alteration of trioctahedral micas. *Clays and Clay Minerals*, **20**, 343- 358.
- Holdren, G.R.Jr. and Berner, R. A. (1979) Mechanism of feldspar weathering. I. Experimental studies. *Geochimica et Cosmochimica Acta*, **43**, 1161-1171.
- Holland, T.H. (1900) The charnockite series , a group of Archean hypersthene rocks in Peninsular India. *Memoir of Geological Survey of India*, **28**, 117-249.
- Hsu, Pa. Ho. (1977) Aluminum hydroxides and oxyhydroxides. In *Minerals in Soil Environments*, J.B. Dixon and S.B. Weed, eds, Soil Science Society of America, Madison. Wisconsin, 99-143.
- Huang, W.H. (1974) Stabilities of kaolinite and halloysite in relation to weathering of feldspars and nepheline in aqueous solution. *American Mineralogist*, **59**, 365-371
- Huertas, F.J., Huertas, F. and Linares, J. (1993) A new approach to the kinetics of kaolinite synthesis. *Proc. 4th Int. Symposium on hydrothermal reaction*, 87-90.
- Hughes, R.E., Moore, D.M. and Reynolds, R.C.Jr. (1993) The nature, detection and occurrence, and origin of kaolinite`/smectite. In *Kaolin Genesis and Utilization*, H.H. Murray, W.M. Bundy and C.C. Harvey, eds., Publication No.1, Clay Mineral Society, Boulder, Colorado, 291-323.
- Hunter, R.J. (2001) *Foundations of colloid science*. Oxford University Press, 806 pp.
- Hurst, V.J. and Pickering Jr, S.M. (1997) Origin and classification of coastal plain kaolins Southeastern USA, and the role of groundwater and microbial action. *Clays and Clay Minerals*. **45**, 274-285.

- Indian Bureau of Mines, Ministry of steel and Mines, Nagpur (1997) Indian Mineral Yearbook Volume 2, Mineral Reviews & Foreign Trade (1999) Issued by Controller General India, Bureau of Mines, Nagpur, Published by the Controller of Publication, Delhi, 645pp
- Indian Bureau of Mines, Ministry of Steels & Mines Nagpur (1997) Indian Mineral Yearbook. General Reviews, issued by Controller General Indian Bureau of Mines, Nagpur (1998), 195pp.
- Indian Bureau of Mines, Mineral Economics Division, Nagpur, (2000) China Clay (Kaolin) A Market Survey, Government of India, Ministry of Mines and Minerals, 144 pp.
- Jackson, M.L. (1969) Soil Chemical Analysis- Advanced Course: 2nd Edition, Published by the author, Madison, Wis., 895 pp.
- Janczuk, B. and Bialopiotrowicz, T. (1988a) Components of surface free energy of some clay minerals. *Clays and Clay Minerals*, **333**, 243-248.
- Janczuk, B., Chibowski, E., Bialopiotrowicz, T. and Stawinski, J. (1989) Influence of exchangeable cations on the surface free energy of kaolinite as determined from contact angles. *Clays and Clay Minerals*, **37**, 269-272.
- Janczuk, B., Chibowski, E., Bialopiotrowicz, T., Holysz, L. and Kliszcz, A. (1990) Influence of dodecylamine chloride on the surface free energy of kaolinite. *Clays and Clay Minerals*, **38**, 53-56
- Jeffery, G.H., Bassette, J., Mendham, J. and Denney, R. C. (1989) Vogel's textbook of quantitative chemical analysis. ELBS/Longman, UK, 877 pp.
- Jeong, G.Y. (1998) Vermicular kaolinite epitactic on primary phyllosilicates in the weathering profiles of anorthosite. *Clays and Clay Minerals*, **46**, 509-520.
- Jepson, W.B. (1988) Structural Fe in kaolinites and in associated ancillary minerals. In *Iron in soils and clay minerals*, J.W. Stucki, ed., D. Reidel Publishing Company, Netherlands, 467- 536.
- Johansson, U., Holmgren, A., Frosling, W. and Frost, R.L. (1999) Adsorption of silane coupling agents on kaolinite surface. *Clay Minerals*, **34**, 239-246.
- Kawano, M. and Tomito, K. (1995) Formation of mica during experimental alteration of K-feldspar. *Clays and Clay Minerals*, **43**, 397-405.
- Kawano, M. and Tomita, K. (1996) Amorphous aluminum hydroxide formed at the earliest weathering stages of K- feldspar. *Clays and Clay Minerals*, **44**, 672-676.
- Keller, W.D. (1962) The principles of chemical weathering. Lucas Brothers Publication, Columbia, Missouri, 111 pp.
- Keller, W. D. (1970) Environmental aspects of clay minerals. *Journal of Sedimentary Petrology*, **40**, 788– 813.
- Keller, W. D. (1976a) Scan electron micrographs of kaolins collected from diverse environments or origin. II. *Clays and Clay Minerals*, **24**, 114 –117.
- Keller, W. D. (1976 b) Scan electron micrographs of kaolins collected from diverse origins. III. Influence of parent material on flint clays and flint like clays. *Clays and Clay Minerals*, **24**, 262-264.
- Keller, W.D. (1977) Scan electron micrographs of kaolin collected from diverse environment of origin. – IV Georgia kaolin and kaolinizing source rocks. *Clays and Clay Minerals*, **25**, 311-345.

- Keller, W.D. (1978) Classification of kaolins exemplified by their texture in scan electron micrographs. *Clays and Clay Minerals*, **26**, 1-20.
- Keller, W.D. (1978a) Progress and problem in rock weathering related to stone decay. In *Engineering Geology Case Histories*, E.M. Winkler, ed., Geological Society of America, 37-46.
- Keller, W.D. (1978b) Kaolinization of feldspar as displayed in scanning electron micrographs. *Geology*, **6**, 184-188.
- Keller, W. D. and Clarke, O. M. Jr. (1984) Resilication of bauxite at Alabama street Mine, Saline County, Arkansas, illustrated by scanning electron micrographs. *Clays and Clay Minerals*, **32**, 139-146.
- Keller, W.D. (1985) The nascence of clay minerals. *Clays and Clay Minerals*, **33**, 161-172.
- Kerala state gazetteer (1986) Vol 1, Ramachandran Nair ed., 401 pp
- King, W. (1882) General sketch of the geology of Travancore state. Record of Geological Survey of India, **15**, 93-102.
- Kittrick, J.A. (1969) Soil minerals in the Al_2O_3 - SiO_2 - H_2O system and a theory of their formation. *Clays and Clay Minerals*, **17**, 157-167.
- Kogel, J.E. and Hall, R.K. (1999) Process for improving the color and brightness of discolored goethite containing materials. United State Patent, 5,891,236, April 6.
- Krishnan, M. S. (1982) Geology of India and Burma. Higginbotham Pub. 6th Edition, 536 pp.
- Kittirck, J. A. (1973) Mica-derived vermiculites as unstable intermediates. *Clays and Clay Minerals*, **21**, 479-488.
- Kubiena, W.L. (1954) Micromorphology of laterite formation in Rio Muni (Spanish Guines). In *Trans. V th International Congress Soil Science (Lepioldville)*, 77- 84.
- Kubler, B. (1968) Evaluation quantitative du metamorphisme par la cristallinite de l'illite: Bull Centre Rech. Pau.SNPA 2, 385-397.
- Kubiena, W.L. (1970) Micromorphological features of soil geography, Rurgerv Univ Press, 254 pp
- Kukharskaya, E.V. and Skorik, Yu.I. (1996) Modification of kaolinite surface by organic and organosilicon polymers by means of ultrasonics. *Kauchuki Rezina*, **25**, 23-24.
- Laslett, R., Wansbrough, K.M., Rizzardo, E., Singh, S. and Mainwaring, D.E. (1992) Modification of kaolinite by surface polymerization. *Polymer International*, **28**, 19-23.
- Lazarev, A.N. (1974) The dynamics of crystal lattices. In *The Infrared Spectras of Minerals*, V.C. Farmer ed., Mineralogical Society, London, 69- 86.
- Libby, P.W., Iannicelli, J. and McGill, C.R. (1967) Elastomer reinforcement with amino silane grafted kaolin. American Chemical Society, Division of Rubber Chemistry, Spring Meeting, 18 pp.
- Liu, Q., Spears, D.A. and Liu, Q. (2001) MAS NMR study of surface modified calcined kaolin, *Applied Clay Science*, **19**, 89-94.
- Loughnan, F.C. (1969) Chemical weathering of the silicate minerals. American Mineralogist, Elsevier, New York, 154 pp.
- Loughnan, F.C. (1969) Chemical weathering of silicate minerals. Elsevier, Amsterdam, 273pp.

- Lundstrom, I. (1970) Etch patterns and twinning in two plagioclases. *Arkiv Mineralogisch Geologi*, **5**, 63 – 91.
- Lynd, L. E. (1960) Alteration of ilmenite. *Economic Geology*, **55**, 1064-1070.
- MacEwan, D.M.C. (1953) Cardenite, biotahedral montmorillonoid derived from biotite, *Clay Mineral Bulletin*, **2**, 120-126.
- MacKenzie, J.D., Brown, I.W.M., Meinhold, R.H. and Bowden, M.E. (1985) Outstanding problems in the kaolinite-mullite sequence investigated by ^{29}Si and ^{27}Al solid state NMR: I metakaolinite. *Journal of American Ceramic Society*, **68**, 293-297.
- Maksimovic Z., White, J.L and Logar, M. (1981) Chromium – bearing dickite and chromium – bearing kaolinite from Teslic, Yugoslavia. *Clays and Clay Minerals*, **29**, 213- 218.
- Manju, C. S., Narayanan Nair, V. and Lalithambika, M. (2001) Mineralogy, geochemistry and utilisation study of Madayi kaolin deposit, North Kerala, India. *Clays and Clay Minerals*, **49**, 355-369.
- Marshall, C. E. (1962) III. Reactions of feldspars and micas with aqueous solutions. *Economic Geology*, **57**, 1219 – 1227.
- Meads, R.E and Malden, P.J. (1975) Electron spin resonance in natural kaolinites containing Fe^{3+} and other transition metal ions. *Clay Minerals*, **10**, 313- 345.
- Menon, K.K. (1966) Sequence and source of the Tertiary near Karruchal, Trivandrum district. *Bulletin of Geological Society of India*, **3**, 75-78.
- Mestdagh, M.M., Vielvoye, L. and Herbillon, A.J. (1980) Iron in kaolinite II. The relationship between kaolinite crystallinity and iron content. *Clay Minerals*, **15**, 1-13.
- Meunier, A and Velde, B. (1979) Biotite weathering in granites of Western France. In *Proceedings of International clay Conference, Oxford, 1978*, M.M. Mortland and V.C. Farmer, eds., Elsevier Amsterdam, 405 –415.
- Meunier, A. and Velde, B. (1979) Weathering mineral facies in altered granites: The importance of local small scale equilibria. *Mineralogical Magazine*, **43**, 261- 268.
- Milewski, J.V; Katz, H.S. (1978) *Handbook of fillers and reinforcements for plastics*, Litton Education, New York, 122pp.
- Miyawaki, K., Tomura, S., Samejima, S., Okazaki, M., Mizuta, H., Maruyama, S. and Shibasaki, Y. (1991) Effects of solution chemistry on the hydrothermal synthesis of kaolinite. *Clays and Clay Minerals*, **39**, 498-508.
- Moore, D.M. and Reynolds, Jr.R.C. (1989) *X-ray diffraction and the identification and analysis of clay minerals*. 332 pp.
- Morse, J. W. and Casey W.H. (1988) Ostwald process and mineral paragenesis in sediments. *American Journal of Science*, **288**, 537- 560.
- Muller, J.-P and Bocquier, G. (1987) Textural and mineralogical relationships between ferruginous nodules and surrounding clayey matrices in a laterite from Cameroon, In *Proceedings of International Clay Conference, Denver, 1985*, L.G Schultz, H. Van Olphen and F.A. Mumpton, eds., The Clay Mineral Society, Bloomington, Indiana, 186-196.
- Murray, H.H. (1963) Industrial applications of kaolin. *Clays and Clay Minerals*, **10**, 291-293.

- Murray, H.H and Keller W.D. (1993) Kaolin, Kaolin and Kaolin. In *Kaolin Genesis and Utilization*, H. Murray, W. Bundy and C. Harvey eds., Special Publication No.1, The Clay Mineral Society, 341 pp.
- Nair, M. M. (1990) Structural trend line patterns and lineaments of Western ghats south of 13 latitude. *Journal Geological Society of India*, **35**,99–105.
- Nagasawa, K. (1978) Kaolin minerals. In *Clays and Clay Minerals of Japan Kodansha*, T. Sudo and S. Shimodo, eds., Tokyo/ Elsevier, Amsterdam, 189- 219.
- Newmann, A.W. and Good, R.J. (1979) Techniques of measuring contact angles. In *Surface and Colloid Science, Vol. II*, R.J. Good and R.R. Stromberg eds., Plenum Press, New York, 31-91.
- Nishiyama, N., Horie, K and Asakura, T (1988) Adsorption of silane coupling agent onto silica surface studied by magnetic resonance. In *Interfaces in polymerceramic and metal matrix composites interfaces, Proceedings of the second International (ICCI-11) 1988 , Cleveland, Ohio, U.S.A.*, Hatsuo Ishida, Ed., Elsevier Science Publishing Co., Inc, 279-289.
- Nixon, R.A. (1979) Differences in incongruent weathering of plagioclase and microcline- cation leaching versus precipitates. *Geology*, **7**, 221-224.
- Norton, S.A. (1980) Geologic factors controlling the sensitivity of aquatic ecosystems to acidic precipitation. In *Atmospheric Sulfur Deposition*, D.S. Shriner et al. eds., pp 521-531.
- Nordstrom, D.K. (1982) Aqueous pyrite oxidation and the consequent formation of secondary iron minerals In *Acid Sulfate Weathering*, J.A Kittrick; D.S. Fanning and L.R. Hossner, eds., Soil Science Society of America, Special Publication 10, Madison, Wisconsin, 37- 55.
- Nugay, N. and Erman, B. (2001) Property optimization in nitrile rubber composites via Hybrid filler systems. *Journal of Applied Polymer Science*, **79**, 366-374.
- Ogawa, M., Okutomo, S. and Kuroda,K. (1998) Control of interlayer microstructures of a layered silicate by surface modification with organochlorosilane. *Journal of American Chemical Society*, **120**, 7361-7362.
- Oliveira, M.G. and Soares, B.G. (2001) Mercapto-modified copolymers in polymer blends. III. The effect of functionalized ethylene-propylene diene rubber (EPDM) on curing and mechanical properties of NBR/EPDM blends; *Journal of Applied Polymer Science*, **82**, 38-52.
- Osaka, J. and Kato T. (1984) Synthesis of clay minerals from loose sands under hydrothermal condition. *Rep Asahi Glass Found Ind Technol*, **45**, 23-28 (in Japanese with English abstract).
- Panias, D., Taxiarchou, M., Paspaliaris, I. and Kontopoulos, A.(1996a) Dissolution of hematite in acidic oxalate solutions. The effect of ferrous ions addition. *Hydrometallurgy*, **43**, 219-230.
- Panias, D., Taxiarchou, M., Paspaliaris, I. and Kontopoulos, A. (1996 b) Mechanism of dissolution of iron oxides in aqueous oxalic acid solution. *Hydrometallurgy* **42**,257-265.
- Parham, W.E.(1969) Formation of halloysite from feldspar: low temperature artificial weathering versus natural weathering. *Clays and Clay Minerals*, **17**, 13-22.
- Paterson, E and Swaffield, R. (1987) Thermal analysis. In *A handbook of determinative methods in clay mineralogy*, M.J. Wilson ed., Blackie, Chapman and Hall, New York, 99-132.
- Paulose, K.V. and Narayanaswami, S. (1968) The Tertiary of Kerala coast. *Memoir of Geological Society of India*, **2**, 300-308.
- Pevear, D.R. and Nagy K.L.(1993) Kaolinite growth on mica in sandstones, bentonites and

- experiments. In *Abstract. 10th Int Clay Conf., 1993*, Adelaide, South Australia, 0-141.
- Plancon, A. and Tchoubar, C. (1977a) Determination of structural defects in phyllosilicates by X- ray powder diffraction- I. Principle of calculation of the diffraction phenomenon. *Clays and Clay Minerals*, **25**, 430-435.
- Plancon, A. and Tchobar, C. (1977b) Determination of structural defects in phyllosilicates by X- ray power diffraction – II. Nature and proportion of defects in natural kaolinites. *Clays and Clay Minerals*, **25**, 436 – 450.
- Plancon, A., Giese, R.F., Snyder, R., Drits, V.A. and Bookin, A.S. (1989) Stacking faults in kaolin- group minerals: defect structures of kaolinite, *Clays and Clay Minerals*, **23**, 249-260.
- Plueddemann, E.P. (1982) *Silane coupling agents*. Plenum press, New York, 17 pp.
- Porro, T.J. and Pattacini, S.C. (1990) The use of diffuse reflection FT-IR spectroscopy for the quantitative analysis of a number of silanized kaolin clays. *Applied Spectroscopy*, **44**, 1170-1175.
- Prabhakar Rao, G. (1968) Age of the Warkallai Formation and the emergence of the present Kerala Coast. *Bulletin of National Institute of Science*, **38**, 449–456.
- Raghava Rao, K. V. (1976) Groundwater exploration, development and long term aquifer management in Kerala. In *Proceedings of the Symposium on Mineral Resources of Kerala and their utilisation, 1975*, 30–36.
- Raiswell, R (1982) Pyrite texture, isotopic composition and the availability of iron. *American Journal of Science*, **282**, 1244-1263.
- Rajendran, C.P. and Narayanaswamy (1987) A note on lateritization cycles associated with sedimentaries, Kasargode district, Kerala. *Journal of Geological Society of India*, **30**, 309- 314.
- Rankama and Sahama, T.H.G. (1952) *Geochemistry*. 2nd edition. University of Chicago Press, Chicago, 659 pp
- Rao, P.S. (1974) Some aspects of structure and tectonics of the Kerala region and related mineralization. In *Proceedings of. symposium on tectonics and metallogeny of South East Asia and Far East*, Geological Survey of India, Miscellaneous Publication, **34**, 51-64.
- Rasheed, D. A. and Ramachandran, K. K. (1978) Foraminiferal biostratigraphy of the Quilon beds, Kerala state, India. *Proc. VII. India Coll. Micropal strat.*, 299 – 230.
- Rausell-Colom, J., Shwheatman, T. R., Wells, C. B. and Norrish, K. (1965) Studies in the artificial weathering of mica In *Proc 11th, School of Agricultural Science, Nottingham, 1965*, Butterworth, London, 40–72.
- Rausell-Colom, J.A. and Serratos, J.M. (1987) Reaction of clays with organic substances. In *Chemistry of clays and Clay Minerals*, A.C.D. Newman, eds., Wiley- Interscience, New York, 371-422.
- Rehner, J., Wiese, H.K. and Gessler, A.M. (1960) Cyclodiénylhalosilane treated mineral pigments. United States Patent, 2,928,802.
- Rendon, J.L and Serna, C.J. (1981) IR spectra of powder hematite: effects of particle size and shapes. *Clay Minerals*, **16**, 375- 382.
- Rengaswamy, P. (1976) Substitution of iron and titanium in kaolinites. *Clays and Clay Minerals*, **24**, 265-266.
- Robertson, I.D.M. and Eggleton, A.A. (1991) Weathering of granite muscovite to kaolinite and

- halloysite and of plagioclase derived kaolinite to halloysite. *Clays and Clay Minerals*, **39**, 113-126.
- Robie R. A. and Waldbaum D. R. (1968) Thermodynamic properties of minerals and related substances at 298.15 °K (25 °C) and one atmosphere (1.013 bars) pressure and at higher temperatures. *US Geological Survey Bulletin*, **1259**, 256 -.259.
- Robie R.A., Hemingway B.S., and Fisher J.R. (1978) Thermodynamic properties of minerals and related substances at 298.15 °K (25 °C) and 1 bar (10 Pascals) pressure and at higher temperatures. *US Geol Surv Bull*, **1452**, 456 p.
- Ross, C.S. and Kerr, P.F. (1931) The kaolin minerals. *U.S. Geological Surv. Prof. Paper* **165 E**, 151-175.
- Ross, C.S. and Kerr, P.F. (1934) Halloysite and allophane. *U.S. Geol. Surv. Prof. Paper* **185-G**, 135-148.
- Resource atlas of Kerala (1984) Centre of Earth Science Studies Pub., Trivandrum..
- Russell, J.D. (1987) Infrared methods. In *A handbook of determinative methods in clay Mineralogy*, M.J. Wilson ed., Blackie, Chapman and Hall, New York, 99-132.
- Sand, L. B. (1956) On the genesis of residual kaolins. *American Mineralogist*, **41**, 28-40.
- Samatoin N.D. and Checkin, S.S. (1993) Helical growth of kaolinite crystal in layer silicate. In *Abstr 10th Int Clay Conference, 1993 Adelaide, South Australia*, 143.
- Satokawa S., Osaki, Y., Samejima S., Miyawaki, R., Tomura S., Shibasaki, Y. and Augahara Y. (1994) Effects of the structure of silica-alumina gel on the hydrothermal synthesis of kaolinite. *Clays and Clay Minerals*, **42**, 288-297.
- Satakawa, S., Miyawaki, R., Osaki, Y., Tomura, S. and Shibasaki, Y. (1996) Effects of acidity on the hydrothermal synthesis of kaolinite from silica- gel and gibbsite. *Clays and Clay Minerals*, **44**, 417-423.
- Sawhney, B.L. (1977) Interstratification in layer silicates. In *Mineral in Soil Environments*, J.B. Dixon and S.B. Weed eds., Soil Society of America, Madison. 405-434.
- Schafer, H.N.S (1966) The determination of the iron (II) oxide in silicate and refractory Materials. *Analyst*, London, **91**, 755-762.
- Schneider, J.W. and Schneider, K. (1990) Indirect method for the determination of pyrite in clays and shale after selective extraction with acid solutions. *Ceramic Bulletin* , **69**, 107-109.
- Schoen, R. and Roberson, E.C. (1970) Structure of aluminum hydroxides and geochemical implications. *American Mineralogist*, **55**, 43-77.
- Schott, J. and Berner R.A. (1983) X- ray photoelectron studies of mechanism of iron silicate dissolution during weathering . *Geochimica et Cosmochimica Acta*, **49**, 1263- 1275.
- Schwertmann, U and Taylor, R.M (1977) Iron oxides. In *Minerals in Soil Environments*, J.B. Dixon and S.B Weed, eds., Soil Science Society of America, Madison, Wisconsin, 379-433.
- Schneider, J.W. and Schneider, K. (1990) Indirect method for the determination of pyrite, in clays and shale after selective extraction with acid solutions. *Ceramic Bulletin*, **69**, 107-109.
- Serna, C.J., Rendon, J.L. and Igleis, J.E. (1982) Infrared surface modes in corundum type microcrystalline oxides, *Spectrochim Acta*, **38A**, 797- 802.
- Sharp, T. G., Olten, M. T. and Buseck, P. R. (1990) Serpentinization of phlogopite phenocrysts from a

- micaceous kimberlite. *Contribution to Mineralogy and Petrology*, **104**, 530–539.
- Shoumkov, S., Dimitrov, Z. and Brakalov, L (1987) High gradient magnetic treatment of kaolin. *Interceram*, **6**, 26-28.
- Siffert, B. (1978) Genesis and synthesis of clays and clay minerals recent developments and future prospects. In *Proceedings of International Clay Conference, Oxford*, 337- 347.
- Singer, F and Singer, S.S. (1978) *Industrial Ceramics*. Chapman and Hall, London, 1455 pp.
- Singh, B. and Gilke, R. J. (1991) Weathering of a chromian muscovite to kaolinite. *Clays and Clay Minerals*, **39**, 571-579.
- Singh, B. and Gilkes, R.J. (1992) An electron optical investigations of the alteration of kaolinite to halloysite. *Clays and Clay Minerals*, **40**, 212-229.
- Sinha-Roy,S., John Mathai and Narayanaswamy (1984) Structure and metamorphic characteristics of cordierite-bearing gneiss of South Kerala. *Journal of Geological Society of India*, **25**, 231-244.
- Soman, K. and Slukin, A.D. (1987) Lateritization cycles and their relation to the formation and quality of kaolin deposits in South Kerala, India. *Chemical Geology*, **60**, 273-280.
- Sposito, G. (1984) *The surface chemistry of soils*. Oxford University Press, New York, 234 pp.
- Srodon, J. (1980) Synthesis of mixed layer kaolinite/smectite. *Clays and Clay Minerals*, **28**, 419-424.
- Starr, R.E. and Young, R.H. (1978) Paprecoating formulations. A study of limitations in the determination and use of the Kubelka-Munk constants. *Tappi*, **61**, 78-80.
- Steeffel, C. I. and Van Cappellen, P. (1990) A new kinetics approach to modelling water- rock interaction. The role of nucleation, precursors and Ostwald ripening. *Geochimica et Cosmochimica Acta*, **54**, 2657-2677.
- Stoch, L. and Sikora,W. (1976) Transformation of mica in the process of kaolinization of granites and gneisses. *Clays and Clay Minerals*, **24**, 156-162.
- Stucki, J.W., Goodman, B.A. and Schwertmann, U. (1988) *Iron in soils and clay Minerals*. D. Reidel Publ. Co., Dordrecht, Holland, 893 pp.
- Stumm, W and Sulzberger, B (1992) The cycling of iron in natural environments: Consideration based on laboratory studies of heterogeneous redox processes. *Geochimica et Cosmochimica Acta*, **56**, 3233-3257.
- Suttner, L.J., Mack, G., James, W.C. and Young, S.W. (1976) Relative alteration of microcline and sodic plagioclase in semi arid and humid climate. *Geological Society of America, Abstract programs*, **8**, 512.
- Tardy, Y., Bocquier, G., Paquet, H. and Millot, G. (1973) Formation of clay from granite and its distribution in relation to climate and topography. *Geoderma*, **10**, 271-284.
- Tardy, Y. and Nahon, D. (1985) Geochemistry of laterites. Stability of Al-goethite, Al- hematite and Fe³⁺ kaolinite in bauxite and ferricretes. An approach to the mechanism of concretion. *American Journal Science* **285**, 865-903.
- Tarzi, J.D. and Protz, R. (1978) Characterisation of morphological features of soil micas using scanning electron microscopy. *Clays and Clay Minerals*, **26**, 352-360
- Tazaki, K. and Fyfe, W.S. (1987) Primitive clay precursors formed on feldspar. *Canadian Journal of Earth Sciences*, **24**, 506-527.

- Temple, A.K. (1966) Alteration of ilmenite. *Economic Geology*, **61**, 695-714.
- Teufer, G. and Temple, A.K. (1966) Pseudorutile, a new mineral intermediate between ilmenite and rutile in the natural alteration of ilmenite. *Nature*, **211**, 179-181.
- Theng, B.K.G. (1979) Formation and properties of clay- polymer complexes. Elsevier, Amsterdam, 362 pp.
- Thomas, D., Lalithambika, M. and Soman, K. (1987) Clay mineral transformation in the weathering crust : Evidence from Lundara clay mine, Kerala. *Journal of Geological Society of India*, **30**, 239-243.
- Thompson, J.G. (1985) Interpretation of solid state ^{13}C and ^{29}Si nuclear magnetic resonance spectra of kaolinite intercalates. *Clays and Clay Minerals*, **33**, 173-180.
- Tomura, S., Shibasaki, Y. and Mizuta, H. (1983) Spherical kaolinite: synthesis and mineralogical properties. *Clays and Clay Minerals*, **31**, 413- 421.
- Tomura, S., Shibasaki, Y., Mizuta, H. and Kitamura, I.(1985) Growth conditions and genesis of spherical and platy kaolinite. *Clays and Clay Minerals*, **33**, 200-206.
- Tsuzuki, Y. and Kawabe, I.(1983). Polymorphic transformation of kaolin minerals in aqueous solution. *Geochimica et Cosmochimica Acta*, **47**, 59-66.
- Ubal dini, S., Piga, L., Fornari, P., Massidda, R. (1996) Removal of iron from quartz sands: A study by column leaching using a complete factorial design. *Hydrometallurgy* **40**, 369-379.
- Valenton, I. (1972) Bauxite. Elsevier, Amsterdam, 226 pp.
- Varadarajan, K. and Balakrishnan, M. K. (1980) Kerala Coast – A landsats views. Proc. Sym. On geology and geomorphology of Kerala. Geological survey of India, Special Publication, **5**, 67– 68.
- Vazquez, F.M. (1981) Formation of gibbsite in soil and saprolites of temperate-humid zones. *Clay Mineral*, **16**, 43-52.
- Velbel, M. A. (1984) Natural weathering mechanisms of almandine garnet, *Geology* **12**, 631-634.
- Velbel, M.A. (1985a) Geochemical mass balances and weathering rates in forested watersheds of Southern Blue Ridge. *American Journal of Science*, **285**, 904-930.
- Velbel, M.A. (1985b) Hydrogeochemical constraints on mass balances in forested watersheds of the southern Appalachians. In *The Chemistry of Weathering*, J.I.Drever and D. Reidel, eds., NATO ASI Series, C 149, 231- 247.
- Waite, T.W. and Morel, F.M.M. (1984) Photoreductive dissolution of colloidal iron oxide: Effect of citrate. *Journal of Colloid Interface Science*, **102**, 121-137.
- Walker, T.L. (1902) The geology of Kalahandi state, central provinces. Memoir of Geological Survey of India, **33**, 1-21.
- Walker, T.R. (1974) Formation of red beds in moist tropical climates: A hypothesis. *Bulletin of GSA*, **85**, 633-638.
- Water Resource of Kerala (1974) Government of Kerala, Pub., 110p.
- Weaver, C.E. (1985) Development in sedimentology 44- Clay, Muds and Shales. Elsevier, Amsterdam, 819 pp.
- White, A.F. and Yee, A. (1985) Aqueous oxidation- reduction kinetics associated with coupled electron- cation transfer from iron containing silicates at 25°C ., **49**, 1263-1275.

- White, G.N., Dixon, J.B., Weaver, R.M. and Kunkle, A.C. (1991) Genesis and morphology of iron sulfides in gray kaolins. *Clays and Clay Minerals*, **39**, 70-76.
- Wilson, M.J. (1966) The weathering of biotite in some Aberdeenshire soils. *Mineralogical Magazine*, **35**, 1080–1093.
- Wilson, M.J. (1987) *A handbook of determinative method in clay mineralogy*. Blackie, Chapman and Hall, New York, 308 pp
- Wollast, R. (1967) Kinetics of the alteration of K- feldspar in buffered solutions at low temperature. *Geochimica et Cosmochimica Acta*, **31**, 635-648.
- Wollast, R. and Chou, L. (1985) Kinetic study of the dissolution of albite with a continuous flow-through fluidized bed reactor. In *The Chemistry of Weathering*, NATO ASI series J. I. Drever, eds., Reidel, Dordrecht, The Netherlands, 75-96.

Summary and Conclusion

Kaolinites, the molecularly engineered layered silicates are widespread in nature and possess many unique properties. The uniqueness of kaolinite arises from its typical layered structure, thin platelet shape, fine particle size, high brightness and whiteness, good rheology in aqueous suspension, relative chemical inertness and the ability to modify its structure in accordance with the surrounding environment.

Geochemical, mineralogical and morphological evaluations of kaolin deposits of Madayi and Kundara from northern and southern parts of Kerala give a very interesting picture on the above aspects. The present study showed that the three factors such as 1) morphology of the minerals, 2) their internal crystal order and 3) the physico-chemical components of the environment in which the clay mineral crystallised are genetically related.

The similarities and differences of formation and properties of clays from the two kaolin deposits are highlighted below. Asterisk “*” indicates the typical feature of the deposits.

Madayi Deposit

North Kerala, Kannur district, thickness of the profile ~ 45 meters

Clay Sequence:

Residual white clay (L1a, L1b and L1c: ~ 14m), formed from Precambrian crystalline rock: quartzo feldspathic mica gneiss, due to pre-Tertiary lateritisation.

Gray carbonaceous clay (L3, L5, L7, L9,

Kundara Deposit

South Kerala, Kollam district, thickness of the profile ~ 55 meters.

Residual white clay (K1a, K1b and K1c: ~15m), formed from pre-Tertiary lateritisation of Precambrian rock, garnetiferous biotite gneiss.

Gray carbonaceous clay (K2, K4, K6 and

L11, L13 and L15 with alternate lignite Seams: ~ 17.5 meters depth) and Hematitic clay (L16, L17 and L18: ~12 meters depth) formed as a part of Warkallai Formation.

***Encrustation of bauxite along with ferricretes indicates long periods of aridity in the climate prior to rainfall.**

Mineralogy:

Residual clay

Mineralogical assemblages include kaolinite, quartz, muscovite, illite and pyrophyllite in upper portion of the profile (L1b & c). Pyrophyllite is absent in the lower most portion (L1a)

***The sequence indicates pyrophyllite to be the intermediate stage in muscovite →kaolinite alteration.**

Gray carbonaceous clay

Associated minerals include kaolinite, quartz (coarse and microcrystalline), marcasite and pyrite with traces of smectite and gibbsite.

***Association of smectite and gibbsite indicates a dual condition of leaching environment.**

***Ample marcasite and pyrite reflect the reducing environment for clay formation/deposition.**

K7 with lignite seams: ~ 19 m) and Hematitic clay (K8, K9 and K10: ~ 24 m) formed as a part of Warkallai Formation.

***Presence of FeS₂ patches in residual white clay.**

***Typical quick yellow pigmentation of white clay soon after the exposure.**

Mineralogical associations include kaolinite, quartz, biotite, ilmenite and trace pseudorutile in the lowermost portion, K1a. Pseudorutile, rutile and anatase present along with kaolinite and quartz in K1b. Minerals present in the black patches include pyrite, melanterite and jarosite. Good amount of rutile and anatase present in addition to kaolinite and quartz in K1c.

***The sequence represent the conversion of biotite to kaolinite and alteration of ilmenite to pseudorutile, anatase and rutile.**

Mineralogical assemblages in these seams consist of kaolinite, quartz, gibbsite, anatase, rutile with traces of marcasite, jarosite, goethite and sillimanite.

***Good amount of gibbsite reflects the intensity of leaching.**

Hematitic clay

Kaolinite, quartz and hematite are the minerals present in L16 and L17. The topmost bauxitic sample consists of higher gibbsite and hematite concentrations with traces of kaolinite. Ferricretes is entirely of hematite.

***High amount of this Fe- mineral shows the aridity of the climate and extent of oxidation**

The associate minerals in this clay include kaolinite, quartz, hematite, sillimanite, rutile and anatase.

Geochemistry:**Residual clay**

Good amount of alkali and alkaline earth metals in the lower layer exhibit the variation in intensity of leaching of parent material with depth

Presence of high water leachable SO_4^{2-} and iron in the K1c, upper portion of the profile indicate the elution of the same from the upper carbonaceous clay seams. On the contrary high FeO in lower most portion of the profile (K1a) indicates the presence of ilmenite and biotite.

***Lowering of the pH soon after the exposure of the clay reflects the leaching of FeS_2 on oxidation**

Gray carbonaceous clay

High Fe_2O_3 / organic carbon and pH substantiate the intensity of reducing condition and the also the acidity of the deposit.

***High acidity for the clays indicates the oxidation of FeS_2 .**

Good amount of Al_2O_3 and lower concentration of Fe_2O_3 further give evidences on SO_4^{2-} leaching.

***Maximum trace element concentration is for laterite (1124 ppm).**

Hematitic clay

Concentration of high Fe_2O_3 in the upper bauxitic layer shows the intensity of incongruent dissolution of Al_2O_3 and SiO_2 , and consequent enrichment of iron.

* Maximum trace element concentration is for bauxite (2788 ppm).

Structural Features:

Hinckley index ranges from 0.44 (L5) to 1.10 (L1a). In addition the presence of doublet between 3694 and 3619 cm^{-1} (OH stretching region) for kaolinite in FTIR, which has a lower Hinckley crystallinity index, reflects the presence of well ordered kaolinite along with the disordered ones.

Thermal properties:

DTA shows a range in the endothermic peak values from 487 to 542°C and exothermic peak values between 955 to 1003.5°C. Weight losses as from TG were consistent with the concentration of organic carbon and FeS_2 .

Morphological features:

Residual clay

Fanning out texture and friated edges of kaolinite is indicative of muscovite kaolinization. Pyrite crystal of cube-octahedral-dodecahedral features were

Concentration of Fe_2O_3 more in the topmost lateritised portion.

Hinckley Index ranges from 0.67 (K10) to 1.1 (K1b). Absence of doublet between 3694 and 3619 cm^{-1} reflects lower order for these kaolinites.

Endothermic and exothermic peak value ranges from 507 to 540°C and 981 to 1003°C respectively. The weight losses around 288°C reflect the concentration of gibbsite and in turn the leaching environment.

Microcrystalline stacks of kaolinite are pseudomorph after feldspar. Kaolinization of biotite is also evident. Pyrite crystals with typical cube-octahedral, pyritohedral

found within the fossilised plant remains in the upper most portion of residual clay profile, indicating a local area of saturation of Fe^{2+} and SO_4^{2-} enriched solution, which get leached out from FeS_2 of gray carbonaceous clay.

Gray carbonaceous clay

This thick sequence of clay seams show kaolinite crystals of three distinct genetic types: 1) swirl texture with face-to-face arrangement of kaolinite platelets showing its detrital character 2) bimodal texture indicative of *in situ* crystallization in a water laden condition 3) *in situ* kaolinite crystallization into the etched pits of cubic pyrite, resulting from an Al-Si enriched solution.

Hematitic clay

Kaolin from hematitic clay exhibit distinct morphology showing 1) agglomerated nature in the presence of iron oxide indicative of detrital origin 2) collomorphous texture for laterites with *in situ* gibbsite crystallization due to Al_2O_3 -

crystals are present in black patched portions. In addition, their oxidation product, melanterite with monoclinic crystal feature is also present. The leached out iron in clay deposit reprecipitates as ferrihydrite in this SO_4^{2-} enriched environment. Garnet grains show two sets of leached pits, which give fingerprints on the influence of dual environment reducing and oxidising on the clay deposit.

***Morphological features also reflect the influence of leaching of SO_4^{2-} ions into the residual clay**

Two distinct types of kaolinites were found 1) *in situ* crystallisation of vermicular kaolinite in unconsolidated sediment enriched in feldspar 2) agglomerated nature of kaolinite showing its detrital origin.

Two distinct type 1) *In situ* kaolinite showing vermicular nature 2) detrital one with face-to-edge arrangements of clay platelets. Feldspar grain shows prismatic etch pits. The iron mineral shows a typical mushroom shaped morphology covering the

SiO₂ remobilization 3) features showing the remobilisation of Fe₂O₃ into tubules indicative of advanced stage of lateritization for this layer. entire surface of the clays.

Optical feature:

Muscovite grains from residual clay shows a varying intensity of weathering of the parent rock in the residual clay profile. The extent of alteration of muscovite increases in the upper portions of the profile owing to increasing acidity.

The optical properties of the mineral grain biotite, ilmenite, anatase/rutile and alterites reflect the influence of dual environment: oxidative and reductive, on the deposit.

Comparison of the stratigraphic, petrological and morphological characteristics of the clays from the above two deposits show that both the deposits: Madayi and Kundara were formed under similar paleoclimatic conditions. The variations in the geochemistry of the two resulted from the variation in the characteristics of the parent rocks such as their mineralogy and the permeability of the deposited parent materials. In addition, the sedimentary deposits show a slight varying depositional environment as evident from the concentration of the organic carbon in the gray carbonaceous and lignite seams and also from the size variation of the deposited minerals. In the case of Kundara kaolinites, since the Tertiary sediments are coarser and much more unconsolidated with lower amounts of reactive ferrous iron, the SO₄²⁻ enriched solution elutes downward into the residual clay seams resulting in FeS₂ crystallization. Here on exposure, the clay shows quick yellow pigmentation resulting from Fe²⁺ oxidation. The sedimentary Warkallai Formation, which overlies the residual clays of both the places, has major role in controlling the quality of kaolinite. In addition, these clays preserve the valuable underlying residual white clays in both the deposits from ongoing lateritisation. Mineralogical, thermal, spectroscopic and morphological analysis give evidences to substantiate the climatic and environmental conditions during the deposition of kaolinite. Thus, the sequence and pattern of

lithologies, mineral content and chemical composition clearly bring out the complete record on geochemistry of the deposits. The texture and morphology of the minerals help to substantiate the conditions of microenvironments under which these valuable deposits have been formed. New insight into the fascinating science of kaolinite—about its formation mechanisms, variation of the chemical and structural properties, geochemistry of the accessory minerals, its stability in the weathering environments etc could be gained from the present investigations.

Studies on the physical and bleaching properties of the economically viable white residual clays from the two locations indicate that the iron mineral, which imparts colour to the residual white clays in Madayi, is goethite (ferric iron). Here bleaching of the raw clay using sodium hydrosulphite and oxalic acid could enhance the property of the clay only to a limited extent. The clay on bleaching after calcination (350°C, 3 h) could improve the properties much better than the uncalcined one. The evaluation of the physical properties of these clays indicates their use as fillers. On the contrary, taking advantage of the presence iron in the ferrous form in the clays of Kundara, deferration of the same clays with oxalic acid as the sequestering agent, could enhance the brightness from 7-8 units and reduce the yellowness by 4-5 units, even at room temperature treatment. Deferration studies indicate fast room temperature dissolution of Fe with oxalic acid by autocatalytic reductive mechanism. This technique was found to be successful for profitable deferration prior to its conversion to the yellow pigmentous material. The physical property evaluation of these clays shows their promising use for paper coating and bone china formulations.

In view of the improved demand of value added products of kaolinite in the world market, the property enhancement study adopted by hydrophobicing the kaolinite surface was found to be successful for its application as filler in natural rubber. Outstanding surface characteristics were obtained when kaolinite was hydrophobised using organosilane. These improvements include water repellency (hydrophobicity), better coating/adhesion to the substrate, controlled rheological properties, improved compatibility and dispersibility. In addition, the enhanced mechanical, thermal, curing

and swelling characteristics of kaolin incorporated natural rubber composites reflect the formation of a higher crosslinked product. Thermal treatment followed by silylation of the kaolinite filler results in enhancements in the composite properties. The study showed that the clay in the natural state or in the modified forms have the potential to produce novel molecular organisations, which show much higher efficiency for certain applications.

The rising demand of clay based products in the world market, remind us of the need for such elaborate investigations on the geochemical, mineralogical and utilitarian aspects of clays. Value addition of clays by surface modification opens a new field of thought in clay research. Studies in this line are still in the initial stages. Prognostics definitely show an increasing demand for the value-added clay based products. Elaborate investigation in geochemistry, mineralogy and value addition is the need of the day to assess the industrial potential of the clay minerals available in our country.

References

- Aagaard, P. and Helgeson, H. C. (1982) Thermodynamic and kinetics constraints on reaction rates among minerals and aqueous solutions I. Theoretical considerations. *American Journal of Sciences*, **282**, 237-285.
- Acker, J.G. and Bricker, O.P. (1992) The influence of pH on biotite dissolution and alteration kinetics at low temperature. *Geochimica et Cosmochimica Acta*, **56**, 3073- 3092.
- Ahn, J. H. and Peacor, D. R. (1987) Kaolinization of biotite: TEM data and implications for an alteration mechanism. *American Mineralogist*, **72**, 353-356.
- Alexander, L.T. and Cady, J.G. (1962) Genesis and hardening of laterite in soils USDA Tech. Bulletin, 90 pp.
- Al-Khalissi, F.Q. and Worrall, W.E. (1982) The effect of crystallinity on the quantitative determination of kaolinite. *Transaction British Ceramic Society*, **81**, 43-46.
- Altschuler, Z.S., Dwornik, E.J. and Kramer, H. (1963) Transformation of montmorillonite to kaolinite during weathering. *Science*, **141**, 148-152.
- Ambikadevi, V.R. and Lalithambika, M. (2000) Effect of organic acids on ferric iron removal from iron stained kaolinite. *Applied clay science*, **16**, 133-145.
- Amigó, J.M., Bastida, J., Garcia Agramut, M.J., Sanz M. and Galván J. (1987). Crystallinity of Lower Cretaceous kaolinites of Teruel. In *EUROCLAY Conf; Sevilla '87; Sevilla; Spain*. Galan E, PerezRodriguez JL, Cornejo J. eds., 74-75.
- Amouric, M. and Olives, J. (1998) Transformation mechanisms and interstratification in conversion of smectite to kaolinite: An HRTEM study. *Clays and Clay Minerals*, **46**, 521-527.
- Anand, R. R. and Gilkes, R. J. (1984) Weathering of ilmenite in a lateritic pallid zone. *Clays and Clay Minerals*, **32**, 363-374.
- Anand, R.R., Gilkes, R.J., Armitage, T.M. and Hillyer, J.W. (1985) Feldspar weathering in lateritic saprolite. *Clays and Clay Minerals*, **33**, 31-43.
- Anovitz, L. M., Perkins, D., Essene, E. J. (1991) Metastability in near-surface rocks of minerals in the system Al_2O_3 - SiO_2 - H_2O . *Clays and Clay Minerals*, **39**, 225- 233.
- Arkles, B. (1977) Tailoring surfaces with silanes. *Chemtech*, **12**, 766-777.
- Bailey, S.W. (1963) Polymorphism of kaolin minerals. *American Mineralogist*, **48**, 1196-1206.
- Bailey, S.W. (1969) Polytypism of trioctahedral 1:1 layer silicates. *Clays and Clay Minerals*, **17**, 355-371.
- Bailey, S.W. (1980) Structures of layer silicates. In *Crystal structure of clay minerals and their X-ray identification*, G. W. Brindley and G. Brown, eds., Mineralogical Society London, Monograph, **44**, 78-114.
- Banfield, J.F. (1985) The mineralogy and chemistry of granite weathering. MSc. Thesis, Australian National University, Canberra, Australia, 229pp.

- Banfield, J. R. and Eggleton, R. A. (1988) Transmission electron microscopic study of biotite weathering. *Clays and Clay Minerals*, **36**, 47–60.
- Banfield, J.F. and Eggleton, R. A. (1990) Analytical transmission electron microscope studies of plagioclase, muscovite and K- feldspar weathering. *Clays and Clay Minerals*, **38**, 77- 89.
- Bandyopadhyay, S., De, P.P., Tripaty, D.K. and De, S.K. (1996) 3- Aminopropyltriethoxysilane as a promoter in the crosslinking of carboxylated nitrile rubber by surface-oxidized carbon black. *Journal of Applied Polymer Science*, **61**, 1813-1820.
- Baron, D and Palmer, C.D. (1996) Solubility of jarosite at 4 – 35°C, *Geochemica et Cosmochimica Acta*, **60**, 185- 195.
- Barrot, R.J. (1968) Interest of lamellar minerals in rubber compounding. Rubber Meeting of the Swedish Institution of Rubber Technology, Falsterbo, 14 pp.
- Bei, Y.L. and Huang, J.T. (1990) Study on clay surface modified by coupling agents. *Journal of Huaqiao University*, **11**, 278-283, in Chinese, with English Abstract.
- Bennett, H. and Reed, R.A. (1971) Chemical methods of silicate analysis. A handbook Academic Press Ind., London, 272 pp.
- Berner, R.A and Holdren, G.R. Jr. (1977) Mechanism of feldspar weathering. I. Some observational evidences. *Geology*, **5**, 369-372.
- Berner, R.A. (1984) Sedimentary pyrite formation: An update. *Geochimica et Cosmochimica Acta*, **48**, 605-615.
- Berry, L.G., Mason, B. and Dietrich, R.V. (1985) Mineralogy concepts description and determination. W.H Freeman and Company, U.S.A., 560 pp.
- Bigham, J.M. (1994) Mineralogy of ochre deposits formed by sulfide oxidation. In. *Handbook on environmental geochemistry of sulfide mine waste*, J. Jambor and D. Blowes eds., Mineralogical Association of Canada, **22**, 103-132.
- Blow, C.M. and Hepburn, C. (1982) Rubber technology and manufacture. Published for the plastics and rubber institute, Butterworth Scientific, London, 608 pp.
- Bonney, C.F. (1994) Removal of iron from kaolin and quartz dissolution with organic acids. *Proceedings of International Symposium on Hydrometallurgy*, London, 313-323.
- Brady, K.S., Bigham, J.M., Jaynes, W.F. and Logan, T.J. (1986). Influence of sulfate on Fe-oxide formation: Comparisons with a stream receiving acid mine drainage. *Clays and Clay Minerals*, **34**, 266-274.
- Braggs, B., Fornasiero, D., Ralston, J. and Smart, R.St. (1994) The effect of surface modification by an organosilane on electrochemical properties of kaolinite. *Clays and Clay Minerals*, **42**, 123-136.
- Brindley, G.W. and Brown, G. (1980) Crystal structure of clay minerals and their X-ray identification, Mineralogical Society, London, 495 pp.
- Brindley, G.W., Zalba E, and Bethke C.M. (1983). Hydrobiotite, a regular 1:1 interstratified cation of biotite and vermiculite layers. *American Mineralogist*, **68**, 420-425.
- Brindley, G.W., Kao, C-C., Harrison, J.L., Lipsicas, M., and Raythatha, R. (1986) Relation between structural disorder and other characteristics of kaolinite dickite. *Clays and Clay Minerals*, **34**, 239 – 249.

- Brown, A.J., Brannen, J.O., Andrews, W., May, J.R. and Raythatha, R.H. (1990) Kaolinitaggregation using organo-silicon compounds. June 19, Patent number.4,935, 062.
- Bruckner, W. (1952) The mantle rock ("laterite") of the Gold coast and its origin. *Geol Rdsch.*, **43**, 307-327.
- Bundy, W.M. and Ishley, J.N (1991) Kaolin in paper filling and coating. *Applied Clay Science*, **5**, 397-420.
- Busenberg, E (1978) The product of the interaction of feldspar with aqueous solution at 25°C. *Geochimica et Cosmochimica Acta*, **42**, 1679-1686.
- Chen, P.-Y. Lin, M.-L and Zheng, Z. (1997) On the origin of the name kaolin and the kaolin deposits of the Kauling and Dazhou areas, Kiangsi, China. *Applied Clay Science*, **12**, 1-25.
- Chiarizia, R., Horwitz, E.P. (1991) New formulation for iron oxides dissolution. *Hydrometallurgy*, **27**, 339-360.
- Churchman G.J. and Gilkes R.J. (1989) Recognition of intermediates in the possible transformation of halloysite to kaolinite in the weathering profiles. *Clay Minerals*, **24**, 549-590.
- Chukrov, F.V., Zvyagin, B.B., Gorshov, A.I., Yermilova, L.P., Korovuskov, V.V., Rudnitskaya Ye. S. and Syakubovskaya. N. Yu (1977) Feroxyhyte a new modification of FeOOH. *Int. Geol. Rev*, **19**, 873-890.
- Clarke, O. M. Jr. (1973) Gibbsite in weathered granitic rocks of Alabama, Southeast. *Geology*, **14**, 203- 212.
- Cleaves E. T., Godfrey, A. E. and Bricker O. P. (1970) Geochemical balance of a small watershed and its geomorphic implications. *Geological Society of America Bulletin*, **81**, 3015 – 3032.
- Cornell, R.M., Posner, A.M. and Quirk, J.P. (1974) Crystal morphology and the dissolution of goethite (α - FeOOH). *Journal of Inorganic Nuclear Chemistry*, **36**, 1937-1946.
- Cornell, R.M., Posner, A.M and Quirk, J.P (1976) Kinetics and mechanisms of the acid dissolution of goethite (α -FeOOH). *Journal of Inorganic Chemistry*, **38**, 563-567.
- Cornell, R. M. and Schindler, P.W. (1987) Photochemical dissolution of goethite in acid/oxalate solution. *Clays and Clay Minerals*, **35**, 347-352.
- Craw, D., Coombs, D.S. and Kawachi, Y. (1982) Interlayered biotite kaolin and other altered biotites and their relevance to the biotite isograd in eastern Otago, New Zealand. *Mineralogical Magazine*, **45**, 79-85.
- Dai, J.C., Bei, Y.L., Lin, Q.Y. and Huang, J.T. (1995b) Reinforcement of rubber by silane modified clay. *Journal of Huaqiao University*. **16**, 159-164, in Chinese, with English Abstract.
- Dai, J.C. and Huang, J.T. (1999) Surface modification of clays and clay- rubber composites. *Applied Clay Science*, **15**, 51-65.
- Dangic', A. (1985) Kaolinization of bauxite: A study in the Vlasenica bauxite area, Yugoslavia. I. Alteration of matrix. *Clays and Clay Minerals*, **33**, 517-524.
- Dangic', A. (1988) Kaolinization of bauxite: A study of the Vlasenica bauxite area, Yugoslavia, II. Alteration of oolites. *Clays and Clay Minerals*, **36**, 439-447.

- Danneberg, E.M. (1975) The effects of surface chemical interactions on the properties of the filler reinforced rubber. *Rubber Chemical Technology*, **48**, 410-444.
- Debnath, S., De, S.K. and Khastigir, D. (1987) Effect of silane coupling agent on vulcanization network structure, polymer-filler interaction, physical properties and failure mode of mica filled styrene butadiene rubber. *Journal of Material Science*, **22**, 44-53.
- Deer, W.A., Howie, R.A. and Zussman, J. (1976) *Rock forming minerals*. Volume 3, Longman Group Limited, London, 270 pp.
- DeKimpe, C., Gastuche, M.C. and Brindley, G.W. (1961) Ionic coordination in alumino-silicic gels in relation to clay mineral formation. *American Mineralogist*, **46**, 1370-1381.
- DeKimpe, C., Gastuche, M. W. and Brindley, G. W. (1964) Low temperature synthesis of clay minerals. *American Mineralogist*, **49**, 1-16.
- De Vijnck, Y. (1976) Action des ions alcalins sur la transformation hydrothermales de gels silico-alumineux . II. Influence de 1 ions K⁺. *Silic. Ind.* **41**, 67- 81.
- Dickson, T. (2000) Global kaolin supply and industrial structure. *Industrial Clays*, **3** 39-47.
- Eberl, D. and Hower, J. (1975) Kaolinite synthesis. The role of the Si/Al and (Alkali)(H⁺) ratio in hydrothermal systems. *Clays and Clay Minerals*, **23**, 301-309.
- Eggleton, R.A. and Buseck, P.R. (1980) High resolution electron microscopy of feldspar weathering. *Clays and Clay Minerals*, **28**, 173-178.
- Eswaran, H. and Raghunathan, N.G. (1973) The microfabric of petroplinthite. *Soil Science Society of America Proceedings*, **37**, 79- 81.
- Eswaran, H., Stoops, C and Sys, C. (1977) The micromorphology of gibbsite forms in soils. *Journal of Soil Science Society of America Proceedings*. **37**, 79-81.
- Eswaran, H. and Bin, W.C. (1978 a) A study of a deep weathering profile on granite in Peninsular Malaysia: III. Alteration of feldspar. *Soil Science Society of American Journal*, **42**, 154-158.
- Eswaran, H. and Bin, W.C. (1978b) A study of a deep weathering profile on granite in Peninsular Malaysia: II Mineralogy of the clay, silt and sand fraction. *Soil Science Society of American Journal*, **42**, 149-153.
- Eswaran, H., Comerma, J. and Sooryanarayanan, V. (1981) Scanning Electron Microscopic observations on the nature and distribution of iron mineral in plinthite and petroplinthite. In *Proceedings of the International Seminar on Lateritisation Processes*, Oxford & IBH Publishing Co. New Delhi, 335-341.
- Farmer, V.C and Russell, J.D. (1966) Effects of particle size and structure on the vibrational sequences of layer silicates. *Spectrochimica Acta*, **22**, 389- 398.
- Farmer, V.C. (1979) Infrared Spectroscopy. In *Data Handbook for Clay Minerals and other Non metallic M*, H. Van Olphen and J.J. Fripiat, eds., Pergamon Press, New York, 285-337.
- Fellahi, S., Chikhi, N. and Bakar, M. (2001) Modification of epoxy resin with kaolin as a toughening agent. *Journal of Applied Polymer Science*, **82**, 861-878.
- Feth, J. H., Roberson, C.E. and Polzer, W.L. (1964) Sources of mineral constituents in water from granitic rocks, Sierra Nevada, California and Nevada, U.S. Geological Survey Water Supply Paper, 170pp.

- Firman, R.J. (1953) On the occurrence of nacrite at Shap, Westmorland. *Mineralogical Magazine*, **30**, 199-200.
- Foot, R. B. (1883) On the geology of south Travancore. *Record of Geological Survey of India*, **16**, 20-35.
- Fowkes, F.M. (1987) Role of acid – base interfacial bonding in adhesion. *Journal of Adhesion Science*, **1**, 7-27.
- Frederickson, A. F. (1951) Mechanism of weathering. *Geological Society of America Bulletin*, **62**, 221-232.
- Freund, F. (1966) Nature of high temperature reaction products of dehydroxylated clay minerals. In *Silicate Science Volume V, Ceramic and Hydraulic Binders*, Wilhelm Eitel, ed., 133-151.
- Fuerstenau, M.C. (1976) *Flotation: American Institute of Mining, Metallurgical and petroleum Engineers*, New York, Vol 2, 1341pp.
- Garrels, R. M. and Howards, P. (1959) Reactions of feldspar and mica with water at low temperature and pressure. In *Clays and Clay Minerals, 1957, A. 6th Natl. Conf., Berkeley California, 1957*, A. Swineford, ed., Pergamon Press, New York, 66- 88.
- Garrels, R. M. and Christ, C. L. (1965) *Solutions, minerals and equilibria*, New York, 450 pp.
- Garrels, R.M. (1984) Montmorillonite/ illite stability diagram. *Clays and Clay Minerals*, **32**, 161-166.
- Giese, R.F. Jr. (1988) Kaolin minerals: structure and stabilities. In *MSA Rev. Mineral Hydrous phyllosilicates (exclusive of micas)*, Bailey S.W, ed., **19**, 29- 66.
- Gilkes, R.J. (1973) The alteration products of potassium depleted oxybiotite. *Clays and Clay Minerals*, **21**, 303-313.
- Gilkes, K.J and Suddhiprakarn, A. (1979) Biotite in deeply weathered granite. Morphologic, mineralogical and chemical properties. II. The oriented growth of secondary minerals. *Clays and Clay Minerals*, **27**, 349 – 367.
- Goldman, M. I. and Tracey, J. I. Jr. (1964) Relation of bauxite and kaolin in the Arkansas bauxite deposits. *Economic Geology*, **14**, 567-575.
- Goldschmidt, V.M. (1958) *Geochemistry*. Oxford University Press, 491 pp.
- Gopalakrishnan, L.S. and Nair, M.M. (1976) Pre and post – sedimentary laterites-critical appraisal of the Karruchal Cliff section. *Proceedings of. Symposium On Geology and Geomorphology of Kerala (Abstr.) Geological Survey of India*, 58 pp.
- Grey, I.E. and Reid, A.F. (1975) The structure of psuedorutile and its role in the alteration of ilmenite. *American Mineralogist*, **60**, 898-906.
- Grim, R.E. (1962) *Applied clay mineralogy*. Mc Graw-Hill Book Company, Inc. London, 422pp.
- Grim, R.E. (1968) *Clay Mineralogy*. McGraw- Hill Book Co., New York, 596 pp.
- Grimshaw, R.W. and Searle, A. B. (1958) *Physics and Chemistry of Clays*. Western Printing Service Ltd., Bristol, 742 pp.

- Gross, M.G. (1971) Carbon Determination. In *Procedure in Sedimentary Petrology*, Robert. E. Carver ed., Wiley Interscience, 573-596.
- Hamilton, R. (1964). A short note on droplet formation in iron crusts. In *Proc IInd. Ind. Work. Meeting on Soil Micromorphology Arnheim*, A. Jogesius ed., Nederlands, Elsevier, Amsterdam, 277-278.
- Hanson, R.F., Zamora, R. and Keller, W.D. (1981) Nacrite, dickite and kaolinite in one deposit in Nayarat, Mexico. *Clays and Clay Minerals*, **29**, 451-453.
- Harris, W.G., Zelazny L.W., Baker, J.C. and Martens D.C. (1985) Biotite kaolinization in Virginia Piedmont Soils: 1. Extent, profile trends and grain morphological effects. *Soil Science Society of American Journal*, **49**, 1290-1297.
- Hawthorne, D.G., Hodgkin, J.H., Loft, B.C. and Solomon, D.H. (1974) Polymerisation of vinyl monomers on mineral surfaces a novel method of preparing reinforcing fillers. *Journal of Macromolecular Science, Chemistry, A*, 649-657.
- Heckroodt, R.O. and Buhmann, D. (1987) Genesis of South African residual kaolins from sedimentary rocks. In *Proceedings of the International Clay Conference, Denver, 1985*, L.G.Schultz, H.van Olphen and F.A.Mumpton, eds., The Clay Minerals Society, Bloomington, Indiana, 128-134.
- Helgeson, H.C. (1971) Kinetics of mass transfer among silicates and aqueous solution. *Geochimica et Cosmochimica Acta*, **35**, 421-469.
- Helmer, B.M., Prescott, P.I. and Sennett, P. (1976) Surface –modified kaolin in plastics. In *Proceedings of 31st Annual Technical Conference, Reinforced Plastics/Composite Institute*, The society of the plastic industry, Inc. Section 8-G, 1-4.
- Hemley, J.J. (1959) Some mineralogical equilibria in the system K_2O - Al_2O_3 - SiO_2 - H_2O . *American Journal of Science*, **257**, 241- 270.
- Hey, M.H. (1941) The determination of ferrous iron in resistant silicates, *Mineralogical Magazine*, **26**, 116-118.
- Hillebrand, W.F., Lundell, G.E.F., Bright, H.A. and Hoffmann, J.I. (1953) *Applied Inorganic Analysis*. John Wiley, New York. 296 pp.
- Hinckley, D.N. (1963) Variability in crystallinity values among the kaolin deposits of the coastal plain of Georgia and South Carolina. *Clays and Clay Minerals*, **11**, 229- 235.
- Hoda, S.N and Hood, W.C. (1972) Laboratory alteration of trioctahedral micas. *Clays and Clay Minerals*, **20**, 343- 358.
- Holdren, G.R.Jr. and Berner, R. A. (1979) Mechanism of feldspar weathering. I. Experimental studies. *Geochimica et Cosmochimica Acta*, **43**, 1161-1171.
- Holland, T.H. (1900) The charnockite series , a group of Archean hypersthene rocks in Peninsular India. *Memoir of Geological Survey of India*, **28**, 117-249.
- Hsu, Pa. Ho. (1977) Aluminum hydroxides and oxyhydroxides. In *Minerals in Soil Environments*, J.B.Dixon and S.B. Weed, eds, Soil Science Society of America, Madison. Wisconsin, 99-143.

- Huang, W.H. (1974) Stabilities of kaolinite and halloysite in relation to weathering of feldspars and nepheline in aqueous solution. *American Mineralogist*, **59**, 365-371.
- Huertas, F.J., Huertas, F. and Linares, J. (1993) A new approach to the kinetics of kaolinite synthesis. *Proc. 4th Int. Symposium on hydrothermal reaction*, 87-90.
- Hughes, R.E., Moore, D.M. and Reynolds, R.C.Jr. (1993) The nature, detection and occurrence, and origin of kaolinite/smectite. In *Kaolin Genesis and Utilization*, H.H. Murray, W.M. Bundy and C.C. Harvey, eds., Publication No.1, Clay Mineral Society, Boulder, Colorado, 291-323.
- Hunter, R.J. (2001) *Foundations of colloid science*. Oxford University Press, 806 pp.
- Hurst, V.J. and Pickering Jr, S.M. (1997) Origin and classification of coastal plain kaolins Southeastern USA, and the role of groundwater and microbial action. *Clays and Clay Minerals*, **45**, 274-285.
- Indian Bureau of Mines, Ministry of steel and Mines, Nagpur (1997) *Indian Mineral Yearbook Volume 2, Mineral Reviews & Foreign Trade (1999)* Issued by Controller General India, Bureau of Mines, Nagpur, Published by the Controller of Publication, Delhi, 645pp.
- Indian Bureau of Mines, Ministry of Steels & Mines Nagpur (1997) *Indian Mineral Yearbook. General Reviews*, issued by Controller General Indian Bureau of Mines, Nagpur (1998), 195pp.
- Indian Bureau of Mines, Mineral Economics Division, Nagpur, (2000) *China Clay (Kaolin) A Market Survey*, Government of India, Ministry of Mines and Minerals, 144 pp.
- Jackson, M.L. (1969) *Soil Chemical Analysis- Advanced Course: 2nd Edition*, Published by the author, Madison, Wis., 895 pp.
- Janczuk, B. and Bialopiotrowicz, T. (1988a) Components of surface free energy of some clay minerals. *Clays and Clay Minerals*, **333**, 243-248.
- Janczuk, B., Chibowski, E., Bialopiotrowicz, T. and Stawinski, J. (1989) Influence of exchangeable cations on the surface free energy of kaolinite as determined from contact angles. *Clays and Clay Minerals*, **37**, 269-272.
- Janczuk, B., Chibowski, E., Bialopiotrowicz, T., Holysz, L. and Kliszcz, A. (1990) Influence of dodecylamine chloride on the surface free energy of kaolinite. *Clays and Clay Minerals*, **38**, 53-56.
- Jeffery, G.H., Bassette, J., Mendham, J. and Denney, R. C. (1989) *Vogel's textbook of quantitative chemical analysis*. ELBS/Longman, UK, 877 pp.
- Jeong, G.Y. (1998) Vermicular kaolinite epitactic on primary phyllosilicates in the weathering profiles of anorthosite. *Clays and Clay Minerals*, **46**, 509-520.
- Jepson, W.B. (1988) Structural Fe in kaolinites and in associated ancillary minerals. In *Iron in soils and clay minerals*, J.W. Stucki, ed., D. Reidel Publishing Company, Netherlands, 467- 536.
- Johansson, U., Holmgren, A., Frosling, W. and Frost, R.L. (1999) Adsorption of silane coupling agents on kaolinite surface. *Clay Minerals*, **34**, 239-246.
- Kawano, M. and Tomita, K. (1995) Formation of mica during experimental alteration of K-feldspar. *Clays and Clay Minerals*, **43**, 397-405.
- Kawano, M. and Tomita, K. (1996) Amorphous aluminum hydroxide formed at the earliest weathering stages of K- feldspar. *Clays and Clay Minerals*, **44**, 672-676.

- Keller, W.D. (1962) The principles of chemical weathering. Lucas Brothers Publication, Columbia, Missouri, 111 pp.
- Keller, W. D. (1970) Environmental aspects of clay minerals. *Journal of Sedimentary Petrology*, **40**, 788–813.
- Keller, W. D. (1976a) Scan electron micrographs of kaolins collected from diverse environments or origin. II. *Clays and Clay Minerals*, **24**, 114–117.
- Keller, W. D. (1976 b) Scan electron micrographs of kaolins collected from diverse origins. III. Influence of parent material on flint clays and flint like clays. *Clays and Clay Minerals*, **24**, 262-264.
- Keller, W.D. (1977) Scan electron micrographs of kaolin collected from diverse environment of origin. – IV Georgia kaolin and kaolinizing source rocks. *Clays and Clay Minerals*, **25**, 311-345.
- Keller, W.D. (1978) Classification of kaolins exemplified by their texture in scan electron micrographs. *Clays and Clay Minerals*, **26**, 1-20.
- Keller, W.D. (1978a) Progress and problem in rock weathering related to stone decay. In *Engineering Geology Case Histories*, E.M. Winkler, ed., Geological Society of America, 37-46.
- Keller, W.D. (1978b) Kaolinization of feldspar as displayed in scanning electron micrographs. *Geology*, **6**, 184-188.
- Keller, W. D. and Clarke, O. M. Jr. (1984) Resilication of bauxite at Alabama street Mine, Saline County, Arkansas, illustrated by scanning electron micrographs. *Clays and Clay Minerals*, **32**, 139-146.
- Keller, W.D. (1985) The nascence of clay minerals. *Clays and Clay Minerals*, **33**, 161-172.
- Kerala state gazetteer (1986) Vol 1, Ramachandran Nair ed., 401 pp.
- King, W. (1882) General sketch of the geology of Travancore state. *Record of Geological Survey of India*, **15**, 93–102.
- Kittrick, J.A. (1969) Soil minerals in the Al_2O_3 - SiO_2 - H_2O system and a theory of their formation. *Clays and Clay Minerals*, **17**, 157-167.
- Kogel, J.E. and Hall, R.K. (1999) Process for improving the color and brightness of discolored goethite containing materials. United State Patent, 5,891,236, April 6.
- Krishnan, M. S. (1982) *Geology of India and Burma*. Higginbotham Pub. 6th Edition, 536 pp.
- Kittirck, J. A. (1973) Mica-derived vermiculites as unstable intermediates. *Clays and Clay Minerals*, **21**, 479–488.
- Kubiena, W.L. (1954) Micromorphology of laterite formation in Rio Muni (Spanish Guines). In *Trans. Vth International Congress Soil Science (Lepoldville)*, 77-84.
- Kubler, B. (1968) Evaluation quantitative du metamorphisme par la cristallinite de l'illite: *Bull Centre Rech. Pau.SNPA* **2**, 385-397.

- Kubiena, W.L. (1970) *Micromorphological features of soil geography*, Rurgerv Univ Press, 254 pp.
- Kukharskaya, E.V. and Skorik, Yu.I. (1996) Modification of kaolinite surface by organic and organosilicon polymers by means of ultrasonics. *Kauchuki Rezina*, **25**, 23-24.
- Laslett, R., Wansbrough, K.M., Rizzardo, E., Singh, S. and Mainwaring, D.E. (1992) Modification of kaolinite by surface polymerization. *Polymer International*, **28**, 19-23.
- Lazarev, A.N. (1974) The dynamics of crystal lattices. In *The Infrared Spectras of Minerals*, V.C. Farmer ed., Mineralogical Society, London, 69- 86.
- Libby, P.W., Iannicelli, J. and McGill, C.R. (1967) Elastomer reinforcement with amino silane grafted kaolin. American Chemical Society, Division of Rubber Chemistry, Spring Meeting, 18 pp.
- Liu, Q., Spears, D.A. and Liu, Q. (2001) MAS NMR study of surface modified calcined kaolin, *Applied Clay Science*, **19**, 89-94.
- Loughnan, F.C. (1969) *Chemical weathering of the silicate minerals*. American Mineralogist, Elsevier, New York, 154 pp.
- Loughnan, F.C. (1969) *Chemical weathering of silicate minerals*. Elsevier, Amsterdam, 273pp.
- Lundstrom, I. (1970) Etch patterns and twinning in two plagioclases. *Arkiv Mineralogisch Geologi*, **5**, 63 – 91.
- Lynd, L. E. (1960) Alteration of ilmenite. *Economic Geology*. **55**, 1064-1070.
- MacEwan, D.M.C. (1953) Cardenite, biodahedral montmorillonoid derived from biotite, *Clay Mineral Bulletin*, **2**, 120-126.
- MacKenzie, J.D., Brown, I.W.M., Meinhold, R.H. and Bowden, M.E. (1985) Outstanding problems in the kaolinite-mullite sequence investigated by ²⁹Si and ²⁷Al solid state NMR: I metakaolinite. *Journal of American Ceramic Society*, **68**, 293-297.
- Maksimovic Z., White, J.L and Logar, M. (1981) Chromium – bearing dickite and chromium – bearing kaolinite from Teslic, Yugoslavia. *Clays and Clay Minerals*, **29**, 213- 218.
- Manju, C. S., Narayanan Nair, V. and Lalithambika, M. (2001) Mineralogy, geochemistry and utilisation study of Madayi kaolin deposit, North Kerala, India. *Clays and Clay Minerals*. **49**, 355-369.
- Marshall, C. E. (1962) III. Reactions of feldspars and micas with aqueous solutions. *Economic Geology*, **57**, 1219 – 1227.
- Meads, R.E and Malden, P.J. (1975) Electron spin resonance in natural kaolinites containing Fe³⁺ and other transition metal ions. *Clay Minerals*, **10**, 313- 345.
- Menon, K.K. (1966) Sequence and source of the Tertiary near Karruchal, Trivandrum district. *Bulletin of Geological Society of India*, **3**, 75-78.
- Mestdagh, M.M., Vielvoye, L. and Herbillon, A.J. (1980) Iron in kaolinite II. The relationship between kaolinite crystallinity and iron content. *Clay Minerals*, **15**, 1-13.
- Meunier, A and Velde, B. (1979) Biotite weathering in granites of Western France. In *Proceedings of International clay Conference, Oxford, 1978*, M.M. Mortland and V.C. Farmer, eds., Elsevier Amsterdam, 405 –415.

- Meunier, A. and Velde, B. (1979) Weathering mineral facies in altered granites: The importance of local small scale equilibria. *Mineralogical Magazine*, **43**, 261- 268.
- Milewski, J.V; Katz, H.S. (1978) Handbook of fillers and reinforcements for plastics, Litton Education, New York, 122pp.
- Miyawaki, K., Tomura, S., Samejima, S., Okazaki, M., Mizuta, H., Maruyama, S. and Shibasaki, Y. (1991) Effects of solution chemistry on the hydrothermal synthesis of kaolinite. *Clays and Clay Minerals*, **39**, 498-508.
- Mondal, S.K and Basu, D.K. (1994) *Rubber Chemical Technology*, **67**, 672.
- Moore, D.M. and Reynolds, Jr.R.C. (1989) X-ray diffraction and the identification and analysis of clay minerals. 332 pp.
- Morse, J. W. and Casey W.H. (1988) Ostwald process and mineral paragenesis in sediments. *American Journal of Science*, **288**, 537- 560.
- Muller, J.-P and Bocquier, G. (1987) Textural and mineralogical relationships between ferruginous nodules and surrounding clayey matrices in a laterite from Cameroon, In *Proceedings of International Clay Conference, Denver, 1985*, L.G Schultz, H. Van Olphen and F.A. Mumpton, eds., The Clay Mineral Society, Bloomington, Indiana, 186-196.
- Murray, H.H. (1963) Industrial applications of kaolin. *Clays and Clay Minerals*, **10**, 291-293.
- Murray, H.H and Keller W.D. (1993) Kaolin, Kaolin and Kaolin. In *Kaolin Genesis and Utilization*, H. Murray, W. Bundy and C. Harvey eds., Special Publication No.1, The Clay Mineral Society, 341 pp.
- Nair, M. M. (1990) Structural trend line patterns and lineaments of Western ghats south of 13 latitude. *Journal Geological Society of India*, **35**, 99-105.
- Nagasawa, K. (1978) Kaolin minerals. In *Clays and Clay Minerals of Japan Kodansha*, T. Sudo and S. Shimodo, eds., Tokyo/ Elsevier, Amsterdam, 189- 219.
- Newmann, A.W. and Good, R.J. (1979) Techniques of measuring contact angles. In *Surface and Colloid Science, Vol. II*, R.J. Good and R.R. Stromberg eds., Plenum Press, New York, 31-91.
- Nishiyama, N., Horie, K and Asakura, T (1988) Adsorption of silane coupling agent onto silica surface studied by magnetic resonance. In *Interfaces in polymer/ceramic and metal matrix composites interfaces, Proceedings of the second International (ICCI-11) 1988 , Cleveland, Ohio, U.S.A.*, Hatsuo Ishida, Ed., Elsevier Science Publishing Co., Inc, 279-289.
- Nixon, R.A. (1979) Differences in incongruent weathering of plagioclase and microcline- cation leaching versus precipitates. *Geology*, **7**, 221-224.
- Norton, S.A. (1980) Geologic factors controlling the sensitivity of aquatic ecosystems to acidic precipitation. In *Atmospheric Sulfur Deposition*, D.S. Shriner et al. eds., pp 521-531.
- Nordstrom, D.K. (1982) Aqueous pyrite oxidation and the consequent formation of secondary iron minerals In *Acid Sulfate Weathering*, J.A Kittrick; D.S. Fanning and L.R. Hossner, eds., Soil Science Society of America, Special Publication 10, Madison, Wisconsin, 37- 55.
- Nugay, N. and Erman, B. (2001) Property optimization in nitrile rubber composites via Hybrid filler systems. *Journal of Applied Polymer Science*, **79**, 366-374.

- Ogawa, M., Okutomo, S. and Kuroda, K. (1998) Control of interlayer microstructures of a layered silicate by surface modification with organochlorosilane. *Journal of American Chemical Society*, **120**, 7361-7362.
- Oliveira, M.G. and Soares, B.G. (2001) Mercapto-modified copolymers in polymer blends. III. The effect of functionalized ethylene-propylene diene rubber (EPDM) on curing and mechanical properties of NBR/EPDM blends; *Journal of Applied Polymer Science*, **82**, 38-52.
- Osaka, J. and Kato T. (1984) Synthesis of clay minerals from loose sands under hydrothermal condition. *Rep Asahi Glass Found Ind Technol*, **45**, 23-28 (in Japanese with English abstract).
- Panias, D., Taxiarchou, M., Paspaliaris, I. and Kontopoulos, A. (1996a) Dissolution of hematite in acidic oxalate solutions. The effect of ferrous ions addition. *Hydrometallurgy*, **43**, 219-230.
- Panias, D., Taxiarchou, M., Paspaliaris, I. and Kontopoulos, A. (1996 b) Mechanism of dissolution of iron oxides in aqueous oxalic acid solution. *Hydrometallurgy* **42**, 257-265.
- Parham, W.E. (1969) Formation of halloysite from feldspar: low temperature artificial weathering versus natural weathering. *Clays and Clay Minerals*, **17**, 13-22.
- Paterson, E and Swaffield, R. (1987) Thermal analysis. In *A handbook of determinative methods in clay mineralogy*, M.J. Wilson ed., Blackie, Chapman and Hall, New York, 99-132.
- Paulose, K.V. and Narayanaswami, S. (1968) The Tertiary of Kerala coast. *Memoir of Geological Society of India*, **2**, 300-308.
- Pevear, D.R. and Nagy K.L. (1993) Kaolinite growth on mica in sandstones, bentonites and experiments. In *Abstract. 10th Int Clay Conf., 1993*, Adelaide, South Australia, 0-141.
- Plancon, A. and Tchoubar, C. (1977a) Determination of structural defects in phyllosilicates by X-ray powder diffraction- I. Principle of calculation of the diffraction phenomenon. *Clays and Clay Minerals*, **25**, 430-435.
- Plancon, A. and Tchobar, C. (1977b) Determination of structural defects in phyllosilicates by X-ray power diffraction – II. Nature and proportion of defects in natural kaolinites. *Clays and Clay Minerals*, **25**, 436 – 450.
- Plancon, A., Giese, R.F., Snyder, R., Drits, V.A. and Bookin, A.S. (1989) Stacking faults in kaolin-group minerals: defect structures of kaolinite, *Clays and Clay Minerals*, **23**, 249-260.
- Plueddemann, E.P. (1982) *Silane coupling agents*. Plenum press, New York, 17 pp.
- Porro, T.J. and Pattacini, S.C. (1990) The use of diffuse reflection FT-IR spectroscopy for the quantitative analysis of a number of silanized kaolin clays. *Applied Spectroscopy*, **44**, 1170-1175.
- Prabhakar Rao, G. (1968) Age of the Warkallai Formation and the emergence of the present Kerala Coast. *Bulletin of National Institute of Science*, **38**, 449-456.
- Raghava Rao, K. V. (1976) Groundwater exploration, development and long term aquifer management in Kerala. In *Proceedings of the Symposium on Mineral Resources of Kerala and their utilisation, 1975*, 30-36.
- Raiswell, R (1982) Pyrite texture, isotopic composition and the availability of iron. *American Journal of Science*, **282**, 1244-1263.

- Rajendran, C.P. and Narayanaswamy (1987) A note on lateritization cycles associated with sedimentaries, Kasargode district, Kerala. *Journal of Geological Society of India*, **30**, 309- 314.
- Rankama and Sahama, T.H.G. (1952) *Geochemistry*. 2nd edition. University of Chicago Press, Chicago, 659 pp.
- Rao, P.S. (1974) Some aspects of structure and tectonics of the Kerala region and related mineralization. In *Proceedings of symposium on tectonics and metallogeny of South East Asia and Far East*, Geological Survey of India, Miscellaneous Publication, **34**, 51-64.
- Rasheed, D. A. and Ramachandran, K. K. (1978) Foraminiferal biostratigraphy of the Quilon beds, Kerala state, India. *Proc. VII. India Coll. Micropal strat.*, 299 – 230.
- Rausell-Colom, J., Shweatman, T. R., Wells, C. B. and Norrish, K. (1965) Studies in the artificial weathering of mica In *Proc 11th*, School of Agricultural Science, Nottingham, 1965, Butterworth, London, 40–72.
- Rausell-Colom, J.A. and Serratoso, J.M. (1987) Reaction of clays with organic substances. In *Chemistry of clays and Clay Minerals*, A.C.D. Newman, eds., Wiley- Interscience, New York, 371-422.
- Rehner, J., Wiese, H.K. and Gessler, A.M. (1960) Cyclodienylhalosilane treated mineral pigments. United States Patent, 2,928,802.
- Rendon, J.L and Serna, C.J. (1981) IR spectra of powder hematite: effects of particle size and shapes. *Clay Minerals*, **16**, 375- 382.
- Rengaswamy, P. (1976) Substitution of iron and titanium in kaolinites. *Clays and Clay Minerals*, **24**, 265-266.
- Robertson, I.D.M. and Eggleton, A.A. (1991) Weathering of granite muscovite to kaolinite and halloysite and of plagioclase derived kaolinite to halloysite. *Clays and Clay Minerals*, **39**, 113-126.
- Robie R. A. and Waldbaum D. R. (1968) Thermodynamic properties of minerals and related substances at 298.15 °K (25 °C) and one atmosphere (1.013 bars) pressure and at higher temperatures. *US Geological Survey Bulletin*, **1259**, 256 -259.
- Robie R.A., Hemingway B.S., and Fisher J.R. (1978) Thermodynamic properties of minerals and related substances at 298.15 °K (25 °C) and 1 bar (10 Pascals) pressure and at higher temperatures. *US Geol Surv Bull*, **1452**, 456 p.
- Ross, C.S. and Kerr, P.F. (1931) The kaolin minerals. *U.S. Geological Surv. Prof. Paper* **165 E**, 151-175.
- Ross, C.S. and Kerr, P.F. (1934) Halloysite and allophane. *U.S. Geol. Surv. Prof. Paper* **185-G**, 135-148.
- Resource atlas of Kerala (1984) Centre of Earth Science Studies Pub., Trivandrum..
- Russell, J.D. (1987) Infrared methods. In *A handbook of determinative methods in clay Mineralogy*, M.J. Wilson ed., Blackie, Chapman and Hall, New York, 99-132.
- Sand, L. B. (1956) On the genesis of residual kaolins. *American Mineralogist*, **41**, 28-40.
- Samatoin N.D. and Checkin, S.S. (1993) Helical growth of kaolinite crystal in layer silicate. In *Abstr 10th Int Clay Conference, 1993 Adelaide, South Australia*, 143.

- Satokawa S., Osaki, Y., Samejima S., Miyawaki, R., Tomura S., Shibasaki, Y. and Augahara Y. (1994) Effects of the structure of silica-alumina gel on the hydrothermal synthesis of kaolinite. *Clays and Clay Minerals*, **42**, 288-297.
- Satakawa, S., Miyawaki, R., Osaki, Y., Tomura, S. and Shibasaki, Y. (1996) Effects of acidity on the hydrothermal synthesis of kaolinite from silica- gel and gibbsite. *Clays and Clay Minerals*, **44**, 417-423.
- Sawhney, B.L. (1977) Interstratification in layer silicates. In *Mineral in Soil Environments*, J.B. Dixon and S.B. Weed eds., Soil Society of America, Madison. 405-434.
- Schafer, H.N.S (1966) The determination of the iron (II) oxide in silicate and refractory Materials. *Analyst*, London, **91**, 755-762.
- Schneider, J.W. and Schneider, K. (1990) Indirect method for the determination of pyrite in clays and shale after selective extraction with acid solutions. *Ceramic Bulletin* , **69**, 107-109.
- Schoen, R. and Roberson, E.C. (1970) Structure of aluminum hydroxides and geochemical implications. *American Mineralogist*, **55**, 43-77.
- Schott, J. and Berner R.A. (1983) X- ray photoelectron studies of mechanism of iron silicate dissolution during weathering . *Geochimica et Cosmochimica Acta*, **49**, 1263- 1275.
- Schwertmann, U and Taylor, R.M (1977) Iron oxides. In *Minerals in Soil Environments*, J.B. Dixon and S.B Weed, eds., Soil Science Society of America, Madison, Wisconsin, 379-433.
- Schneider, J.W. and Schneider, K. (1990) Indirect method for the determination of pyrite, in clays and shale after selective extraction with acid solutions. *Ceramic Bulletin*, **69**, 107-109.
- Serna, C.J., Rendon, J.L. and Iglesias, J.E. (1982) Infrared surface modes in corundum type microcrystalline oxides, *Spectrochim Acta*, **38A**, 797- 802.
- Sharp, T. G., Olten, M. T. and Buseck, P. R. (1990) Serpentinization of phlogopite phenocrysts from a micaceous kimberlite. *Contribution to Mineralogy and Petrology*, **104**, 530-539.
- Shoumkov, S., Dimitrov, Z. and Brakalov, L (1987) High gradient magnetic treatment of kaolin. *Interceram*, **6**, 26-28.
- Siffert, B. (1978) Genesis and synthesis of clays and clay minerals recent developments and future prospects. In *Proceedings of International Clay Conference, Oxford*, 337- 347.
- Singer, F and Singer, S.S. (1978) *Industrial Ceramics*. Chapman and Hall, London, 1455 pp.
- Singh, B. and Gilke, R. J. (1991) Weathering of a chromian muscovite to kaolinite. *Clays and Clay Minerals*, **39**, 571-579.
- Singh, B. and Gilkes, R.J. (1992) An electron optical investigations of the alteration of kaolinite to halloysite. *Clays and Clay Minerals*, **40**, 212-229.
- Sinha-Roy,S., John Mathai and Narayanaswamy (1984) Structure and metamorphic characteristics of cordierite-bearing gneiss of South Kerala. *Journal of Geological Society of India*, **25**, 231-244.
- Soman, K. and Slukin, A.D. (1987) Lateritization cycles and their relation to the formation and quality of kaolin deposits in South Kerala, India. *Chemical Geology*, **60**, 273-280.
- Sposito, G. (1984) *The surface chemistry of soils*. Oxford University Press, New York, 234 pp.

- Srodon, J. (1980) Synthesis of mixed layer kaolinite/smectite. *Clays and Clay Minerals*, **28**, 419-424.
- Starr, R.E. and Young, R.H. (1978) Paprecoating formulations. A study of limitations in the determination and use of the Kubelka-Munk constants. *Tappi*, **61**, 78-80.
- Steeffel, C. I. and Van Cappellen, P. (1990) A new kinetics approach to modelling water- rock interaction. The role of nucleation, precursors and Ostwald ripening. *Geochimica et Cosmochimica Acta*, **54**, 2657-2677.
- Stoch, L. and Sikora, W. (1976) Transformation of mica in the process of kaolinization of granites and gneisses. *Clays and Clay Minerals*, **24**, 156-162.
- Stucki, J.W., Goodman, B.A. and Schwertmann, U. (1988) *Iron in soils and clay Minerals*. D. Reidel Publ. Co., Dordrecht, Holland, 893 pp.
- Stumm, W and Sulzberger, B (1992) The cycling of iron in natural environments: Consideration based on laboratory studies of heterogeneous redox processes. *Geochimica et Cosmochimica Acta*, **56**, 3233-3257.
- Suttner, L.J., Mack, G., James, W.C. and Young, S.W. (1976) Relative alteration of microcline and sodic plagioclase in semi arid and humid climate. *Geological Society of America, Abstract programs*, **8**, 512.
- Tardy, Y., Bocquier, G., Paquet, H. and Millot, G. (1973) Formation of clay from granite and its distribution in relation to climate and topography. *Geoderma*, **10**, 271-284.
- Tardy, Y. and Nahon, D. (1985) Geochemistry of laterites. Stability of Al-goethite, Al-hematite and Fe³⁺ kaolinite in bauxite and ferricretes. An approach to the mechanism of concretion. *American Journal Science* **285**, 865-903.
- Tarzi, J.D. and Protz, R. (1978) Characterisation of morphological features of soil micas using scanning electron microscopy. *Clays and Clay Minerals*, **26**, 352-360.
- Tazaki, K. and Fyfe, W.S. (1987) Primitive clay precursors formed on feldspar. *Canadian Journal of Earth Sciences*, **24**, 506-527.
- Temple, A.K. (1966) Alteration of ilmenite. *Economic Geology*. **61**, 695-714.
- Teufer, G. and Temple, A.K. (1966) Pseudorutile, a new mineral intermediate between ilmenite and rutile in the natural alteration of ilmenite. *Nature*, **211**, 179-181.
- Theng, B.K.G. (1979) *Formation and properties of clay- polymer complexes*. Elsevier, Amsterdam, 362 pp.
- Thomas, D., Lalithambika, M. and Soman, K. (1987) Clay mineral transformation in the weathering crust : Evidence from Lundara clay mine, Kerala. *Journal of Geological Society of India*, **30**, 239-243.
- Thompson, J.G. (1985) Interpretation of solid state ¹³C and ²⁹Si nuclear magnetic resonance spectra of kaolinite intercalates. *Clays and Clay Minerals*, **33**, 173-180.
- Tomura, S., Shibasaki, Y. and Mizuta, H. (1983) Spherical kaolinite: synthesis and mineralogical properties. *Clays and Clay Minerals*, **31**, 413- 421.
- Tomura, S., Shibasaki, Y., Mizuta, H. and Kitamura, I. (1985) Growth conditions and genesis of spherical and platy kaolinite. *Clays and Clay Minerals*, **33**, 200-206.

- Tsuzuki, Y. and Kawabe, I. (1983). Polymorphic transformation of kaolin minerals in aqueous solution. *Geochimica et Cosmochimica Acta*, **47**, 59-66.
- Ubaladini, S., Piga, L., Fornari, P., Massidda, R. (1996) Removal of iron from quartz sands: A study by column leaching using a complete factorial design. *Hydrometallurgy* **40**, 369-379.
- Valenton, I. (1972) *Bauxite*. Elsevier, Amsterdam, 226 pp.
- Varadarajan, K. and Balakrishnan, M. K. (1980) Kerala Coast – A landsats views. Proc. Sym. On geology and geomorphology of Kerala. Geological survey of India, Special Publication, **5**, 67– 68.
- Vazquez, F.M. (1981) Formation of gibbsite in soil and saprolites of temperate-humid zones. *Clay Mineral*, **16**, 43-52.
- Velbel, M. A. (1984) Natural weathering mechanisms of almandine garnet, *Geology* **12**, 631-634.
- Velbel, M.A. (1985a) Geochemical mass balances and weathering rates in forested watersheds of Southern Blue Ridge. *American Journal of Science*, **285**, 904-930.
- Velbel, M.A. (1985b) Hydrogeochemical constraints on mass balances in forested watersheds of the southern Appalachians. In *The Chemistry of Weathering*, J.I. Drever and D. Reidel, eds., NATO ASI Series, C 149, 231- 247.
- Waite, T.W. and Morel, F.M.M. (1984) Photoreductive dissolution of colloidal iron oxide: Effect of citrate. *Journal of Colloid Interface Science*, **102**, 121-137.
- Walker, T.L. (1902) The geology of Kalahandi state, central provinces. Memoir of Geological Survey of India, **33**, 1-21.
- Walker, T.R. (1974) Formation of red beds in moist tropical climates: A hypothesis. *Bulletin of GSA*, **85**, 633-638.
- Water Resource of Kerala (1974) Government of Kerala, Pub., 110p.
- Weaver, C.E. (1985) Development in sedimentology 44- Clay, Muds and Shales. Elsevier, Amsterdam, 819 pp.
- White, A.F. and Yee, A. (1985) Aqueous oxidation- reduction kinetics associated with coupled electron- cation transfer from iron containing silicates at 25 °C., **49**, 1263-1275.
- White, G.N., Dixon, J.B., Weaver, R.M. and Kunkle, A.C. (1991) Genesis and morphology of iron sulfides in gray kaolins. *Clays and Clay Minerals*, **39**, 70-76.
- Wilson, M.J. (1966) The weathering of biotite in some Aberdeenshire soils. *Mineralogical Magazine*, **35**, 1080–1093.
- Wilson, M.J. (1987) A handbook of determinative method in clay mineralogy. Blackie, Chapman and Hall, New York, 308 pp.
- Wollast, R. (1967) Kinetics of the alteration of K- feldspar in buffered solutions at low temperature. *Geochimica et Cosmochimica Acta*, **31**, 635-648.
- Wollast, R. and Chou, L. (1985) Kinetic study of the dissolution of albite with a continuous flow-through fluidized bed reactor. In *The Chemistry of Weathering*, NATO ASI series J. I. Drever, eds., Reidel, Dordrecht, The Netherlands, 75-96.

Publications/ Papers Presented

Publications (SCI Journals):

1. Mineralogy, geochemistry and utilization study of the Madayi kaolin deposit, North Kerala, India. **Manju, C.S.**, V. Narayanan Nair. and M. Lalithambika, Clays and Clay Minerals, Vol. 49, N0. 4, 2001, 355-369.
2. Geochemical and mineralogical investigation on Kundara kaolin deposit, South Kerala, India. **Manju, C.S.**, V. Narayanan Nair and M. Lalithambika (2001) Clays and Clay Minerals (Accepted).
3. Surface modified kaolinite as filler in natural rubber. **Manju, C.S.**, C.K.S. Pillai, A.R.R. Menon, V.S. Prasad, I. Balakrishnan, T.G.Nelson and M. Lalithambika (2002) Applied Clay Science (Communicated)

Papers presented (International Seminars):

1. Morphology and geochemistry of clays in Kundara, South Kerala. **Manju C.S.** and M. Lalithambika, **International Symposium** on Clays in Relation to Environment and Industry (ISCREI – 2000), November 2000, held at Annamalai University, Chidambaram.
2. Value addition of kaolin by an easy deferration technique. **Manju C.S.**, Ambikadevi. V.R. and M. Lalithambika, **International Seminar** on Mineral Processing Technology (MPT-2002), January 2002, held at Indian Institute of Science, Bangalore.